Spin-Orbit Interactions in Low Dimensional Systems and Spin Transport Properties of Single Molecular Transistor

A thesis submitted for the degree of **DOCTOR OF PHILOSOPHY IN PHYSICS**

By

Pooja Saini (16PHPH05)



Under the supervision of **Prof. Ashok Chatterjee**

School of Physics,
University of Hyderabad
Hyderabad- 500046
India

DECLARATION

I hereby declare that this thesis titled "Spin-Orbit Interactions in Low Dimensional Systems and Spin Transport Properties of Single Molecular Transistor" submitted by me, under the guidance and supervision of Prof. Ashok Chatterjee, is a bonafide research work and is free from plagiarism. I also declare that it has not been submitted previously, in part or in full to this university or any other university or institution, for the award of any degree or diploma. I hereby agree that my thesis can be deposited in Shodhganga or INFLIBNET.

A report on plagiarism statistics from the university librarian is enclosed.

Place: Hyderabad

Date: 27/12/2022

Pooja Saini Pooja Saini

(Reg. No. 16PHPH05)

Prof. ASKOK CHATTERJEE SCHOOL OF PHYSICS UNIVERSITY OF HYDERABAD HYDERABAD - 500 046, INDIA

Prof. Ashok Chatterjee

(Thesis Supervisor)

CERTIFICATE

This is to certify that the research work described in this thesis entitled "Spin-Orbit Interactions in Low Dimensional Systems and Spin Transport Properties of Single Molecular Transistor" is being submitted to the University of Hyderabad by Pooja Saini with Reg. No. 16PHPH05, in partial fulfillment for the award of Doctor of Philosophy in physics, is a bona fide work done by her under my supervision. This thesis is free from plagiarism and has not been submitted previously in part or in full to this or any other University or Institution for the award of any degree or diploma.

Further, the student has the following publication before submission of the thesis for adjudication:

- 1. "Effect of Rashba and Dresselhaus spin-orbit interactions on a donor impurity in a Gaussian GaAs Quantum Dot in the presence of a Magnetic field" **Pooja Saini**, A. Boda, Ashok Chatterjee, J. Mag. Mag. Mat. 485, 407 (2019).
- "Effect of confinement potential shape and Spin-Orbit Coupling on the D⁰ Impurity in a
 GaAs quantum dot placed in a magnetic field" Pooja Saini, Ashok Chatterjee,
 Superlattices and Microstructures 146, 106641 (2020).
- 3. "Spin-orbit interaction effects on binding energy and susceptibility of an off-centre D⁰ impurity in a Gaussian dot in magnetic field" **Pooja Saini**, S. Mukhopadhyay, Ashok Chatterjee, Physica B Condensed matter, 617, 413099 (2021).
- 4. "Spin-orbit interaction effect on a hydrogenic D^0 centre in a three-dimensional asymmetric Gaussian GaAs quantum dot in a magnetic field" **Pooja Saini** and A. Chatterjee, (to be communicated).

- 5 "Diamagnetic Susceptibility of a D⁻ Impurity in a GaAs Gaussian Quantum Dot in the presence of Rashba and Dresselhaus spin-orbit interactions and a magnetic field" Pooja Saini, A. Boda, Ashok Chatterjee (Accepted in Micro and Nanostructure)
- 6. "Thermoelectric properties of single molecular transistor" **Pooja Saini**, Manasa Kalla, Ashok Chatterjee (Manuscript under preparation)

Conference proceedings

1. **Pooja Saini,** Aalu Boda and Ashok Chatterjee, Effect of Rashba and Dresselhaus spin orbit interactions on the ground state properties of a D⁰ impurity in a Gaussian GaAs quantum dot placed in a magnetic field. *AIP Conference Proceedings 2115, 030450 (2019)*.

Presentations in National and International Conferences

- 1. Poster Presentation: **Pooja Saini** and Ashok Chatterjee, "Spin orbit intractions and magnetic field effect on off centre D^0 impurity for GaAs Gaussian QD", (**Poster**), International Conference on Advanced basic sciences, February 7-9, 2018, GDC Memorial College, Bahal, Bhiwani district, Haryana.
- 2. Pester presented: Pooja Saini, Aalu Boda and Ashok Chatterjee, "Effect of Rashba and Dresselhaus spin-orbit interactions on the ground state properties of a D0 impurity in a Gaussian GaAs quantum dot placed in a magnetic field.", (Poster), 'DAE SSPS 2018', December 18-22 2018, Guru Jambeshwar University of Science and Technology, Hisar, Haryana.
- **3.** Workshop attened: **Pooja Saini**, "Integrable systems in Mathematics, Condensed matter and Statistical physics", July 16 August 10, 2018, ICTS, Bangalore, Karnataka.
- 4. Poster presented: **Pooja Saini**, Aalu Boda and Ashok Chatterjee, "Tuning diamagnetic susceptibility on D^- impurity of Gaussian QD in the presence of magnetic field and Rashba

and Dresselhaus spin orbit interactions", (Poster), 2nd Annual Conference on Quantum Condensed Matter, July 8-10, 2019, IISc, Bangalore.

Further, the student has passed the following courses towards the fulfillment of the course required for Ph. D.

Course code	Name	Credits	Pass/Fail	
PY601	Research Methodology	4	Pass	
PY602	Advanced Quantum Mechanics	4	Pass	
PY60305	Advanced Experimental Technique	4	Pass	
PY60309	Advanced Mathematical Methods	4	Pass	

Prof. ASKOK CHATTERJEE
SCHOOL OF PHYSICS
UNIVERSITY OF HYDERABAD
WYDERABAD - 500 046, INDIA

M. Than arbyam
Dean
School of physics

CDE N
School of Physics
University of Hyderabad
HYDERABAD - 500 046

Prof. Ashok Chatterjee Supervisor

ACKNOWLEDGEMENTS

I consider myself extremely fortunate to have had a chance to work with Prof. Ashok Chatterjee. He has always been encouraging, guiding, while at the same time, he gave me enough freedom to pursue my research interests. He always helped me morally and mentally. Without his guidance, this thesis would not have been possible.

I am incredibly grateful to my collaborator Prof. Soma Mukhopadhyay for valuable suggestions and discussions, my senior and collaborator Dr. Aalu Boda for insightful inputs. They were always available for me to help whenever needed.

I want to express my gratitude to my doctoral committee members, Prof. Srinath and Prof. S. V. S. Nageswara Rao, for their fruitful suggestions during review meetings. I also express my sincere thanks to the current Dean Prof. KC James Raju and former Deans of the school, Prof. Vipin Srivasthava, Prof. Bindu. A. Bambah and Prof. Seshubai. I convey my sincere regards to all the condensed matter faculty members.

I am thankful to the non-teaching staff Mrs. Deepika, Mr. Abraham, Mrs. Vijayalakshmi, Mr. Sudarshan and Mrs. Sasikalla for their help in administrative matters.

I acknowledge the financial assistance provided by the CSIR-JRF fellowship. My regards to Mr. Devender of finance section for processing fellowship bills.

I thank all my seniors and colleagues, Dr. Sanjeev kumar, Dr. Shankar, Dr. Narsimha Raju, Dr. Uma lavanya, Dr. Luhluh Jahan, Dr. Manasa Kalla, Dr. Hemant Sharma, Zahid Malik, Kuntal Bhattacharya and Debika Debnath. Especially, I thank my friend, late Dr. Ruchika seth for her unconditional love and support. I thank to my college and school friends Hemlata, Preeti, Sunita, Priyanka, Anita, Manoj, Narendre, Rajbala, Dr. Anita, Dr. Zeba and Dr. Kamlesh for their constant encouragement over the years. I am also grateful to my friends Dr. Atasi, Dr. Dinesh, Vinod, Muhammed Sharif and Praveen, for their constant support. I thank all my seniors Dr. Suchismitha, Dr. Shivaramakrishna, Dr. Nisha, Dr. Anupama, and Dr. Atiya, Avishek, Dr. Leelasree, Dr. Muhammad Rasi, Naresh, Dr. Pranetha and Dr. Muhammad Tahir. I thank all my juniors

Bishupriya, Pawan, Akashay, Nitin, Mitesh, Dinesh, Aishwarya, Susmita, Karthik. I thank my hostel friends Jhansi Rani and Rekha. I am thankful to my College teachers Rakesh Dhaka Sir, Rajesh Sir, Prof. Seshadri for their immense support.

I want to dedicate this thesis to my parents Shri Satyanarayan Saini and Smt. Rameshwari Devi, my grandparents Shri. Omkar Saini and Smt. Bimla Devi, who supported me and believed in my abilities. I would like to acknowledge my siblings Ravi, Ram, Ved, Shyam, Uma, Om and Varsha for their unconditional love. Lastly I would like to give special thanks to Ashim Dutta for his love, help and encouragement.

PREFACE

This thesis focuses on the effect of the Rashba and Dresselhaus spin-orbit interactions on the hydrogenic impurity in a quantum dot (QD) and the effect of electron-phonon interaction, electron-electron interaction and quantum dissipation on the electric conductance, Seebeck effect and the spin Seebeck effect. A QD is a low-dimensional system in which the motion of the electrons is restricted in all three directions. The natural length scale of a QD is the order of a few nm which makes these systems highly interesting because at this length scale strong quantum effects are expected to appear. The confinement potential is one of the essential parameters one needs to consider while studying a QD theoretically. According to the recent experimental findings, the confinement potential is anharmonic and has a finite depth. It has been suggested that the Gaussian potential is an appropriate model for a QD's confinement potential.

Generally, we can have two types of spin-orbit interactions in a solid. One is the Rashba spin-orbit (RSO) interaction (RSOI) which arises when a material loses its structural inversion symmetry (SIS), and the other one is the Dresselhaus spin-orbit (DSO) interaction (DSOI) which arises from the breaking of the bulk inversion symmetry (BIS).

The generation of the electric voltage by a temperature gradient is known as the Seebeck effect. In Spintronics, the central focus is on spin transport in place of charge transport. Similarly, a spin analog of the Seebeck effect has received a lot of attention in recent years. The spin Seebact effect refers to the generation of the spin voltage by placing a temperature gradient in a ferromagnet. In 2008, Uchida et al. reported the possibility of creating a pure spin current by the temperature gradient in magnetic metals. The thesis is organized as follows:

We begin the thesis by presenting an overall introduction to the subject of QDs and spin-orbit interactions in Chapter 1. Here, we first give a brief review of some of the basic properties of QDs, discuss a few fabrication techniques, highlight some of their important applications and introduce the concept of confinement potential. Next, we discuss the donor impurity in the QDs and a brief introduction to the spin-orbit interactions. Next, we introduce the single molecular transistor (SMT). In SMT device, it is possible to successfully regulate the current by adjusting the gate voltage. Investigations have shown that SMTs and molecular electronic devices have tremendous

potential for applications in spin filters, switching devices, sensors, etc. Finally, we discuss the brief introduction of Seebeck effect and spin Seebeck effect. One of the main objectives of this thesis is to study the effect of Rashba and Dresselhaus spin-orbit interactions on the impurity states in a QD and the thermal transport properties of a single molecular transistor.

In Chapter 2, we study the effect of Rashba and Dresselhaus spin-orbit interaction on the bound state of an on-centre D^0 hydrogenic impurity in a three-dimensional GaAs GQD in the presence of an external magnetic field (B). To deal with the spin-orbit interaction part, we first apply a unitary transformation on the Hamiltonian of the system and then use the Rayleigh-Ritz variational method to calculate the ground state energy (GS). We obtain the binding energy (BE), magnetic moment and the diamagnetic susceptibility. We show that the GS energy of the D^0 system increases with decreasing QD size and it decreases with increasing confinement strength. Also, the GS energy is found to decrease with increasing RSOI and DSOI. However, the effect of DSOI is found to be less than RSOI. So, one may conclude that RSOI is more dominating than DSOI in a QD. We also show the variation of binding energy (BE) with respect to both Rashba and Dresselhaus parameters. The BE appears to be independent of both Rashba and Dresselhaus parameters. The effect of spin-orbit interactions in the presence of a magnetic field, however, turns out to be more interesting. In the presence of a magnetic field, the Rashba parameter decreases the BE while the Dresselhaus parameter increases it. Finally, we calculate the magnetic moment (M) and diamagnetic susceptibility (S) of the D^0 impurity as a function of the magnetic field for a different sets of Rashba and Dresselhaus interaction parameters. We show that |M| increases with B and decreases with the reduction in the effective QD radius R. S is also found to increase with B. We furthermore show that |S| increases with increasing QD size at small magnetic fields, but above a critical magnetic field, it decreases with increasing QD radius. This leads to a crossing behaviour in the diamagnetic susceptibility. Finally, we calculate the electron distribution for different values of the QD parameters. It is shown that, in general, as the QD size decreases, the electron localization becomes stronger. However, the behaviour starts reversing below a certain QD size because of the uncertainty principle.

In Chapter 3, we consider the spin-orbit interaction effects on BE and susceptibility of an offcentre D^0 impurity in a GQD in the presence of a magnetic field (B). Again we eliminate the spinorbit interactions by a unitary transformation. The resulting problem cannot be solved exactly. So we use the Ritz variational method. We apply our result to a GQD of GaAs and present the behavior of the GS energy (GSE) (E) of the off-centre D^0 impurity as a function of the impurity position D for B=0 and $B\neq 0$ and for different RSOI and DSOI coefficients α_R and β_D . As D increases, GSE initially increases quite rapidly, but asymptotically saturates to a constant value. This can be easily understood from the simple semi-classical argument, which suggests that GS corresponds to the minimum of the potential. The RSOI and DSOI effects on GSE are found to be low at small values of D and large at higher values of D. GSE decreases in the presence of both SOIs at low B, but the effects of RSOI and DSOI are opposite at higher values of B. RSOI reduces GSE, but DSOI enhances it at higher values of B. We show that the binding of a D^0 complex is strongest for the on-centre complex (D = 0) and BE decreases with increasing D and eventually saturates. Our results reveal that the effect of SOIs on the D-dependence of BE is very small, though the magnetic field can influence the D-dependence of BE at small D values. However, if D is large, then none of the parameters R, B, α_R , or β_D would have any effect on the E_B vs D curve. We present the contour plots and 3D plots of BE of the system with respect to different system parameters. Finally, the susceptibility (S) of the off-centre D^0 in a GQD system is calculated using statistical mechanics and is shown to be diamagnetic. With increasing D, |S| initially increases and eventually saturates to a constant. We observe that when RSOI is absent, and only DSOI is present, |S| decreases both with β_D and B. However, in the case when DSOI is absent, and only RSOI is present, at small values of B, |S| initially increases with increasing α_R , reaches a maximum and then decreases with α_R . But at large B, |S| increases monotonically with α_R .

In Chapter 4, we study the effect of the shape of the confinement potential on D^0 system in a GaAs QD in the presence of a magnetic field and spin-orbit interactions. In this problem, we use for the confinement potential, a spherically symmetric power exponential potential (PEP) with a steepness (or a shape) parameter (p). A QD with PEP will be referred to as a power exponential QD (PEQD). By changing the value of p, we can change the shape of PEQD from a Gaussian potential to a rectangle potential. We employ the Ritz variational method and study the variation of GSE and BE of a D^0 Centre in a PEQD as a function of the shape parameter p, the effective QD size R, the Rashba and Dresselhaus spin-orbit interaction constants α_R and β_D and the external magnetic field B. As a function of R, BE shows peaks and the peak height increases as p increases. After reaching the peak, BE decreases with R faster for higher p and gives interesting crossing behaviour. We explore the behaviour of the magnetic moment and diamagnetic susceptibility with respect to the magnetic field for different values of the steepness parameter p. The susceptibility (S) increases with p at small p and at large p, it decreases with increasing p. At intermediate p, it decreases with increasing p. At intermediate p,

S first decreases with increasing p, develops a minimum at some value of p and then increases with further increase in p.

In chapter 5, we investigate the behavior of GS binding energy of a hydrogenic donor impurity in an asymmetric 3D GQD of GaAs with respect to effective QD size R, confinement potential depth V_0 , magnetic field B, asymmetry parameter b, and RSOI and DSOI coefficients. We also examine the dependence of magnetic moment (M) and susceptibility (S) on B for different values of the asymmetry parameter B. As expected, the susceptibility is found to be diamagnetic in nature. Also the magnitude of S is found to decrease with increasing B. However, it increases as the asymmetry increases at small B and decreases with increasing asymmetry at large B. This gives rise to an interesting crossing behavior. The Rashba coupling decreases BE, while Dresselhaus coupling increases it and the asymmetry in the confinement potential enhances these effects.

In chapter 6, we study the energetics of a negative hydrogenic impurity D^- in a GaAs GQD in the presence of a magnetic field, and the Rashba and Dresselhaus SOIs. The D^0 system studied earlier, is spherically symmetric, so there cannot exist any dipole moment. However, in the case of a D^- centre system, the situation is different. Classically, of course, there cannot be any dipole moment in this system because the Coulomb correlation would try to force the electrons to lie on the diametrically opposite sides of the nucleus giving rise to zero dipole moment. Quantum mechanically, however, there would be fluctuations, and because of this quantum fluctuation, electron distribution would be such as to minimize the system's energy. We calculate the GS energy and BE of the D^- system by the Ritz variational method and obtain the dipole moment as a function of the QD size, confinement depth, magnetic field, and the Rashba and Dresselhaus parameters. We show that the magnetic field and Dresselhaus interaction decrease the dipole moment while the Rashba parameter increases it. We also calculate the susceptibility of the negative hydrogenic impurity system and show that the behavior of the susceptibility of D^- is also diamagnetic. Interestingly, the susceptibility of D^- system exhibits a deep minimum in the presence of RSOI.

In Chapter 7, we consider an SMT system in which a central QD is coupled to two metallic leads which act as a source and a drain respectively. A temperature gradient is applied across the source and the drain and electrons can travel from the source to the drain through the QD giving rise to a

tunneling current. The entire SMT system is placed on an insulator substrate to which a gate is attached. By applying a gate voltage, the tunneling current can be manipulated. The substrate contains a large number of uncoupled harmonic oscillators and thus acts as a phonon bath. The QD contains a single energy level and a local phonon mode. The QD electrons interact with each other by the Hubbard onsite interaction and with the local phonon mode through the Holstein onsite el-ph interaction. The substrate phonons can interact with the local QD phonon by a linear interaction of the Caldeira-Leggett type which gives rise to a dissipative effect in the phonon dynamics of the QD. We describe the entire SMT system by the Anderson-Holstein-Caldeira-Leggett model and investigate the tunneling conductance, Seebeck effect and the spin Seebeck effect in the presence of el-el coupling, el-ph coupling, and quantum dissipation. We treat the interaction between the QD phonon and the substrate phonons by using a canonical transformation. This renormalizes the frequency of the QD phonon. The el-ph interaction is decoupled using the conventional Lang-Firsov transformation followed by a zero-phonon averaging. Finally, using the Keldysh approach and the equation of motion method, the transport parameters are determined. In particular, we studied the behaviour of the conductance $(G_{\uparrow}, G_{\downarrow}, G^c)$ and G^s) with respect to different parameters such as the temperature, e-e interaction, e-p interaction, damping parameter, magnetic field, quantum dot energy and chemical potential. It is found that the charge conductance G^c is maximum while the spin conductance G^s is zero in the absence of the magnetic field. However, as the magnetic field increases, the peak height of G^c decreases and the peaks split into two peaks while the peak height of G^s increases and shifts towards the right on the chemical potential axis. We study the variation of the spin-up and spin-down electric conductance as a function of different parameters like temperature, magnetic field, QD energy ϵ_d and the chemical potential μ . We also study the behaviour of the charge Seebeck effect and the spin Seebeck effect with respect to the magnetic field and QD energy. We have also shown that temperature, magnetic field and the above-mentioned interactions have interesting effects on the thermopowers (S_1, S_1, S_2, S_3) S_c and S_s). As a function ϵ_d , the behaviour of the spin-up and spin-down Seeback coefficients are the same, but their amplitudes are slightly different. The spin-up and spin-down thermopowers are the same at zero magnetic field. So the charge Seebeck coefficient is maximum and the spin Seebeck coefficient is zero in this case. However, S_c decreases and S_s increases at higher values of the magnetic field. Thus, as the magnetic field increases, the spin current and the spin Seebeck coefficient also increase.

Finally, in chapter 7, we summarize the main results of the thesis and make some concluding remarks.

TABLE OF CONTENTS

Declaration
Certificate
Acknowledgments
Preface
List of publications

Chapter 1: A Brief Overview of Quantum Dots and Spin Orbit Interactions 16

- 1.1 Introduction
- 1.2 Fabrication of the quantum dot
- 1.3 Application of the quantum dot
- 1.4 Confinement potential
- 1.5 Donor impurities in the quantum dot
- 1.6 Origin of the spin-orbit interaction
 - 1.6.1 Rashba spin-orbit interaction
 - 1.6.2 Dresselhaus spin-orbit interaction
- 1.7 Introduction of single molecular transistor
- 1.8 Seebeck effect and spin Seebeck effect
- 1.9 Aim of the thesis
- 1.10 References

Chapter 2: The effect of Rashba and Dresselhaus Spin Orbit Interactions and Magnetic Field on D^0 Impurity in a Gaussian Quantum Dot 34

- 2.1 Introduction
- 2.2 Theory
- 2.3 Numerical results and discussion
- 2.4 Conclusion
- 2.5 References

Chapter 3: Spin-Orbit Interaction effects on Binding Energy Susceptibility of an Off-Centre D^0 Impurity in a	
Dot in Magnetic Field	52
3.1 Introduction	
3.2 Model Hamiltonian	
3.3 Formulation	
3.4 Numerical results and discussion	
3.5 Conclusion	
3.6 References	
Chapter 4: Effect of Confinement Potential Shape and Spin-on the D^0 Impurity in a GaAs Quantum Dot place Field	
4.1 Introduction	
4.2 Theory	
4.3 Numerical results and discussion	
4.4 Conclusion	
4.5 References	
Chapter 5: Spin-orbit interaction effect on a hydrogenic D^0 of dimensional asymmetric Gaussian GaAs quantum magnetic field	
5.1 Introduction	
5.2 Model and Formulation	
5.3 Results and discussion	
5.4 Conclusion	
5.5 References	

Chapter 6: Enhancement in binding of D^- in a GaAs—Gaussian Quantum Dot in the presence of spin-orbit interactions and a magnetic field—104

6.1	Introduction	
6.2	Model and Formulation	
6.3	Numerical results and discussion	
6.4	Conclusion	
6.5	References	
Chai	pter 7: Thermoelectric properties of single molecular transistor	119
Cita	pter 7. Thermoelectric properties of single molecular transistor	11)
7.1	Introduction	
7.2	The Model	
7.3	Formulation	
	7.3.1 Decoupling of coupling between QD and bath phonons interaction	
	7.3.2 Elimination of phonons	
	7.3.3 Tunnelling current: non-equilibrium Keldysh Green function formalism	
	7.3.4 Conductance, charge and spin Seebeck coefficients	
7.4	Results and discussion	
7.5	Conclusion	
7.6	References	
Chap	ter 8: Conclusions	151

Chapter ~1

A brief overview of quantum dots and spin-orbit Interactions

1.1 Introduction

Quantum dots have generated tremendous interest in the last few decades for their role in providing a platform to test quantum mechanics at the laboratory scale as well as for their potential applications in semiconductor technology at the microscopic level [1-6]. A quantum dot (QD) is a low-dimensional system in which electron transport is restricted in all the three directions [7-10]. Most of the quantum dots (QDs) that are useful from the point of view of nano-technology, are compound semiconductors composed of materials from the periodic groups of II-VI, III-V, or IV-VI.

The typical size of a QD is of the order of a few nanometres and can be thought of as a giant artificial atom. However, they are much more flexible than atoms because they can be fabricated in different shapes and sizes as required depending upon the fabrication process. It is known that materials behave differently at very small sizes, a phenomenon known as the quantum size effect, and the properties of quantum dots have been found to be in between those of bulk semiconductors and discrete atoms or molecules. Additionally, QD structures have an unprecedented tunability and hence a tremendous potential for application in microelectronic device technology such as QD lasers and super-fast computers [12].

Due to quantum confinement, the energy levels of the electrons become discrete with a finite separation between them. Some of these energy levels are unoccupied and constitute the band gap. Most of the electrons occupy the valence band, which are energy levels below the band gap and the levels above constitute the conduction band. When the QD is hit by an incident light of energy

higher than that of the band gap of the semiconductor, electrons from the valence band absorb this light and go the conduction band producing excitons. These excited electrons (exciton) return to a lower energy level resulting in a narrow, symmetric energy band emission [13]. Quantum dots confine their charge carriers in a small spatial domain that is of the order of a few nanometres. This is known as quantum confinement and can be approximately described by an infinite potential having the following energy levels:

$$E_n = \frac{n^2 \pi^2 \hbar^2}{2m^* L^2} \quad , \tag{1.1}$$

$$E_{n+1} = \frac{(n+1)^2 \pi^2 \hbar^2}{2m^* L^2} \ . \tag{1.2}$$

The energy difference between the (n + 1) - th level and the n - th level in a QD is thus given by

$$\Delta E = E_{n+1} - E_n = \frac{(2n+1)\pi^2\hbar^2}{2m^*L^2} , \qquad (1.3)$$

where m^* is the Bloch mass of the particle and L is the effective length scale of the QD well. Eq. (1.3) suggests that as a system becomes extremely small, the energy level difference between two consecutive levels becomes very large and the system becomes fully quantum.

Fig. 1 shows how the band gap between the energy levels influences the colours and size of the QDs. The QD allows us to control its band gap by adjusting its size hence controlling the output wavelength with extreme precision. An immediate optical feature of colloidal QDs is their coloration. While the material which makes up a QD defines its intrinsic energy signature, the nano-crystals quantum-confined size is more significant at energies near the band gap. Thus QD's of the same material, but with different sizes, can emit light of different colours. The physical reason is the quantum confinement effect. The larger the dot, the redder (lower energy) is its fluorescence spectrum. Conversely, smaller dots emit bluer (higher energy) light. The coloration is directly related to the energy levels of the QD. Quantitatively speaking, the band gap energy that determines the energy (and hence colour) of the fluorescent light is inversely proportional to the square of the size of the QD. Larger QDs have more energy levels which are also more closely spaced. This allows the QD to absorb photons containing less energy, i.e., those closer to the red

end of the spectrum. Recent Observations have shown that the shape of the crystal lattice also might change the colour [13].

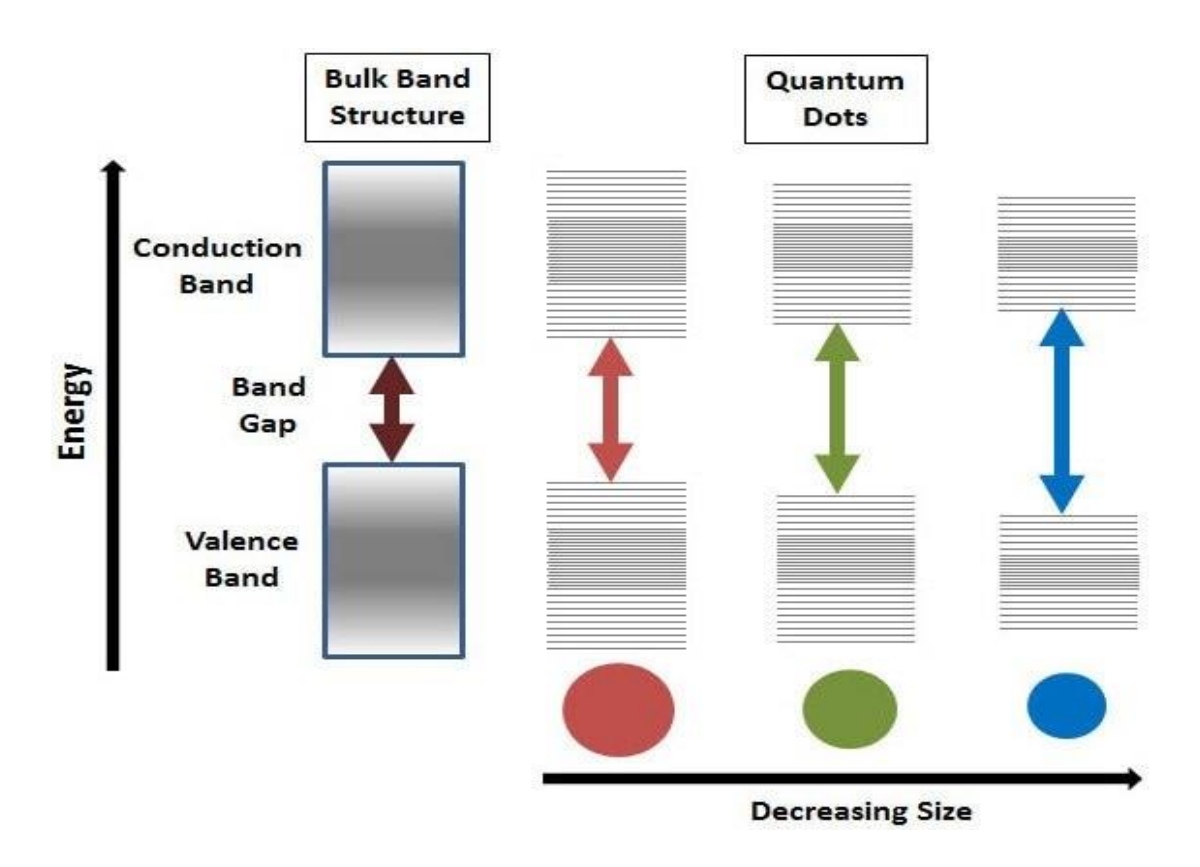


Fig. 1 Size dependence of the QD energy band gap [14].

The density of states (DOS) function describes the number of states per energy difference and determines the distribution of carrier density in a physical system. The DOS is defined by,

$$g(E) = \frac{dN}{dE} \tag{1.4}$$

where dN = g(E)dE is the number of electrons dN with an energy E lying within a narrow range of energy $dE = E_2 - E_1$ and is proportional to the density of state at E. An overview of quantum confinement in nanostructures is shown in Figure 1.2. The DOS behaves as a square root of the energy $E^{1/2}$ in the 3D bulk system. In this structure, electrons are not confined and they can move freely in any direction. In the two-dimensional (2D) quantum well (QW) structure, the DOS

behaves like a Heaviside step function and electrons are free to move in two spatial directions and their motion is confined in the third direction. Thus in a QW structure, electrons are said to constitute a quasi-two-dimensional electron gas (2DEG). In the 1D quantum wire

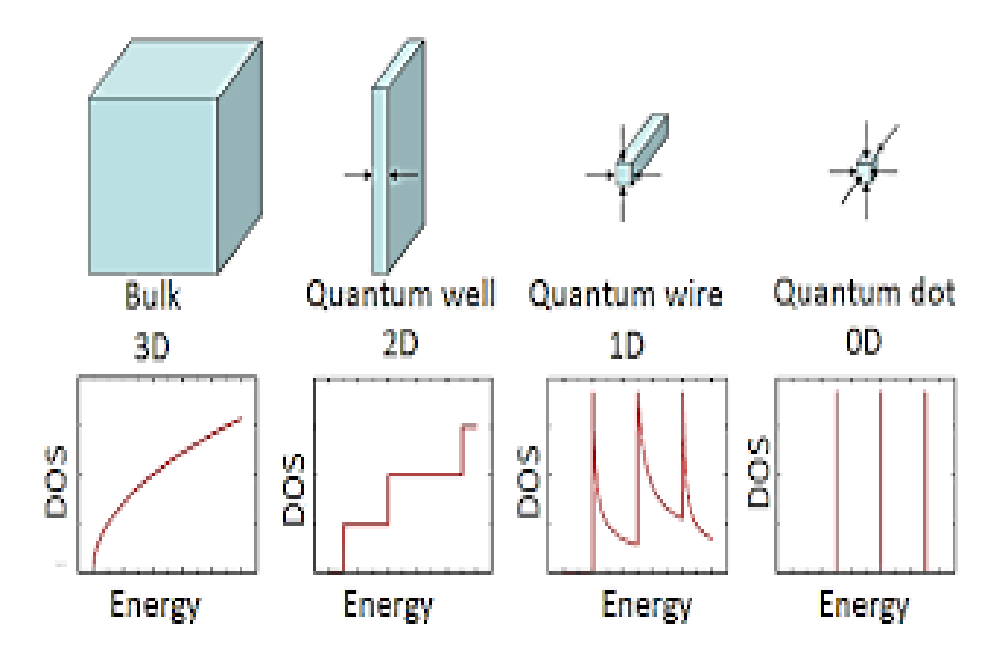


Fig. 2 Quantum confinement behaviour in all three directions.

structure, the DOS is proportional to $E^{-1/2}$ and electron's motion is confined in two directions while they have significant freedom to move freely in the other direction. Such a system of electrons is called a quasi-one-dimensional electron gas. In the QDs or zero-dimensional materials, the DOS is given by a series of Dirac delta functions. In this structure, the electrons do not have any free directions and the de Broglie wavelength of the electrons is of the same order as the confinement length which makes these systems show astounding quantum effects. If the confinement length of the QD is of the same order in all the three directions, it is called a three-dimensional (3D) QD. If the confinement length in one particular direction happens to be much smaller as compared to rest of other two directions, then the resulting system is referred to as a quasi-two dimensional (quasi-2D) QD. For the sake of mathematical simplification, sometimes a quasi-2D QD is treated as a purely 2D QD theoretically. This approximation would be valid if the confinement length in one particular direction say, the z direction is extremely small which may be possible if the material is extremely thin in this direction. In the present work, we consider both 2D and 3D QDs.

1.2 Fabrication of the quantum dot

Quantum dots can be fabricated by several methods. The main aim is to confine the electrons or any other charge carriers in a small region. A metal particle can be surrounded by insulators in order to achieve this. By providing an electric field [15], we can also restrict the motion of electrons inside the semiconductor. With the development of modern fabrication techniques like molecular beam epitaxy it is now possible to manufacture a single atomic layer of semiconductor crystal (eg. GaAs) at a time. A 2D electron gas can be made by sandwiching a thin layer (roughly 10 nm) of a GaAs semiconductor between two thicker layers of a semiconductor with a larger band gap than GaAs [16]. Generally, AlGaAs is chosen for this purpose because its crystal structure and lattice constant are almost identical to GaAs. AlGaAs behaves as an insulator whereas in GaAs electrons can move freely. It is clear that the steps in energy at the GaAs/AlGaAs interfaces produce a potential well and hence discrete energy levels in both the valance and conduction bands. A 2D electron gas can now be created if one of the AlGaAs layers is doped with Si donors. Then even at low temperatures, electrons of a donor atom can go to the conduction band. Once it does that, it can easily land itself into the potential well, where it gets trapped with others to form a 2D electron gas. The dopant impurities are usually placed at some distance from the well so that they produce a very low scattering of the carriers. This is called modulation doping which gives high mobility and large mean free path. The electron gas confined in the GaAs QW is essentially twodimensional. The QW is so thin that at low temperatures, only the lowest quantum energy state is occupied by the electrons. The electrons have no freedom to move in the perpendicular direction of the well, but may only move laterally in it. Now QDs can be made from this QW layered structure. One method is to use a mask of resist material defined on top of the layered QW structure [16]. This resist is a polymer which is either sensitive to electrons or x-rays depending on the type of lithography, which is then performed to define the dot. Another method of achieving lateral confinement in a QW structure is to use a metallic gate on its surface. When this gate is negatively biased, it causes a depletion in the numbers of electrons in the area below it, leading to the formation of the QD.

There has also been an interest on synthesizing arrays of small QDs with uniform spatial ordering. The epitaxial growth of a QW followed by controlled etching does provide the requisite size and uniformity. But the etching process apparently produces surface defects and the subsequent regrowth introduces interface states which make the quality of these materials unacceptable. It has

been claimed that self-organised QDs are the structures that can provide the desired properties most satisfactorily.

1.3 Application of quantum dots

Research on QDs has generated interest in different fields of study [17]. QDs have potential applications in quantum information processing and have paved the way for supercomputers called quantum computers. They can store information as qubits which are the elementary units of the quantum information processes and can be created using the two spin states of the electron. Precision measurements of the spin and other properties can be made by controlling the flow of electrons through the QD using small voltages applied to the leads. Organic dyes can be

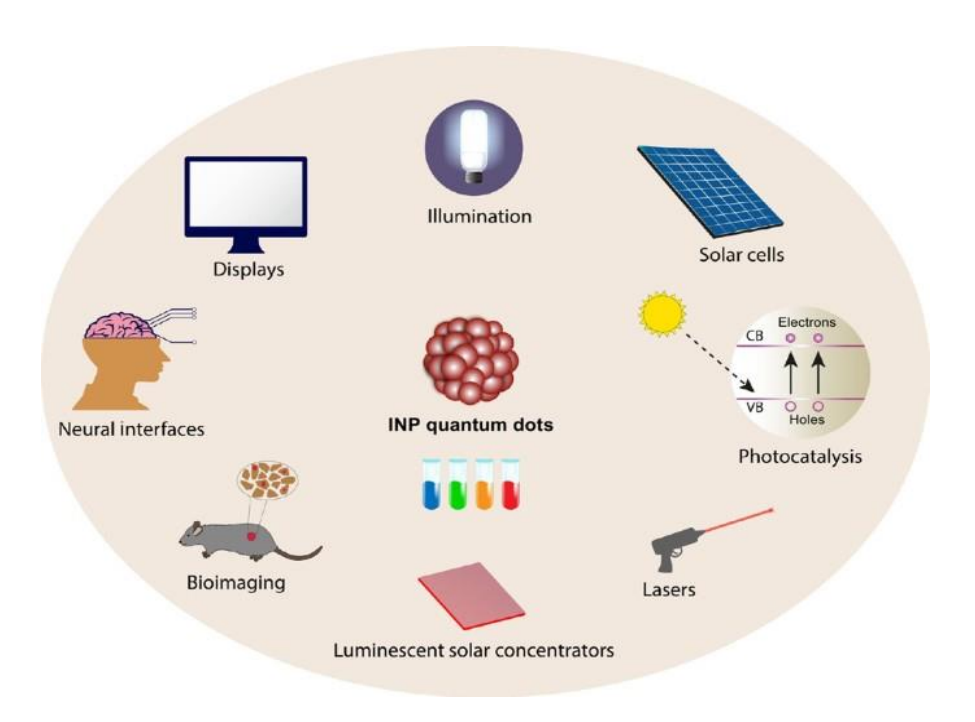


Fig. 4 Use of the quantum dot in different sectors [17].

replaced with QDs. QDs can have wide range of biomedical uses in drug delivery, live imaging, medical diagnosis and in producing images of cancer tumours [18]. As discussed, semiconductor nanoparticles exhibit size and compositionally tunable band gaps. Therefore, QDs of different types and sizes engineered to perfectly match and absorb the light of the solar spectrum can be

brought together into the same cell. QD-based solar cells include luminescent concentrator cells, QD dye sensitized solar cells, multiple exciton generation and intermediate band solar cells.

Recently, display technology has started to incorporate QD light emitting diodes (QLED). QLED displays are getting a lot of attention in the scientific community because of their outstanding colour purity, great brightness, low operation voltage, and simple processability. A longer system life is made possible by the inorganic QDs' high thermal and air stability. Additionally, recent progress in patterning methods has made it possible to create an ultrahigh-resolution QLED array with a full colour spectrum. Conventional display technologies are unable to employ the QDs' implementation methods [19].

1.4 Confinement potential

One of most important parameters for a QD or a QW system from a theorist's point of view is the confinement potential. QDs can be fabricated in different shapes and sizes to have certain required properties. One simple choice would be to work with an infinite potential well as the confinement potential. However, this model is an over-simplification for the actual confinement potential (CP). A more realistic model for the CP could be a finite square well. However, the force experienced by an electron within such a model potential is zero, which is a little unrealistic. Nevertheless, a finite square well has turned out to be a popular and useful model for the study of the behaviour of QD systems.

Experimental research by Sirkosky and Merkt [20-21] has revealed that the resonance frequency in a QD does not depend on the number of electrons in the dot. The independence of the excitation energy on the number of electrons indicates that the excitation spectrum of a QD is not influenced by the electron-electron (e-e) interaction. The above experimental result together with the generalized Kohn theorem suggests that the CP in a QD is more or less parabolic. Motivated by this observation, several investigations have been carried out in the past considering the potential in QD or QW as parabolic [22-27] and various electronic and other properties of QDs have been investigated [28-34]. A QD with a parabolic or harmonic CP is denoted as a parabolic QD (PQD).

Although in most investigations, harmonic potential model has been used to describe the confinement in a QD, some recent experimental results suggest that the actual CP in a QD is

anharmonic in nature and possesses a finite well-like shape with a minimum. Adamowski et al. [35] have suggested that a Gaussian potential can describe the experimental results with a good amount of accuracy. This potential has a finite depth and is consistent with some realistic phenomena like ionization etc... We would like to mention in passing that the Gaussian potential has proved to be a useful potential in various branches of physics and has been solved approximately for a single-particle problem by several authors [36-37]. In this thesis, we will refer to a QD with Gaussian confinement as a Gaussian QD (GQD). Recently, Ciurla [38] has suggested a more generalised CP which is known as the power exponential potential. QDs with power exponential CP will be referred to as PEQD. One important advantage with the power-exponential potential is that it can lead to different CPs in different limiting cases. Jahan et al. [39] have recently investigated the effect of the shape of the CP on the electronic, magnetic thermodynamic and transport properties of a GaAs QD at finite temperature using the power exponential potential.

1.5 Donor impurities in a quantum dot

It is essentially impossible to have, in reality, a QD without any impurity. A hydrogen-like neutral impurity in a QD is normally referred to a donor impurity, for it can easily give away an electron to the conduction band. Such a neutral donor impurity is denoted by the symbol D^0 , while a D^- centre refers to a complex which consists of a single positive ion and two electrons forming a negative hydrogen ion [40].

Bastard [41] was the first to study the confinement effect on a D^0 impurity in a QD. Many researchers have subsequently analysed the energetics of the D^0 impurity in several low-dimensional systems including QDs [42-43]. Later, several works [44–46] on off-centre impurities in QDs, which are more realistic, have also been reported. Movilla and Planelles [47] have presented a computational scheme yielding exact (numerical) wave functions and energies of a spherical nanocrystallite with a shallow donor impurity located anywhere inside.

The existence of stable bound states of D^- complexes in bulk semiconductors was suggested theoretically by Lampert [48] way back in 1958. A D^- impurity in a low-dimensional system is an interesting system because it is a simple two-particle correlated system with a single bound state [49]. The experimental confirmation of the existence of bound state of D^- , however, took a long time to come primarily because of the very feeble nature of the binding of the system. To our knowledge, Huant et al. [50] were the first to observe experimentally the existence of a D^- bound

state in a GaAlAs heterostructure from photoionization transitions through far-infrared magnetooptical experiments. They have reported the binding energy of the D^- impurity in a GaAsmultiple QW structure for several values of the magnetic field strength.

1.6 Origin of the spin-orbit interaction

Another interaction of profound significance that has captured the attention of researchers in the case of low-dimensional systems is the spin-orbit (SO) interaction, which plays the most crucial role in the fascinating area of spintronics. The idea here is to fabricate devices, where spin will be the carrier of current rather than the charge [51] and thus in these devices the information will be carried by the spins. Recently, the importance of spin-orbit interactions has been investigated quite extensively in QD systems and semiconductor nanostructures. According to quantum mechanics, the electron spin can couple with the magnetic field generated by the electron's motion giving rise to the SO interaction (SOI). The general form of the SOI can be obtained from the Dirac equation [52]. From the Dirac theory, we have

$$\left(\frac{\boldsymbol{p}^2}{2m} + V - \frac{p^4}{8 m^3 c^2} - \frac{\hbar}{4m^2 c^2} \boldsymbol{\sigma}. (\boldsymbol{p} \times \mathbf{E}) + \frac{\hbar^2}{8m^2 c^2} \nabla^2 v\right) \psi = \epsilon \psi . \tag{1.5}$$

where the fourth term is known as the Thomas term (H_T) . This term represents the interaction of the moving electron with the electric field and represents the spin-orbit interaction.

1.6.1 Rashba spin orbit interaction:

In 1984, Bychkov and Rashba [53] proposed a simple type of spin-orbit (SO) coupling to explain a specific electron spin resonance phenomenon in 2D semiconductors. In crystals that lack structure inversion symmetry, a spin-orbit interaction comes into play. This is called the Rashba spin-orbit (RSO) interaction (RSOI). The RSO coupling was first introduced for non-centrosymetric Wurtizite semiconductors. The zero-field spin-splitting in III - V heterostructures also occurs because of RSOI arising from the structure inversion asymmetry (SIA) of the heterojunction. Due to the difference in the bandgap, there would be an asymmetry in the space charge accumulated on either side of the heterojunction, which creates an electric field

perpendicular to the 2DEG leading to RSOI [54-56]. As RSOI can be influenced by an external electric field across the junction and it can have many experimental applications.

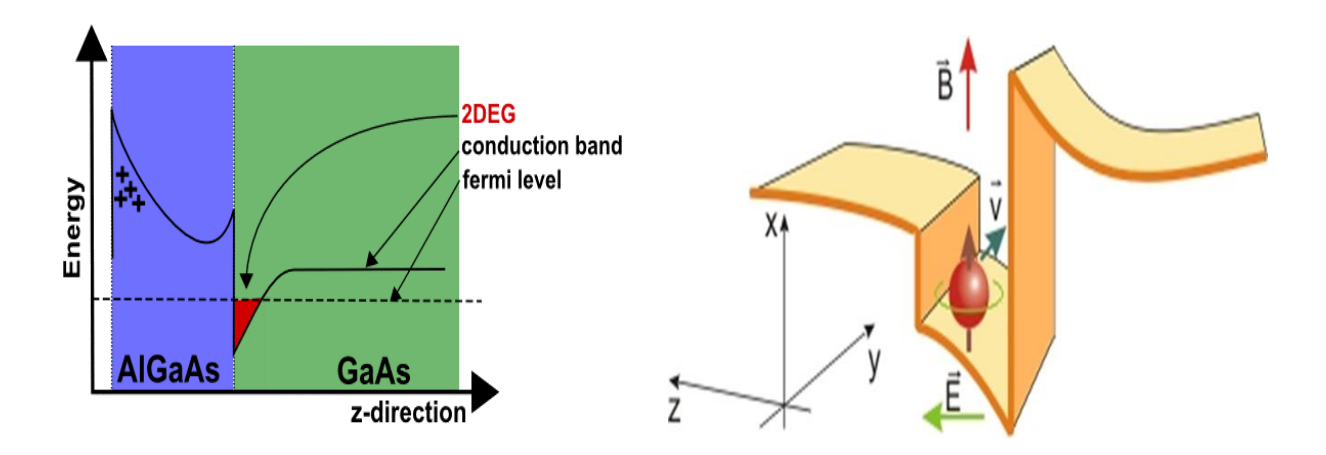


Fig.5 Rashba spin-orbit interaction

As we have already mentioned, one can obtain the form of RSOI Hamiltonian (H_R) from the Thomas term of the Dirac theory. In the presence of an electric field perpendicular to the 2DEG $(\mathbf{E} = E \hat{\mathbf{z}})$, the system loses the inversion symmetry at the surface and the Thomas term reads,

$$H_T = H_R = -\frac{\hbar \sigma \mathbf{E} \cdot (\hat{\mathbf{z}} \times \mathbf{p})}{4m^2 c^2}$$
 (1.6)

$$= \frac{\hbar}{4m^2c^2} \mathbf{E} \cdot (\boldsymbol{\sigma} \times \boldsymbol{p}) \Big|_z = \alpha_R (\sigma_x p_y - \sigma_y p_x), \tag{1.7}$$

where $\alpha_R (= \hbar E/4m^2c^2)$ is the Rashba parameter. It is clear that the breaking of inversion symmetry occurs because of the linearity of the electron momentum in the Rashba term. Theoretically, the lack of inversion symmetry not only creates an additional electric field but also distorts the electron wave function close to nuclei. The Rashba parameter α_R can be controlled by tuning the confining potential, the external electric field and gate voltage. The application of a gate voltage is a well-known method of controlling the structure inversion asymmetry. The study of Rashba physics is now at the heart of spintronics, with a focus on manipulating non-equilibrium material properties via SO coupling.

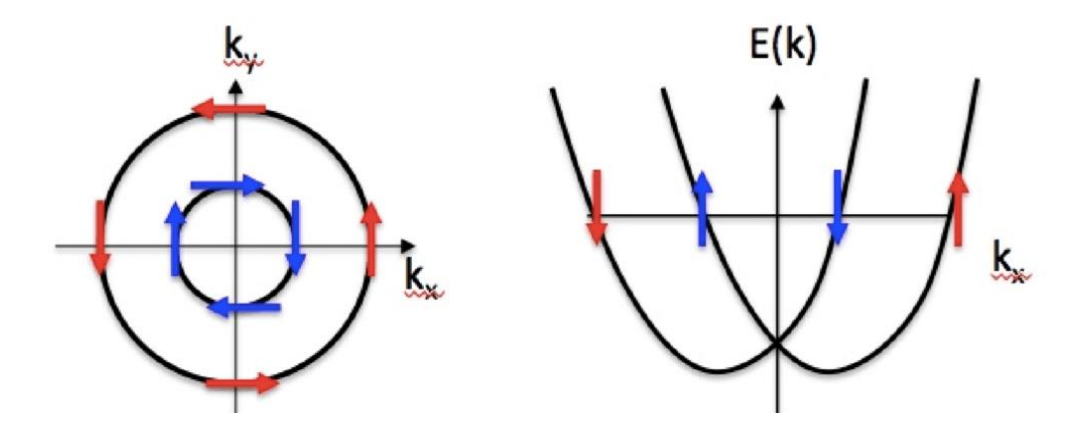


Fig.6 (a) Fermi surface of a 2DEG; (b) Structure inversion asymmetry

1.6.2 Dresselhaus spin-orbit interaction (DSOI)

Another type of spin-orbit interaction that may exit in a solid state system is called the Dresselhass spin-orbit interaction [57]. This arises due to bulk inversion asymmetry (BIA). This type of asymmetry occurs in zinc blende type semiconductors. The strength of the BIA

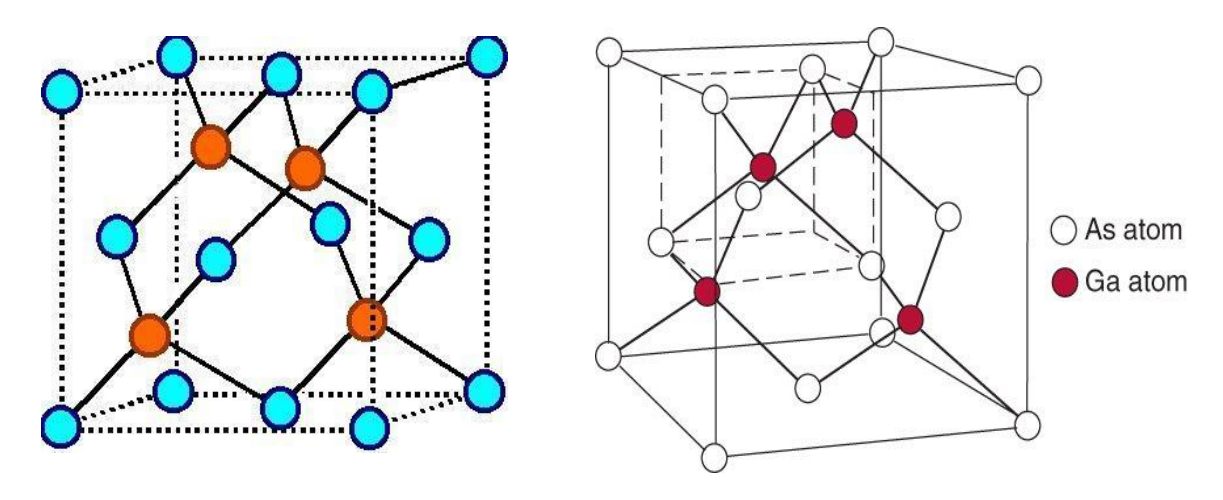


Fig.7 zinc blende type diamond and GaAs crystal structure.

parameter depends on crystal field, QD width, temperature and electron density. The Dresselhaus Hamiltonian is given by [58],

$$H_D = \frac{\beta_D}{\hbar} \left(k_x \sigma_x - k_y \sigma_y \right) + \frac{\gamma}{\hbar} \left(-k_y^2 k_x \sigma_x + k_x^2 k_y \sigma_y \right) \tag{1.8}$$

where $\beta_D(-\gamma k_z^2)$ is the Dresselhaus parameter, σ_x and σ_y are the pauli matrices. While the Rashba term is linear in momentum k, and the Dresselhauss term consists of both linear and cubic terms in k. However, the cubic interaction term is neglected especially for materials with weak SOI such as GaAs semiconductor.

1.7 Introduction to Single molecular transistor (SMT)

Over the last few decades, there has been a shift from bulk systems to nanoscale semiconductors and magnetic systems. As evident from the above discussion, quantum phenomena need to be taken into account in the study of such systems. Early research has revealed a variety of important aspects of nanosystems such as the fascinating physics at the nanoscale, quantum transport properties, and device applications. Datta [59] has provided an excellent overview of the field. Due to advancements in fabrication techniques and the availability of measurement facilities, extensive research of the electrical, optical, transport, and magnetic characteristics of diverse nanosystems have been carried out in recent years. Aviram and Ratner [60] have proposed the theoretical design of a molecular device based on a single organic molecule in 1974, and found that the device's response in an applied field acts as a rectifier. A few research groups later used organic molecules to manufacture a single molecular transistor [61, 62]. An SMT device typically comprises a core molecule or any nanosystem with discrete energy levels, such as a quantum dot (QD). The transport properties of SMT have been investigated by using different theoretical and numerical methods like kinetic equation method [63, 64], rate equation approach [65], slave-boson mean-field method [66], non-crossing approximation method [67], numerical renormalization method [67-69] and non-equilibrium Green's function approaches [70-73]. In our work, we use a non-equilibrium Green function technique to study the thermal transport properties of the single molecular transistor.

We consider an SMT system in which a central QD is coupled to two metallic leads which act as a source and a drain respectively. A temperature gradient is applied across the source and the drain and electrons can travel from the source to the drain through the QD giving rise to a electric current. The entire SMT system is placed on an insulator substrate to which is attached a gate. The substrate contains a large number of uncoupled harmonic oscillators which act as a phonon bath. The QD contains a single energy level and a local phonon mode. The QD electrons interact with each other by the Hubbard onsite interaction and with the local phonon mode through the Holstein onsite el-

ph interaction. The substrate phonons can interact with the local QD phonon by a linear interaction of the Caldeira-Leggett type which gives rise to a dissipative effect in the phonon dynamics of the QD.

1.8 Seebeck effect and spin-Seebeck effect

Thermoelectric materials have the ability to convert the waste heat into electricity based on Seebeck effects, when temperature gradient is applied across the system. This effect has applications in thermal sensing devices such as thermocouples [74]. The efficiency of the Seebeck effect is measured by the Seebeck coefficient S, which is defined as:

$$S = -\frac{V}{(T_2 - T_1)} \tag{1.9}$$

where V is the electric voltage and T_2 , T_1 are the temperature of the hot (source) region and cold (drain) region respectively.

The spin-Seebeck effect (SSE) generates a spin voltage or current from a temperature difference in a ferromagnet. SSE was first discovered by Uchida et al. [75] in a ferromagnetic metal. It has also been observed in ferromagnetic insulators [76] and semiconducting materials [77], nonmagnetic materials with a magnetic field [78], paramagnetic materials [79], antiferromagnetic materials [80], metal-ferromagnet insulators [81] and also in topological insulators [82]. When two charge carriers of spin components, S_{\uparrow} and S_{\downarrow} exhibit equal magnitude of charge but of opposite sign, the charge-Seebeck coefficient ($S_c \propto (S_{\uparrow} + S_{\downarrow})$) vanishes while the spin-Seebeck coefficient becomes finite ($S_s \propto S_{\uparrow} - S_{\downarrow}$)) resulting in the net spin voltage with the charge voltage being zero. SSE can be described by the spin-resolved Seebeck coefficient (or thermo-power).

1.9 Aim of the present thesis

In this thesis, our main aim is to present our results on the effect of Rashba and Dresselhaus spin orbit interactions and magnetic field on D^0 and D^- impurities in a QD. We shall mostly assume that the confinement potential is Gaussian which appears to be a reasonably good assumption as has been suggested by serval investigations. For sake of concreteness, we shall apply our results

to GaAs QD. We shall also study the thermoelectric properties of a single molecular transistor. The organization of the thesis is as follows.

In Chapter 2, we shall study the effect of both the Rashba and Dresselhaus SOIs on neutral hydrogenic donor impurity D^0 complex in a 2D Gaussian QD. To decouple the spin-orbit coupling, we apply a unitary transformation that was first given by Aleiner and Falco [83]. To obtain the ground state (GS) energy and the binding energy (BE), we use the Rayleigh-Ritz variational method [84] and also present our results of magnetisation and susceptibility. In Chapter 3, we study the effect of spin-orbit interactions and an external magnetic field on an off-centre impurity D^0 in a GQD, which is a more realistic system, using an improved variational method [85].

An exponential power potential is a much more general form of a confinement potential and has the advantage that it can lead to different confinement potentials in different limiting cases. In Chapter 4, we shall study effect of the shape of the confinement potential on the properties of a D^0 complex in QD in the presence of RSOI and DSOI and magnetic field [86] using the power exponential CP.

In Chapter 5, we shall consider a D^0 system in an asymmetric 3D GQD in a magnetic field in the presence of Rashba and Dresselhaus SOIs and present our results of GS energy, BE and diamagnetic susceptibility.

A negative hydrogenic donor D^- in a low-dimensional system is another interesting system because it is a simple two-particle correlated system with a single bound state [78]. The experimental confirmation of the existence of bound state of D^- , however, took a long time to come primarily because of the very feeble nature of the binding of the system. In Chapter 6, we shall consider a D^- impurity in a GQD in the presence of a magnetic field and the Rashba and Dresselhaus SOIs. We calculate the GS energy and BE by the Ritz variational technique. We shall also calculate the resultant dipole moment, magnetisation and susceptibility.

In Chapter 7, we consider a single molecular transistor (SMT) system in which a central QD is coupled to two metallic leads which act as a source and a drain respectively. The QD is considered to have a single electron energy level and a single phonon. It also has Hubbard correlation and local Holstein electron-phonon interaction. The source is kept at a higher temperature with respect to the drain. The entire SMT device is placed on an insulator substrate to which is attached a gate.

The substrate contains a large number of uncoupled phonons which can interact with the local phonon of the QD through a linear coupling. This gives rise to dissipation in the QD system. We also apply a magnetic field across the system. Because of the temperature difference between the source and the drain, electrons can tunnel from the source to the drain through the QD leading to thermoelectric effects. We analyse the thermoelectric and spintronic transport in this system using the non-equilibrium Keldysh Green function technique and calculate quantities like charge, spin and thermal conductance, and charge and spin Seebeck coefficients.

Finally, in chapter 8, we present the conclusion of the thesis.

1.10 References

- [1] M.A. Reed, R.T. Bate, K. Bradshaw, W.M. Duncan, W.R. Frensly, J.W. Lee and H.D. Shih, J. Vac. Sci. Technol. B 4, 358 (1986).
- [2] M.A. Reed, Sci. Am. **268** (1993) 118;
- [3] D. Loss, D.P. Divicenzo, Phys. Rev. A 57 (1998) 120;
- [4] Y.V. Pershin, J.A. Nesteroff, V. Privman, Phys. Rev. B 69 (2004) 121306(R);
- [5] B. Vaseghi, R. Khordad, M.M. Golshan, Phys. Stat. Sol. (B) 243 (2006) 2772;
- [6] S. Zhang, R. Liang, E. Zhang, L. Zhang, Y. Liu, Phys. Rev. B 73 (2006);
- [7] E. Kasapoglu, F. Ungan, H. Sari, I. Sokmen, Superlatt. Microstr. 45 (2009) 618;
- [8] K. Kash, A. Schrer, J.M. Worlock, H.G. Craighead and M.C. Tamargo, Appl. Phys. Lett. 49, 1043 (1986).
- [9] M.A. Reed, J.N. Randall, R.G. Aggewal, J.R. Matyi, T.M. Moore and A.E. Wetsel, Phys. Rev. Lett. **60**, 535 (1988).
- [10] M.A. Kastner, Phys. Today 46, 24 (1993).
- [11] Ch. Sikorski and U. Merkt, Phys. Rev. Lett. **62**, 2164 (1989);
- [12] W. Kohn, Phys. Rev. **123**, 1242 (1963);
- [13] Azzazy HME et al. From diagnostic to therapy: Prospects of quantum dots. Clinical Biochemistry, **40** 917-927, (207);
- [14] Wang HZ et al. Acta Biochimica et Biophysica Sinica. 36, 681-686 2004;
- [15] M. A. Kastner, Artificial Atoms, Phys. Today **46**, 24 (1993).
- [16] D. Heitmann and J. Kotthaus, Phys. Today 46, 56 (1993).
- [17] A. A. Abdellatif, M.A. Yonis, M. Alsharidah, O. A. Rugaie, H. M. Tawfeek, Int. J. nanomedicine,

- **17**, 1951 (2022).
- [18] Moon Kee Choi, Jiwoong Yang, Taeghwan Hyeon and Dae-Hyeong Kim,npj Flexible Electronics **2**, Article No:10 (2018);
- [19] T. Jamieson, R. Bakhshi, D. Petrova, R. Pocock, M. Imani& A.M. Seifalian, 28 4717 (2007).
- [20] Ch. Sikorski and U. Merkt, Phys. Rev. Lett. 62, 2164 (1989).
- [21] Ch. Sikorski and U. Merkt, Surf. Sci. 229, 282 (1990).
- [22] P.A. Maksym, T. Chakraborty, Phys. Rev. Lett. 65 (1990) 108;
- [23] W. Que, Phys. Rev. B 45 (1992) 11036; [b]
- [24] U. Merkt, J. Huser, M. Wagner, Phys. Rev. B 43 (1991) 7320;
- [25] H. Oh, K.J. Chang, G. Ihm, S.J. Lee, Phys. Rev. B 50 (1994) 15397;
- [26] F. Albzoor, M.K. Elsaid, K. Ilaiwi, J King Saud. University- Science 30, (2017) 1;
- [27] S. Tarucha, D.G. Austing, T. Honda, R.J. Vander Hage, L.P. Kouwenhoven, Phys. Rev. Lett. 77 (1996) 3613;
- [28] S. Mukhopadhyay & A. Chatterjee, Phys. Rev. B 55, 9279 (1997).
- [29] S. Mukhopadhyay & A. Chatterjee, Phys. Rev. B 58, 2088–2093(1998).
- [30] S. Mukhopadhyay & A. Chatterjee, Phys. Lett. A **240**, 100 (1998).
- [31] S. Mukhopadhyay & A. Chatterjee, Phys. Lett. A 242, 355 (1998).
- [32] S. Mukhopadhyay & A. Chatterjee, *Rev. B* **59**, R7833 (1999).
- [33] M. K. Elsaid, M. Ali, A.A. Shaer, Modern Phys Lett. B 33, 1950422 (2019).
- [34] R. Khordad, H. R. Rastegar Sedehi, Optical and Quantum electronics 50, 294 (2018).
- [35] J. Adamowski, A. Kwasniowski and B. Szzfran, J. Phys.: Condens. Matter 17, 4489 (2005).
- [36] B. Meurer, D. Heitmann and K. Ploog, Phys. Rev. Lett. 68, 1371 (1992).
- [37] R.C. Ashoori, H.L. Stormer, J.S. Weiner, L.N. Pfeiffer, S.J. Pearton, K.W. Balswin and K.W. West, Phys. Rev. Lett. 68, 3088 (1992).
- [38] M. Ciurla, J. Adamowski, B. Szafran, S. Bednarek, Physica E 15 (2002) 261.
- [39] L. Jahan, B. Boyacioglu, A. Chatterjee, Scintific Report 9, 2019.
- [40] M.A. Lamper, Phys. Rev. Lett. 1, 450 (1958).
- [41] G. Bastard, Phys. Rev. B 24 (1981) 4714.
- [42] D. S. chuu, C. M. Hsiao and W. N. Mai Phys. Rev. B **46**, 7 (1992);

- [43] B. Vaseghi, R. Khordad, M.M. Golshan, Phys. Stat. Sol (B) 243, 2772 (2006);
- [44] J.L. Zhu, X. Chen, Phys. Rev. B 50 (1994) 4497.
- [45] F.J. Robeiro, A. Latge, Phys. Rev. B 50 (1994) 4913.
- [46] W.F. Xie, Physica B 403 (2008) 2828.
- [47] J.L. Movilla and J. Planelles, Comput. Phys. Commun.170, 144 (2005).
- [48] M.A. Lampert, Phys. Rev. Lett. 1, 450 (1958).
- [49] R.N. Hill, Phys. Rev. Lett. 38 643 (1977).
- [50] S. Huant, S.P. Najda, B. Etienne, Phys. Rev. Lett. 65, 1486 (1990).
- [51] S. Datta, B. Das, Appl. Phys. Lett. 56 (1990) 665.
- [52] J. J. Sakurai, Advance quantum mechanics
- [53] E.I. Rashba, Sov. Phys. Solid State 2 (1960) 1109.
- [54] E.I. Rashba, V.I. Sheka, New. J. Phys. Phys.-Solid State. 17, 50202, (2015).
- [55] Y.A. Bychkov, E.I. Rashba, J. Phys. C Solid State Phys. 17, 6039, (1984).
- [56] G. Bihlmayer, O. Rader, R. Winkler, New J. Phys. 17, 050202, (2015).
- [57] G. Dresselhaus, Phys. Rev. 100 (1955) 580.
- [58] Spintronics in Nanoscale Devices, CRC Press, (2013).
- [59] S. Datta (Cambridge University Press, 1997).
- [60] A. Aviram, M. A. Ratner. Molecular Rectifiers. Chem. Phys. Lett. 29, 277(1974).
- [61] W. Liang, M. P. Shores, M. Bockrath, J. R. Long. & H. Park. Nature 417, 725-729(2002).
- [62] H. Park et al. Nature 407, 57-60 (2000).
- [63] Boese, D. & Schoeller, H. Europhys. Lett. **54**, 668 (2001).
- [64] Mitra. A Aleiner. I. & Millis. A. J. Phys. Rev. B **69**, 245302–21(2004).
- [65] Meir. Y, Wingreen. N. S and Lee. P. A. Phys. Rev. Lett. 70, 2601 (1993).
- [66] Wingreen. N. S and Meir. Y. Phys. Rev. B 49, 11 040 (1994).
- [67] Hewson. A. C & Meyer. D. J. Phys. Cond. Matter 14, 427 (2002).

- [68] Khedri. A Costi. T.A, Meden V. Phys. Rev.B **96**, 195155 (2017).
- [69] Khedri. A Costi. T.A, Meden V. Phys. Rev.B 98, 195138 (2018).
- [70] Keldysh. L. V. Sov. Phys. JETP 20, 1018–1026 (1965).
- [71] Datta, S. (Cambridge University Press, 2005).
- [72] Haug, H. & Jauho, A. P. (Springer, 1996).arXiv:0711.4881v1.
- [73] Song. J, Sun. Q. F, Gao. J and Xie. X. C. Phys. Rev B.75, 195320(2007).
- [74] Neil W, Ashcroft N and Mermin D 1976 Solid State Physics 1st edn (New York: Thomson Learning)
- [74] I.L. Aleiner, V.I. Fal'ko,, Phys. Rev. Lett. 87 (2001) 256801.
- [75] K. Uchida, S. Takahashi, K. Harii, J. Ieda, W. Koshibae, K. Ando, S. Maekawa, and E. Saitoh, Na ture 455, 778 (2008).
- [76] Uchida K, Adachi H, Ota T, Nakayama H, Maekawa S, Saitoh E (2010) Observation of longitudinal spin-Seebeck effect in magnetic insulators. Appl Phys Lett 97:172505
- [77] Uchida K, Xiao J, Adachi H, Ohe J, Takahashi S, Ieda J, Ota T, Kajiwara Y, Umezawa H, Kawai H, Bauer GEW, Maekawa S, Saitoh E (2010) Spin Seebeck insulator. Nat Mater 9:894–897
- [78] Jaworski C, Myers R, Halperin JE, Heremans J (2012) Nature (London) 487:210–212
- [79] Wu SM, Pearson JE, Bhattacharya A (2015) Phys Rev Lett 114:186602
- [80] Wu SM, Zhang W, Kc A, Borisov P, Pearson JE, Jiang JS, Lederman D, Hoffmann A, Bhattacharya A (2016) Phys Rev Lett 116:097204
- [81] Tang GM, Chen XB, Ren J, Wang J (2018) Phys Rev B 97:081407(R)
- [82] Chang PH, Mahfouzi F, Nagaosa N, Nikolic BK (2014) Phys Rev B 89:195418
- [83] A. Boda and A. Chatterjee, Physica E 45, 36 (2012).
- [84] P. Saini, A. Boda, A. Chatterjee, J. Magn. Magn Mater. 485 (2019) 407.
- [85] P. Saini, Ashok Chatterjee, Superlattice and microstructure **146**, 36 (2020).
- [86] R.N. Hill, Phys. Rev. Lett. 38 643 (1977).

Chapter ~2

Effect of Rashba and Dresselhaus Spin-Orbit Interactions on a D^0 Impurity in a Gaussian GaAs Quantum Dot in the presence of an external Magnetic field

2.1 Introduction

As we have already mentioned in Chapter 1, Quantum dots (QDs) have continued to evoke interest over the last four decades for their fully quantum attributes, novel physical properties and their potential application in nanotechnology [1]. Indeed, the literature is replete with investigations that have unravelled a large number of important and interesting properties of QDs [2-7] that have the potential to revolutionize the semiconductor technology. It is hardly possible to have a realistic system without an impurity and therefore the study of impurity states and their effect on the physical properties of QDs are of utmost practical importance.

Another issue of profound significance that has captured the attention of researchers in the case of low-dimensional systems is the spin-orbit (SO) interaction, which plays the most crucial role in the fascinating area of spintronics. The idea here is to fabricate devices where spin will be the carrier of current rather than the charge [9] and thus in these devices the information will be carried by the spins. Normally two types of SO interactions can originate in a solid material. One is the Rashba spin-orbit (RSO) interaction (RSOI) [10] which arises when a material loses its structural inversion symmetry (SIS). The other one arises from the breaking of the bulk inversion-symmetry (BIS) [11] and is referred to as the Dresselhaus spin-orbit (DSO) interaction (DSOI). While the DSO strength largely depends on the QD parameters, the RSO coupling depends both on the QD parameters and the external electric and magnetic fields [12]. This particular aspect of RSO is actually taken advantage of in the field of spintronics [13]. Understandably, in recent years, considerable effort has been made to study the effects of spin-orbit interactions on several important properties of low-dimensional systems. Kumar et al. [14] have examined the role of RSOI on the energy levels and magnetic properties of a many-electron harmonic QD taking the

Johnson-Payne model potential [15] for the electron-electron interaction. Li *et al.* [16] have explored the role of Rashba SO coupling on the electronic levels of a neutral hydrogenic donor centre D^0 in a GaAs/GaAlAs quantum well by effective-mass envelope function theory. Gisi *et al.* [17] have investigated the effect of magnetic field and RSOI on the optical absorption in a parabolic quantum wire using the compact-density matrix formalism and iterative scheme. Kumar et al. [18] have obtained the GS energy of a D^0 centre in a GaAs QD with Gaussian confinement incorporating the RSOI effect by the Ritz variational method.

To our knowledge, the combined effect of RSO and DSO interactions on the properties of a D⁰ centre in a GQD in the presence of a magnetic field has not yet been studied. The primary aim of this chapter is to present our work on the role of Rashba and Dresselhaus interactions on the GS energy, binding energy, donor distribution, zero-temperature magnetic moment and susceptibility in a three-dimensional (3D) GQD of GaAs placed in an externally applied magnetic field.

2.2 Theory

A D^0 complex placed in a 3D GQD with RSO and DSO interactions in the presence of an externally applied magnetic field \mathbf{B} (0,0, B) can be modelled by the following Hamiltonian

$$H = H_{D^0} + H_R + H_D (2.1)$$

with

$$H_{D^0} = \left(\frac{1}{2m^*}(\mathbf{p} + \frac{e}{c}\mathbf{A})^2 - \frac{e^2}{\varepsilon r} - V_0 e^{-\frac{r^2}{2R^2}}\right) I, \tag{2.2}$$

$$H_R = \frac{\alpha_R}{\hbar} \left[\boldsymbol{\sigma} \times \left(\boldsymbol{p} + \frac{e}{c} \boldsymbol{A} \right) \right]_Z, \qquad (2.3)$$

$$H_D = \frac{\beta_D}{\hbar} \left[\boldsymbol{\sigma}_x \left(\boldsymbol{p}_x + \frac{e}{c} \boldsymbol{A}_x \right) - \boldsymbol{\sigma}_y \left(\boldsymbol{p}_y + \frac{e}{c} \boldsymbol{A}_y \right) \right]$$
 (2.4)

where H_{D^0} denotes the Hamiltonian of the D^0 centre in a GQD in an external magnetic field B, e and m^* being respectively to the charge and the Bloch mass of the electron, r(x, y, z) its position and p the canonically conjugate momentum operator, A denoting the vector potential defined by

the equation: $\mathbf{B} = \nabla \times \mathbf{A}$, ε the dielectric constant of the medium, V_0 and R representing respectively the depth and range of the confinement potential, and I the unit matrix of order 2, H_R and H_D are respectively the Rashba and Dressehaus SOI Hamilonians in the presence of the magnetic field respectively, σ_x , σ_y and σ_z being the Pauli spin matrices and α_R and β_D denoting the RSOI and DSOI constants. It may be noted that R gives essentially the effective size of the GQD. We use the symmetric gauge so that $\mathbf{A} = B \ (-y/2, x/2, 0)$. To proceed further, we have to deal with the SOI's. In order to incorporate the effect of SOI's, we first apply on H a unitary transformation $U = e^S$ [19] with

$$S = i \frac{m^*}{\hbar^2} \left[\alpha_R (y \sigma_x - x \sigma_y) + \beta_D (x \sigma_x - y \sigma_y) \right]. \tag{2.5}$$

The Hamiltonian *H* transforma to

To determine \widetilde{H} , we have to calculate the [S,H], [S,[S,H]] etc. We obtain

$$[S,H] = -\frac{\alpha_R}{\hbar} \left[\boldsymbol{\sigma}_x \left(\boldsymbol{p}_y + \frac{e}{c} \boldsymbol{A}_y \right) - \boldsymbol{\sigma}_y \left(\boldsymbol{p}_x + \frac{e}{c} \boldsymbol{A}_x \right) \right]$$

$$-\frac{\beta_D}{\hbar} \left[\boldsymbol{\sigma}_x \left(\boldsymbol{p}_x + \frac{e}{c} \boldsymbol{A}_x \right) - \boldsymbol{\sigma}_y \left(\boldsymbol{p}_y + \frac{e}{c} \boldsymbol{A}_y \right) \right] - \frac{2m^* \sigma_z L_z}{\hbar^3} (\alpha_R^2 - \beta_D^2)$$

$$-\frac{2m^*}{\hbar^2} (\alpha_R^2 + h_D^2) - \frac{m^*}{\hbar^3} \omega_c \sigma_z \rho^2 (\alpha_R^2 - \beta_D^2), \tag{2.7}$$

$$\frac{1}{2}[S,[S,H]] = \frac{m^*}{\hbar^2}(\alpha_R^2 + \beta_D^2) + \frac{m^*}{\hbar^3}L_z\sigma_z(\alpha_R^2 - \beta_D^2) + \frac{m^*}{2\hbar^3}\omega_c\sigma_z\rho^2(\alpha_R^2 - \beta_D^2), \tag{2.8}$$

where

$$\omega_c = \frac{eB}{m^*c} \,, \tag{2.9}$$

$$\rho^2 = (x^2 + y^2),\tag{2.10}$$

$$L_z = -i\hbar \, \frac{\partial}{\partial \phi}.\tag{2.11}$$

After substituting Eqs. (2.7) and (2.8) in (2.6), the transformed Hamiltonian \widetilde{H} is expanded in powers of α_R and β_D . Neglecting terms higher than α_R^2 and β_D^2 , we obtain

$$\widetilde{\mathcal{H}} = \left(\frac{p^2}{2m^*} + \frac{1}{8}m^*\omega_c^2\rho^2 - \frac{e^2}{\varepsilon r} - V_0 e^{-\frac{r^2}{2R^2}}\right)I - \frac{m^*}{\hbar^2}(\alpha_R^2 + \beta_D^2)I - \frac{m^*}{\hbar^3}(\alpha_R^2 - \beta_D^2)\sigma_Z L_Z
+ \frac{\omega_c}{2}L_Z - \frac{m^*}{2\hbar^3}(\alpha_R^2 - \beta_D^2)\omega_c\sigma_Z \rho^2,$$
(2.12)

We consider the orbital angular momentum to be zero for the GS. To obtain a variational GS energy of $\widetilde{\mathcal{H}}$, we try a function:

$$\psi(\mathbf{r}) = Ne^{-\alpha r^2 - \beta r - im\varphi},\tag{2.13}$$

which is expected to capture the most important features of the GS of (2.9). The variational GS energy $E(D^0)$ of the system is given by

$$E(D^{0}) = \frac{\langle \psi(\mathbf{r}) | \widetilde{\mathcal{H}} | \psi(\mathbf{r}) \rangle}{\langle \psi(\mathbf{r}) | \psi(\mathbf{r}) \rangle}.$$
 (2.14)

Let us define $E(e^-)$ and $E(D^0)$ as the GS energies of the electron and the D^0 complex in the GQD respectively. The binding energy of the D^0 complex $((E_R(D^0)))$ is then defined as:

$$E_B(D^0) = E(e^-) - E(D^0).$$
 (2.15)

In the presence of a magnetic field (B), the GS energy will always be a function of B. The change of the GS energy with B gives the information about the magnetization and susceptibility of the system. Study of the magnetic field becomes particularly important if the system has SOIs. Once the GS energy is obtained, the magnetic moment (M) and susceptibility (S) can be easily determined. The magnetic moment (M) and susceptibility (S) of the D^0 complex are given by

$$M = -\frac{\partial E}{\partial B}; \quad S = -\frac{\partial M}{\partial B}.$$
 (2.16)

2.3 Numerical results and discussion

Though our formulation should work for any QD system, we shall implement it in the case of GaAs QD for the sake concreteness. All quantities will be expressed in SI units; so the unit of energy is chosen as: (meV) and that of length as: (nm), where, for a GaAs QD, $\varepsilon = 12.4$ and $m^* = 0.06m_0$, m_0 being the bare electron mass. The magnetic field will be expressed in Tesla (T) and the SOI constants in meV - nm unless otherwise mentioned. In Fig. 1, we show the behavior of the GS energy (E) of the D^0 centre in a GQD of GaAs with respect to the effective size of the QD (R) for B = 0 and for two values of V_0 and different sets of values of the SOI constants α_R and β_D . The sharp rise in energy as R is reduced below a critical value is clearly visible. The figure also shows that the effects of RSO and DSO interactions are same in the case of B = 0, that is, both the interactions reduce the energy equally. The energy however decreases significantly with increasing V_0 .

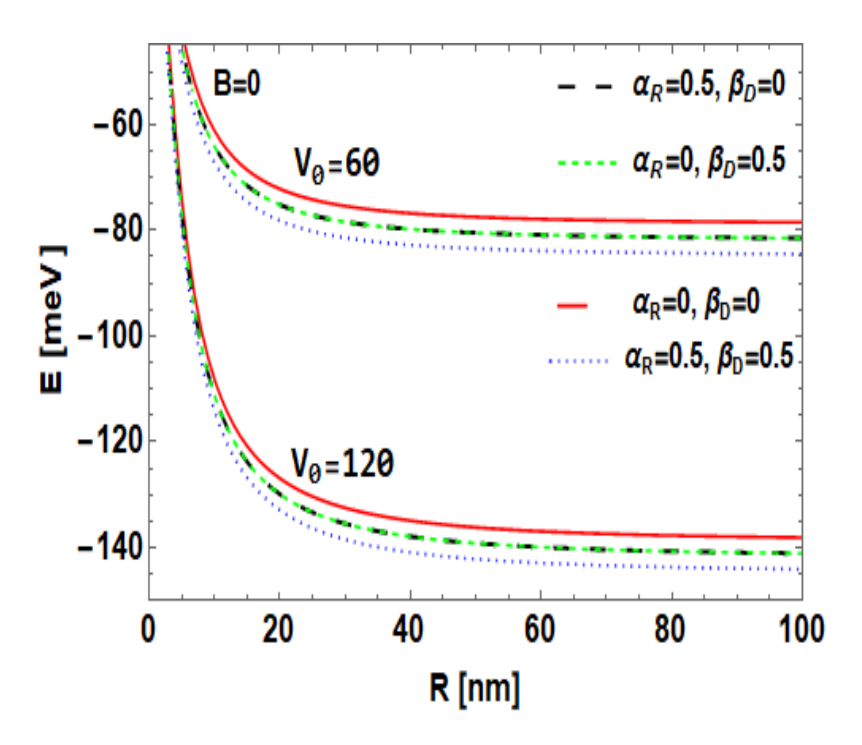


Fig. 1 GS energy (*E*) vs the effective dot radius (*R*) for a D^0 complex in a Gaussian GaAs QD with $V_0 = 60,120 \text{ meV}$, B = 0 T and a few combinations of $\alpha_R(\text{nm-meV})$ and β_D (nm-meV).

Fig. 2 shows how E varies with R for a Gaussian GaAs QD with $V_0 = 60$ nm for different values of α_R and β_D and for B = 5 and 10T. The figure reveals that, in general, the magnetic field enhances the energy which is indeed an expected behaviour. However, the interesting point is that in the case of $B \neq 0$, the energy exhibits a qualitatively different behaviour with the RSO interaction. One can see that though for B = 5T, the energy values for $\beta_D = 0$ and $\beta_D = 0.5$ are almost equal, the energy values for $\alpha_R = 0.5$ are significantly smaller than those for $\alpha_R = 0$. For B = 10T, on the other hand, the energy values for $\beta_D = 0.5$ are marginally higher than those for $\beta_D = 0$ while the energy for $\alpha_R = 0.5$ is again substantially lower than that that for $\alpha_R = 0$.

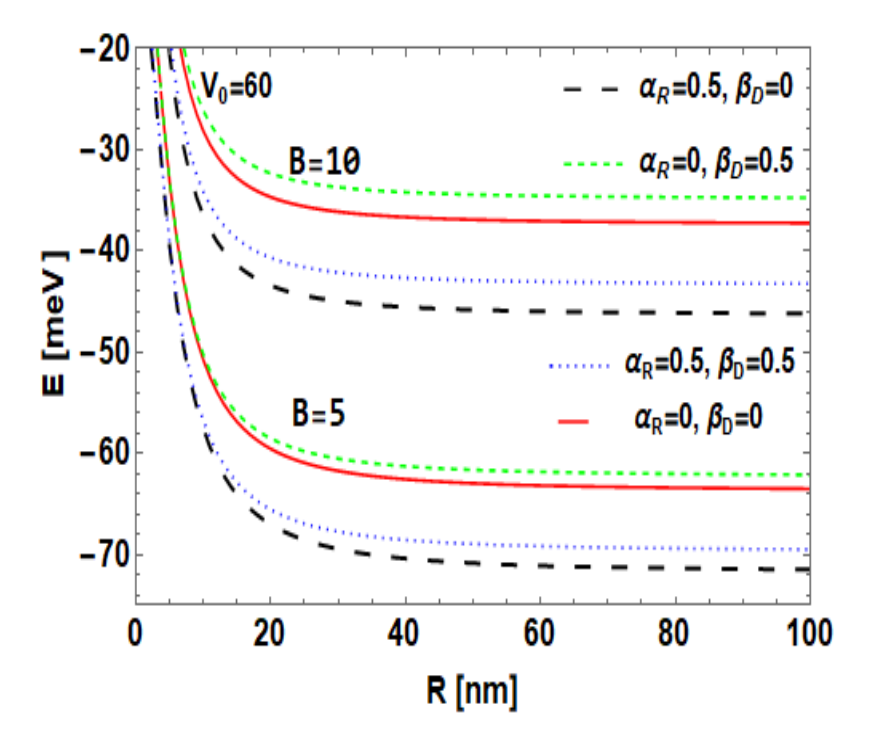


Fig. 2 E vs. R for a D^0 centre in a Gaussian GaAs QD with $V_0 = 60$ meV, B = 5, 10 T and a few combinations of $\alpha_R(\text{nm-meV})$ and β_D (nm-meV).

In Figs. 3 and 4, we show the variation of E with respect to α_R and β_D respectively for B=1 T, $V_0=60$ meV and a few values of R. The figures demonstrate that E is a decreasing function of both α_R and β_D . Variation with respect to β_D is rather slow. In other words, the Rashba term reduces the energy much more than the Dresselhaus term and thus has a more dominating effect in a QD.

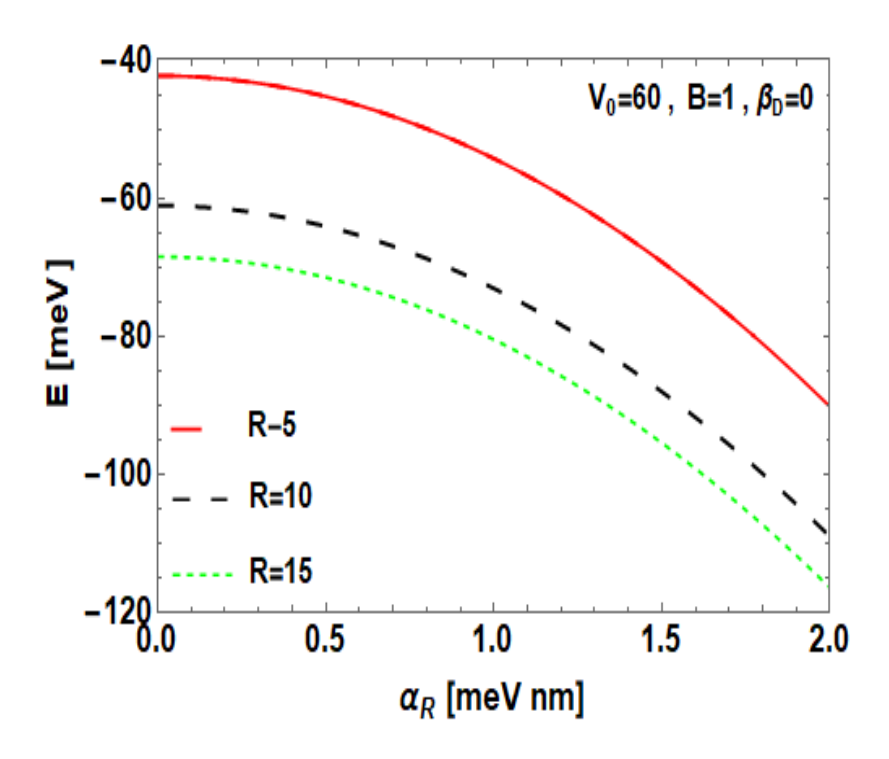


Fig. 3 E vs. α_R for a D^0 centre in a Gaussian GaAs QD with $V_0 = 60$ meV, B = 1 T and $\beta_D = 0$ nm meV and a few combinations of R (nm).

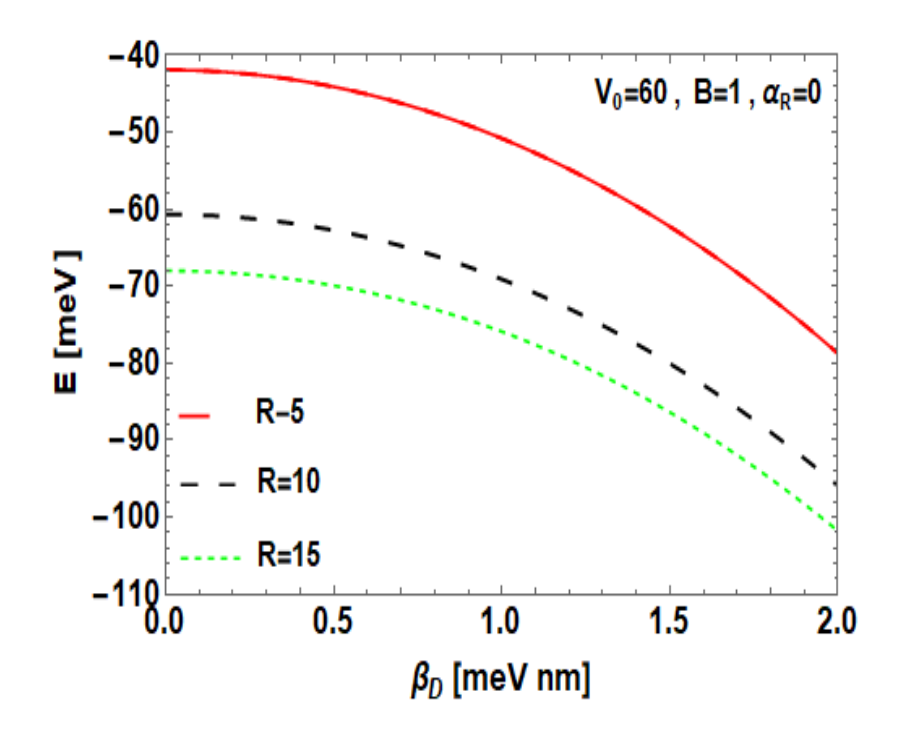


Fig. 4 E vs. β_D for a D^0 centre in a Gaussian GaAs QD with $V_0 = 60$ meV, B = 1 T and $\beta_D = 0$ nm meV and a few combinations of R (nm).

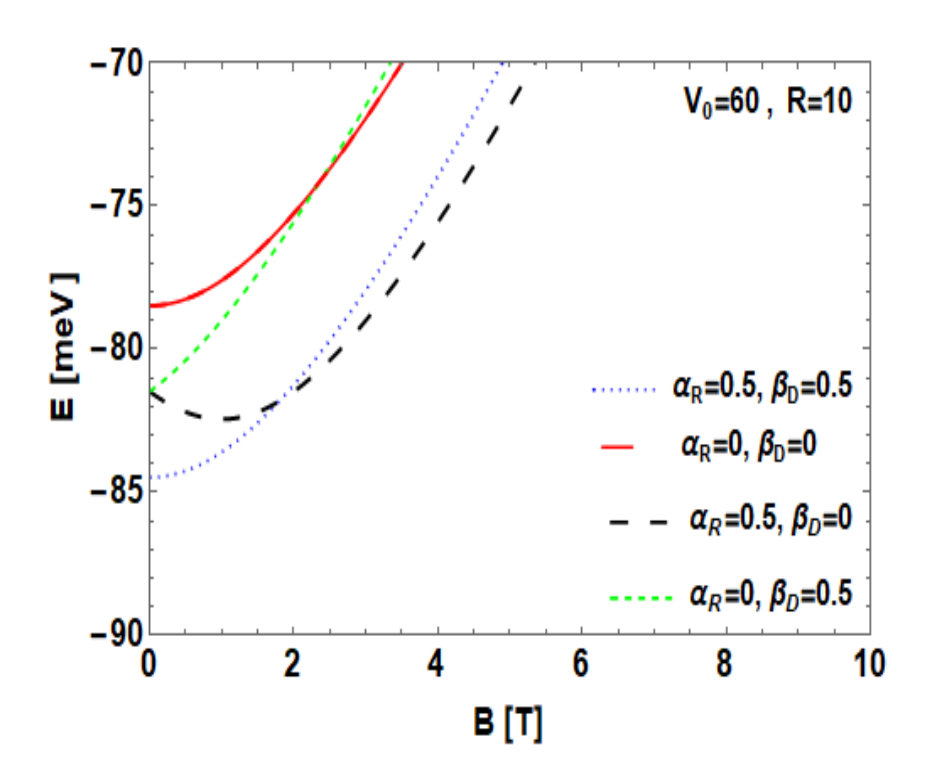


Fig. 5 E vs. B for a D^0 centre in a Gaussian GaAs QD with $V_0 = 60$ meV, R = 10 nm and a few combinations of $\alpha_R(\text{nm-meV})$ and β_D (nm-meV).

In Fig. 5, we plot E vs. B for V = 60 meV and R = 10 nm and for different sets of values of α_R and β_D . As expected, E increases with increasing B. However, when B is small, the variation is very slow while as B increases, the variation of E with B becomes more rapid and almost linear.

Fig. 6 describes the behavior of the GS BE (E_B) of a D^0 complex with respect to R for B=5T, $V_0=120$ nm and in the presence and absence of RSO and DSO interactions. It is clearly evident from the positive values of E_B that the D^0 complex can exist as a stable system in a GaAs QD which is indeed an expected result. Also, the binding becomes stronger as the size of the QD decreases implying that the quantum confinement enhances the binding. As R increases, E_B decreases and finally saturates to the bulk limit. Interestingly, one can observe that the RSOI lowers the binding energy while DSOI enhances it. However, in the case of B=0, E_B does not show any dependence on SOIs. Fig. 6 also reveals the existence of a critical value of R (R_c) at which the D^0 complex is most stable and as the dot size decreases below R_c , the binding begins to decrease very fast. The BE peaks are shown in a magnified way in Fig. 7. The reduction in binding energy below R_c has its genesis in quantum mechanics. When the size of the QD is made very

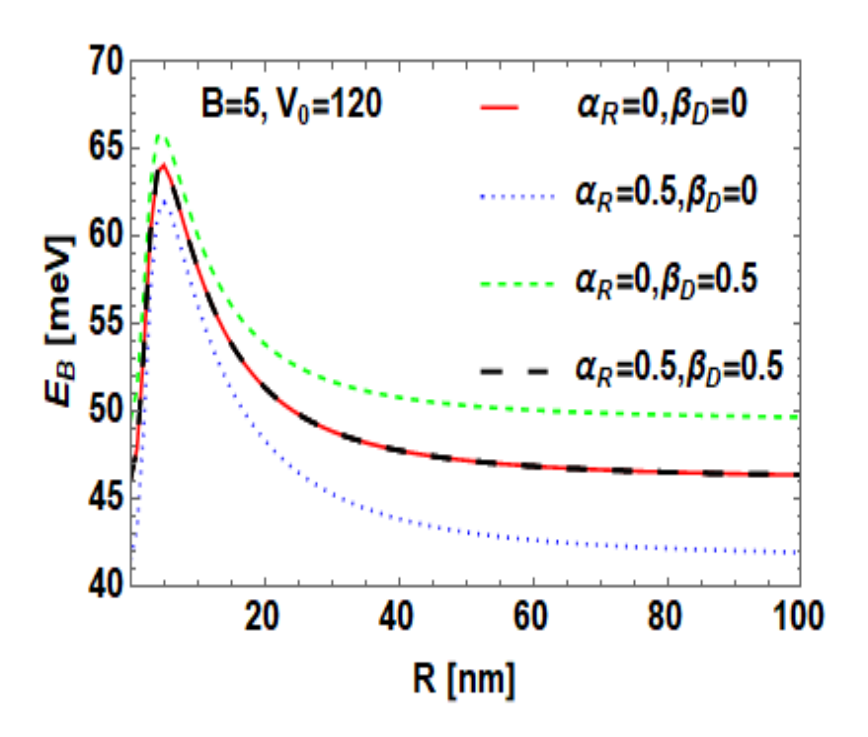


Fig. 6 BE (E_B) vs R for a D^0 centre in a GQD of GaAs with $V_0 = 120$ meV, B = 5 T and a few combinations of α_R (nm-meV) and β_D (nm-meV).

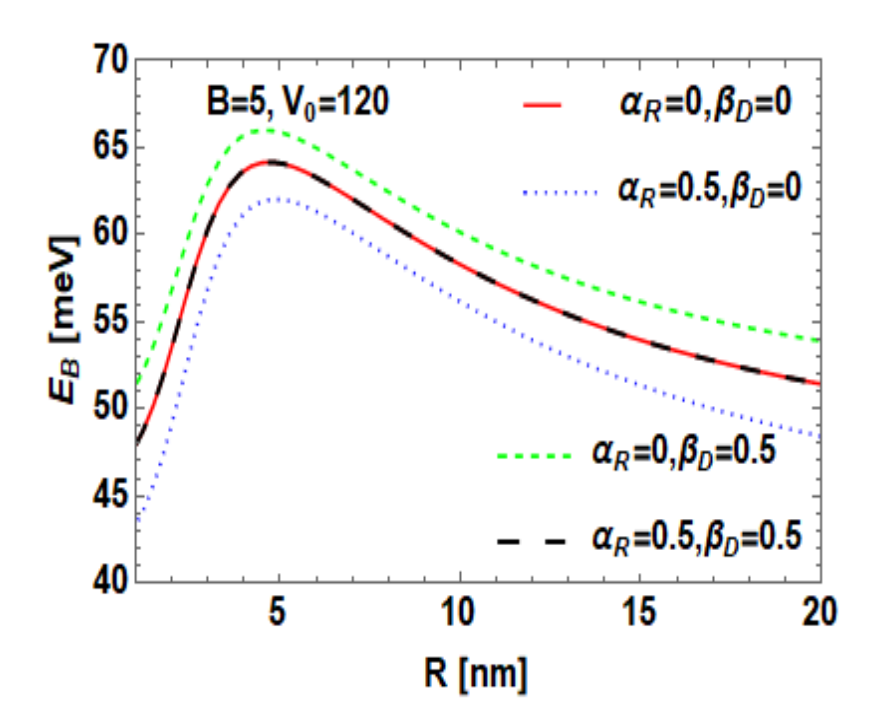


Fig. 7 BE peak for a D^0 centre in a GQD of GaAs with $V_0 = 120$ meV , B = 5 T and a few combinations of α_R (nm-meV) and β_D (nm-meV).

small, the uncertainty in the position of the electron which has to be smaller than the QD size, becomes concomitantly very small. Obviously the momentum uncertainty would then be very large and so the momentum which should be larger than its uncertainty must also be very large. This will naturally lead to a very large kinetic energy. Under these circumstances, it would become really difficult to localize the electrons within the confines of the QD and as a result the binding energy will undergo a substantial reduction.

In Fig. 8, we show the behaviour of the GS BE (E_B) of the D⁰ complex in a GQD of GaAs with respect to the magnetic field for R=10 nm, $V_0=120$ meV and different sets of values of α_R and β_D . In Fig. 9, we plot E_B vs. V_0 for B=5 and R=10 nm. Though the binding of the D⁰ complex is enhanced by both the magnetic field and the confinement potential depth, in the former case the behaviour is concave from above while in the latter case it is concave from below. The explicit variation of the binding energy with α_R and β_D are shown in Figs. 10 and 11.

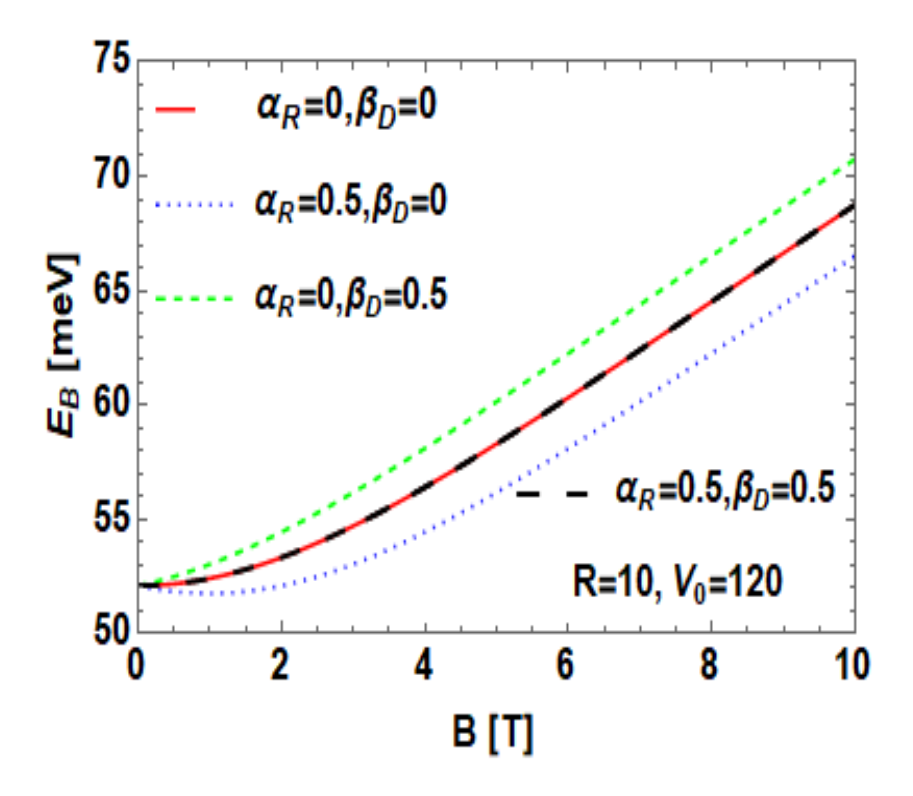


Fig. 8 E_B vs. B for a D^0 centre in a GQD of GaAs with $V_0=120$ meV , R=10 nm and a few combinations of $\alpha_R(\text{nm-meV})$ and β_D (nm-meV).

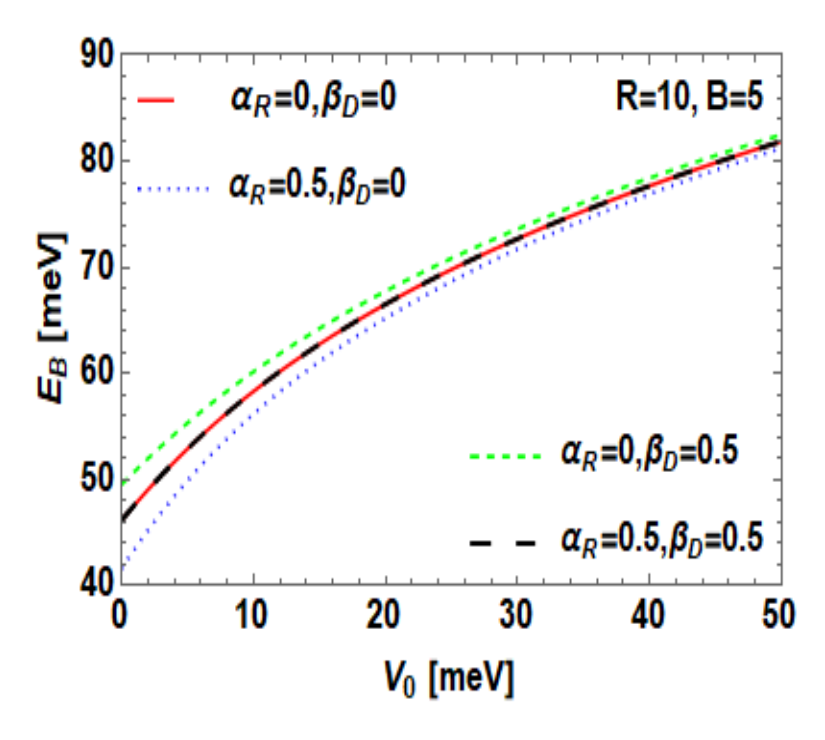


Fig. 9 E_B vs. V_0 for a D^0 centre in a GQD of GaAs with B=5 T, R=10 nm and a few combinations of α_R (nm-meV) and β_D (nm-meV).

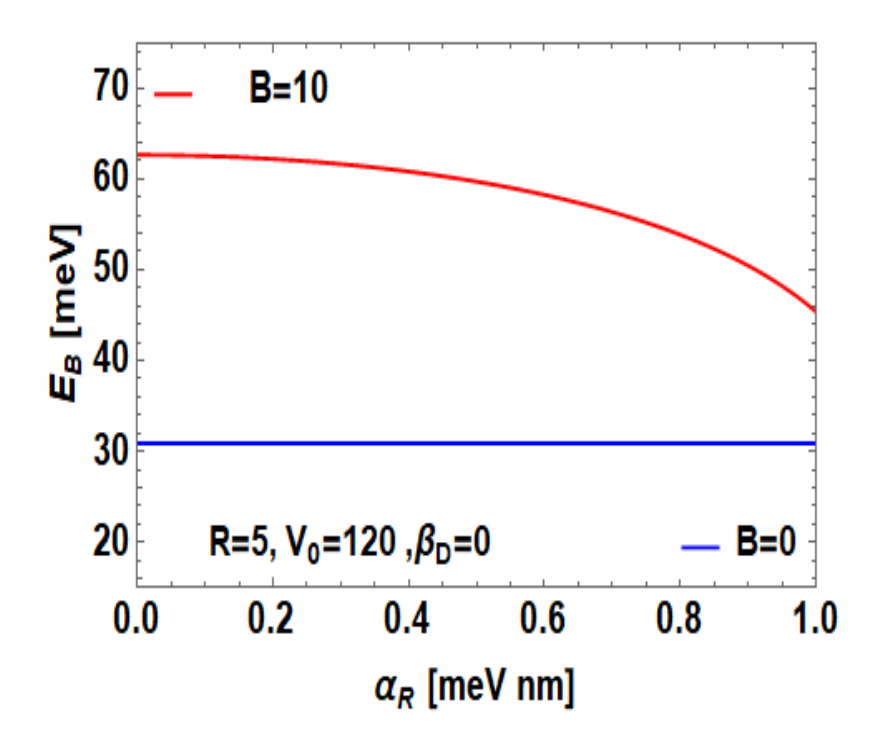


Fig. 10 E_B vs. α_R for a D^0 complex in a GQD of GaAs for R=5 nm, $V_0=120$ meV, $\beta_D=0$ mev nm and B=0 and ST.

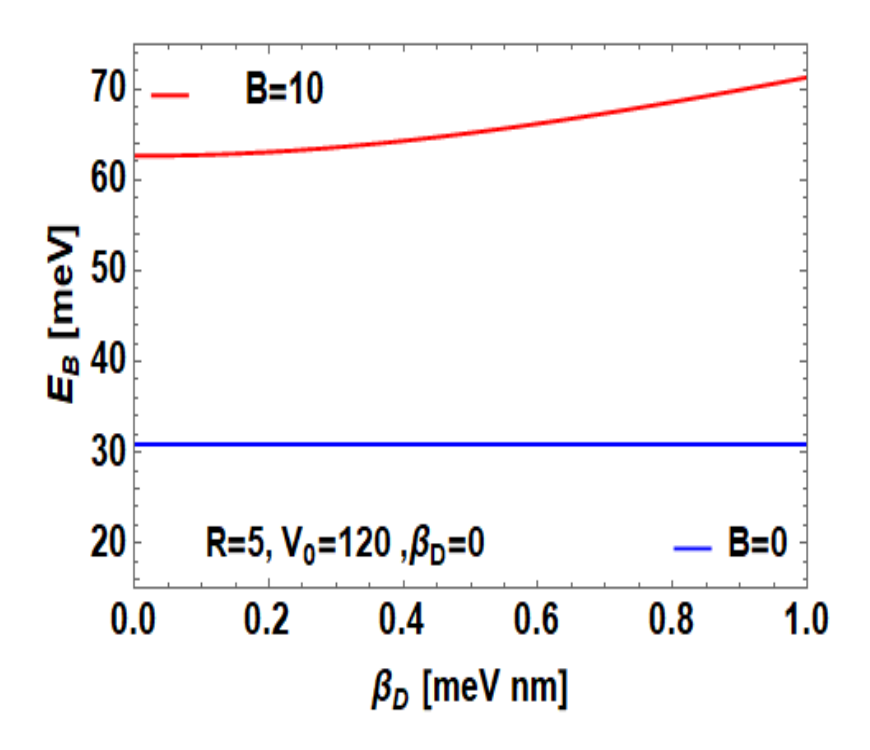


Fig. 11 E_B vs. β_D for a D^0 complex in a GQD of GaAs for R=5 nm, $V_0=120$ meV, $\alpha_R=0$ meV nm and B=0 and 5T.

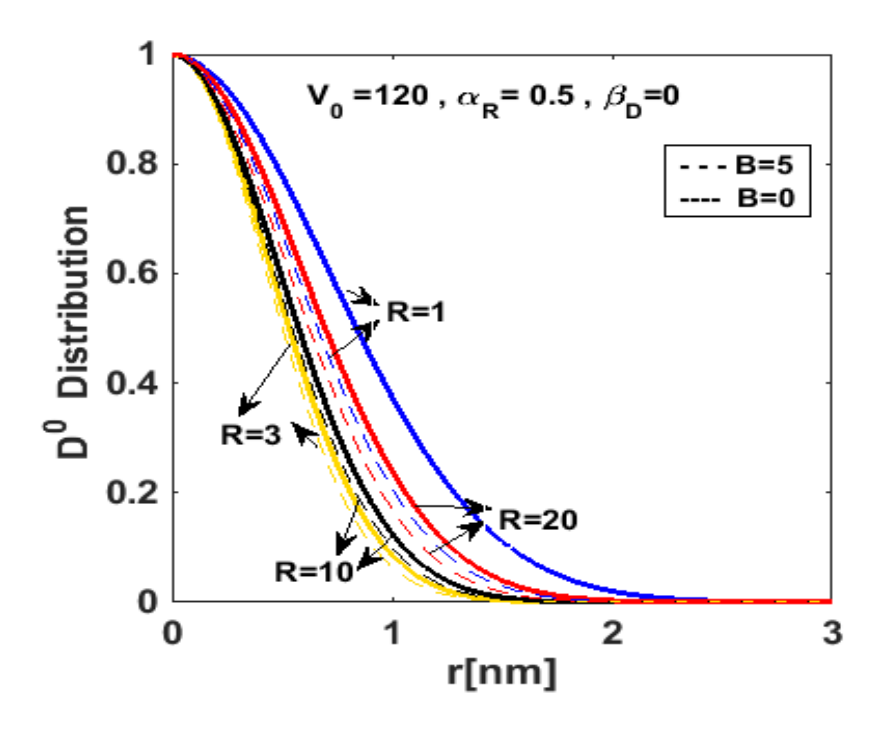


Fig. 12 Donor electron distribution in a GQD of GaAs with $V_0 = 120$ meV, $\alpha_R = 0.5$ meV nm, $\beta_D = 0$ meV nm, B = 0 and 5T and different values of R (nm).

In Figs. 12 and 13 we show the behaviour of the donor electron distribution in a GQD of GaAs with $V_0 = 120 \, nm$ and different values of R in the presence of DSO and RSO interactions respectively. Fig. 12 gives the results for DSO interaction while those for RSO interaction are shown in Fig. 13. It is evident that the electron localization becomes more and more stronger with the reduction in the QD size as can be seen from the curves for $R = 20, 10, 3, 1 \, nm$. However the figures show that localization for $R = 10 \, nm$ is less than that for $R = 3 \, nm$. This is because below a certain R, the kinetic energy becomes so large because of uncertainty principle that localization starts reducing. The figures also show that the localization is stronger in the presence of DSO interaction. It is also evident that the magnetic field provides an additional localization as expected.

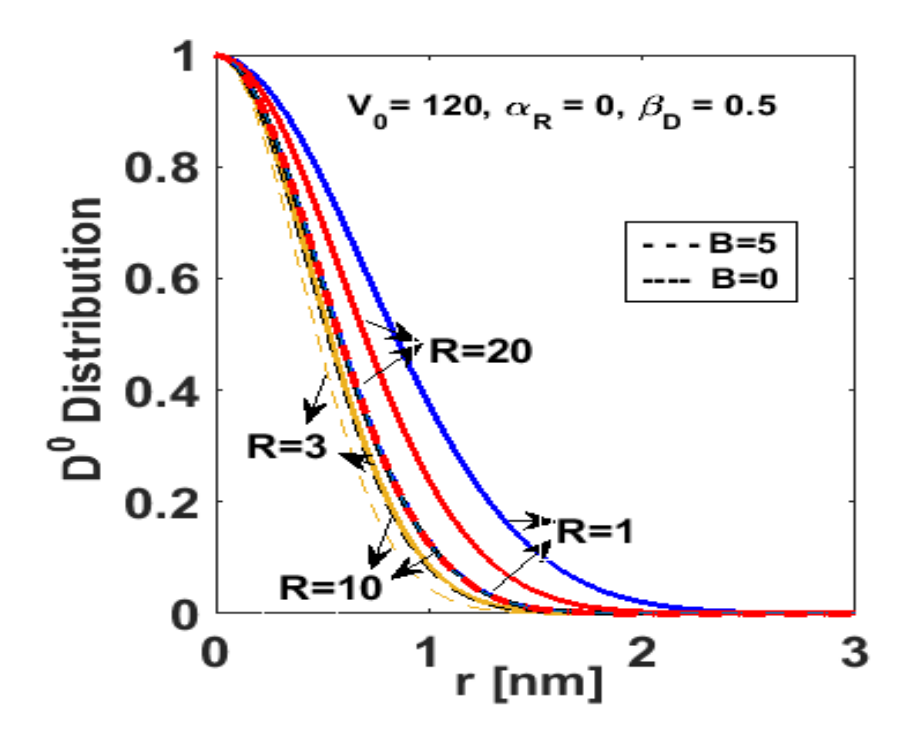


Fig. 13 Donor electron distribution in a GQD of GaAs with $V_0 = 120R_y^*$, $\beta_D = 0.5$ meV-nm B = 0 and 5T and different values of R (nm).

In Fig. 14 we plot the magnetic moment (M) with respect to B for $V_0 = 120$ meV, R = 10,20 nm and for different values of α_R and β_D . The curves clearly reveal that M is diamagnetic in the D^0 complex. One can observe from Fig. 14 that the magnitude of M increases with increasing B. Furthermore, |M| increases with R. However, for both small and very large values of B, the magnetic moment depends rather weakly on the QD size. At low values of B, the RSO interaction reduces the diamagnetic moment while DSO enhances it. At large B, the magnetic

moment becomes independent of SOI.

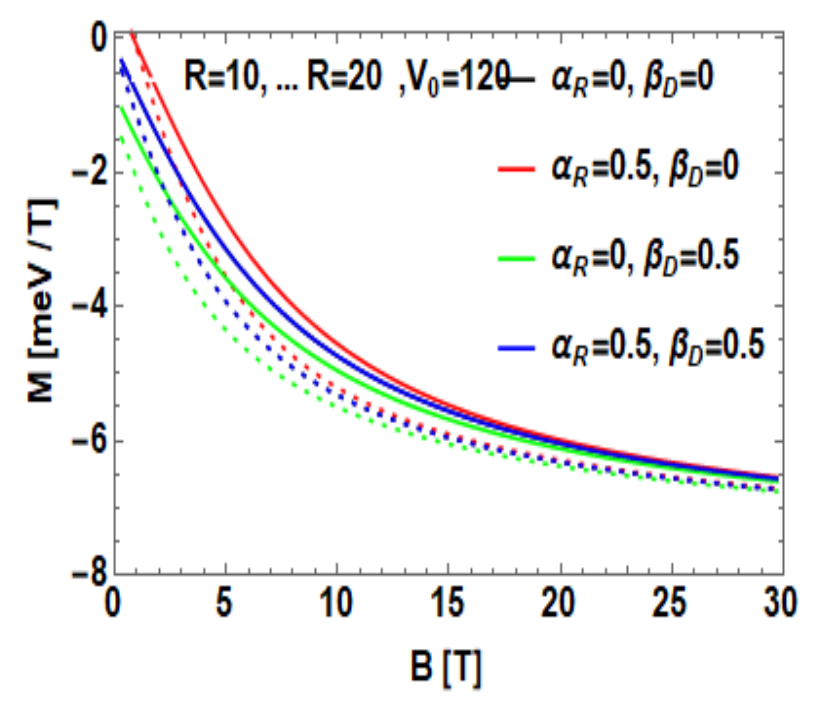


Fig. 14 Magnetic moment (*M*) **vs.** *B* for a D^0 centre in a GQD of GaAs with $V_0 = 120$ meV , R = 10 nm and 20 nm and a few combinations of α_R (nm-meV) and β_D (nm-meV).

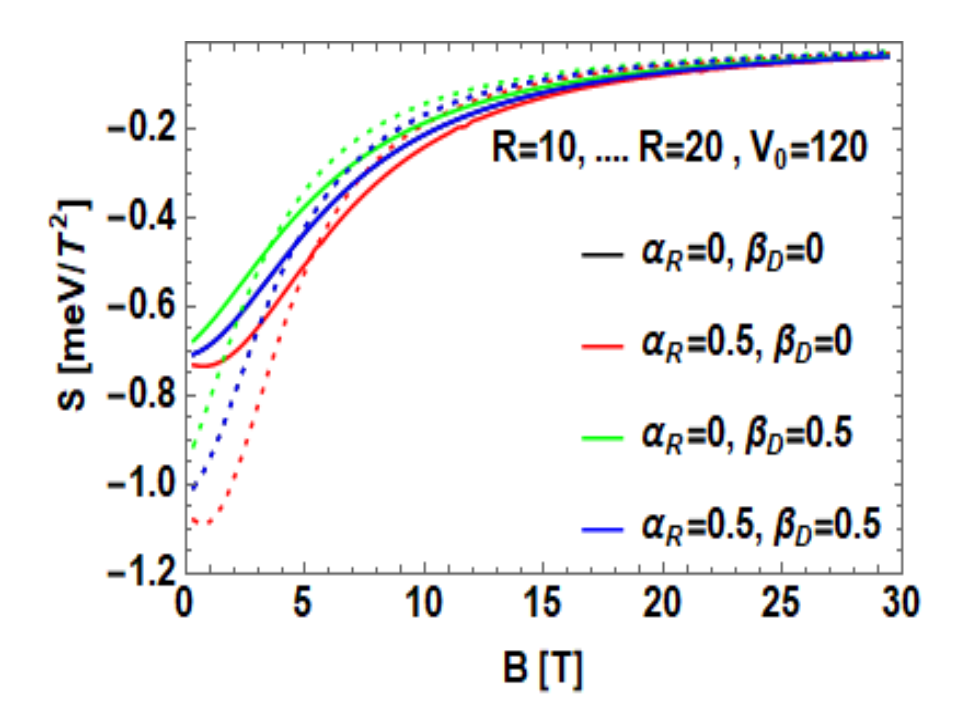


Fig. 15 Magnetic susceptibility (S) vs. B for a D^0 centre in a GQD of GaAs with $V_0 = 120$ meV, R = 10 nm and 20 nm and a few combinations of α_R (nm-meV) and β_D (nm-meV).

Fig.15 shows how the magnetic susceptibility (S) of a D^0 system varies with B. The diamagnetic nature of the susceptibility is clearly visible from the figure. Secondly, in the case of a small QD, the susceptibility varies rather slowly with B at small values of B. But for a larger QD, the susceptibility is found to increase quite rapidly at low values of B. As B increases, the rate of increase of S with B becomes slower beyond a certain value of B that is weakly dependent on the size of the QD. This leads to a crossing behaviour in S as a function of B. At large B, S, however, tends to saturate asymptotically to a value which is a constant independent of R.

2. 4 Conclusion

In this chapter, we have calculated the GS energy (E) and the GS BE (E_B) of a D^0 centre system in a GQD of GaAs as a function of the effective QD radius, confinement strength, external magnetic field and RSO and DSO interactions. The GS energy of the D^0 system has been shown to increase with decreasing QD size and to decrease with increasing confinement strength. Also the GS energy has been shown to decrease with increasing RSOI and DSOI, though the decrease in the case of DSOI has been shown to be much slower. It has been furthermore suggested that in the case of $B \neq 0$, the GS BE decreases with increasing RSOI whereas it increases with DSOI. In the case of B = 0, however, neither of the SOIs has any effect on the GS BE.

We have also presented results for the diamagnetic moment (M) and susceptibility (S) for the donor centre at zero temperature (T=0). We have shown that |M| increases with B and decreases with the reduction in R. S has also been shown to increase with B. We have furthermore shown that |S| increases with increasing QD size at small magnetic fields, but above a critical magnetic field, it decreases with increasing QD radius. This leads to a crossing behaviour in the diamagnetic susceptibility. Finally, we have calculated the electron distribution for different values of the QD parameters. It has been shown that in general, as the QD size decreases, the electron localization becomes stronger. However, the behaviour starts reversing below a certain QD size because of the uncertainty principle.

2.5 References

- [1] M.A. Reed, Sci. Am. **268**, 118 (1993);
 - D. Loss, D.P. Divicenzo, Phys. Rev. A 57, 120 (1998);
 - Y.V. Pershin, J.A. Nesteroff, V. Privman, Phys. Rev. B 69, 121306(R) (2004);
 - B. Vaseghi, R. Khordad, M.M. Golshan, Phys. Stat. Sol. (B) 243, 2772 (2006);
 - S. Zhang, R. Liang, E. Zhang, L. Zhang, Y. Liu, Phys. Rev. B 73, 155316 (2006);
 - E. Kasapoglu, F. Ungan, H. Sari, I. Sokmen, Superlatt. Microstr. 45, 618 (2009);
 - R. Khordad, S.K. Khaneghah, Phys. Stat. Sol. (B) 248, 243249 (2011);
 - G. Rezaei, B. Vaseghi, R. Khordad, H. Azadi Kenary, Physica E 43, 1853 (2011);
 - S. Bandyopadhyay, Physics of Nanostructured Solid State Devices, Springer, 2012;
 - A. Boda and A. Chatterjee, Superlatt. Microstr. 97 268 (2016).
- [2] L. E. Brus, J. Chem. Phys. **80**, 4403 (1984);
 - V. Halonen, T. Chakraborty and P. Pietilainen, Phys. Rev. E 45, 5980 (1992);
 - G. W. Bryant, Phys. Rev. B 37, 8763 (1988); G. W. Bryant, Phys. Rev. B 41, 1243 (1990);
 - J. Y. Marzin and G. Bastard, Soid State Commun. 92, 437 (1994);
 - B. Boyacioglu, M. Saglam and A. Chatterjee, J. Phys.: Condens. Matter 19, 456217 (2007);
 - A. Boda, B. Boyacioglu and A. Chatterjee, J. Appl. Phy. 114, 044311 (2013).
- [3] J. C. Oh, K. J. Chang, G. Ihm, and S. J. Lee, J. Korean Phys. Soc. 28, 132 (1995);
 - J. J. S. De Groote, J. Hornos, and A. Chaplik, Phys. Rev. B 46, 12773 (1992);
 - P. A. Maksym and T. Chakraborty, Phys. Rev. Lett. 65, 108 (1990);
 - B. Boyacioglu and A. Chatterjee, J. Appl. Phys. **112**, 083514 (2012).
- [4] S. Mukhopadhyay and A. Chatterjee, Int. J. Mod. Phys. B 10, 2781 (1996);
 - S. Mukhopadhyay and A. Chatterjee, Phys. Lett. A 240, 100 (1998);
 - S. Mukhopdhyay and A. Chatterjee, Acta Phys. Pol. B 32, 473 (2001);
 - P. M. Krishna, S. Mukhopadhyay and A. Chatterjee, Solid State Commun. 138, 285 (2006).
- [5] S. W. Gu and K. X. Guo, Solid State Commun. 89, 1023 (1993).
 - P. M. Krishna, S. Mukhopadhyay and A. Chatterjee, Int. J. Mod. Phys. B 16, 1489 (2002).
- [6] U. Merkt, J. Huser and M. Wagner, Phys. Rev. B 43, 7320 (1991);
 - J. H. Oh, K. J. Chang, G. Ihm, and S. J. Lee, Phys. Rev. B 50, 15397 (1994);
 - O. Voskoboynikov, O. Bauga, C. P. Lee, and O. Tretyak, J. Appl. Phys. 94, 5891(2003);
 - P.A. Maksym, T. Chakraborty, Phys. Rev. B 45, 1947 (1992);
 - W. C. Tan, J.C. Inkson, Phys. Rev. B **60**, 5626 (1999);
 - O. Voskoboynikov, C.P. Lee, Physica E **20**, 278 (2004);
 - Y. Meir, O. Entin-Wohlman, Y. Gefen, Phys. Rev. B 42, 8351 (1990);

- A. Ralko, T.T. Truong, Phys. Lett A 323, 395 (2004);
- A. Boda, G. Madhusudhan and A. Chatterjee, Superlattices and Microstructures, 71, 261 (2014);
- A. Boda and A. Chatterjee, J. Nanosc . Nanotech. 15, (2015);
- L. Jahan, A. Boda and A. Chatterjee, Scientific Reports;
- A. Boda, D. S. Kumar, I. V. Sankar and A. Chatterjee, J. Mag. and Mag. Mat., 418, 242 (2016);
- A. Boda and A. Chatterjee, Superlattices and Microstructures 97, 268 (2016).
- [7] B. Boyacioglu and A. Chatterjee, Physica B 407, 3535 (2012).
- [8] Zhigang Xiao, Jiqian Zhu, Fenglai He, phys. status sol. (b) 191, 401 (1995);
 - T. Szwacka, J. Phys.: Condens. Matt. 8, 10521 (1996);
 - N. Porras-Montenegro, Phys. Rev. B 46 9780 (1992);
 - J.L. Zhu, X. Chen, Phys. Rev. B 50, 4497 (1994);
 - W. F. Xie, Phys. Lett. A 263, 127 (1999);
 - J.L. Zhu, J.J. Xiong, B.L. Gu, Phys. Rev. B 41, 6001 (1990);
 - Y.P. Bao, W.F. Xie, Commun. Theor. Phys. **50**, 1449 (2008);
 - W.F. Xie, Physica B 403, 2828 (2008);
 - A. Boda, A. Chatterjee, Physica E **45**, 36 (2012);
 - A. Kh. Manaselyan and A. A. Kirakosyan, *Physica E* **28**, 462 (2005);
 - N.P. Sandier and C. R. Proetto, *Phys. Rev. B* 46, 7707 (1992).
- [9] S. Datta, B. Das, Appl. Phys. Lett. 56, 665 (1990);
 - I. Zutic, J. Fabian, S. Das Sarma, Rev. Mod. Phys. 76, 223 (2004);
 - J.-F. Liu, Z.-C. Zhong, L. Chen, D. Li, C. Zhang, Z. Ma, Phys. Rev. B 76, 195304 (2007);
 - F. Malet, M. Pi, M. Barranco, L. Serra, E. Lipparini, Phys. Rev. B 76, 115306 (2007).
- [10] E.I. Rashba, Sov. Phys. Solid State 2, 1109 (1960).
- [11] G. Dresselhaus, Phys. Rev. **100**, 580 (1955).
- [12] R. Winkler, Spin Orbit Coupling Effects in Two-Dimensional Electron and Hole Systems, Springer, Berlin, 2003.
- [13] S. A. Wolf, J. Supercond. **13**, 195 (2000);
 - I. Zutic, J. Fabian, S. D. Sarma, Rev. Mod. Phys 76, 323 (2004);
 - C. Kurdak, N. Biyikli, U. Ozgur, H. Morkoc, V. I. Litvinov, Phys. Rev. B 74, 113308 (2006);
 - J. Fabian, A. Matos-Abiague, C. Ertler, P. Stano, I. Zutic, Acta Phy. Slovaca 57, 565 (2007).
- [14] D. S. Kumar, S. Mukhopadhyay, Ashok Chatterjee, J. Mag. Mag. Mat. 418, 169 (2016).
- [15] N.F. Johnson, M.C. Payne, Physical Review Letters 67, 1157 (1991)
- [16] Shu-Shen Li and Jain-Bai Xia, Appl. Phys. Lett. **92**, 022102 (2008).

- [17] B. Gisi, S. Sakiroglu, E. Kasapoglu, H. Sari, and I. Sokmen, Superlatt. Microstr. 86,166 (2015).
- [18] D. Sanjeev Kumar, Aalu Boda, Soma Mukhopadhyay and A. Chatterjee, Superlattices and Microstructures 88, 174 (2015).
- [19] D. Sanjeev Kumar, S. Mukhopadhyay and A. Chatterjee, Physica E, 47, 270 (2013).

Chapter ~3

Spin-Orbit Interaction effects on the Binding Energy and Susceptibility of an Off-Centre D^0 Impurity in a 2D Gaussian Dot in the presence of a Magnetic Field

3.1 Introduction

As we discussed in Chapter 2, a large number of investigations have been carried out for an oncentre D^0 impurity in a QD [1-10]. The off-centre D^0 impurity problem in the QD has also received considerable attention by several authors [11-35]. Indeed, the energetics of an off-centre D^0 impurity have been studied in square well, parabolic and Gaussian QDs using variational method [10-25], perturbation method [26-30], effective mass approximation [31], finite element method and Arnoldi algorithm [32] and it has been demonstrated that BE of an off-centre D^0 reduces when the impurity is shifted away from the dot centre. Many researches [32-35] have been studied the effect of magnetic field on BE and susceptibility of an off centre D^0 impurity in the QDs.

SOIs has become an interesting probe for studying the physical properties of low-dimensional structures, from both the theoretical and technical points of view. In this chapter, we employ a variational method to study the effect of Rashba and Dresselhaus SOIs on the GS and binding energies of an off centre D^0 impurity in a Gaussian QD in the presence of a magnetic field. We apply our theory to obtain results for a GaAs QD.

3.2 Model Hamiltonian

The system of an off-centre D^0 centre in a 2D GQD in the presence of RSOI and DSOI and an external magnetic field B(0,0,B) is governed by the Hamiltonian:

$$\mathcal{H} = \left(\frac{1}{2m^*}(\boldsymbol{p} + \frac{e}{c}\boldsymbol{A})^2 - \frac{e^2}{\varepsilon|\boldsymbol{\rho} - \boldsymbol{D}|} - V_0 e^{-\frac{\rho^2}{2R^2}}\right) I + \frac{\alpha_R}{\hbar} \left[\boldsymbol{\sigma} \times \left(\boldsymbol{p} + \frac{e}{c}\boldsymbol{A}\right)\right]_Z$$

$$+\frac{\beta_{D}}{\hbar}\left[\boldsymbol{\sigma}_{x}\left(\boldsymbol{p}_{x}+\frac{e}{c}\boldsymbol{A}_{x}\right)-\boldsymbol{\sigma}_{y}\left(\boldsymbol{p}_{y}+\frac{e}{c}\boldsymbol{A}_{y}\right)\right],\tag{3.1}$$

where $\rho(p)$ is the coordinate (conjugate momentum) of an electron of effective mass m^* and charge e, A refers to the vector potential which is defined as: $B = \nabla \times A$, ε is the permittivity of the material medium, D represents the location of the D^0 impurity, R and V_0 stand for the range and the depth of the confinement potential, I denotes the unit matrix of order 2, σ_x , σ_y and σ_z describe the Pauli spin matrices and α_R and β_D are respectively the RSOI and DSOI coefficients. We work in the symmetric gauge and choose: A = B (-y/2, x/2, 0).

To deal with SOIs, we apply a transformation $U = e^S$ to \mathcal{H} , as in Chapter 2. The generator S is given by

$$S = i \frac{m^*}{\hbar^2} \left[\alpha_R (y \sigma_x - x \sigma_y) + \beta_D (x \sigma_x - y \sigma_y) \right]$$
 (3.2)

We expand the transformed Hamiltonian $\widetilde{\mathcal{H}} = e^S \mathcal{H} e^S$ in a power series in terms of α_R and β_D and consider terms up to quadratic in α_R and β_D . This leads to

$$\widetilde{\mathcal{H}} = \left(\frac{p^2}{2m^*} + \frac{1}{8}m^*\omega_c^2\rho^2 - \frac{e^2}{\varepsilon|\rho - D|} - V_0 e^{-\frac{\rho^P}{2R^P}}\right)I - \frac{m^*}{\hbar^2}(\alpha_R^2 + \beta_D^2)I - \frac{m^*}{\hbar^3}(\alpha_R^2 - \beta_D^2)\sigma_Z L_Z + \frac{\omega_c}{2}L_Z - \frac{m^*}{2\hbar^3}(\alpha_R^2 - \beta_D^2)\omega_c\sigma_Z \rho^2, \tag{3.3}$$

where

$$\omega_c = \left(\frac{eB}{m^*c}\right), \qquad \rho^2 = (x^2 + y^2), \qquad L_z = -i\hbar\left(\frac{\partial}{\partial\phi}\right).$$
 (3.4)

3.3 Formulation

To calculate the GS energy of the electron and D^0 in Gaussian QD we use the Ritz variational method and choose a simple variational wave function:

$$\psi_{e^{-}}(\boldsymbol{\rho}) = e^{-\beta \rho^2 - im\varphi},\tag{3.5}$$

$$\psi_{D^0}(\boldsymbol{\rho}) = \left[1 + \gamma e^{-\alpha(\rho - D)}\right] e^{-\beta \rho^2 - im\varphi},\tag{3.6}$$

where γ , α , and β will be treated as variational parameters. The variational energies of the e^- and D^0 system are given by

$$E_{S=e^{-},D^{0}} = \frac{\langle \psi_{S}(\boldsymbol{\rho})|\widetilde{\mathcal{H}}|\psi_{S}(\boldsymbol{\rho})\rangle}{\langle \psi_{S}(\boldsymbol{\rho})||\psi_{S}(\boldsymbol{\rho})\rangle},$$
(3.7)

where E_{e^-} is the GS energy of an electron in GQD and E_{D^0} is that of the off-centre D^0 complex in GQD. The BE of the off-centre D^0 impurity $(E_{B(D^0)})$ is given, as usual, by

$$E_B(D^0) = E(e^-) - E(D^0). (3.8)$$

We are also interested in the magnetization and susceptibility which are given by:

$$M = -\frac{\partial E}{\partial B}; \quad M = -\frac{\partial M}{\partial B}.$$
 (3.9)

3.3 Numerical results and discussion

We choose to measure energy in meV, length in nm, magnetic field in Tesla (T), and SOI coefficients in meV-nm. We shall apply our results to GaAs QD for the sake of concreteness for which we take $\varepsilon = 12.4$ and $m^* = 0.067m_0$, m_0 being the bare electron mass. In Fig 1, we show the GS energy levels for different values of the impurity position D in a GQD with $V_0 = 300$ meV and R = 10 nm. The GS energy level rises with increasing D. Thus one can tune the energy levels if one can have a control on the position of the impurity.

In Fig. 2, we present the behavior of GS energy (GSE) (E) of an off-centre D^0 impurity in a GaAs GQD as a function of impurity position D for B = 0 and $B \neq 0$ and for different RSOI and

DSOI coefficients α_R and β_D . As D increases, GSE initially increases quite rapidly, but asymptotically saturates to a constant value.

This can be easily understood from the simple semi-classical argument, which suggests that GS corresponds to the minimum of the potential. The RSOI and DSOI effects on GSE are found to be low at small values of D and large at higher values of D. GSE decreases in the presence of both SOIs at low B, but the effects of RSOI and DSOI are opposite at higher values of B. RSOI reduces GSE but DSOI enhances it at higher values of B.

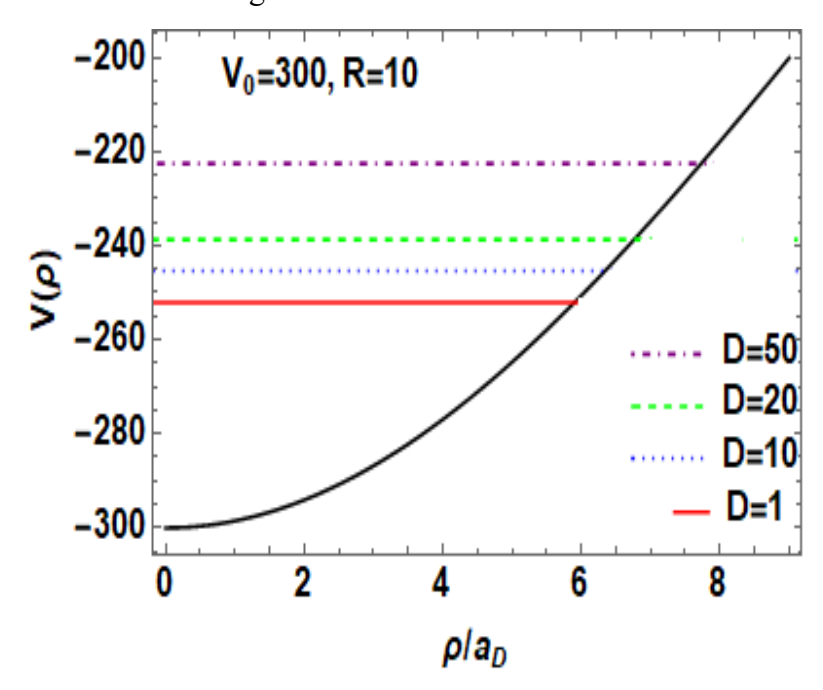


Fig. 1 GSE levels (E) vs ρ for an off-centre D^0 centre in a GaAs GQD with $V_0 = 300$ meV and R = 10 nm and for different values of D (nm).

Fig. 3 depicts the behavior of E with respect to R for a GQD of GaAs semiconductor with $V_0 = 60$ meV and $V_0 = 120$ meV for a few combinations of α_R and β_D and at B = 0. With increasing R, GSE falls off initially rapidly, particularly so for a larger V_0 , but finally appears to saturate to the bulk value. The figure clearly shows that the donor system becomes more confined as V_0 increases. This behavior follows from the commonplace notion of quantum mechanics. It is also revealed by the figure that RSOI and DSOI have the same effects on GSE at B = 0. Comparison of the present results with those of [13] reveals that GSE increases with D.

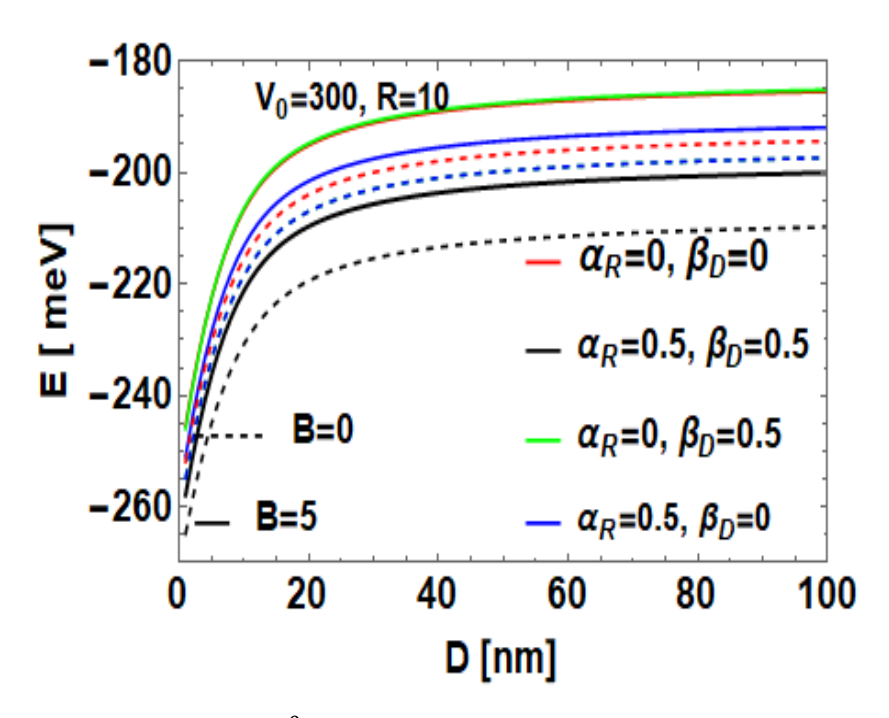


Fig. 2 E vs D for an off-centre D⁰ impurity in a Gaussian GaAs QD with $V_0 = 300$ meV, R = 10 nm, B = 0, 5T and a few different values of α_R (nm-meV) and β_D (nm-meV).

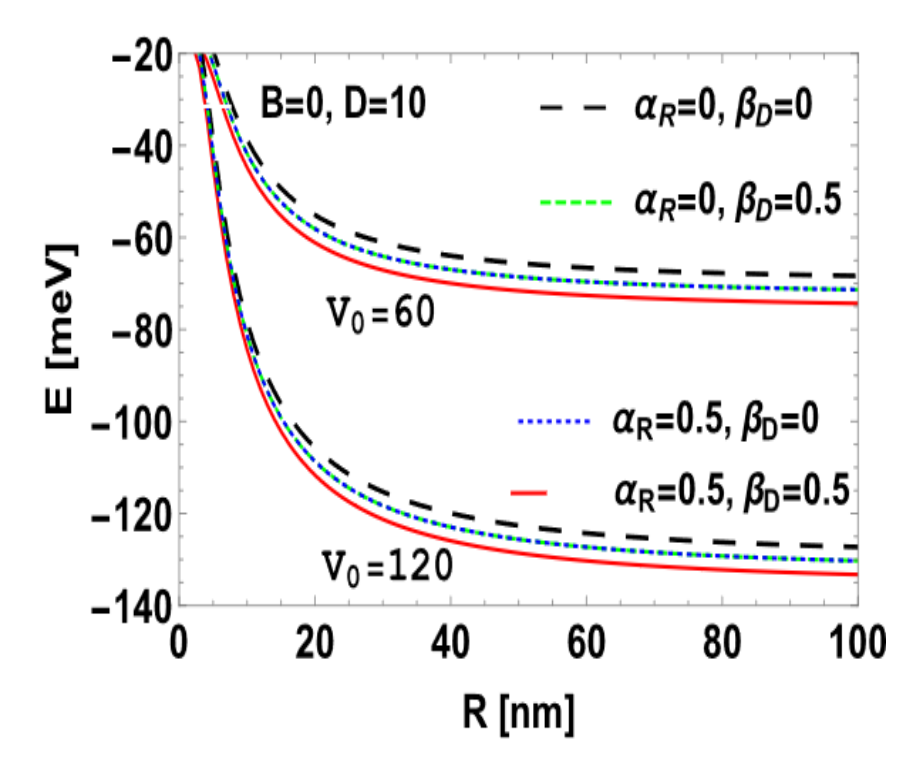


Fig. 3 E vs R for an off-centre D^0 impurity in a Gaussian GaAs QD with B=0, D=10 nm, $V_0=60$ meV and 120 meV and a few different values of α_R (nm-meV) and β_D (nm-meV).

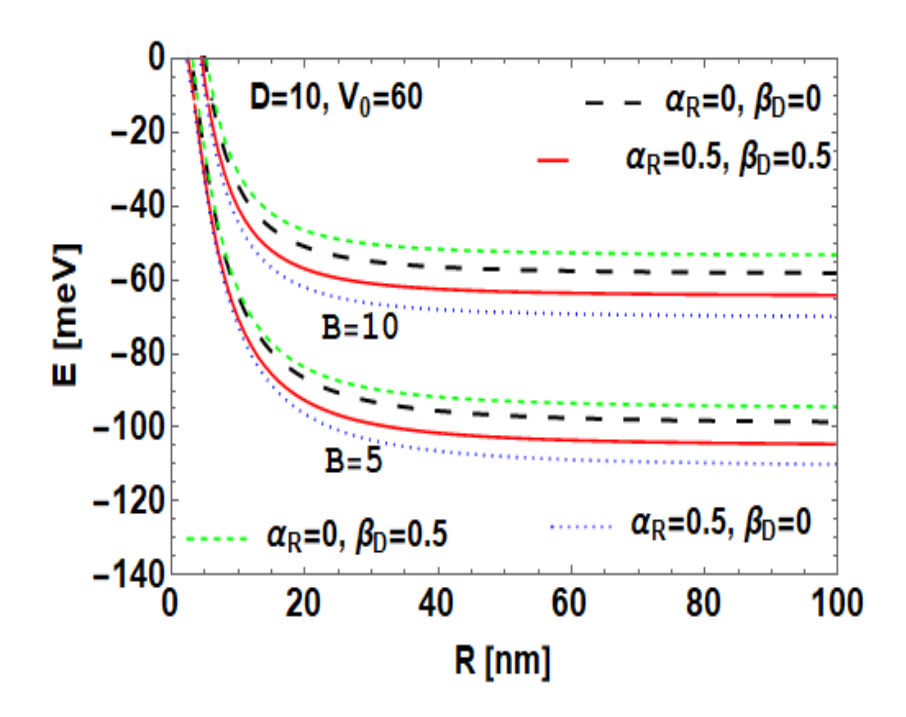


Fig. 4 E vs R for an off-centre D^0 impurity in a Gaussian GaAs QD with D=10 nm, $V_0=60$ meV, B=5 T, 10T and for few values of α_R (nm-meV) and β_D (nm-meV).

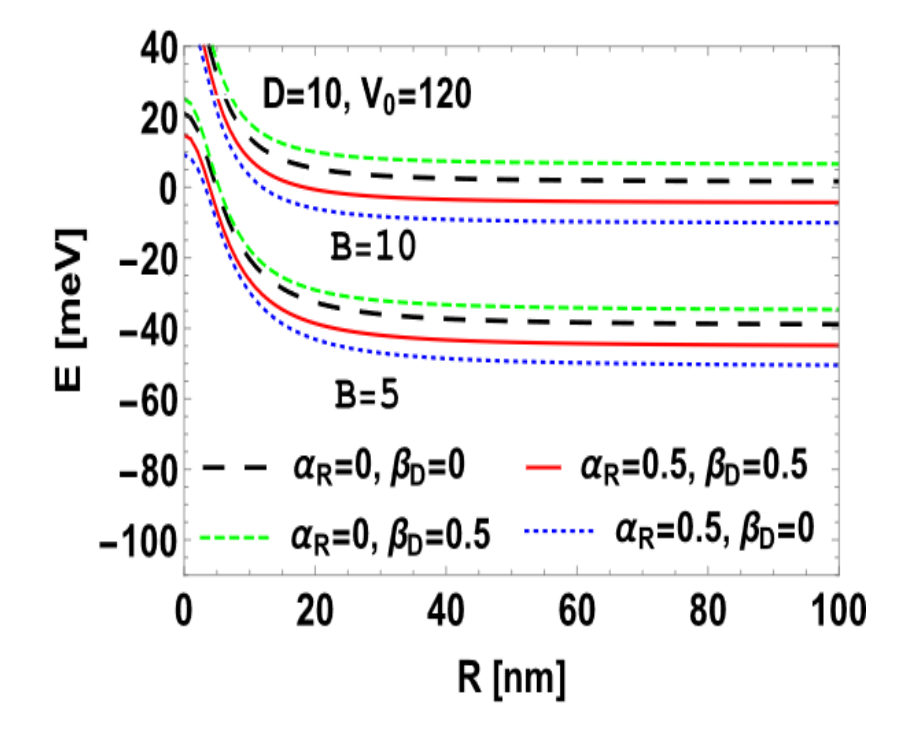


Fig. 5 E vs R for an off-centre D^0 impurity in a Gaussian GaAs QD with D=10 nm, $V_0=120$ meV, B=5 T, 10T and for a few values of α_R (nm-meV) and β_D (nm-meV).

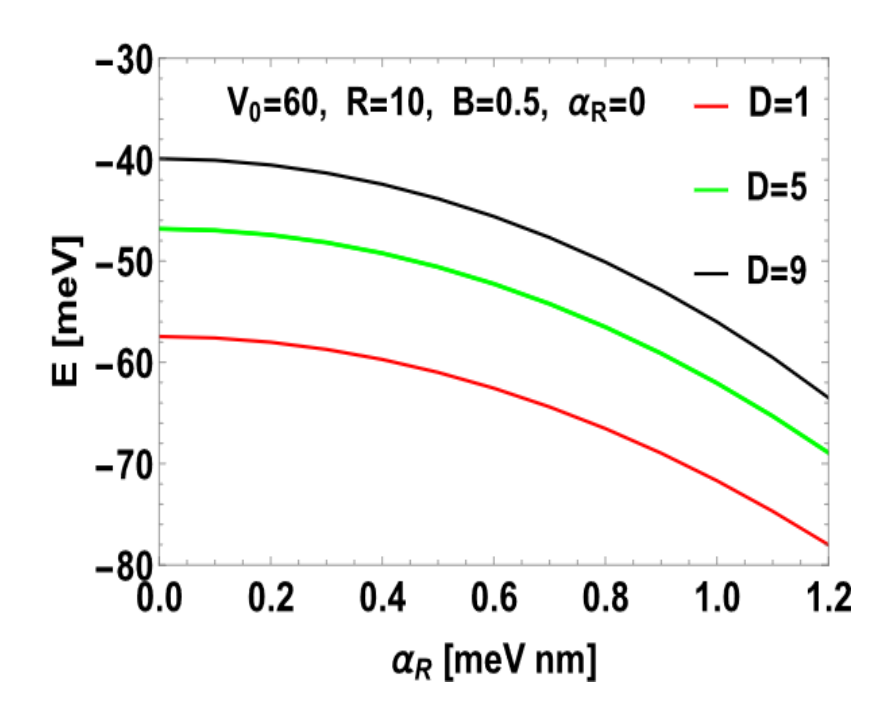


Fig. 6 E vs. α_R for an off-centre D^0 in a Gaussian GaAs QD with $V_0 = 60$ meV, R=10 nm, B=0.5 T, $\beta_D=0$ and for different values of D (nm).

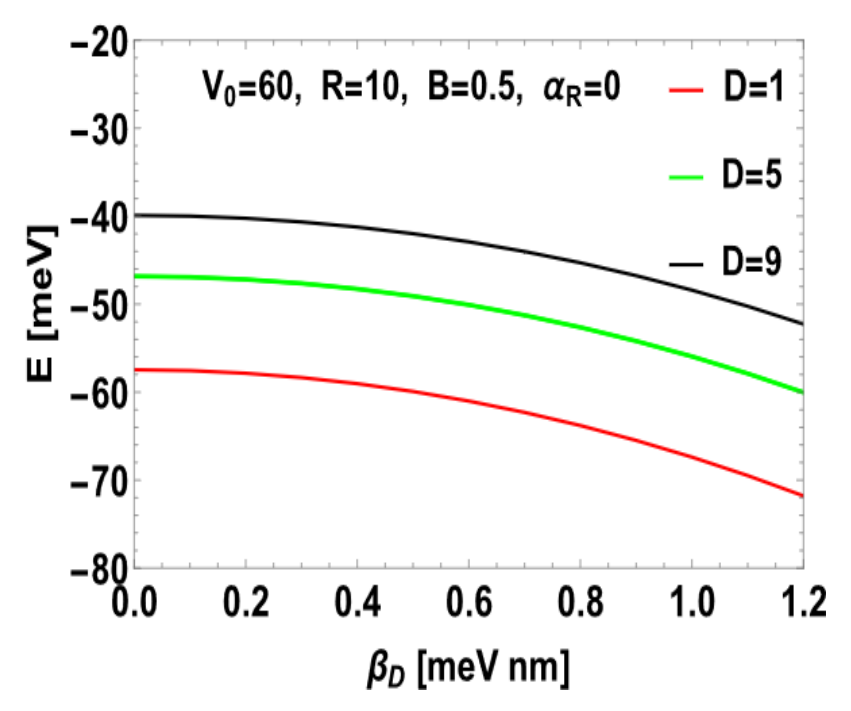


Fig. 7 E vs. β_D for an off-centre D^0 in a Gaussian GaAs QD with B=0.5 T, R=10 nm, $V_0=60$ meV, $\alpha_R=0$ and for different values of D (nm).

We show in Fig. 4 and Fig. 5, the behaviour of E with R for a 2D GaAs GQD for a few combinations of α_R and β_D - values at B=5 and B=10 T and $V_0=60$ meV and $V_0=120$ meV respectively. The figure shows that GSE increases with B, which is an expected behaviour. Furthermore, GSE reduces in value as R increases and eventually saturates to the bulk limit. This effect is understandable from the point of view of simple quantum mechanics.

In Figs. 6 and 7, we show the variation of E as a function of α_R and β_D respectively with B = 0.5 T, $V_0 = 60$ meV and R=10 nm and for a few values of D. One can see from the figure that the value of GSE diminishes with increasing α_R and β_D , but the decrease with respect to α_R is faster. Thus the energy is lowered more by the Rashba coupling than by the Dresselhaus interaction and the Rashba coupling has a stronger effect in a QD. Fig. 7 suggests that the location of impurity plays a more important role at higher values of β_D .

In Fig. 8, we show the plot of E vs. B with V = 300 meV, R = 10 nm, D = 5 nm and for different values of α_R and β_D . In the case of $\alpha_R = 0 = \beta_D$, one can see that E is an increasing function of B, which is however is an expected behaviour. When DSOI is switched on, the E vs B – curve becomes more steeper and almost linear.

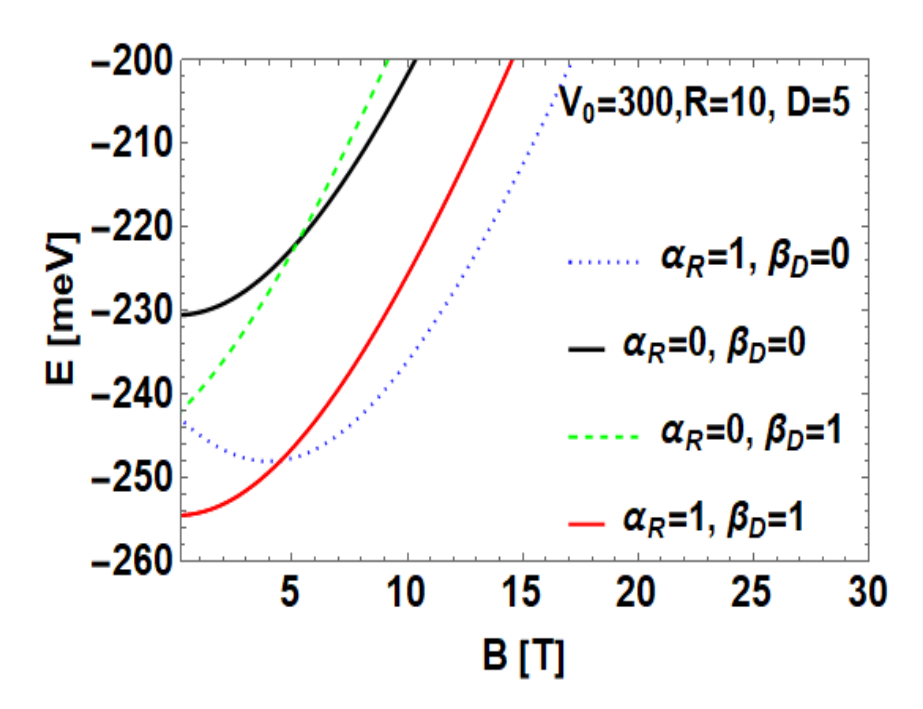


Fig. 8 E vs B for an off-centre D^0 in a Gaussian GaAs QD with $V_0 = 300$ meV, R=10 nm, D=5 nm and for different values of α_R (nm-meV) and β_D (nm-meV).

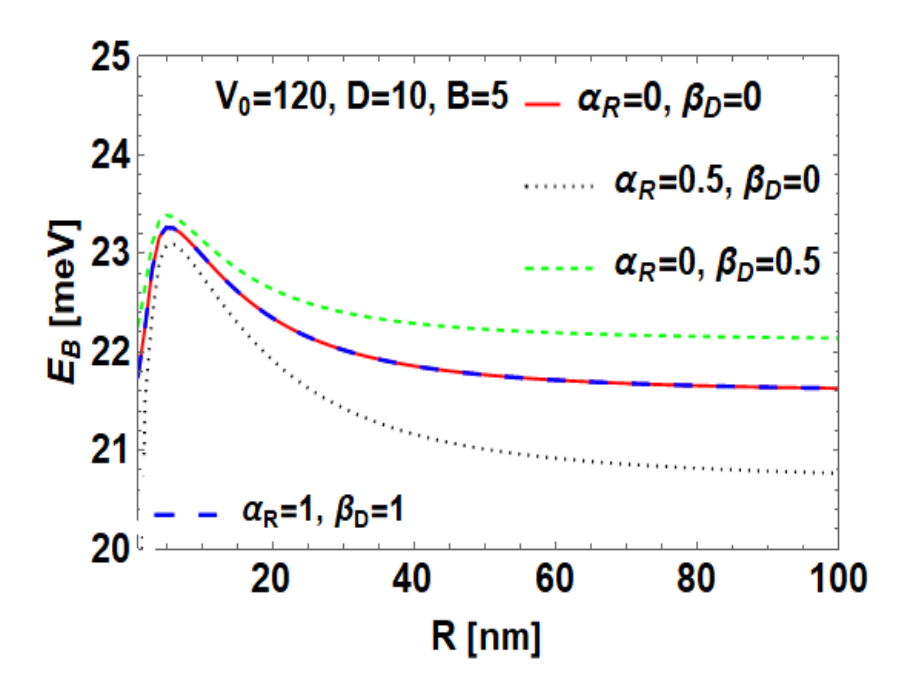


Fig. 9 E_B vs R for an off-centre D^0 in a Gaussian GaAs QD with $V_0 = 120$ meV, D=10 nm, B=5 T for different values of α_R (nm-meV) and β_D (nm-meV).

Thus in this case, E increases with B more rapidly but linearly. If RSOI is switched on keeping $\beta_B = 0$, the behaviour of GSE becomes interesting. At small B, it decreases with increasing B, reaches a minimum and then increases monotonically. Now if DSOI is additionally swiched on, E shows again an increasing behaviour with E. Of course the nitty-gritty of the behaviour would be determined largely by the relative values of E0. The bottom-line is that E1 is raised by the magnetic field and DSOI.

In Fig. 9, we plot the GS BE (E_B) of an off-centre D^0 system as a function of R with B=5T, $V_0=120$ meV, D=10 and for different combinations of α_R and β_D . The BE E_B turns out be positive, which means that the system is always stable. Comparison of the results of the present work with the corresponding values for the on-centre D^0 complex [13] suggests that the binding is weaker in the case of an off-centre D^0 complex than for the corresponding off-centre system. One can see from Fig.9 that the role of SOI on E_B is more visible at larger values of R. DSOI enhances the binding while it is reduced by RSOI. One can see that the curves for $\alpha_R=0=\beta_D$ and $\alpha_R=1=\beta_D$ exactly coincide. This is not fortuitous, but a general trend. The effect of RSOI and DSOI are exactly equal and opposite. Fig. 9 also reveals that the BE of an off centre D^0

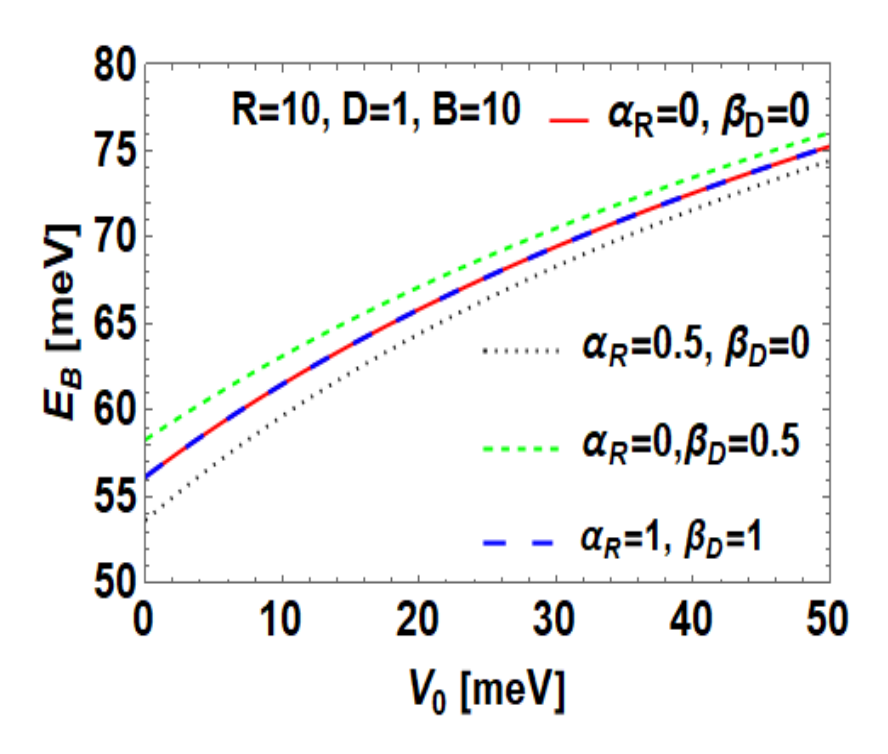


Fig. 10 E_B vs. V_0 for an off-centre D^0 in a Gaussian GaAs QD with R=10 nm, D=1 nm, B=10 T for different values of α_R (nm-meV) and β_D (nm-meV).

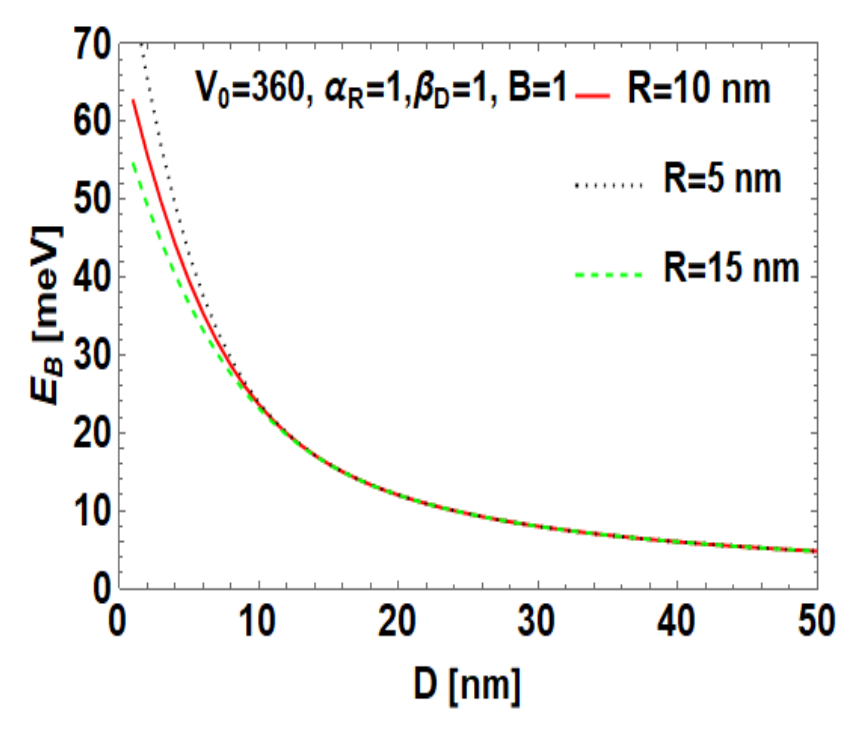


Fig. 11 E_B vs D for an off-centre D^0 in a Gaussian GaAs QD with $V_0 = 360$ meV, $\alpha_R = 1$ nm-meV, $\beta_D = 1$ nm-meV, B = 1 T and for different values of R (nm).

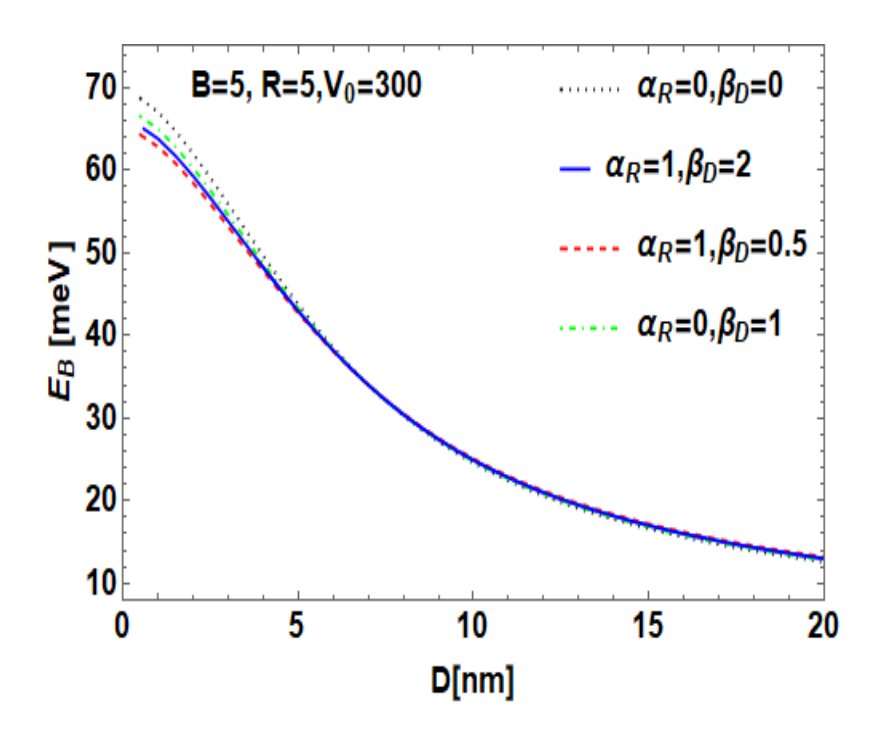


Fig. 12 E_B vs D for an off-centre D^0 in a Gaussian GaAs QD with B=5 T, R=5 nm, $V_0=300$ meV for different values of α_R (nm-meV) and β_D (nm-meV).

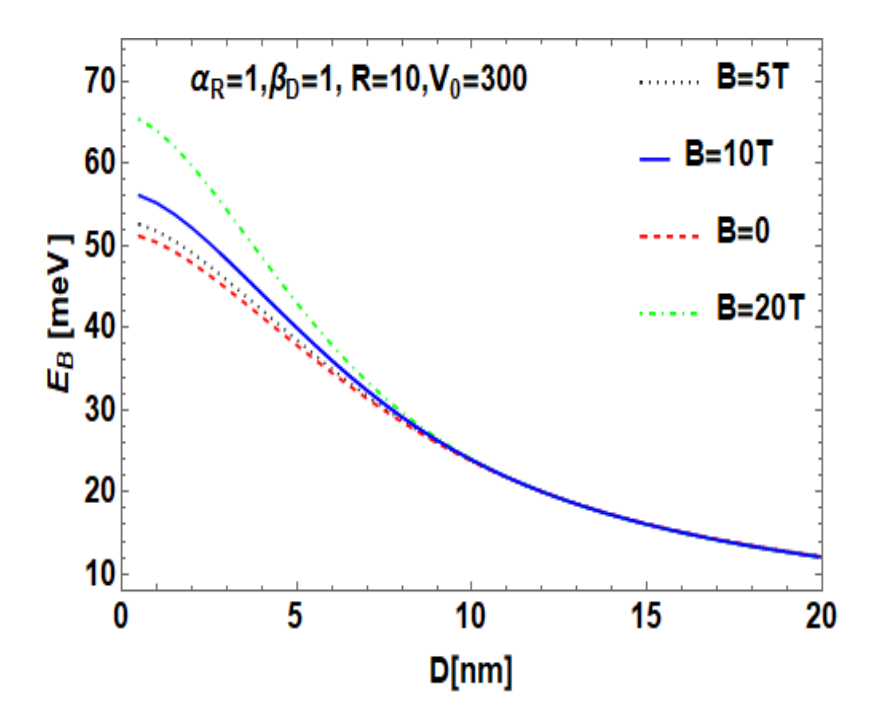


Fig. 13 E_B vs D for an off-centre D^0 in a Gaussian GaAs QD with $\alpha_R = 1$ nm-meV, $\beta_D = 1$ nm-meV, R=10 nm, $V_0 = 300$ meV and for different values of B(T).

becomes stronger as R is decreased and it attains a peak at a critical value of R (R_c) below which it decreases very fast The rapid fall in BE below R_c is purly a quantum mechanical phenomenon and has been explained in [13]. In Fig. 10, we plot E_B vs. V_0 for R=10nm, D=1nm and B=5T. We can see that BE increases with V_0 . Also RSOI decreases BE while DSOI enhances it.

We plot E_B vs D in Fig. 11 for a few values R, in Fig. 12 for a few combinations of α_R and β_D – values and in Fig. 13 for a few values of B. Fig. 11 suggests that the binding is strongest when D^0 is placed at the centre of the QD i. e., when D=0. As D increases, BE decreases and eventually saturates. The figure also shows that QD size influences the E_B-D - curve essentially at small D values only, where BE increases with decreasing QD size R.

Fig. 12 reveals that the SOI effect on *D*-dependence of BE is rather negligible, while Fig. 13 suggests that at small *D* values, the magnetic field plays a significant part in deciding the *D*-dependence of BE. However, if *D* is large, then none of *R*, *B*, α_R , or β_D has any effect on the E_B vs *D* curve.

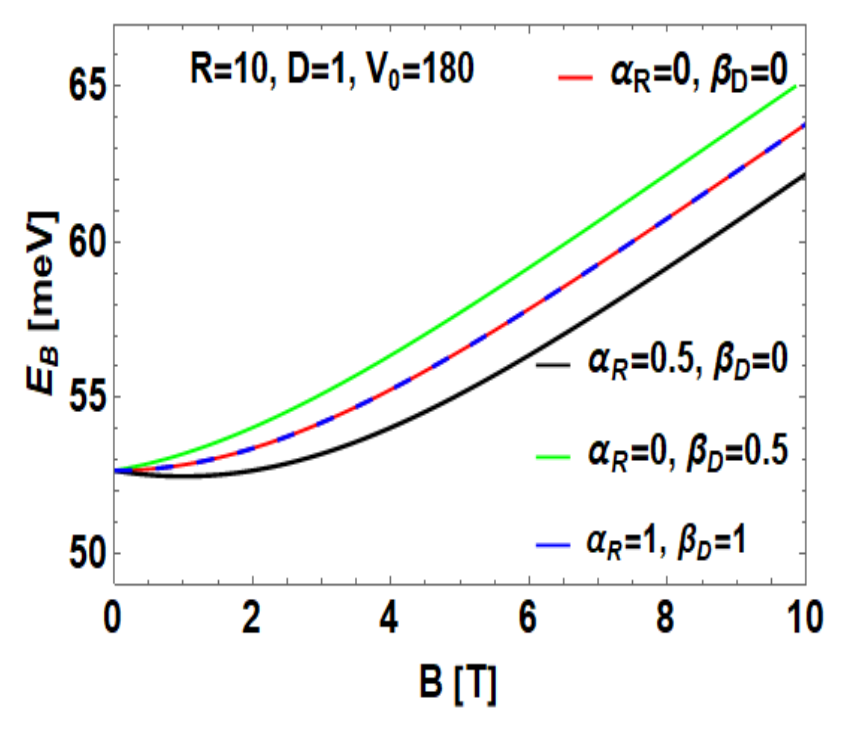


Fig. 14 BE vs. *B* for an off-centre D^0 in a Gaussian GaAs QD with R = 10 nm, D=1 nm, $V_0 = 180$ meV for different values of α_R (nm-meV) and β_D (nm-meV).

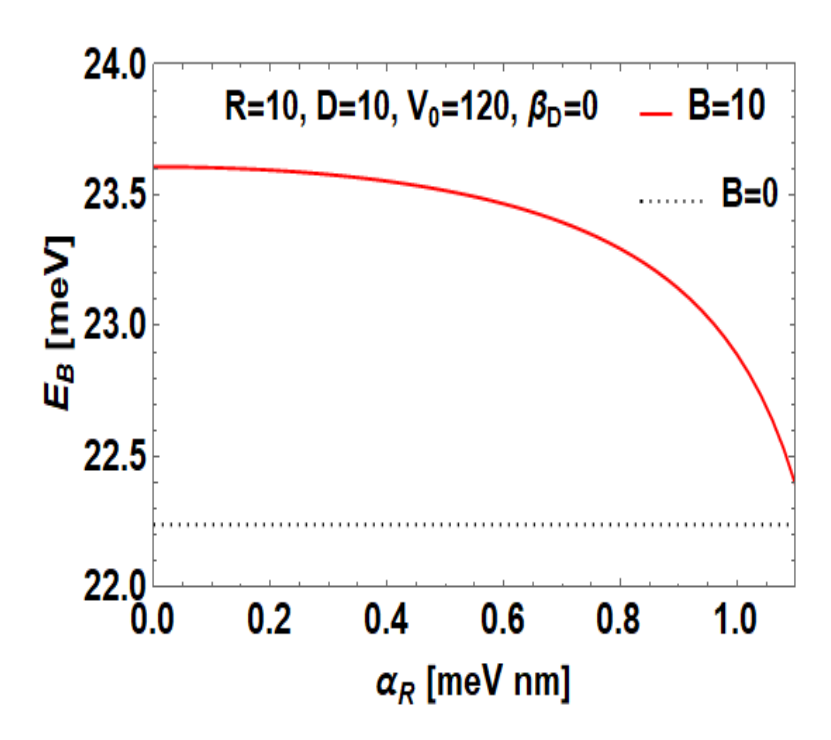


Fig. 15 E_B vs. α_R for an off-centre D^0 in a Gaussian GaAs QD with $\it R=10$ nm, $\it D=10$ nm, $\it V_0=120$ meV and $\it \beta_D=0$ nm-meV and for $\it B=0$ and $\it B=10$ T.

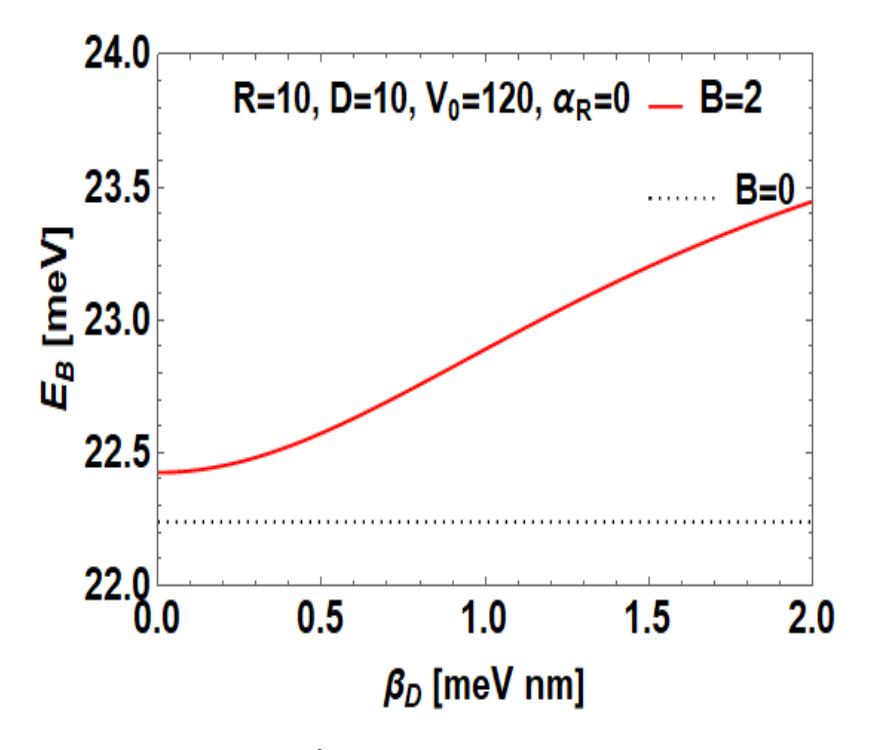


Fig. 16 E_B vs. β_D for an off-centre D^0 in a Gaussian GaAs QD with R=10 nm, D=10 nm, $V_0=120$ meV and $\alpha_R=0$ nm-meV for B=0 and B=2T.

In Fig. 14, we have shown the behaviour of E_B of an off-centre D^0 impurity in a GaAs GQD with respect to B for R=10 nm, D=1 $V_0=180$ and different values of α_R and β_D . As expected, E_B increases with B. We also see that DSOI increases E_B while RSOI increases it, as observed earlier. The BE of a system with of $\alpha_R=\beta_D$ is same of a system without SOIs.

In Figs. 15 and 16, we show directly the variation of BE as a function of α_R and β_D for R = 10, D = 10, $V_0 = 120$ for both B = 0 and $B \neq 0$ respectively. It is evident that BE decreases with the RSO parameter and increases with the DSO parameter in the presence of B and it is independent of SOIs in the case of B = 0.

Fig. 17 describes the behaviour of the magnetic moment (M) with respect to B for $V_0 = 300 meV$, D = 5, R = 10 nm and for a few combinations of α_R and β_D . The figure suggests that depending on the value of B and SOI constants, M can assume positive or negative values. For example, in the presence of DSOI alone, M is negative for all values of B. In fact, the negativity of M increases with the increase in B. At low B, M is positive in the presence of RSOI alone, but M decreases as B is increased and beyond a critical value of B, M undergoes a transition and becomes negative. For the same value of α_R and β_D , M is negative for all values of B.

In Fig. 18, we present the susceptibility (S) of an off-centre D^0 system against B for different combinations of RSOI and DSOI constants. In the absence of SOIs, the diamagnetic effect decreases with the increase in magnetic field and |S| reaches zero asymptotically. The behaviour is essentially similar in the presence of only DSOI. In the presence of RSOI alone, the magnitude of the susceptibility increases at lower magnetic field up to a critical field where |S| shows a minimum and after this the diamagnetic effect starts decreasing monotonically and |S| saturates to zero eventually with the rise in the magnetic field. The minimum in |S| occurs at the magnetic field where M changes sign from positive to negative. It is clearly visible that while DSOI decreases the diamagnetic effect, RSOI increases it. When $\alpha_R = \beta_D$, the opposite effects caused by RSOI and DSOI cancel each other and the result becomes same as the case where both RSOI and DSOI are absent. The S-B curve becomes independent of both B and SOIs at large B. The diamagnetic nature of D^0 is understandable from fundamental principles of physics. Indeed, it is easy to see that in the case of the ground state of the D^0 complex, if the electron's spin is not taken into account, the only contribution to susceptibility comes from the Larmour or Langevin diamagnetism.

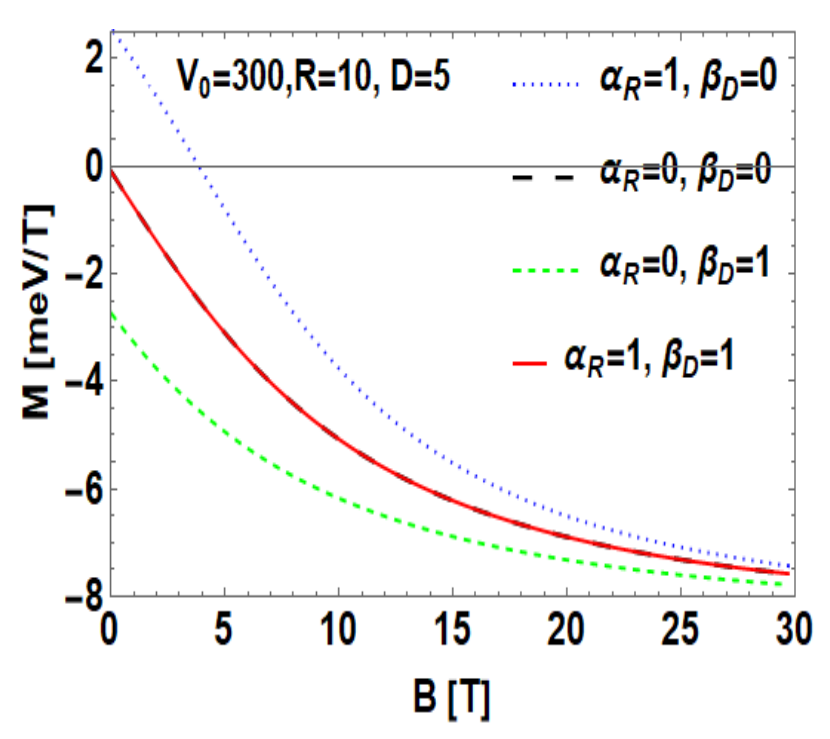


Fig. 17 *M* vs *B* for an off-centre D^0 in a Gaussian GaAs QD with $V_0 = 300$ meV, R=10 nm, D=5 nm for different values of α_R (nm-meV) and β_D (nm-meV).

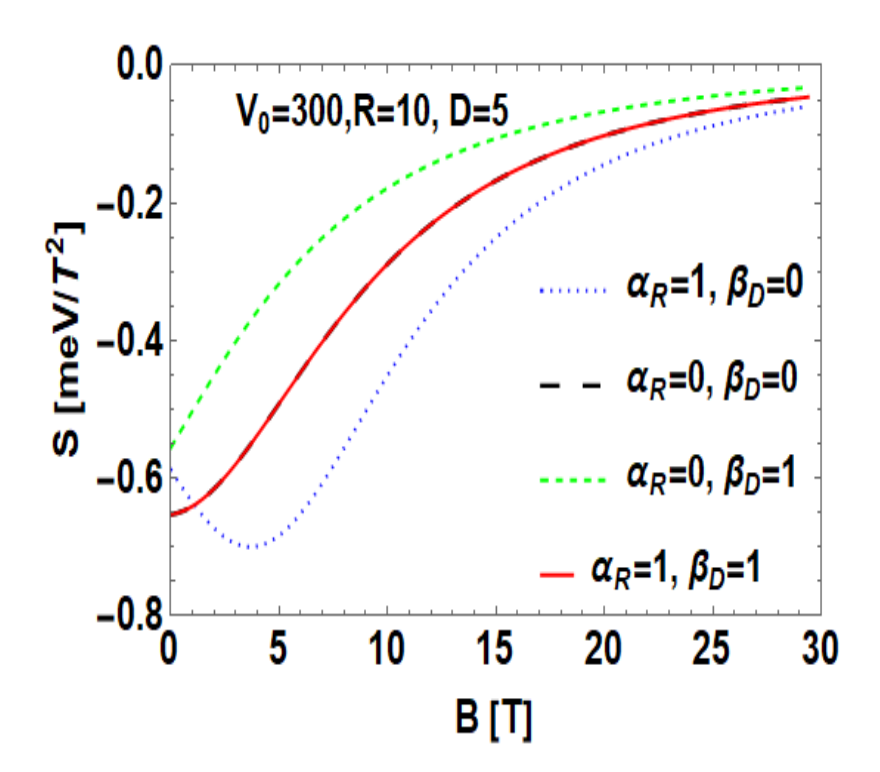


Fig. 18 *S* vs. *B* for an off-centre D^0 in a Gaussian GaAs QD with $V_0 = 300$ meV, R = 10 nm, D = 5 nm for different values of α_R (nm-meV) and β_D (nm-meV).

This is precisely what is happening here. If the spin of the electron is taken into account, the spin-Zeeman interaction would give rise to a paramagnetic effect which is commonly known as the Langevin paramagnetism.

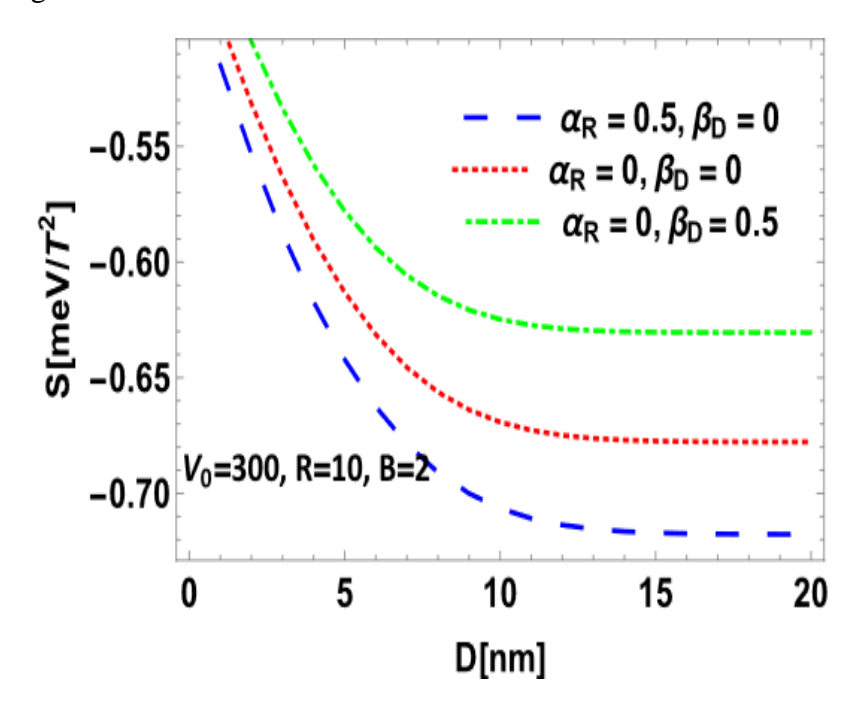


Fig. 19 *S* vs. *D* for an off-centre D^0 in a Gaussian GaAs QD with $V_0 = 300$ meV, R=10 nm, B=2T and for different values of α_R (nm-meV) and β_D (nm-meV).

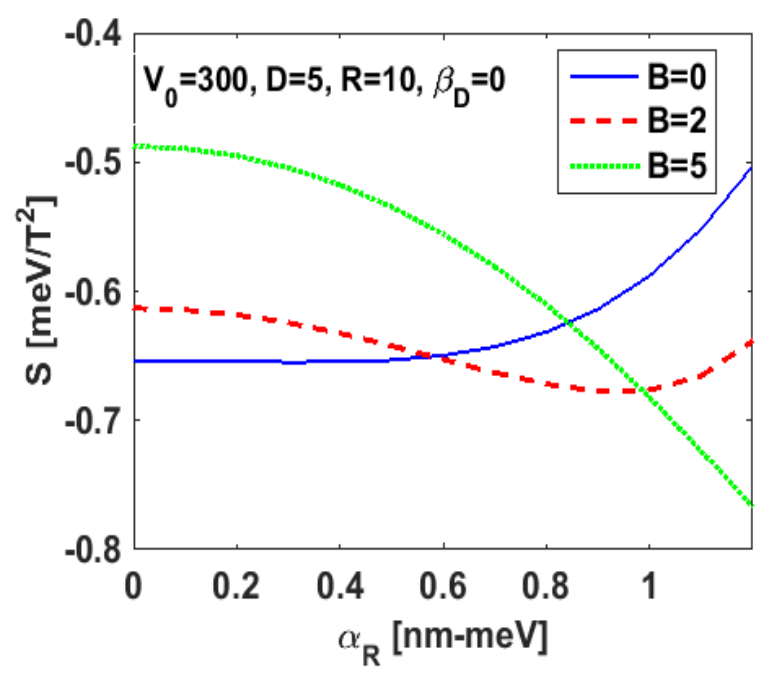


Fig. 20 S vs α_R for an off-centre D⁰ in a Gaussian GaAs QD with $V_0=300$ meV, D = 5 nm R = 10 nm and $\beta_D=0$ nm-meV for few values of B (T)

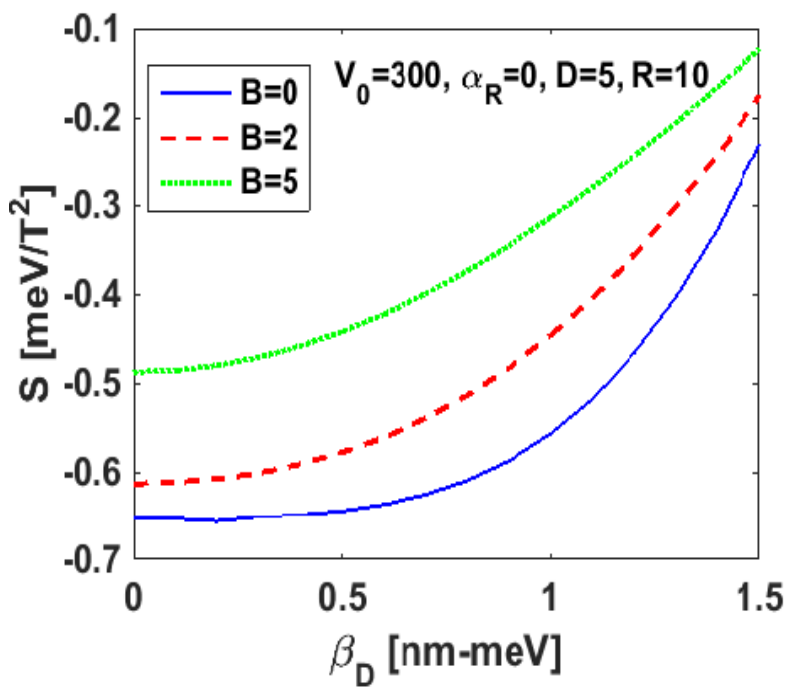


Fig. 21 *S vs.* β_D for an off-centre D⁰ in a Gaussian GaAs QD with $V_0 = 300$ meV, D = 5 nm R = 10 nm and $\alpha_R = 0$ nm-meV for few values of B (T).

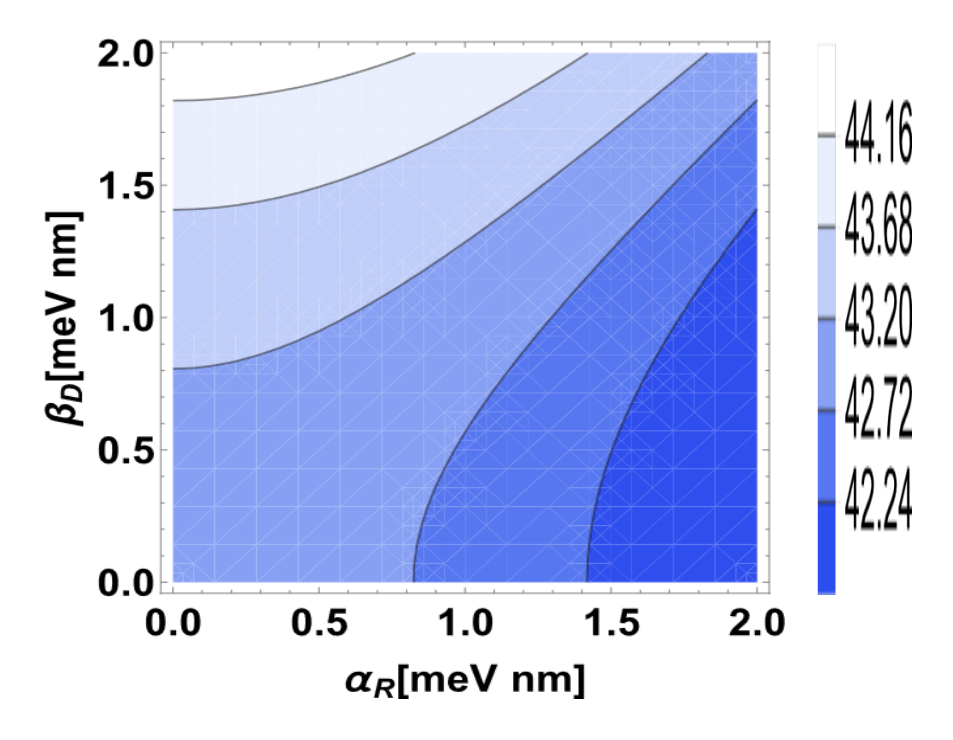


Fig. 22 Contour plot of the BE as a function of α_R and β_D for an off-centre D^0 in a Gaussian GaAs QD

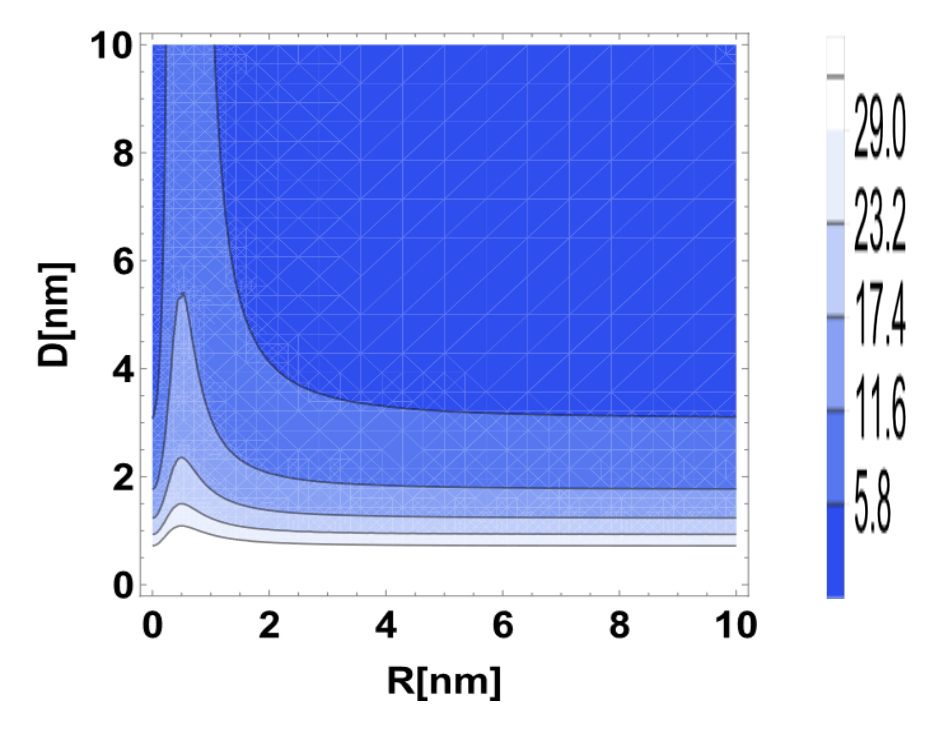


Fig. 23 Contour plot of BE as a function of R and D for an off-centre D^0 in a Gaussian GaAs QD.

Thus in the presence of the electron spin, there would be a competition between the two magnetic effects and the ground state magnetic susceptibility would depend on both the magnetic field and temperature.

Fig.19 shows how the susceptibility S varies with the impurity position D for $V_0 = 300$ meV, R = 10 nm, B = 2 T and for various combinations of Rashba and Dresselhaus parameters. One may note that as D is increased, |S| increases and finally reaches a saturation value.

We study the nature of the susceptibility with respect to RSOI and DSOI coefficients in Figs. 20 and 21 respectively for $V_0 = 300 \ meV$, $D = 5 \ nm$, $R = 10 \ nm$ and a few values of B. In case of B = 0, |S| is found to decrease with respect to both α_R and β_D . However, when the magnetic field is switched on, though |S| still decreases monotonically with β_D , with α_R it has an interesting behaviour. At small B, it first increases, then develops a broad hump-like structure and finally decreases, while at large B, it increases monotonically with α_R .

In Fig.22, we show the contour plot of BE for different combinations of α_R and β_D for $V_0 = 300 \, meV$, $R = 10 \, nm$, $B = 1 \, T$ and $D = 5 \, nm$. Black lines in the plot correspond to constant BE values. BE decreases from light blue region to dark blue region. BE is high at large values of β_D and small values of α_R . The contour plot of BE as a function of R and D for $V_0 = 300 \, meV$, $B = 1 \, T$, $\alpha_R = 1 \, mev \, nm$ and $\beta_D = 0$ is presented in Fig.23. BE decreases from the light blue to the dark blue region and the black lines are constant energy curves. So in general, for the same R, an increase in D decreases BE. The figure also shows that beyond a certain value of R, BE does not change much with R if D is fixed. At small R, however, there is a window of D-values for which BE is same.

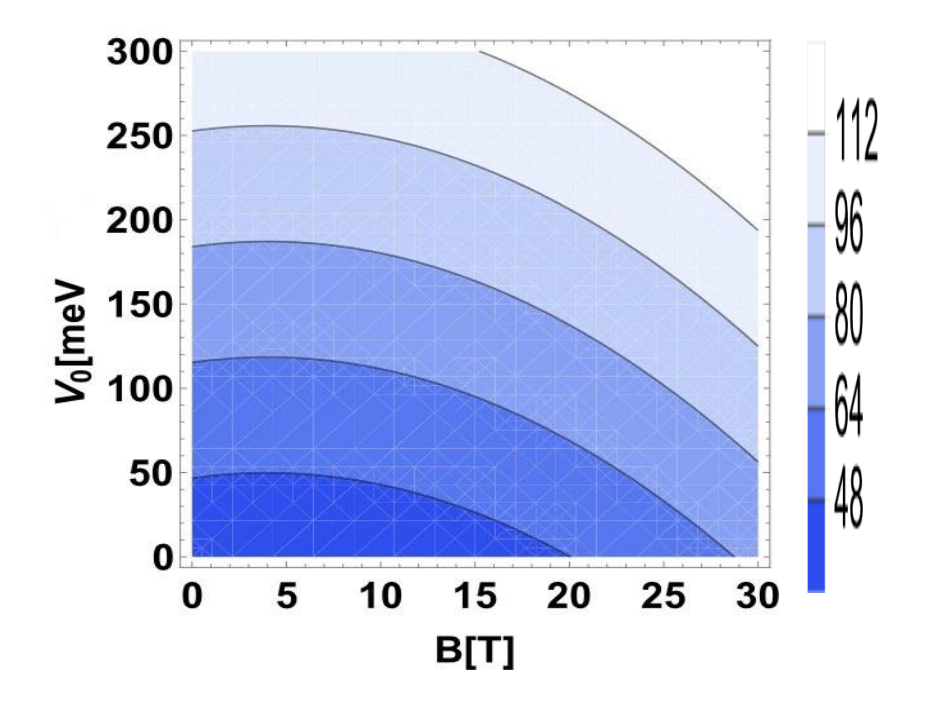


Fig. 24 Contour plot of the BE as a function of B and V_0 for an off-centre D^0 in a Gaussian GaAs QD.

Fig. 24 shows the contour plot of BE with respect to B and for V_0 with R=10 nm, D=5 nm, $\alpha_R=1$ mev-nm and $\beta_D=0$. BE increases from dark blue to light blue region and thus it is small at small values of B and V_0 and large at higher values of B and V_0 . In Figs. 25-27, we present the 3D plots of the BE as a function of different system parameters. Fig. 25 shows that BE decreases as α_R increases while it increases as β_D increases. Thus BE is maximum in a material with large β_D and small α_R . It is also observed that at equal values of α_R and β_D , BE is same as that in the absence of SOIs.

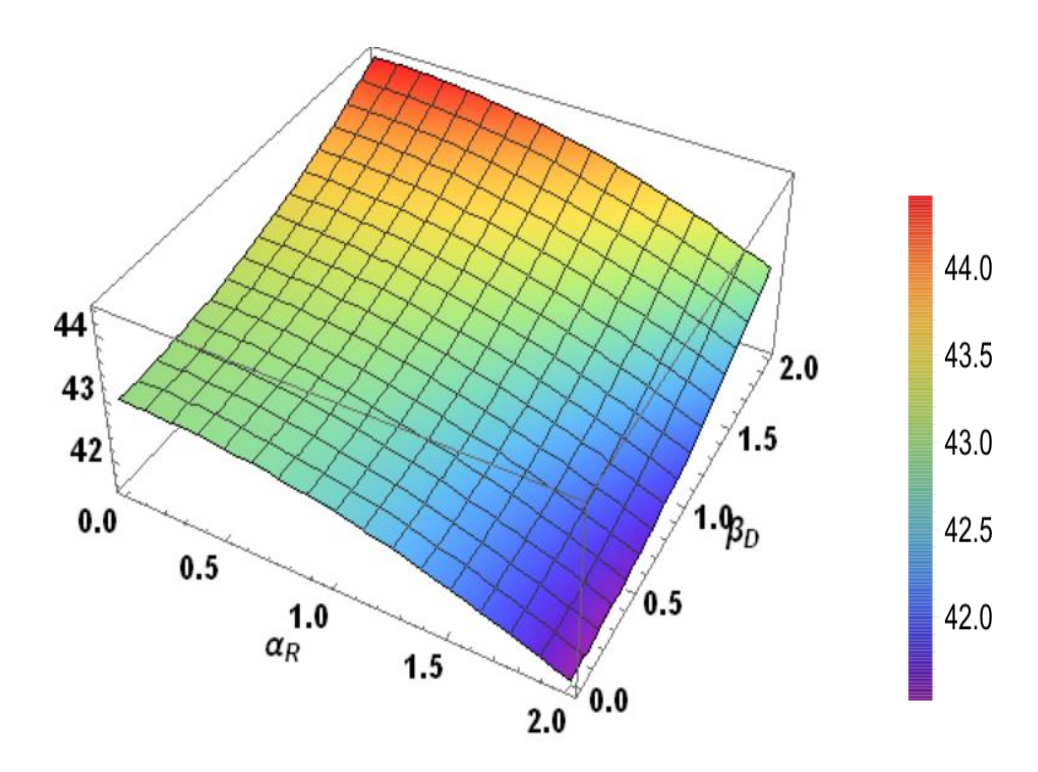


Fig. 25 3D plot of the BE as a function of $\alpha_R(nm-meV)$ and $\beta_D(nm-meV)$ for an off-centre D^0 in a Gaussian GaAs QD.

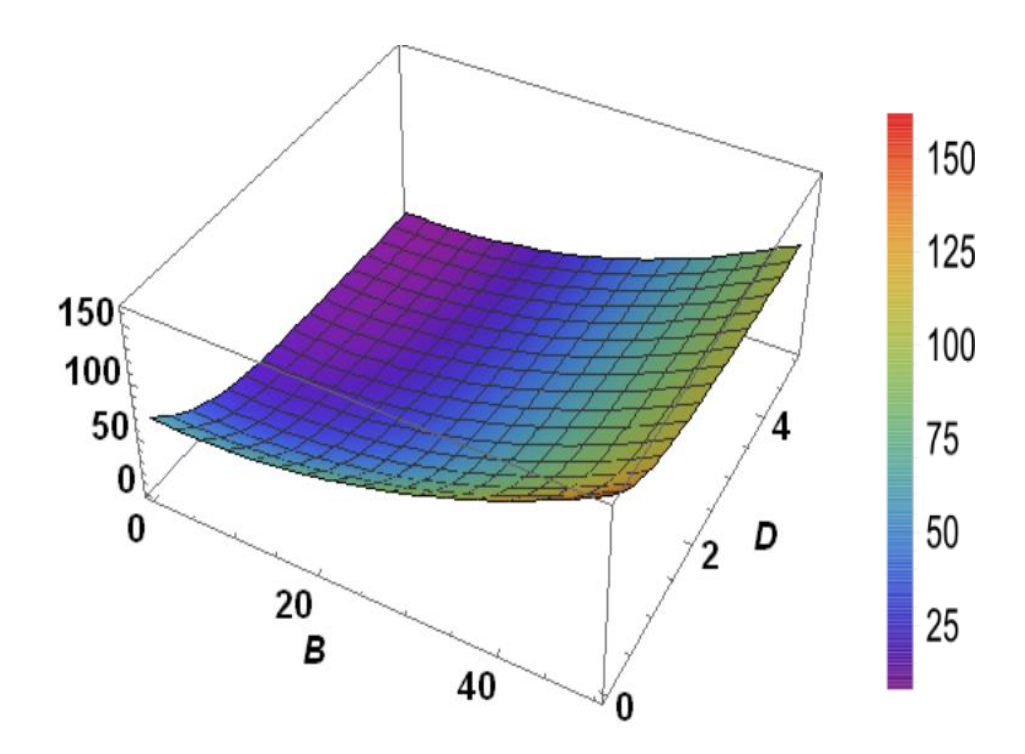


Fig. 26 3D plot of the BE as a function of B (T) and D (nm) for an off-centre D^0 in a Gaussian GaAs QD.

It is because in the presence of a magnetic field, the amount of BE enhanced by DSOI is same as that reduced by RSOI. Fig. 26 shows the plot of BE as a function of B and D for $V_0 = 300 \ meV$, $R = 10 \ nm$, $\alpha_R = 1 \ mev - nm$ and $\beta_D = 0$. The plot shows that BE increases as B increases and D decreases. The 3D curve given by Fig. 27 shows that BE can be large in a window of R values.

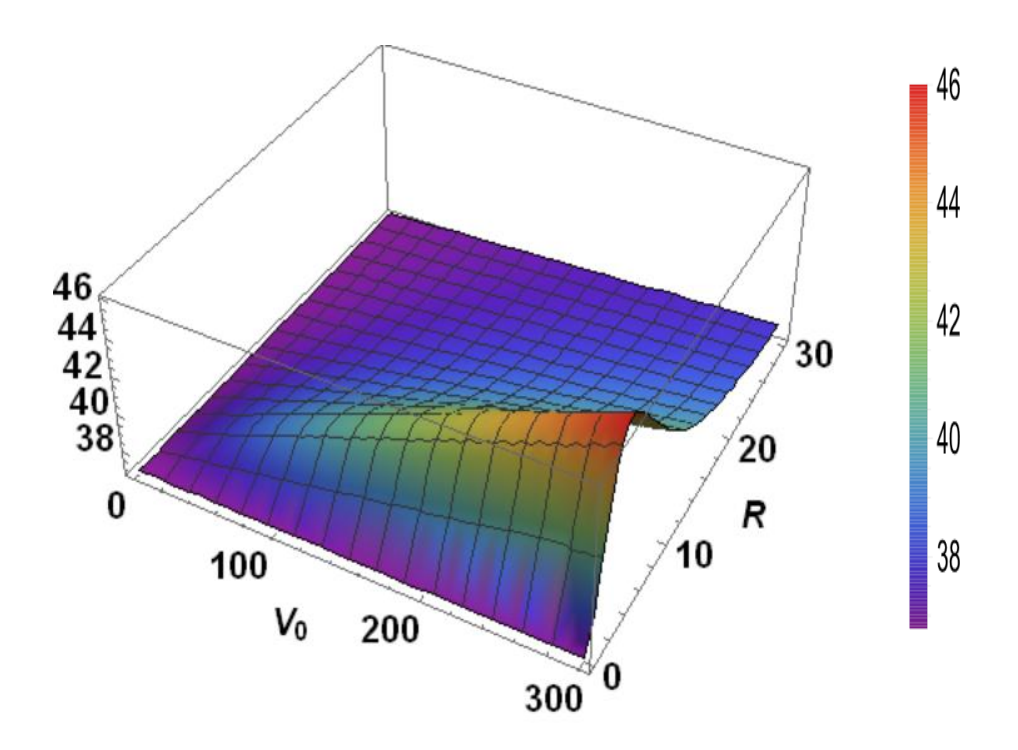


Fig. 27 3D plot of the BE as a function of $V_0(meV)$ and QD size R (nm) for an off-centre D^0 in a Gaussian GaAs QD.

3.4. Conclusion

In conclusion, an off-centre D^0 impurity is considered in a 2D Gaussian GaAs QD incorporating the effects of RSOI and DSOI and an external magnetic field and the GS BE of the system is calculated. It is shown that the binding of a D^0 complex is strongest for the on-centre complex (D=0) and BE decreases with increasing D and eventually saturates. Our results reveal that the effect of SOIs on the D-dependence of BE is very small, though magnetic field can influence the D-dependence of BE at small D values. However, if D is large, then none of R, B, α_R , or β_D would have any effect on the E_B vs D curve. We have also presented the contour plots and 3D plots of BE of the system with respect to different system parameters.

Finally, the susceptibility (S) of the off-centre D^0 in a GQD system is calculated using statistical mechanics. It is shown that S is diamagnetic. With increasing D, |S| initially increases and eventually saturates to a constant. It is observed that when RSOI is absent and only DSOI is present, |S| decreases both with β_D and B. However, in the case when DSOI is absent and only RSOI is present, at small values of B, |S| initially increases with increasing α_R , reaches a maximum and then decreases with α_R , but at large B, |S| increases monotonically with α_R .

3.5 References

- [1] D. Chandramohan, S. Balasubramanian, M. Tomak, Phys. Rev. B 37, 7102 (1988).
- [2] D. S. Chuu, C. M. Hsiao, and W. N. Mei, Phys. Rev. B 46, 7 (1992).
- [3] Y.P. Varshni, Superlattice. Microst. 23, 1 (1998).
- [4] Q. Xie, W. Hai and G. Chong, mod. Phys. Let. B 17, 1111 (2003).
- [5] B. Yuan-Peng and X. Wen-Fang, Commun. Theor. Phys. 50, 1449 (2008).
- [6] A. Boda and A. Chatterjee, Physica E 45, 36 (2012)
- [7] W.F. Xie, Phys. B Condens. Matter 407 1134 (2012).
- [8] R. Khordad, Int. J. Theor. Phys. 52,837 (2013).
- [9] A. Boda, B. Boyacioglu and A. Chatterjee, J. Appl. Phys. 114, 044311 (2013).
- [10] A. Boda, G. Madhusudhan, A. Chatterjee, Superlattice. Microst. 71 261 (2014).
- [11] N. Porras-Montenegro and S. T. Pérez-Merchancano, Phys. Rev. B 46, 9780 (1992).
- [12] N. Porras-Montenegro, S. T. Pérez-Merchancano, and A. Latgé, J. Appl. Phys. 74, 7624 (1993).
- [13] J. L. Zhu and X. Chen, Phys. Rev. B 50, 4497 (1994)
- [14] J. L. Zhu and X. Chen, J. Phys.: Condens. Matter 6, L123 (1994).

- [15] Z. Y. Deng, J. K. Guo, and T. R. Lai, J. Phys.: Condens. Matter 6, 5949 (1994).
- [16] H. Paredes-Gutiérrez, J. C. Cuero-Yépez, and N. PorrasMontenegro, J. Appl. Phys. 75, 5150 (1994).
- [17] Z. Xiao, J. Zhu, and F. He, J. Appl. Phys. 79, 9181 (1996).
- [18] C.A. Duque, A. Montes, N. Porras-Montenegro and L.E. Oliveira, Semicond. Sci. Technol. 14, 496 (1996).
- [19] Z. Xiao, J. Zhu and F. He, Superlattice Microstruct. 19, 137 (1996).
- [20] J. Silva-Valencia and N. Porras-Montenegro, J. Appl. Phys. 81, 901 (1997).
- [21] C. Bose, J. Appl. Phys. 83, 3089 (1998).
- [22] A. Corella-Madueño, R. Rosas, J. L. Marín, and R. Riera, J. Appl. Phys. 90, 2333 (2001).
- [23] H. Ham and H. N. Spector, J. Appl. Phys. 93, 3900 (2003).
- [24] I. F. I. Mikhail and I. M. M. Ismail, Phys. stat. sol. (b) 244, 3647 (2007)
- [25] R.L.M. melono, D. Dobgima and O. Motapon Candian journal of phys. 96 (2018).
- [26] C. Bose and C.K. Sarkar, Physica B 253, 238 (1998).
- [27] C. Bose, Physica E 4, 180 (1999).
- [28] J. L. Movilla and J. Planelles, Phys. Rev. B 71 075319 2005.
- [29] J. H. Yuan, C. Liu, Physica E 41, 41 (2008).
- [30] Y. J. Hui, H. J. Sheng, Y. Miao, Z. Q. Jun and Z. J. Pei, Commun. Theor. Phys. 54 369 (2010)
- [31] E. Sadeghi, A. Avazpour, Physica B, 406, 241 (2011).
- [32] Z. Avazzadeh, H. Bahramiyan, R. khordad, S.A. Mohammadi, Eur. Phys. J. Plus 131, 121 (2016).
- [33] S. wang, G. Wei, G. Yi, Internat. J. mod. Phys 22, 22 (2010).
- [34] A. Boda, A. Chatterjee, J. Nanosci. and Nanotech. 15, 6472 (2015).
- [35] M. H. Tanhaei, G. Rezaei, Superlattice Microstruct. 98, 29 (2016).

Chapter ~4

Effect of confinement potential shape and Spin-Orbit Coupling on the D^0 Impurity in a GaAs quantum dot placed in a magnetic field

4.1 Introduction

One of most important parameters for a quantum dot (QD) system from a theorist's point of view is the confinement potential. QDs can be fabricated in different shapes and sizes to have certain required properties. The nature of the confinement potential in a QD depends on the shape of QD, gate voltage, lateral voltage and on the fields applied from outside. Motivated by some early experiments and generalized Kohn's theorem, several investigations have been carried out in the past considering the potential in QD as parabolic [1]. Later investigations have suggested that the confinement potential in a QD is generally anharmonic and has a finite depth. This has led to a large number of studies on QDs using Gaussian confinement potential [2]. Such a QD can be called a Gaussian QD (GQD).

Recently, Ciurla et. al. [3] have proposed a more generalized confinement potential namely, the power-exponential potential (PEP) given by

$$V(\boldsymbol{\rho}) = -V_0 e^{-\left(\frac{\rho}{R}\right)^p},\tag{4.1}$$

where V_0 measures the depth of the potential, R its range and p can be called the steepness parameter which describes the hardness of the confinement potential. The higher the value of p, the harder the potential at the boundary. One important advantage with PEP is that it can lead to

different confinement potentials in different limits. For p = 2, we get the Gaussian potential and confinement potential is soft, i.e. the electron can partially penetrate through the potential well. As p increases, the probability of the electron tunneling becomes smaller. For large p, the PEP mimics the rectangular well and becomes hard [3]. Fig. 1 shows the form of PEP for different values of p.

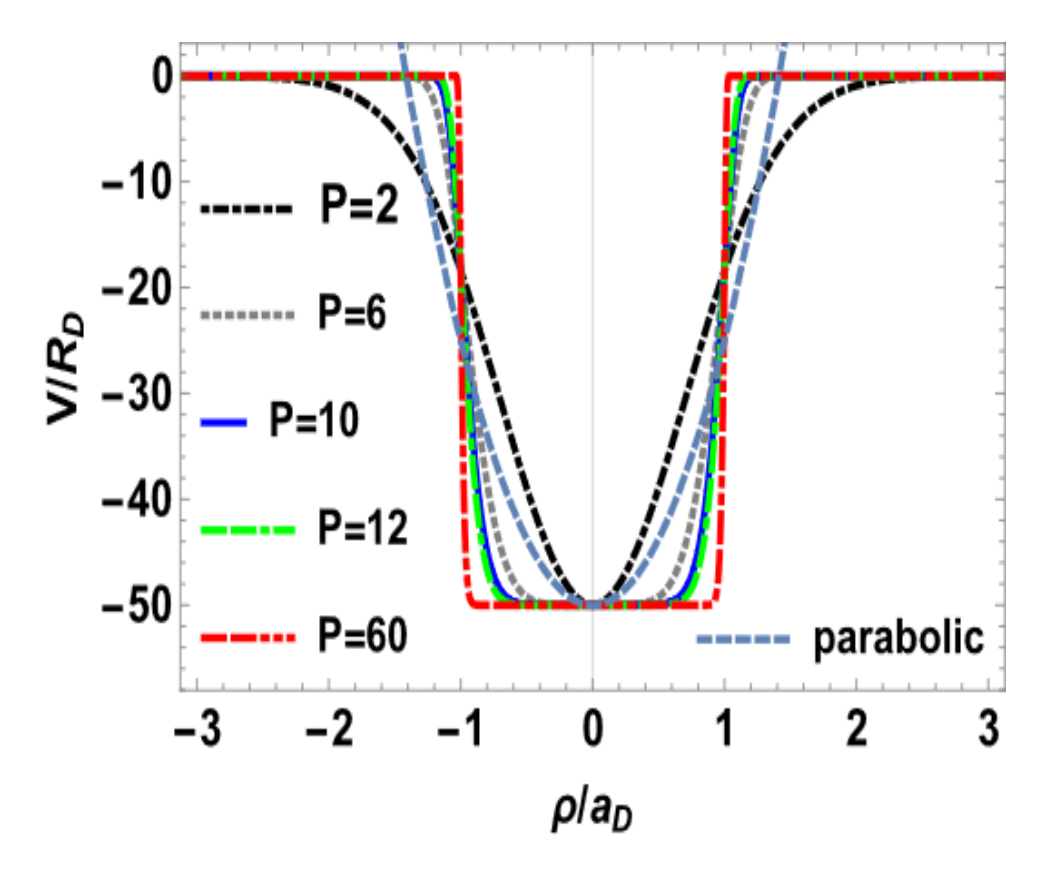


Fig.1. Power-exponential potential for p = 0.5, 2, 5, 30, 100 and comparison with a parabolic potential.

Ciurla et al. [3] have studied the spectra of this potential and its applicability as a confinement potential. Hereafter, QDs with power exponential confinement potential will be referred to as PEQD. Xie [4] has studied the effect of the shape of the confinement potential on photoionization cross section of a D^0 impurity in a QD using the power-exponential potential (PEP). Jahan at el. [5] have recently investigated the effect of the shape of the confinement potential on the electronic, magnetic thermodynamic and transport properties of a GaAs QD at finite temperature.

The spin-orbit interaction (SOI) effects are also important in a QD. Khordad [6] has studied the diamagnetic susceptibility of a hydrogenic impurity in a quantum pseudo-dot in the presence of SOI with harmonic potential. Kumar at el. [7] have investigated the effect of Rashba SOI on the GS energy of a D^0 centre in a GQD of GaAs. Saini et. al. [8] have studied the effect of RSOI and DSOI on the susceptiblity of a D^0 impurity in GQD placed in an external magnetic field. In previous chapters, we have presented these works.

In the present chapter, we shall study the effect of the shape of the confinement potential on the properties of a D^0 complex in a PEQD the presence of both RSOI and DSOI and an external magnetic field. We shall calculate, in particular, the GS energy (GSE), binding energy (BE), magnetic moment (MM) and the magnetic susceptibility (MS) of the D^0 complex.

4.2 Theory

The Hamiltonian of a D^0 complex in a 2D PEQD system with RSOI and DSOI and placed in a magnetic field \mathbf{B} (0,0, B) can be written as

$$\mathcal{H} = \left(\frac{1}{2m^*}(\boldsymbol{p} + \frac{e}{c}\boldsymbol{A})^2 - \frac{e^2}{\varepsilon\rho} - V_0 e^{-\left(\frac{\rho}{R}\right)^p}\right) I + \frac{\alpha_R}{\hbar} \left[\boldsymbol{\sigma} \times \left(\boldsymbol{p} + \frac{e}{c}\boldsymbol{A}\right)\right]_Z$$
$$+ \frac{\beta_D}{\hbar} \left[\boldsymbol{\sigma}_x \left(\boldsymbol{p}_x + \frac{e}{c}\boldsymbol{A}_x\right) - \boldsymbol{\sigma}_y \left(\boldsymbol{p}_y + \frac{e}{c}\boldsymbol{A}_y\right)\right], \tag{4.2}$$

where all the notations have already been defined.

To eliminate SOIs, we apply as before, the unitary transformation

$$U = e^{S} \quad , \qquad S = i \frac{m^*}{\hbar^2} \left[\alpha_R (y \sigma_x - x \sigma_y) + \beta_D (x \sigma_x - y \sigma_y) \right], \tag{4.3}$$

on the Hamiltonian. The transformed Hamiltonian can be written as,

$$\widetilde{\mathcal{H}} = e^{S} \mathcal{H} e^{-S} = \mathcal{H} + [S, \mathcal{H}] + \frac{1}{2} [S, [S, \mathcal{H}]] + \cdots \qquad (4.4)$$

Straight-forward calculation yields

$$[S,H] = -\frac{\alpha_R}{\hbar} \left[\sigma_x \left(p_y + \frac{e}{c} A_y \right) - \sigma_y \left(p_x + \frac{e}{c} A_x \right) \right] - \frac{2 m^*}{\hbar^2} (\alpha_R^2 + \beta_D^2)$$

$$-\frac{\beta_D}{\hbar} \left[\sigma_x \left(p_x + \frac{e}{c} A_x \right) - \sigma_y \left(p_y + \frac{e}{c} A_y \right) \right] - \frac{m^*}{\hbar^3} \omega_c \sigma_z L_z \rho^2 (\alpha_R^2 - \beta_D^2)$$

$$-\frac{2}{\hbar^3} m^* \sigma_z L_z (\alpha_R^2 - \beta_D^2) , \qquad (4.5)$$

$$\frac{1}{2}[S,[S,\mathcal{H}]] = \frac{m^*}{\hbar^2}(\alpha_R^2 + \beta_D^2) + \frac{m^*}{2 \,\hbar^3} \omega_c \sigma_z L_z \rho^2 (\alpha_R^2 - \beta_D^2) + \frac{m^*}{\hbar^3} \sigma_z L_z (\alpha_R^2 - \beta_D^2), \tag{4.6}$$

and the transformed Hamiltonian is given by

$$\widetilde{\mathcal{H}} = \left(\frac{p^2}{2m^*} + \frac{1}{8}m^*\omega_c^2\rho^2 - \frac{e^2}{\varepsilon r} - V(\vec{\rho})\right)I - \frac{m^*}{\hbar^2}(\alpha_R^2 + \beta_D^2)I - \frac{m^*}{\hbar^3}(\alpha_R^2 - \beta_D^2)\sigma_Z L_Z + \frac{\omega_c}{2}L_Z - \frac{m^*}{2\hbar^3}(\alpha_R^2 - \beta_D^2)\omega_c\sigma_Z\rho^2,$$
(4.7)

where $\omega_c=(eB/m^*c)$, $\rho^2=(x^2+y^2)$ and $L_z=-i\hbar(\partial/\partial\phi)$.

We wish to obtain GSE of D^0 by the Ritz variational principle and choose the trial wave function as

$$\psi(\boldsymbol{\rho}) = N e^{(-\alpha \rho^2 - \beta \rho - im\varphi)}. \tag{4.8}$$

Denoting GSE of the electron in PEQD by $E(e^-)$, GSE of the D^0 complex in the same system by $E(D^0)$ and BE of the D^0 complex by $E_B(D^0)$, we can write, as before, the binding energy of the D^0 complex as

$$E_B(D^0) = E(e^-) - E(D^0).$$
 (4.9)

The magnetic moment (M) and the magnetic susceptibility (S) of the of the D^0 complex are given by

$$M = -\frac{\partial E(D^0)}{\partial R}; \qquad S = \frac{\partial^2 E(D^0)}{\partial R^2} . \tag{4.10}$$

4.3 Numerical Results and Discussion

We use meV as the unit of energy, nm as the unit of length, and T (Tesla) as the unit of magnetic field. SOIs are then given in meV - nm. For concreteness, we shall apply our results to a GaAs QD for which $m^* = 0.067 m_0$, where m_0 is the bare electron mass and $\epsilon = 12.4 \epsilon_0$ [4,14].

Fig. 2 shows the behavior of the wave function as a function of ρ for different values of the parameter p (with B=1T, $V_0=120$ meV, R=10 nm, $\alpha_R=1$, $\beta_D=1$). Interestingly, the wave functions show a crossing behavior with respect to p.

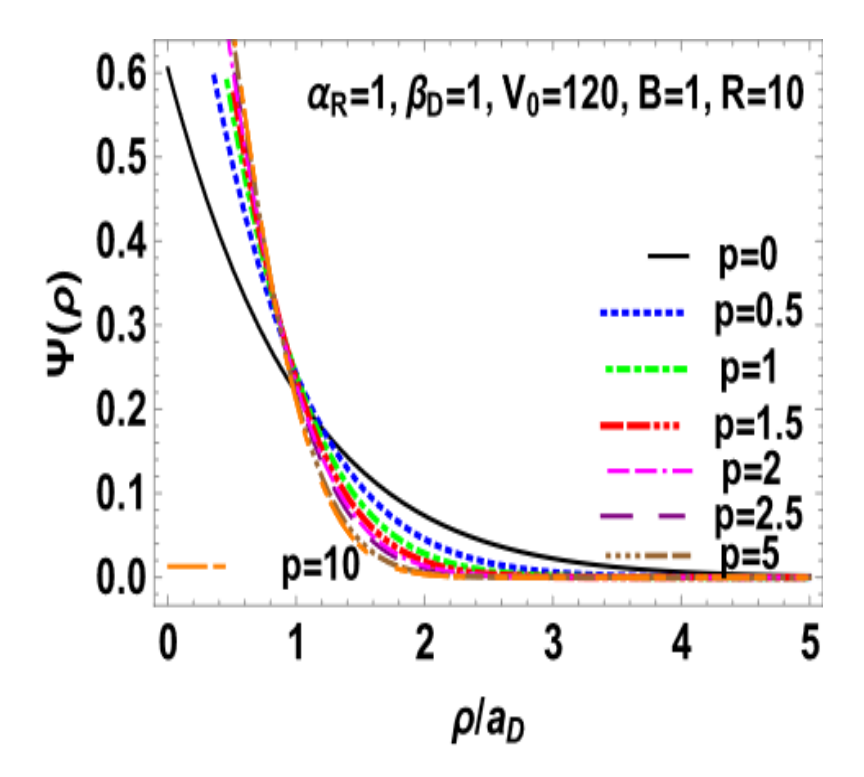


Fig. 2 The GS Wave-function vs ρ for a D^0 centre in a GaAs GQD with B=1 T, $V_0=120$ meV, R=10 nm, $\alpha_R=1$ meV – nm and $\beta_D=1$ meV – nm for a few different values of p.

In Fig.3, we plot GSE of a D^0 donor $E(D^0)$ in a GaAs QD with respect to the steepness parameter p in the absence of RSOI and DSOI, in the presence of either of them, and in the presence of both. In all cases, GSE decreases as p increases but eventually saturates as p becomes large. One can also observe that both RSOI and DSOI lower the energy, DSOI having a larger effect.

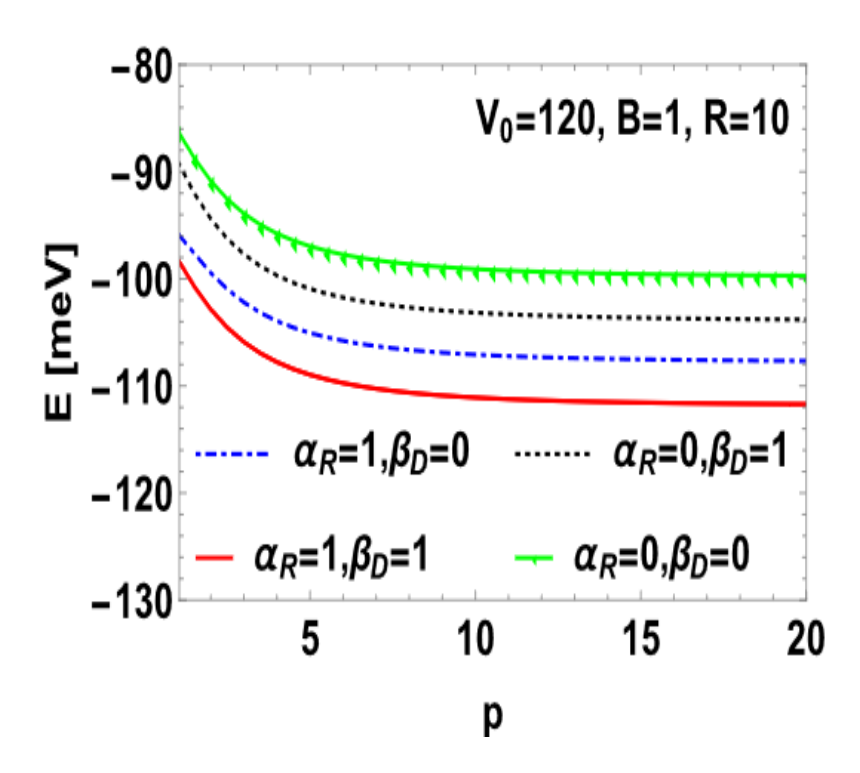


Fig. 3 GSE (E) vs p for a D^0 centre in GaAs GQD with $V_0 = 120$ meV, B = 1 T, R=10 nm, for different values of α_R (meV – nm) and β_D (meV – nm).

In Fig. 4, we plot GSE of a D^0 donor $E(D^0)$ in a GaAs QD with respect to the steepness parameter p for B=1 T, $V_0=120$ meV, $\alpha_R=1$, $\beta_D=1$ and for different values of R. We observe that for $R \leq 8$, GSE initially increases with p but eventually reaches a saturation value as p becomes sufficiently large, while for $R \geq 8$, GSE initially decreases with increasing p and eventually reaches a saturation value for large p. For $R \approx 8$, GSE is almost independent of p. Fig. 5 shows the variation of GSE with respect to R for different values of p. It is clearly evident that GSE decreases as R increases, and saturates to the bulk value as R becomes large. At small R, GSE increases quite rapidly with decreasing R. This can of course be easily explained by simple quantum mechanics.

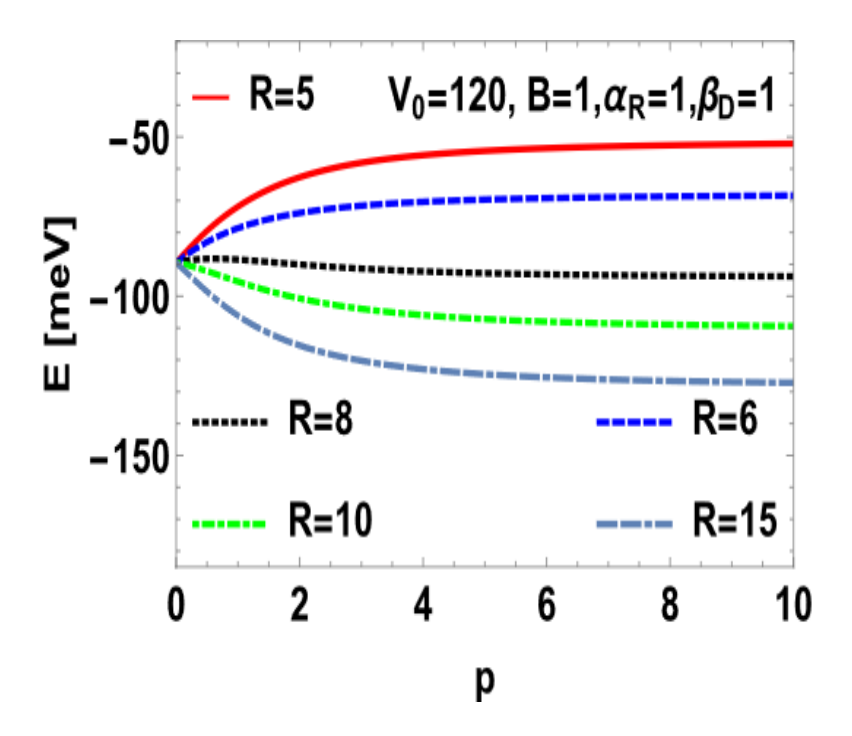


Fig. 4 E vs p for a D^0 centre in GaAs GQD with $V_0 = 120$ meV, B = 1 T, $\alpha_R = 1$ meV nm and $\beta_D = 1$ meV nm for different values of R (nm).

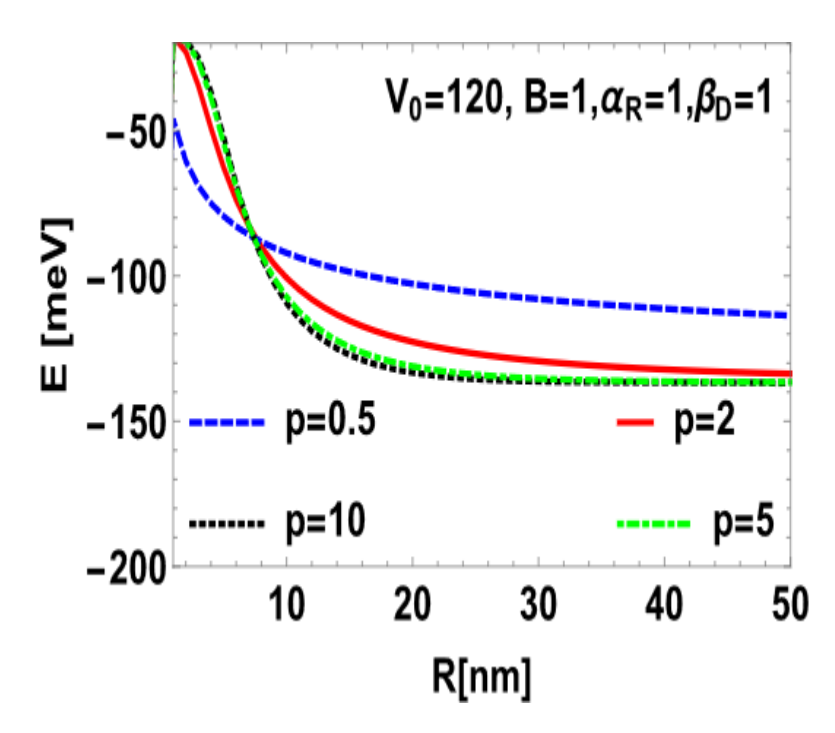


Fig. 5 E vs R for a D^0 centre in GaAs GQD with $V_0 = 120$ meV, B = 1 T, $\alpha_R = 1$ meV nm and $\beta_D = 1$ meV nm for different values of p.

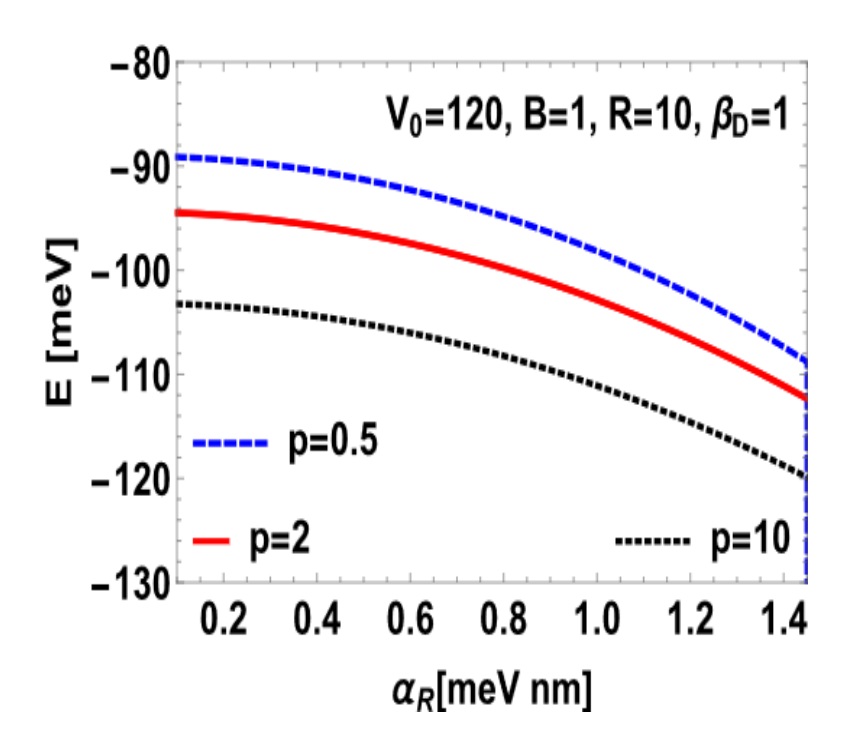


Fig. 6 E vs α_R for a D^0 centre in GaAs GQD with $V_0 = 120$ meV, B = 1 T, R = 10 nm, and $\beta_D = 1$ meV nm for three values of p.

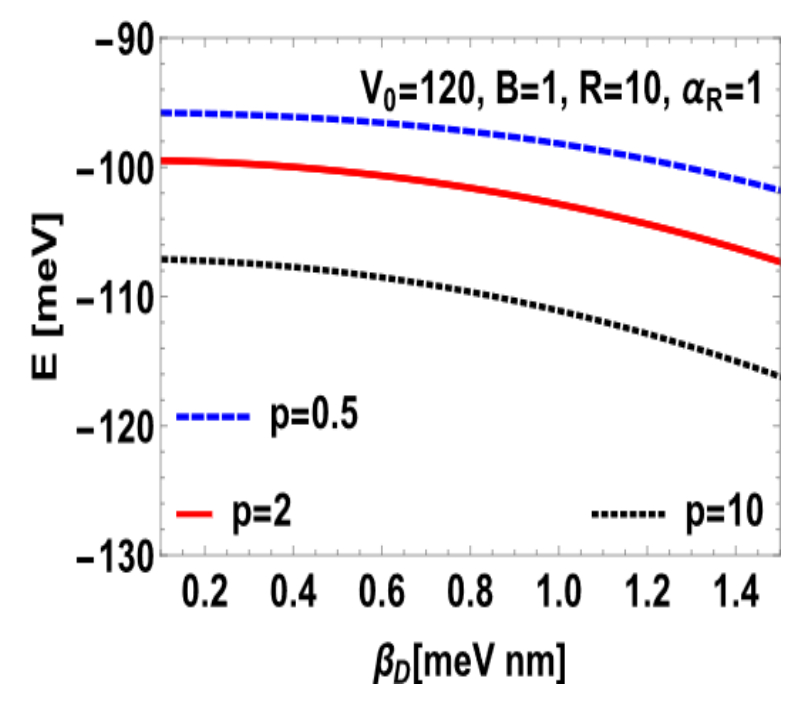


Fig. 7 E vs β_D for a D^0 centre in GaAs GQD with $V_0 = 120$ meV, B = 1 T, R = 10 nm, and $\alpha_R = 1$ meV nm for three values of p.

In Figs. 6 and 7, we show the variation of GSE E as a function of α_R and β_D respectively for a few values of p with B=1 T, $V_0=120$ meV and R=10 nm. GSE is found to decrease with increase in both α_R and β_D . But the decrease in GSE with respect to β_D is slower than that with respect to α_R . In other words, the Rashba term reduces GSE more than the Dresselhaus term and thus has a stronger effect in a QD.

Fig. 8 depicts the behavior of BE as a function of p for different values of R with B=1T, $V_0=120$ meV, $\alpha_R=1$, and $\beta_D=1$. According to our result, BE E_B is positive for D^0 system in GaAs which implies that in a GaAs QD, D^0 always exists in a stable bound state, which is of course an expected result. At small p, BE is almost linear in p. One interesting observation that one can make from this figure is that for a small QD, BE as a function of p shows a peak. The peak broadens in width and shifts towards higher values of p as p increases. Beyond a certain values of p, BE does not exhibit any peak with respect to p. For higher values of p, BE just increases with p monotonically and eventually saturates.

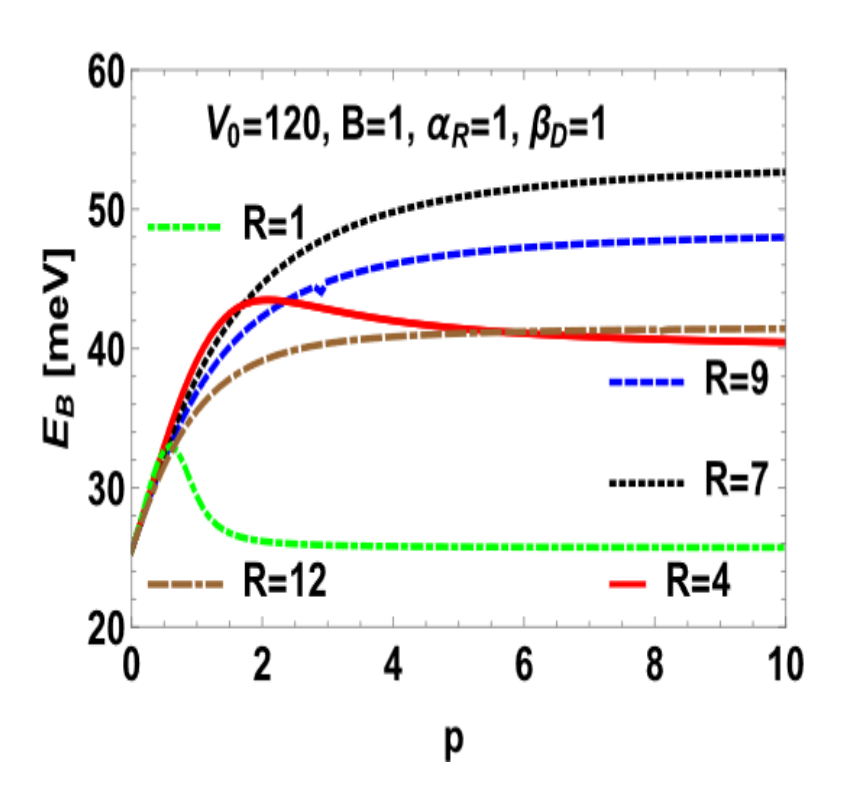


Fig. 8 BE (E_B) vs. p for a D^0 centre in GaAs GQD with $V_0 = 120$ meV, B = 1 T, $\alpha_R = 1$ meV nm and $\beta_D = 1$ meV nm for different values of R (nm).

The behaviour of BE with respect to R is shown explicitly in Fig. 9. One can see that BE increases as R decreases and becomes maximum at a critical value of R below which BE rapidly decreases. Again this behaviour is consistent with quantum mechanics. If R is very small, then the uncertainty in position is also small and the uncertainty in momentum as well as in kinetic energy must be large. In this case, it would be very difficult to localise the electron inside the QD and concomitantly BE would decrease rapidly. One can see from the figure that the peak height of BE increases as p increases. Also the peak position changes with p. After the maximum, BE decreases with R faster for higher p giving rise to a crossing behaviour. The BE graph crossing each other at different value of p. The reason of that the wavefunction is also crossing each other at different value of p.

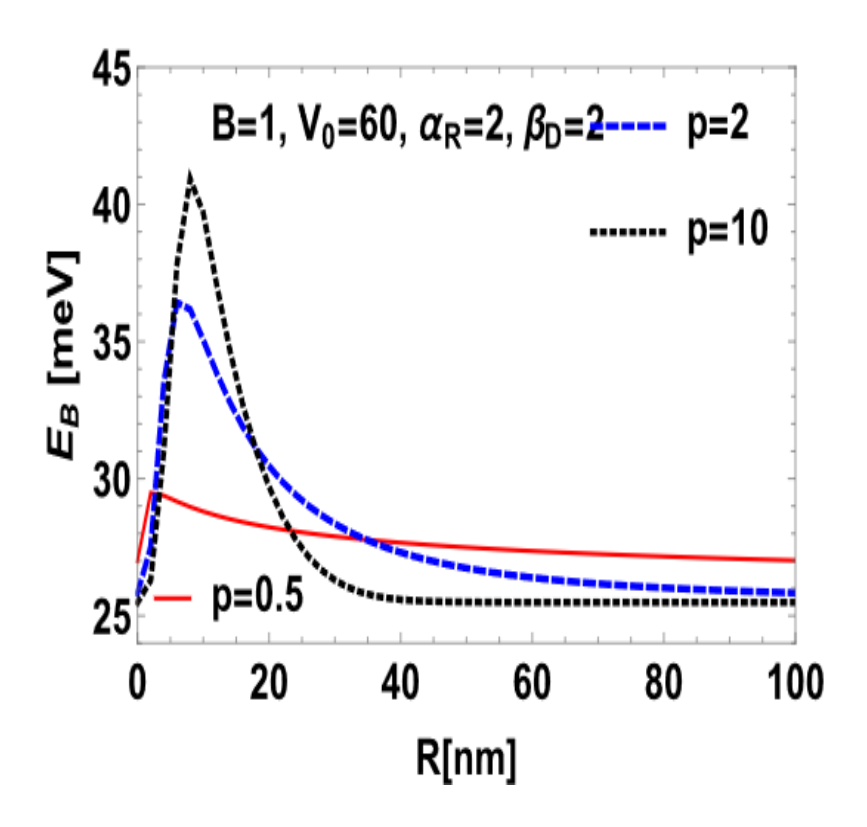


Fig. 9 E_B vs. R for a D^0 centre in GaAs GQD with B=1 T, $V_0=60$ meV, $\alpha_R=2$ meV nm and $\beta_D=2$ meV nm for different values of p.

In Fig. 10, we present the variation of our results for the GS BE (E_B) with B. From the figure, E_B is found to increase with B. It is clear that the shape of the confinement potential plays an important role at small B, while at large B, E_B does not have much significant dependence on p.

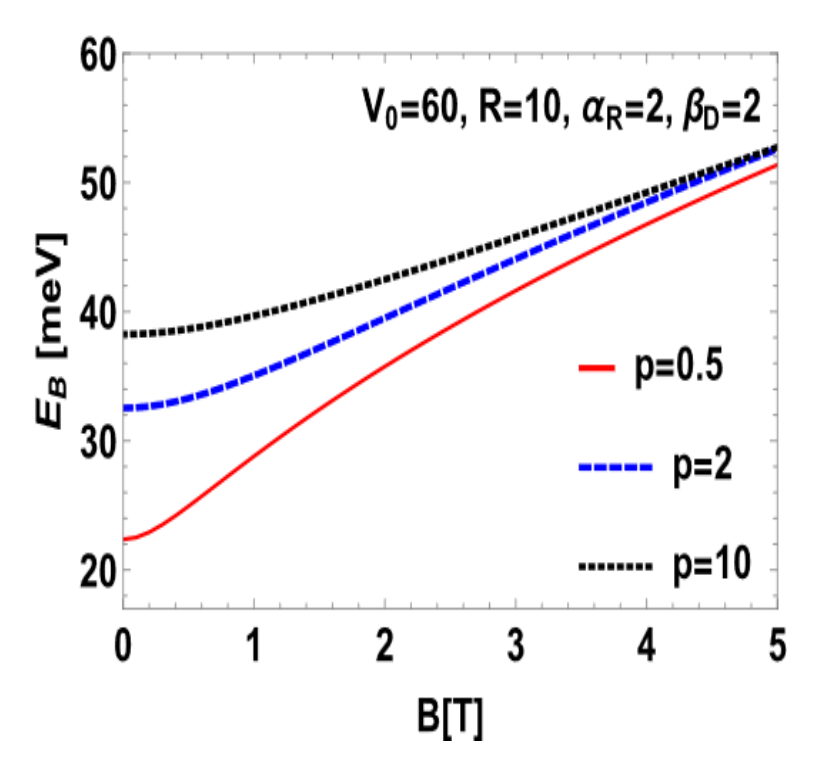


Fig. 10 E_B vs. B for a D^0 centre in GaAs GQD with R=10 nm, $V_0=60$ meV, $\alpha_R=2$ meV nm and $\beta_D=2$ meV nm and for different values of p.

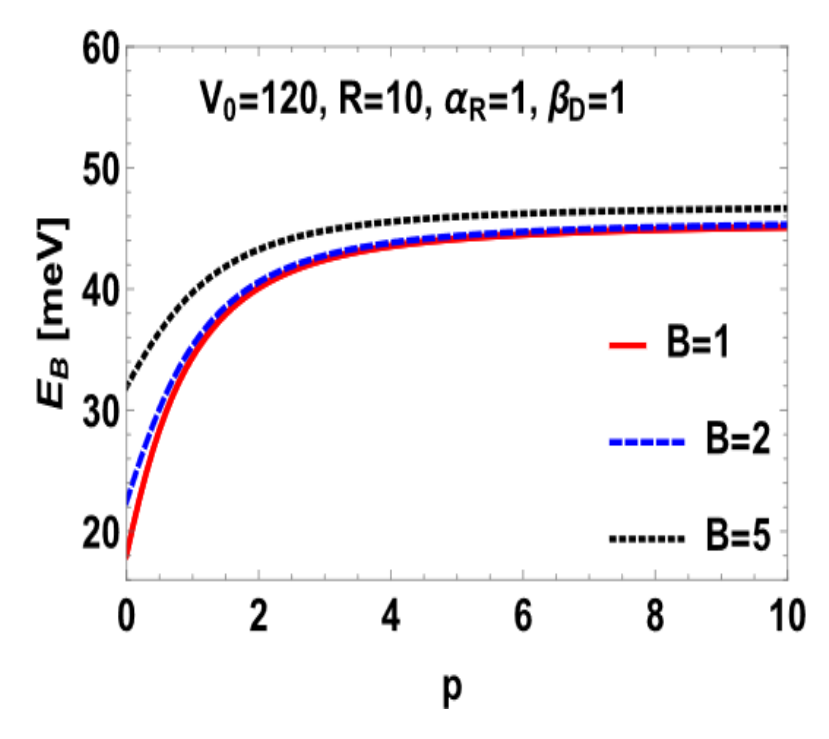


Fig. 11 E_B vs. p for a D^0 centre in GaAs GQD with $V_0 = 120$ meV, R = 10 nm, $\alpha_R = 1$ meV nm and $\beta_D = 1$ meV nm for different values of B (T).

In Fig. 11, we plot BE as a function of p for three different value of B with R = 10nm, $V_0 = 120$ meV, $\alpha_R = 1$ and $\beta_D = 1$ to show the explicit p-dependence of BE for different values of B. One can see that BE increases rapidly with p at small p and seems to saturate at p increases. Also the MF-dependence is significant only low p.

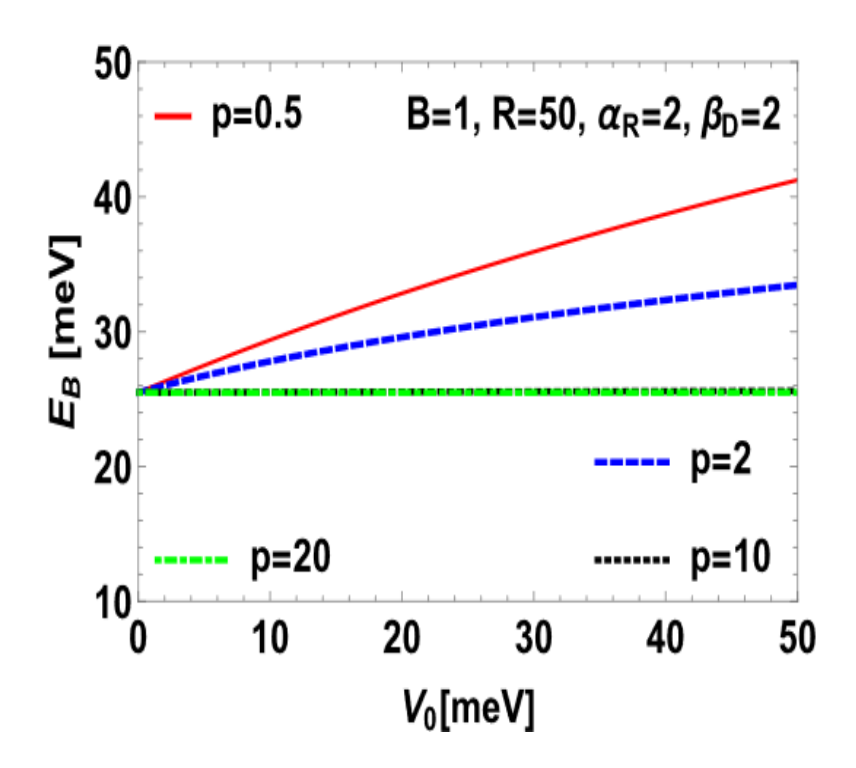


Fig. 12 E_B vs. V_0 for a D^0 centre in GaAs GQD with B = 1 T, R = 50 nm, $\alpha_R = 2$ meV nm and $\beta_D = 2$ meV nm for different values of p.

Figs. 12 and 13 show the variation of BE as a function of V_0 . Fig. 12 gives the results for R=50, while the results for R=10 are plotted in Fig. 13. Fig. 12 suggests that the binding increases with V_0 for p=0.5 and p=2 while for p=10 and p=20, BE is essentially independent of V_0 . For large p, the confinment potential becomes more or less like a square well potential and then any change in p does not change the potential much and therefore in that limit E_B becomes almost independent of p. Again we observe that the shape of the confinement potential plays a more important role for large values of V_0 which is of course an expected behaviour because as the depth of the potential increases, binding becomes stronger. Fig. 13 shows that a decrease in QD size in general enhances BE. One can see that even for p=10 and 20, BE now increases with V_0 , though the E_B vs V_0 — curves for these cases coincide.

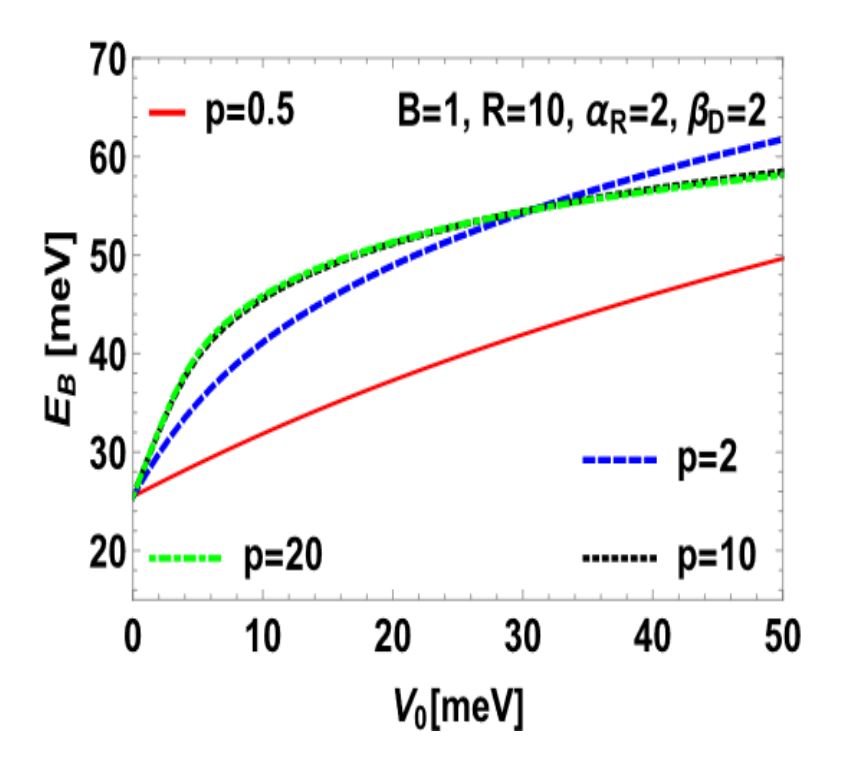


Fig. 13 E_B vs. V_0 for a D^0 centre in GaAs GQD with B=1 T, R=10 nm, $\alpha_R=2$ meV nm and $\beta_D=2$ meV nm for different values of p.

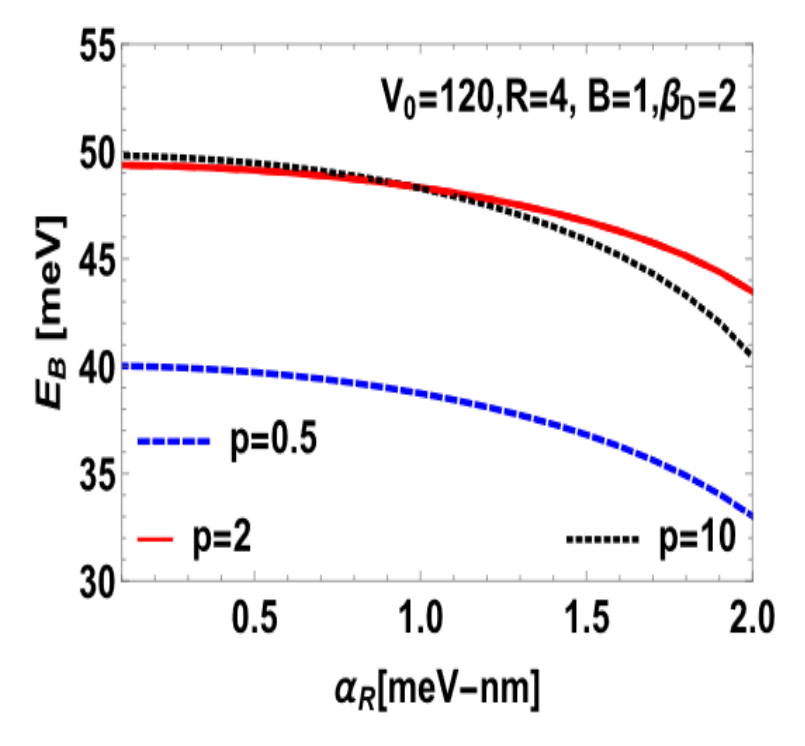


Fig. 14 E_B vs. α_R for a D^0 centre in GaAs GQD with $V_0 = 120$ meV, R = 4 nm, B = 1 T, and $\beta_D = 2$ meV nm for different values p.

١

In Figs. 14 and 15 we plot BE E_B vs α_R and β_D respectively for different values of p with $V_0 = 120$, R = 4, B = 1T. The figures show that BE decreases with increasing α_R while it increases with β_D .

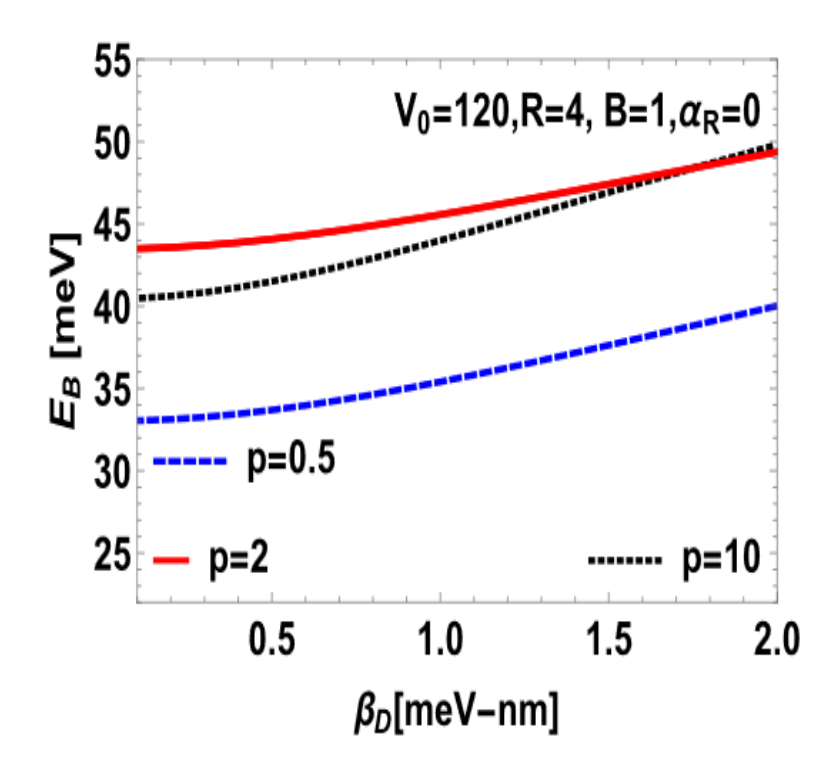


Fig. 15 E_B vs. β_D for a D^0 centre in GaAs GQD with $V_0 = 120$ meV, R = 4 nm, B = 1 T, and $\alpha_R = 0$ meV nm for different values p.

We study the magnetic field dependence of Magnetisation (M) and Susceptibility (S) in Figs. 16 and 17 respectively for different values of p with R = 10nm, $V_0 = 60$ meV and $\alpha_R = 1$, $\beta_D = 1$. The magnitude of M is found to increse with B. Furthermore, |M| increses with decreasing p. Fig. 17 shows that the susceptibility is diamagnetic in nature. The diamagnetic susceptibility decreases with increasing B and it saturates as B becomes sufficiently large. It appears that the diamagnetic effect of suceptibility is more at smaller values of p. However, the suceptibility is very weakly dependent on the shape of the potential at large B.

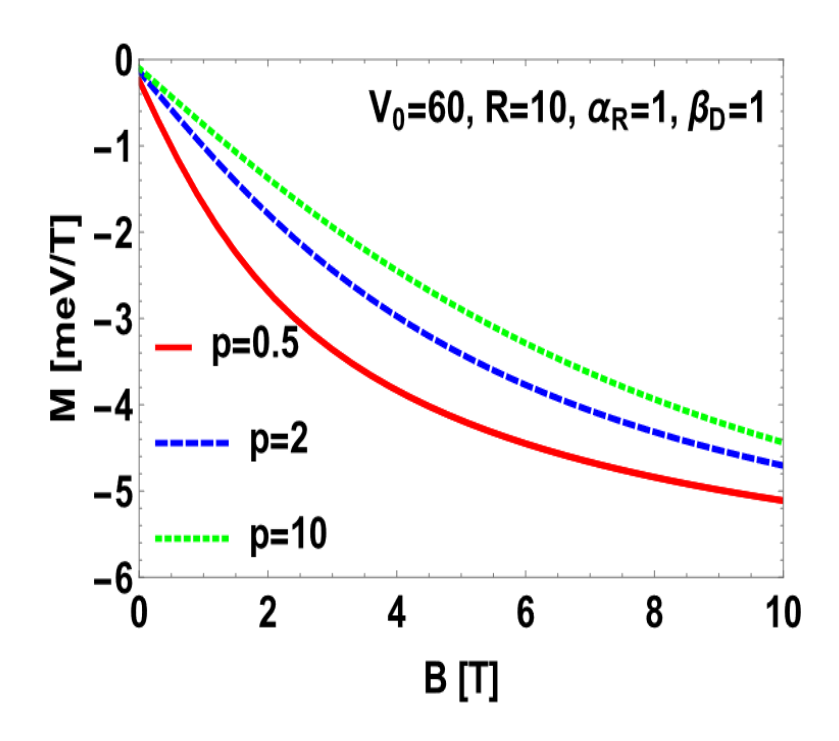


Fig. 16 M vs B for a D^0 centre in GaAs GQD with R=10 nm, $V_0=60$ meV and $\alpha_R=1$ meV nm, $\beta_D=1$ meV nm for different values of p.

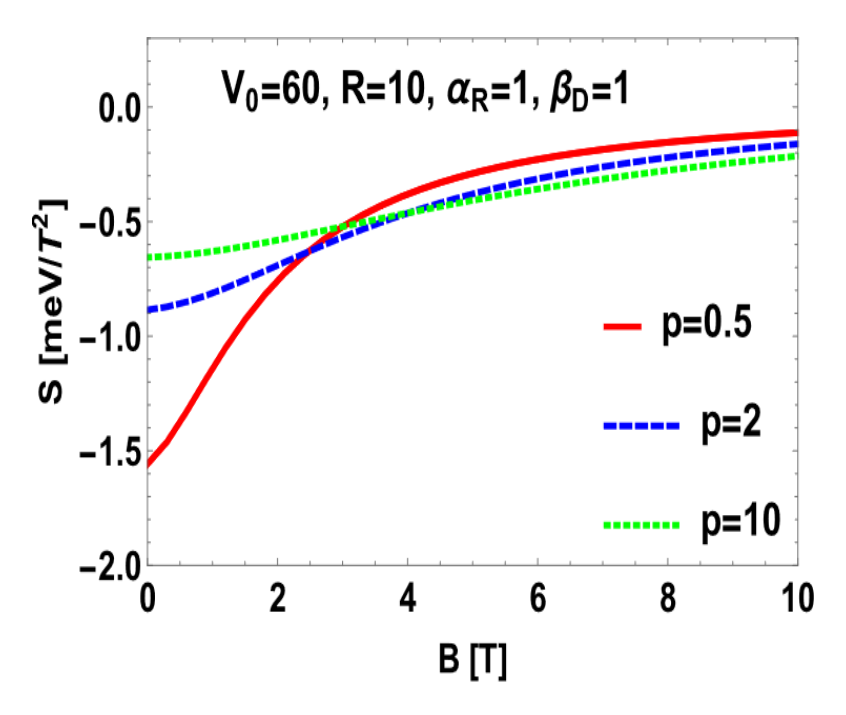


Fig. 17 S vs *B* for a D^0 centre in GaAs GQD with R=10 nm, $V_0=60$ meV and $\alpha_R=1$ meV nm, $\beta_D=1$ meV nm for different values of p.

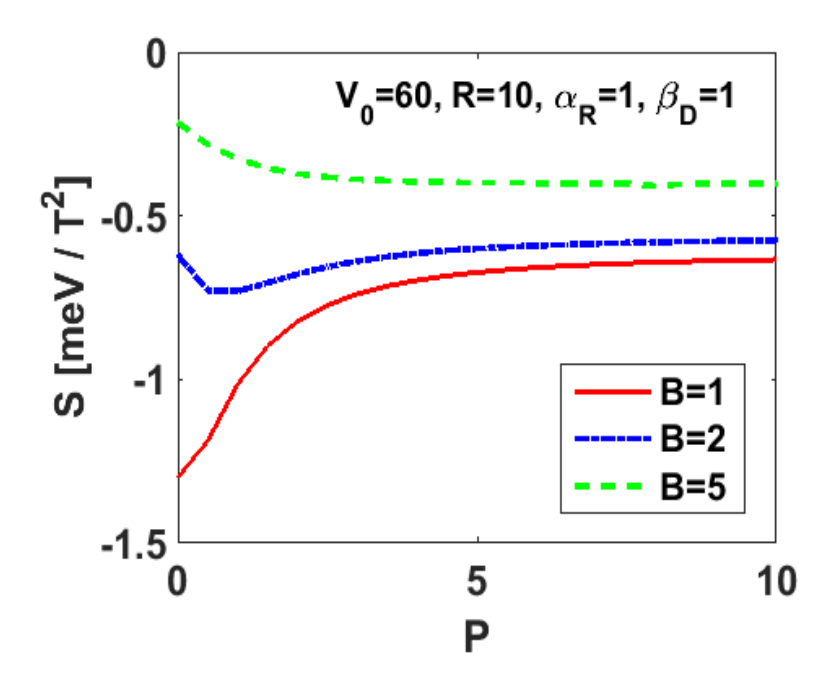


Fig. 18 *S* vs p for a D^0 centre in GaAs GQD with R = 10 nm, $V_0 = 60$ meV and $\alpha_R = 1$ meV nm, $\beta_D = 1$ meV nm for different values of B (T).

In Fig. 18, we show the behaviour of S directly as a function shape of p for different values of B with $V_0 = 60$, R = 10, $\alpha_R = 1$, $\beta_D = 1$. At low B, S initially increases with increasing p and eventually saturates at large p. At larger values of B, S initially decreases with increasing p and again saturates at large p eventually.

4.4 Conclusions

In this chapter, we have calculated the GS energy and BE of a D^0 Centre in PEQD as a function of the shape (or the steepness) parameter p, the effective QD size R, the Rashba and Dresselhaus spin-orbit interaction constants α_R and β_D and the external magnetic field B. We have shown that for $R \le 8$, the GS energy increases with p while for R > 8, it decreases. However, in both cases, the GS saturates as p becomes large. This is because when p becomes large, the confinement potential hardly changes with p.

For a small dot, the GS BE as a function of p exhibits a peak at a small value of p and saturates

to a constant as p increases. As the size of the QD increases, the peak becomes flatter though its height increases. Furthermore, the peak shifts towards higher values of p. As R becomes still larger, the peak disappears and the GS BE just monotonically increases with p at small p and eventually saturates. As a function of R too, BE shows peaks and the peak height increases as p increases. After reaching the peak, BE decreases with R faster for higher p giving rise to a crossing behaviour.

As a function of B, BE increases with B, as the magnetic field provides an additional confinement. It is shown that at small B, the shape of the confinement potential has a significant influence on BE, while at large B, E_B does not depend much on p. We have also shown that for BE, the shape of the confinement potential becomes more important when its depth is large.

RSOI and DSOI have competing roles on BE of the D^0 system. RSOI is found to reduce the binding while DSOI enhances it. Finally we show that the susceptibility of a D^0 impurity in PEQD is diamagnetic and this diamagnetic susceptibility (S) increases with p at small B and at large B, it decreases with increasing p. At intermediate B, S first decreases with increasing p, develops a minimum at some value of p and then increases with further increase in p. Eventually, however, S saturates to a constant as p becomes large.

4.5 References

- [1] P.A. Maksym, T. Chakraborty, Phys. Rev. Lett. 65, 108 (1990);
 - U. Merkt, J. Huser, M. Wagner, Phys. Rev. B 43, 7320 (1991);
 - W. Que, Phys. Rev. B 45, 11036 (1992);
 - H. Oh, K.J. Chang, G. Ihm, S.J. Lee, Phys. Rev. B 50, 15397 (1994);
 - S. Mukhopadhyay, A. Chatterjee, Phys. Lett. 204, 411 (1995);
 - S. Tarucha, D.G. Austing, T. Honda, R.J. Vander Hage, L.P. Kouwenhoven, Phys. Rev. Lett. 77, 3613 (1996);
 - S. Mukhopadhyay, A. Chatterjee, Int. J. Mod. Phys. B 10, 2781 (1996);
 - S. Mukhopadhyay, A. Chatterjee, Phys. Rev. B 58, 2088 (1998);
 - S. Mukhopadhyay, A. Chatterjee, Phys. Lett. 240, 100 (1998);
 - W.C. Tan, J.C. Inkson, Phys. Rev. B 60, 5626 (1999);
 - S. Mukhopadhyay, A. Chatterjee, J. Phys. Condens. Matter 11, 2071 (1999);
 - A. Chatterjee, S. Mukhopadhyay, Acta Phys. Pol. B 32, 473 (2001);
 - M.K. Phani, S. Mukhopadhyay, A. Chatterjee, Solid State Commun. 138, 285 (2006);
 - M.K. Phani, S. Mukhopadhyay, A. Chatterjee, Phys. Lett. 360, 655 (2007);

- S. Mukhopadhyay, B. Boyacioglu M. Saglam, A. Chatterjee, Physica E 40, 2776 (2008);
- D.S. Kumar, S. Mukhopadhyay, A. Chatterjee, Physica E 47, 270 (2013);
- D.A. Galiautdinov, Phys. Lett. 382, 72 (2018).
- [2] X.W. Fang, Chin. Phys. 15, 203 (2006);
 - B. Boyacioglu, M. Saglam, A. Chatterjee, J. Phys. Condens. Matter 19, 456217 (2007);
 - B. Boyacioglu, A. Chatterjee, J. Appl. Phys. 112, 83514 (2012);
 - B. Boyacioglu, A. Chatterjee, Physica B 407, 3535 (2012);
 - B. Boyacioglu, A. Chatterjee, Physica E 44, 1826 (2012);
 - B. Boyacioglu, A. Chatterjee, Int. J. Mod. Phys. B 26, 1250018 (2012);
 - A. Boda, A. Chatterjee, Physica B 448 244 (2014);
 - D.S. Kumar, S. Mukhopadhyay, A. Chatterjee, Physica E 47, 270 (2017);
 - L.L. Jahan, A. Boda, I.V. Sankar, N.R. Chebrolu, A. Chatterjee, Scintific Report 8 5073 (2018);
 - H.K. Sharma, A. Boda, B. Boyacioglu, A. Chatterjee, J. Magn. Magn Mater. 469, 171 (2018).
- [3] M. Ciurla, J. Adamowski, B. Szafran, and S. Bednarek, Physica E 15, 261 (2002).
- [4] W. F. Xie, Superlattices and Microstructures 65, 271 (2014).
- [5] L. Jahan, B. Boyacioglu, , A. Chatterjee, Scintific Report 9 (2019).
- [6] R. Khordad, Int. J. Theor. Phys. 52 837 (2013).
- [7] D.S. Kumar, A. Boda, S. Mukhopadhyay, A. Chatterjee, Superlattice. Microst. 88 174 (2015).
- [8] P. Saini, A. Boda, A. Chatterjee, J. Magn. Magn Mater. 485, 407 (2019).

Chapter ~5

Spin-orbit interaction effect on a hydrogenic D^0 centre in a three-dimensional asymmetric Gaussian GaAs quantum dot in a magnetic field

5.1 Introduction

In the earlier chapters, we have considered symmetric Gaussian and power exponential potentials as the confinement potential for the QD [1-12]. Several investigations have also been carried out on asymmetric QDs [13-20]. Shan et al. [14] have studied the temperature and impurity effects on the GS energy and the GS binding energy in an asymmetric QD by using the linear combination operator method. Chen and Zhang [15] have calculated the first excited state energy of the polaron in an asymmetric QD in the presence of magnetic field using the Pekar type variational method. Bandyopadhyay et al. [17] have obtained the total spin- splitting energy expression in an asymmetric QD (AQD) with ferromagnetic contacts, subjected to a transfer field. They have shown that the Zeeman splitting can be tuned with a transfer electric field in the presence of RSO coupling in AQD. Zhang et al. [18] has studied the BE of a shallow donor impurity in an asymmetric QW by using the variational method. Hao [19] has examined the SOI effect in an asymmetric quantum well by varying the internal inversion asymmetry. Singh et al. [20] have studied the magnetic field-dependence of the spin and tuning dynamics in a double AQD in the presence of RSOI and DSOI.

In the present chapter, we wish to study the effect of RSOI and DSOI on the GS energy, binding energy, susceptibility and magnetic moment of a D^0 complex in a 3D asymmetric GQD (AGQD) placed in a magnetic field. To obtain results for a realistic system, we apply our theory to a GaAs QD.

5.2 Model and Formulation

A D^0 complex in a 3D AGQD with RSOI and DSOI and placed in a magnetic field \boldsymbol{B} (0,0, \boldsymbol{B}) can be modelled by the Hamiltonian

$$\mathcal{H} = \left(\frac{1}{2m^*}(\boldsymbol{p} + \frac{e}{c}\boldsymbol{A})^2 - \frac{e^2}{\varepsilon r} - V_0 e^{-\frac{a(x^2 + y^2) + b z^2}{2R^2}}\right) I + \frac{\alpha_R}{\hbar} \left[\boldsymbol{\sigma} \times \left(\boldsymbol{p} + \frac{e}{c}\boldsymbol{A}\right)\right]_Z$$
$$+ \frac{\beta_D}{\hbar} \left[\sigma_x \left(p_x + \frac{e}{c}A_x\right) - \sigma_y \left(p_y + \frac{e}{c}A_y\right)\right], \tag{5.1}$$

where a gives the length scale over which the confinement potential becomes zero in the x-y plane and b describes that along the z axis and the rest of the notations have been defined already. To eliminate SOIs, we carry out the same transformation as before,

$$U = e^{S} \quad , \qquad S = i \frac{m^*}{\hbar^2} \left[\alpha_R (y \sigma_x - x \sigma_y) + \beta_D (x \sigma_x - y \sigma_y) \right], \tag{5.2}$$

and expand the transformed Hamiltonian in a power series in terms of α_R and β_D and neglect terms beyond α_R^2 and β_D^2 . This gives

$$\widetilde{\mathcal{H}} = \left(\frac{p^2}{2m^*} + \frac{m^*}{8}\omega_c^2 \rho^2 - \frac{e^2}{\varepsilon r} - V_0 e^{-\frac{a(x^2 + y^2) + b z^2}{2R^2}}\right) I + \frac{\omega_c}{2} L_z - \frac{m^*}{\hbar^2} (\alpha_R^2 + \beta_D^2)
- \frac{m^*}{\hbar^3} (\alpha_R^2 - \beta_D^2) \sigma_z L_z - \frac{m^*}{2\hbar^3} (\alpha_R^2 - \beta_D^2) \omega_c \sigma_z \rho^2,$$
(5.3)

where

$$\rho^2 = x^2 + y^2$$
, $L_z = -i\hbar(\partial/\partial\phi)$, $\omega_c = (eB/m^*c)$. (5.4)

To find the GS energy variationally, we try the function:

$$\psi(\mathbf{r}) = e^{-\alpha r^2 - \beta r - im\varphi} \tag{5.5}$$

where α and β are treated as variational parameter. As before, we define the BE of the D^0 hydrogenic impurity ($E_B(D^0)$) as

$$E_B(D^0) = E(e^-) - E(D^0).$$
 (5.6)

where $E(e^-)$ and $E(D^0)$ and are respectively the GS energies of the electron and D^0 impurity in the AGQD. The magnetisation and susceptibility are defined, as usual, by

$$M = -\frac{\partial E(D^0)}{\partial B}; \qquad S = \frac{\partial^2 E(D^0)}{\partial B^2}. \tag{5.7}$$

5.3 Results and Discussion

We plot the GS energy (E) in Fig.1 with respect to the effective QD size R for B = 1T, $V_0 = 60 \text{ meV}$, $\alpha_R = 1 \text{ meV} - nm$, $\beta_D = 1 \text{ meV} - nm$ and a few values of the asymmetry parameter b. The GS energy is found to decrease nonlinearly as the effective dot size R is increased and to eventually saturate to the bulk value. Furthermore, if the material growth is increased in the z direction, then the GS energy decreases. Of course, the energy becomes independent of the parameters a and b in the bulk limit. This is expected because when b becomes very large, the potential becomes essentially constant and the values of b and b do not affect the energy.

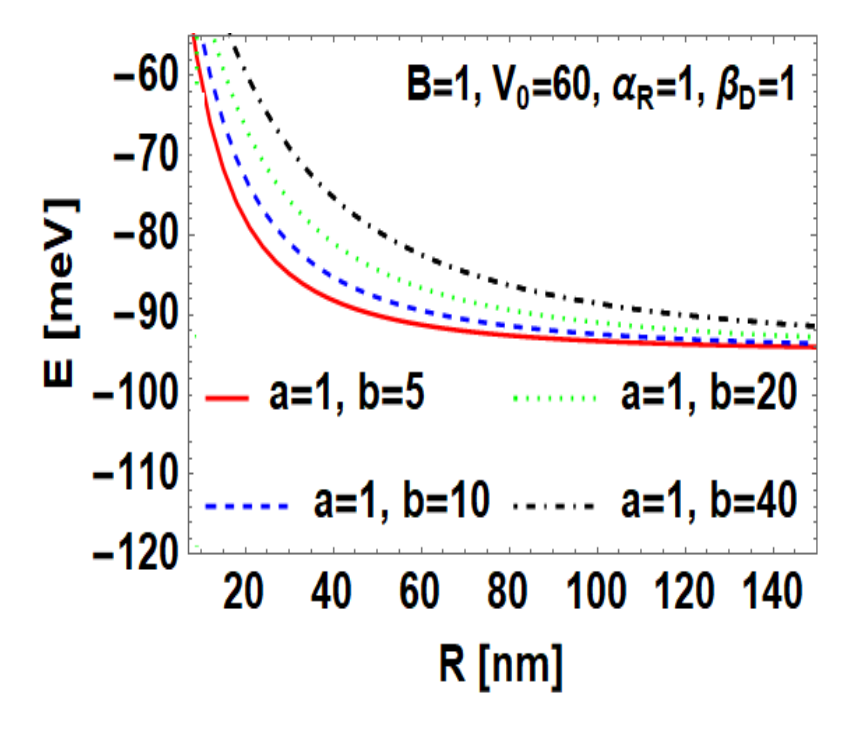


Fig.1 GS energy (E) vs. R for a D^0 centre in AGQD with B = 1T, $V_0 = 60$ meV, $\alpha_R = 1$ meVnm, $\beta_D = 1$ meVnm and for different values of asymmetric parameter b.

In Fig.2, we display the behaviour of the GS energy with respect to the magnetic field B for $R = 10 \, nm$, $V_0 = 60 \, meV$, $\alpha_R = 1 \, meV nm$, $\beta_D = 1 \, meV nm$. The GS energy increases non-linearly with increasing B. It also increases with the increase in the asymmetry parameter b, as expected.

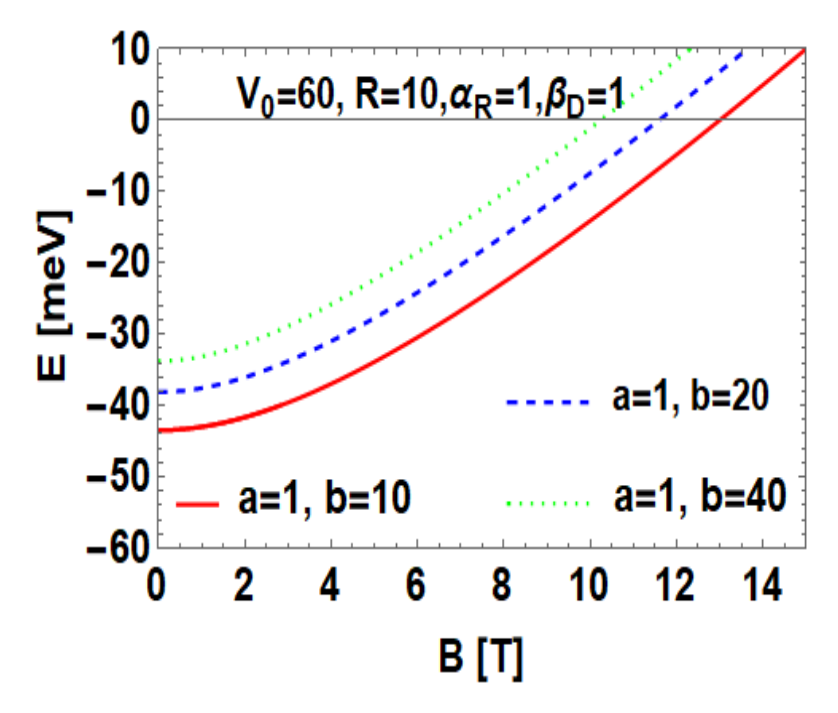


Fig. 2 E vs. B for a D^0 centre in AGQD with R = 10nm, $V_0 = 60$ meV $\alpha_R = 1$ meVnm, $\beta_D = 1$ meVnm and for different values of the asymmetric parameter b.

In Fig. 3, we study the behaviour of the GS energy with respect to b for R=50nm, $V_0=120~meV$, B=1T, a=1 and a few sets of RSOI and DSOI coefficients. As expected, the GS energy is lowered by both RSOI and DSOI, while with the increase in the parameter b, the GS energy is found to increase. Fig. 4 presents the variation of the results for the GS binding energy (BE) with respect to R for B=1T, $V_0=60~meV$, $\alpha_R=0$, $\beta_D=1~meV$ nm and different b values. BE of D^0 turns out to be positive, as expected. This implies that the system has a stable bound state. The binding is observed to be maximum at a certain value of the QD size R_m . For $R>R_m$, BE decreases with increase in R and eventually reaches a saturation value which is the bulk limit. This of course understandable. As R is reduced below R_m , BE starts decreasing rapidly. The rapid fall in BE below R_m is solely a quantum phenomenon. As R decreases, the uncertainty in position also decreases. Concomitantly, the uncertainty in momentum becomes larger leading to an increase in the momentum itself and hence the kinetic energy. Thus, if the size of QD is made very small, restricting the electron's motion inside QD would become very

difficult. This results in a reduction in BE. The figure reveals that the height of the peak in BE decreases and its width increases with increasing asymmetry and furthermore the peak shifts to the higher value of R.

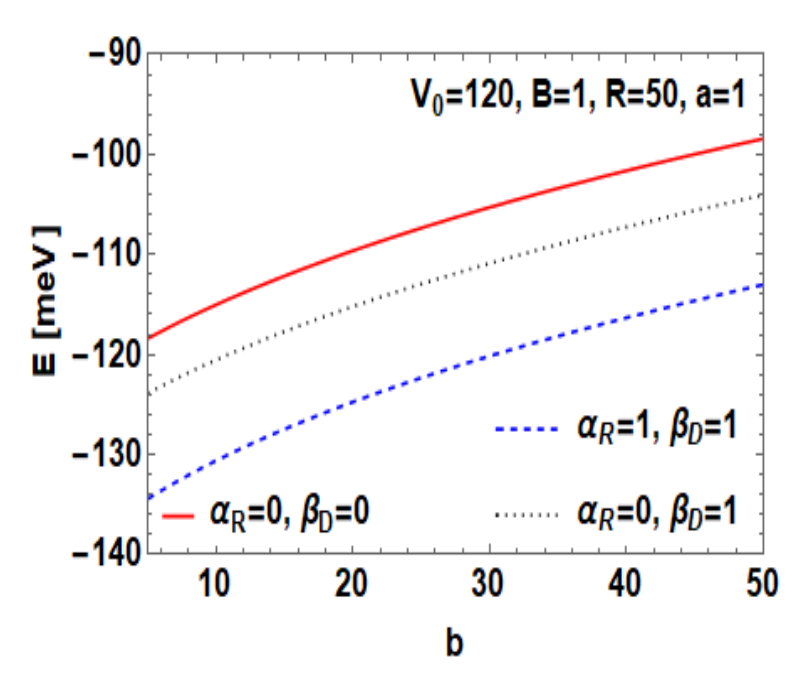


Fig. 3 E vs. b for a D^0 centre in AGQD with $V_0 = 120$ meV, B = 1 T, R = 50nm, a = 1 for different values of $\alpha_R(meVnm)$ and $\beta_D(meVnm)$.

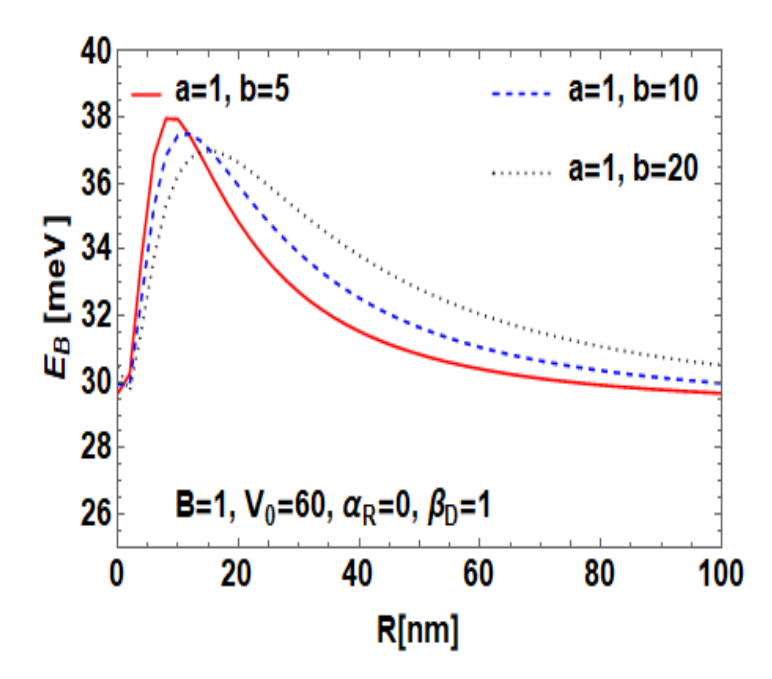


Fig. 4 GS BE (E_B) vs. R for D^0 centre in a GaAs AGQD with B=1T, $V_0=60$ meV $\alpha_R=0$ and $\beta_D=1$ meVnm for different values of asymmetric parameters b.

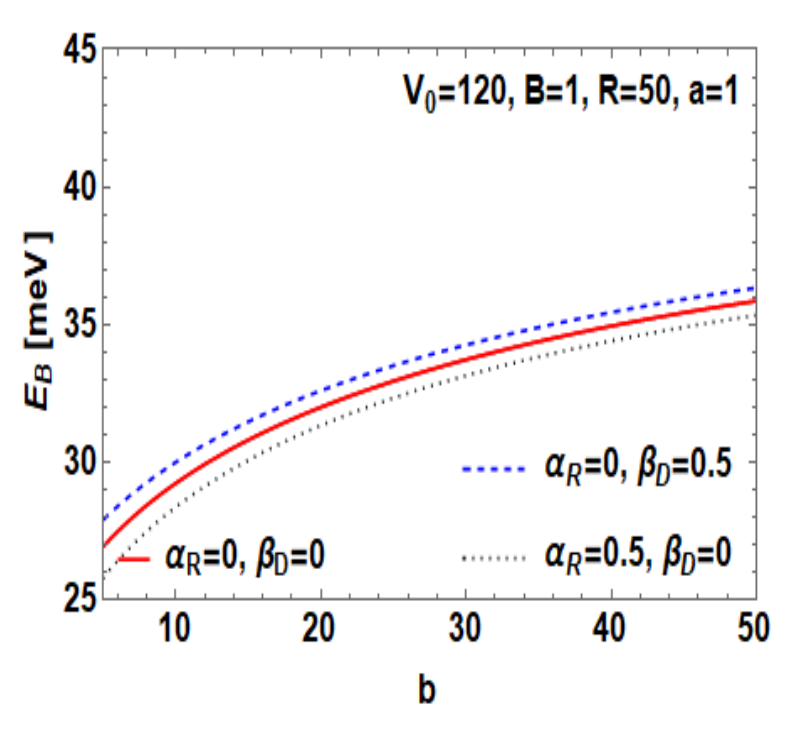


Fig. 5 E_B vs. b for D^0 centre in a GaAs AGQD with $V_0 = 120$ meV, B = 1 T, R = 50nm and a = 1 for different combination of $\alpha_R(meVnm)$ and $\beta_D(meVnm)$.

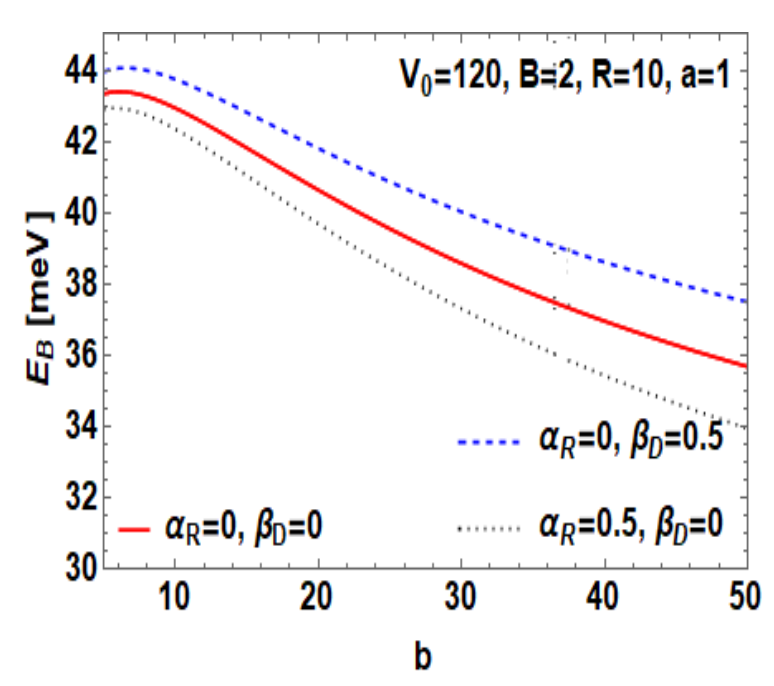


Fig. 6 E_B vs. b for D^0 centre in a GaAs AGQD with $V_0=120$ meV, B=2 T, R=10nm and a=1 for different combination of α_R (meVnm) and β_D (meVnm).

Fig. 5 shows explicitly how BE of D^0 varies with the asymmetry parameter b of AGQD. The figure clearly reveals that BE increases with increasing b. However, for a small QD, BE reduces if b is increased. This is shown in Fig. 6. It is also observed from Fig. 5 and 6 that the Rashba coupling decreases BE, while Dresselhauss coupling increases it. The presence of asymmetry in the confinement potential enhances these effects separately.

In Fig. 7 we depict the variation of BE of D^0 with respect to a magnetic field B in AGQD. BE is found to increase with increasing B. At small B, BE decreases with increasing b, while at high B, BE is essentially independent of b. In Fig. 8, we show the behavior of BE of D^0 in AGQD with respect to V_0 for B = 1T, R = 50 nm and a few values of the parameter b. BE increases with V_0 , as would be normally expected and the curve is concave from below. For a small QD also, BE increases with V_0 , but now the curve is concave from above. This is shown in Fig. 9. Interestingly, for $R \lesssim 10$, BE decreases with increasing b while for $R \gtrsim 10$, BE increases with b.

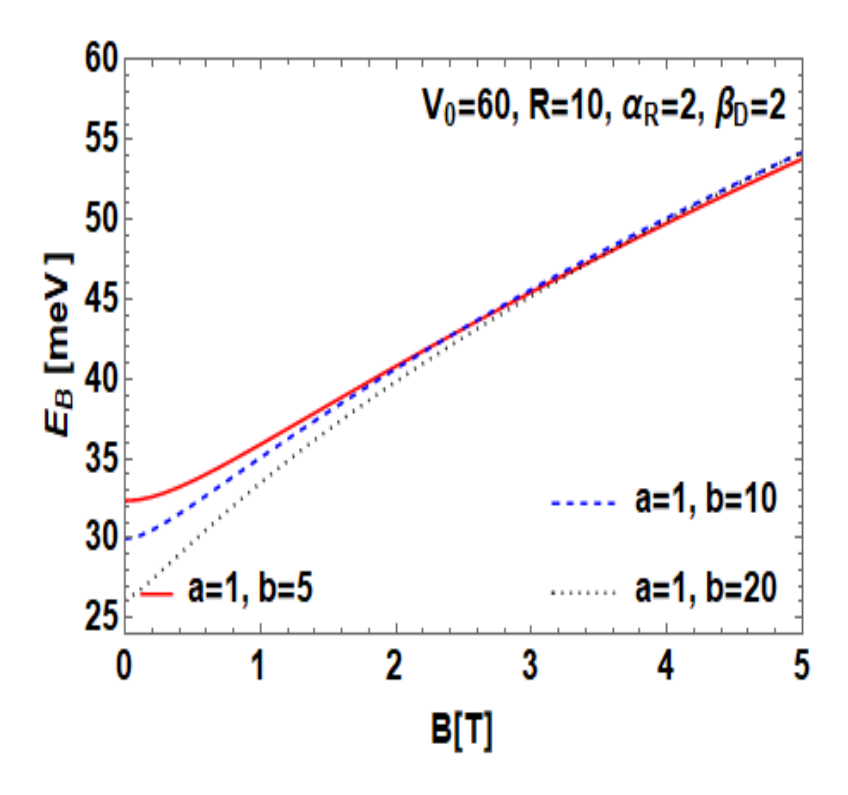


Fig. 7 E_B vs. B for a D^0 complex in AGQD with $V_0 = 60$ meV, R = 10 nm $\alpha_R = 2$ and $\beta_D = 2$ meV nm and for different values of asymmetric parameters b.

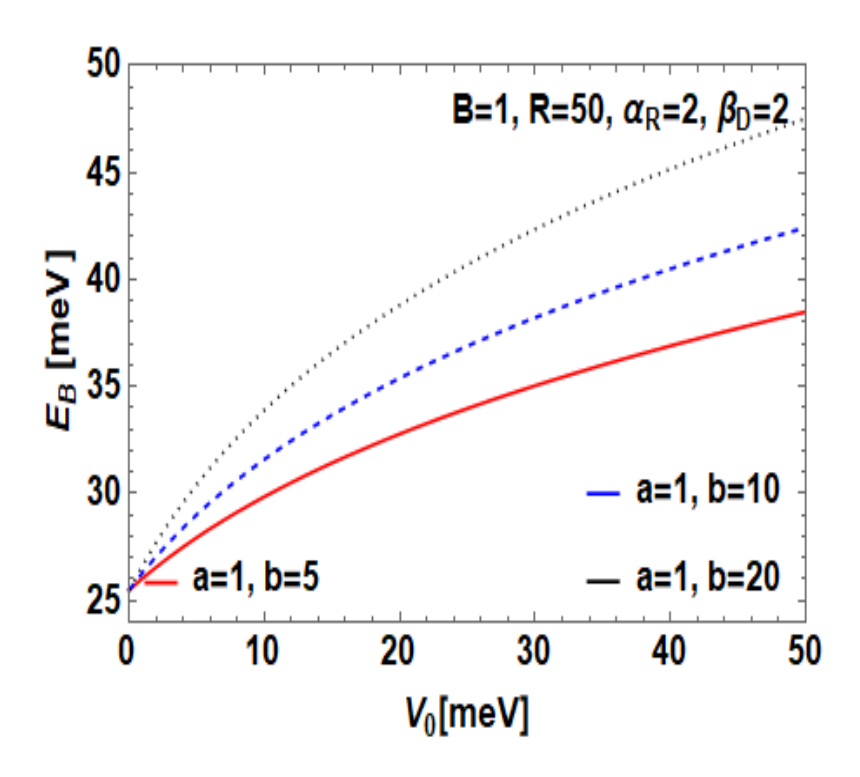


Fig. 8 E_B vs. V_0 for a D^0 complex in AGQD B=1 T, R=50 nm $\alpha_R=2$ and $\beta_D=2$ meVnm and for different values of asymmetric parameters b.

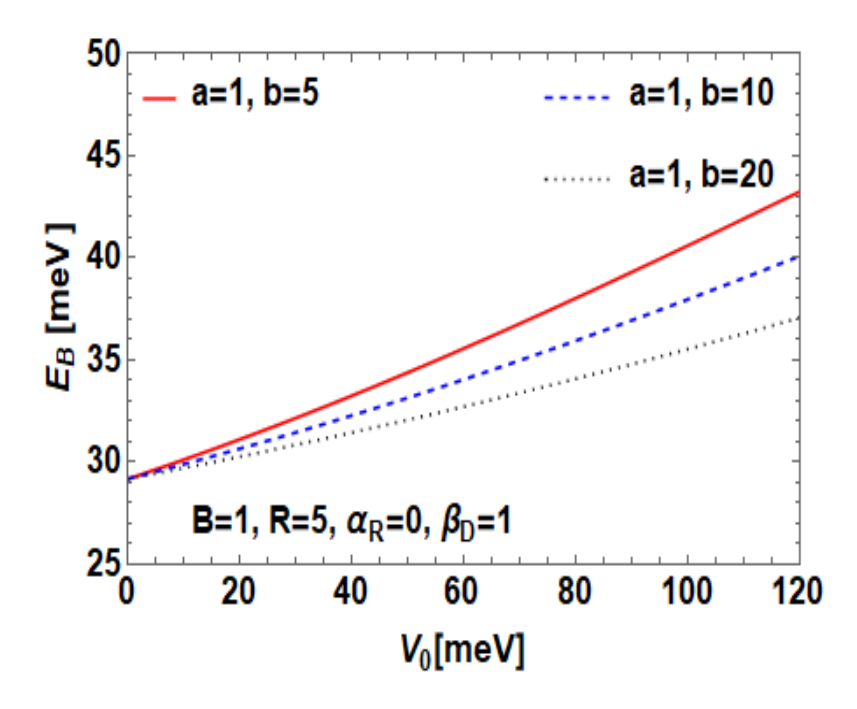


Fig. 9 E_B vs. V_0 for a D^0 complex in AGQD B=1 T, R=5 nm $\alpha_R=0$ and $\beta_D=1$ meVnm for different values of asymmetric parameters b.

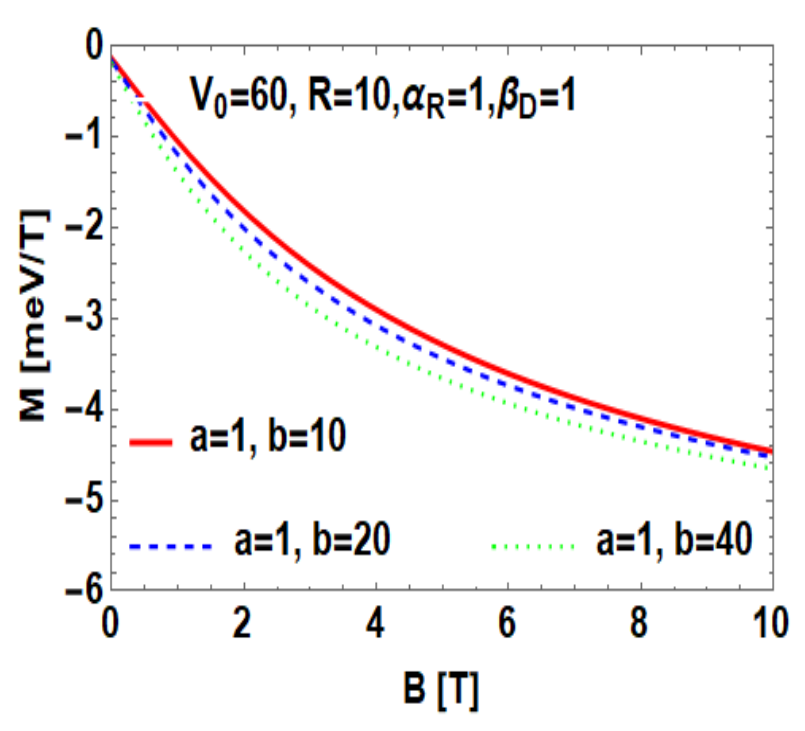


Fig. 10 M vs B for a D^0 complex in AGQD with $V_0 = 60$ meV, R = 10 nm $\alpha_R = 1$ and $\beta_D = 1$ meVnm for different values of asymmetric parameters b.

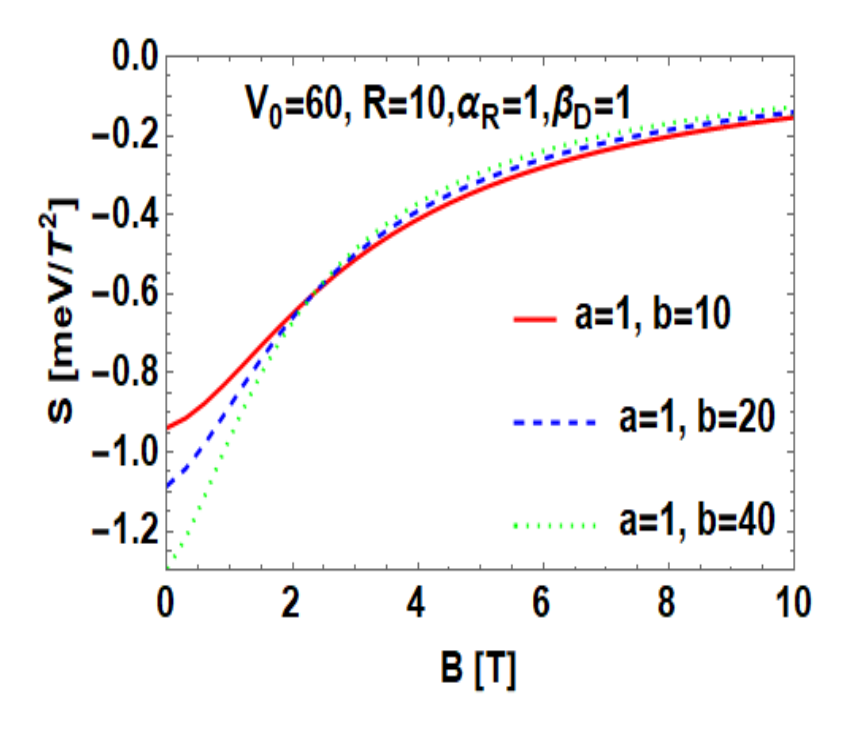


Fig. 11 S vs B for a D^0 complex in AGQD with $V_0 = 60$ meV, R = 10 nm, $\alpha_R = 1$ meVnm and $\beta_D = 1$ meVnm for different values of asymmetric parameters b.

We show in Fig. 10, how the magnetic moment (M) of D^0 varies with B for R=10nm, $V_0=60$ meV, $\alpha_R=1$ nm meV, $\beta_D=1$ nm meV and for three different value of asymmetric parameter b. As expected, the nature of M is diamagnetic. The diamagnetic moment increases in magnitude with the increase in B. If the asymmetry parameter b is increased, then also |M| increases at smaller values of B. In Fig. 11, we show the behavior of susceptibility with respect to B for R=10nm, $V_0=60$ meV, $\alpha_R=1$ nm meV, $\beta_D=1$ nm meV and for a few values of b. The behavior of susceptibility is found to be diamagnetic. It increases a little rapidly with B at small B, but as B increases, its increase slows down and finally it saturates as B becomes large. From Fig. 11, one can also see the B-dependance of B. At low B, B decreases with increasing B, but as B becomes large, B shows a slow increase with B. This gives rise to an interesting crossing behavior.

5.4 Conclusion

The behavior of GSE (E) and BE (E_B) of a hydrogenic donor impurity in an asymmetric 3D GQD of GaAs has been studied with respect to effective QD size R, confinement potential depth V_0 , magnetic field B, asymmetry parameter B, and RSOI and DSOI coefficients. We have shown that GSE increases with the increase in the asymmetry parameter B. We have also shown that with respect to the QD size B, GS BE exhibits a peak which shifts towards larger B as B increases. Also BE is found to decrease with increasing B. Finally, we have examined the dependence of magnetic moment B0 and susceptibility B1 on B2 for different values of the asymmetry parameter B2. As expected, the susceptibility is found to be diamagnetic in nature. Also the magnitude of B3 is found to decrease with increasing B3. However, it increases as the asymmetry increases at small B3 and decreases with increasing asymmetry at large B3. This gives rise to an interesting crossing behavior. The Rashba coupling decreases BE, while Dresselhauss coupling increases it and the asymmetry in the confinement potential enhances these effects.

5.5 References

- [1] J. Adamowski, M. Sobkowicz, B. Szafran, S. Bednarek, Phys. Rev. B 62, 4234 (2000);
- [2] Erratum: Phys. Rev. B 62, 13233 (2000).
- [3] A. Boda, G. Madhusudhan, A. Chatterjee, Superlattices Microstruct. 71, 261 (2014).
- [4] A. Boda, A. Chatterjee, J. Nanosci. Nanotechnol. 15 (2015).

- [5] A. Boda, A. Chatterjee, Physica B 448, 244 (2014).
- [6] Juan Gu, Jiu-Qing Liang, Phys. Lett. A 335 (2005) 451.
- [7] Aalu Boda, A. Chatterjee, Physica E 45 (2012) 36.
- [8] W. Xie, Physica B 403 (2008) 2828.
- [9] Aalu Boda, A. Chatterjee, Physica B 448 (2014) 244.
- [10] A. Gharaati, R. Khordad, Superlattices Microstruct. 48 (2010) 276.
- [11] Aalu Boda, G. Madhusudhan, A. Chatterjee, Superlattices Microstruct. 71 (2014) 261.
- [12] Yuan-Peng Bao, Wen-Fang Xie, Commun. Theor. Phys. 50 (2008) 1449 (Beijing, China).
- [13] C. S. wang, Y. F. Chen and J. J. Xiao, International journal of nanoscience, 11 1250026 (2012).
- [14] S. P. Shan, Y. M. Liu and J. L. Xiao, Low Temp. Phys. 39, 607 (2013).
- [15] Y.J. Chen, P. Y. Zhang, Journal of low temp. phys. 194, 262 (2019).
- [16] H. Akbas, S. Suku, S. Minez, C. Dane, O. Akankay, I. Erdogan, Superlatt. Microstr. 94 131 (2016).
- [17] S. Bandyopadhyay, M. Cahay, Superlatt. Microstr. 32, 4 (2002).
- [18 C. Zhang, Z. wang, Y. Liu, K. Guo, Physica E; Low Dimensional systems and nanostructures 43, 372 (2010).
- [19] Y.F. Hao, Phys. Lett. A **379**, 2853 (2015).
- [20] M.K. Singh, P.K. Jha, A. Bhattacherjee, J. Appl. Phys. **122**, 11 (2017).

Chapter-6

Enhancement in binding of D^- in a GaAs Gaussian Quantum Dot in the presence of spin-orbit interactions and a magnetic field

6.1 Introduction

In the earlier chapters, we have studied the effect of spin-orbit interactions on some of the properties of hydrogenic D⁰ impurities confined in QDs. In this chapter, we shall consider a negative hydrogenic donor impurity (D⁻) which consists of a system of two electrons bound to a hydrogenic nucleus. The existence of stable bound states in negative donor complexes in bulk semiconductors was suggested theoretically by Lampert [1] way back in 1958. A D⁻ complex confined in a low-dimensional material is an interesting system because it is a simple two-particle correlated system with a single bound state [2]. The experimental confirmation of the existence of a bound state of D^- , however, took a long time to come primarily because of the very feeble nature of the binding of the system. To our knowledge, Huant et al. [3] were the first to observe experimentally the existence of a bound state in a D⁻ impurity in a GaAlAs heterostructure from photoionization transitions through far-infrared magneto-optical experiments. They have reported the BE of the D⁻ impurity in a GaAs- multiple quantum well structure for several values of the magnetic field strength. Using a variational method, Phelps and Bajaj [4] have shown that the ratio of BE of D^- to that of D^0 is only about 5.55%. Armistead et al. [5] have studied the D^- problem in GaAs by far-infrared magneto-optical experiments and reported that a D^- complex forms only under metastable conditions. Pang et al. [6] have theoretically calculated BE of a D⁻ centre in a GaAs quantum well by diffusion quantum Monte Carlo method. Their results are in good agreement with the results of Huant et al. [3]. It is certainly interesting to examine the possibility of existence of a D⁻ centre in a QD from the point of view of opto-electronic applications. Several

authors have calculated the energy levels of a D^- system in both PQDs and GQDs [6]. Boda et al. [7] have considered a D^- impurity in the presence of a magnetic field in a GQD and studied its electric and magnetic properties.

To our knowledge, no investigation has so far been devoted to examine the spin-orbit coupling effects on the properties of a D^- system in a GQD. In the present chapter, we shall make an attempt in this direction. We shall calculate the GS energy and binding energy of a D^- system in a 3D GQD in the presence of Rashba and Dresselhaus spin-orbit interactions and an external magnetic field.

6.2 Model and Formulation

A D^- impurity in a GQD with RSOI and DSOI, placed in a magnetic field can be described by the Hamiltonian

$$H = H_{D^-} + H_R + H_D , (6.1)$$

where

$$H_{D^{-}} = \sum_{i=1}^{2} \left[\frac{1}{2m^{*}} \left(\boldsymbol{p}_{i} + \frac{e}{c} \boldsymbol{A}_{i} \right)^{2} - V_{0} e^{-\frac{r_{i}^{2}}{2R^{2}}} - \frac{e^{2}}{\epsilon r_{i}} \right] + \frac{e^{2}}{\epsilon r_{12}}, \tag{6.2}$$

$$H_R = \sum_{i=1}^{2} \frac{\alpha_R}{\hbar} \left[\sigma_i \times \left(p_i + \frac{e}{c} A_i \right)_z \right] , \qquad (6.3)$$

$$H_D = \sum_{i=1}^{2} \frac{\beta_D}{\hbar} \left[\sigma_{ix} \left(p_{ix} + \frac{e}{c} A_{ix} \right) - \sigma_{iy} \left(p_{iy} + \frac{e}{c} A_{iy} \right) \right]. \tag{6.4}$$

Here $r_i(x_i, y_i, z_i)$ represents the position of the *i*-th electron, $p_i(p_{ix}, p_{iy}, p_{iz})$ its canonically conjugate momentum, $r_{12} = |r_1 - r_2|$ refers to the distance between the two electrons, A_i is the vector potential experienced by the *i*-th electron, $\sigma_{ik}(k=x,y,z)$ represent the Pauli matrices and α_R and β_D denote the Rashba and Dreselhaus spin-orbit coupling parameters respectively. We choose the symmetric gauge and therefore take: $A_i = \frac{B}{2}(-y_i, x_i, 0)$.

To eliminate the SOIs, we apply the following unitary transformation

$$U = e^{i(m^*/\hbar^2)[\alpha_R(y_i\sigma_{ix} - x_i\sigma_{iy}) + \beta_D(x_i\sigma_{ix} - y_i\sigma_{iy})]}$$
(6.5)

and express the resulting Hamiltonian in powers of α_R and β_D and neglect terms of order higher than α_R^2 and β_D^2 . The transformed Hamiltonian then reads in Rydberg units,

$$\widetilde{\mathcal{H}} = \sum_{i=1}^{2} \left[-\nabla_{r_{i}}^{2} + \frac{1}{16} \omega_{c}^{2} \rho_{i}^{2} - V_{0} e^{-\frac{r_{i}^{2}}{2R^{2}}} - \frac{2}{r_{i}} - \frac{1}{2} (\alpha_{R}^{2} + \beta_{D}^{2}) I - \frac{1}{2} (\alpha_{R}^{2} - \beta_{D}^{2}) \sigma_{Z} L_{z_{i}} + \frac{\omega_{c}}{2} L_{z_{i}} - \frac{1}{4} (\alpha_{R}^{2} - \beta_{D}^{2}) \omega_{c} \sigma_{Z} \rho^{2} \right] + \frac{2}{r_{12}}$$

$$(6.6)$$

where $\omega_c = eB/m^*c$, $\rho_i^2 = x_i^2 + y_i^2$ and $L_{z_i} = -i\hbar(\partial/\partial\phi_i)$. We seek a variational solution of $\widetilde{\mathcal{H}}$ and make the following choice for the variational function:

$$\psi_{D^{-}}(r_1, r_2) = [1 + \lambda r_{12}^m] e^{-\mu(r_1^2 + r_2^2) + \iota(m_1 + m_2)\phi}$$
(6.7)

where λ , μ and m are variational parameters and m_1 and m_2 denote the magnetic quantum numbers. We have included the generalized Jastrow function r_{12}^m in the wave function to incorporate the effect of Coulomb correlation. We now implement the transformations:

$$u = \frac{r_1 + r_2}{\sqrt{2}}$$
 , $v = \frac{r_1 - r_2}{\sqrt{2}}$ (6.8)

In terms of \boldsymbol{u} and \boldsymbol{v} , both $\widetilde{\mathcal{H}}$ and ψ_{D^-} look simpler and calculation of the energy becomes easier. We perform the integration and minimization numerically. The BE of the D^- impurity can be written as

$$E_B(D^-) = E(D^0) + E(e^-) - E(D^-)$$
(6.9)

where $E(e^-)$ represents the GS energy of a single-electron-GQD, $E(D^0)$ represents that of a D^0 impurity in GQD and $E(D^-)$ represents that of a D^- centre in the same QD.

Because of symmetry, the dipole moment in a D^0 centre is expected to be zero. On the contrary, the D^- system has a different scenario. Classically, however, even for a D^- complex, the dipole moment is expected to be zero. The explanation is simple. The Coulomb correlation will tend to keep the electrons as far away from each other as possible and therefore the GS would correspond to a configuration in which the electrons are expected to settle in positions that would be diametrically opposite to each other. According to quantum mechanics, however, one would

expect quantum fluctuations in the electrons' positions and the equilibrium positions of the electrons will be such as will lead to the minimum energy. Thus, quantum mechanically, the expected electron position vectors will have an angle that is less than 180° leading to a finite dipole moment. The average distance between the two electrons $\langle r_{12} \rangle$ and the resultant dipole moment $|\mathbf{P}|$ are given by

$$\langle \mathbf{r}_{12} \rangle = \langle \psi_{D^{-}}(r_{1}, r_{2}) | (\mathbf{r}_{1} - \mathbf{r}_{2}) | \psi_{D^{-}}(r_{1}, r_{2}) \rangle = \langle \psi_{D^{-}} | (\mathbf{r}_{1}^{2} + \mathbf{r}_{2}^{2} - 2\mathbf{r}_{1}\mathbf{r}_{2}\cos\theta)^{1/2} | \psi_{D^{-}} \rangle, (6.10)$$

$$|\mathbf{P}| = \langle \psi_{D^{-}}(r_{1}, r_{2}) | (\mathbf{r}_{1} + \mathbf{r}_{2}) | \psi_{D^{-}}(r_{1}, r_{2}) \rangle = \langle \psi_{D^{-}} | (\mathbf{r}_{1}^{2} + \mathbf{r}_{2}^{2} + 2\mathbf{r}_{1}\mathbf{r}_{2}\cos\theta)^{1/2} | \psi_{D^{-}} \rangle$$

$$= \sqrt{2} \langle \psi_{D^{-}} | u | \psi_{D^{-}} \rangle$$

$$(6.11)$$

where $cos\theta = cos\theta_1 cos\theta_2 + sin\theta_1 sin\theta_2 \cos(\phi_1 - \phi_2)$, θ being the angle between r_1 and r_2 . At zero temperature, the magnetic moment and susceptibility of the system under consideration can be defined as

$$M = -\frac{\partial E}{\partial B}$$
 ; $\chi = \frac{\partial M}{\partial B}$. (6.13)

6.3 Numerical results and discussion

We compute the energies in $R_y^* = (m^*e^4/\varepsilon^2\hbar^2) = 12$ meV, lengths in $a_B^* = (\varepsilon\hbar^2/m^*e^2) = 9.8$ nm, magnetic field in Tesla (T), and SOI constants in $R_y^*-a_B^*$. We apply our theory to a GaAs QD for concreteness and so we choose $\varepsilon = 12.4$ and $m^* = 0.067m_0$, m_0 being the electron bare mass. We show in Fig. 1, the behaviour of the GS energy E as a function of QD size R for different sets of Rashba and Dresselhaus coefficients α_R and β_D with $V_0 = 25$, B = 2. With respect to R, E exhibits a decreasing behaviour. When both RSOI and DSOI are present, the decrease becomes a little faster. The DSO coupling lowers the energy more at small R while beyond a certain R, the RSO coupling lowers the energy more. Fig. 2 shows how E varies with the magnetic field E for different sets of E0 and E1 with E2 shows how E3 with RSOI alone, as E3 increases from zero, E4 first displays a slow decrease, reaches a shallow minimum and then increases monotonically with further increase in E3. However, with DSOI alone, E4 monotonically increases with E5. When both the interactions are present, E3 becomes again essentially a monotonically increasing function of E5.

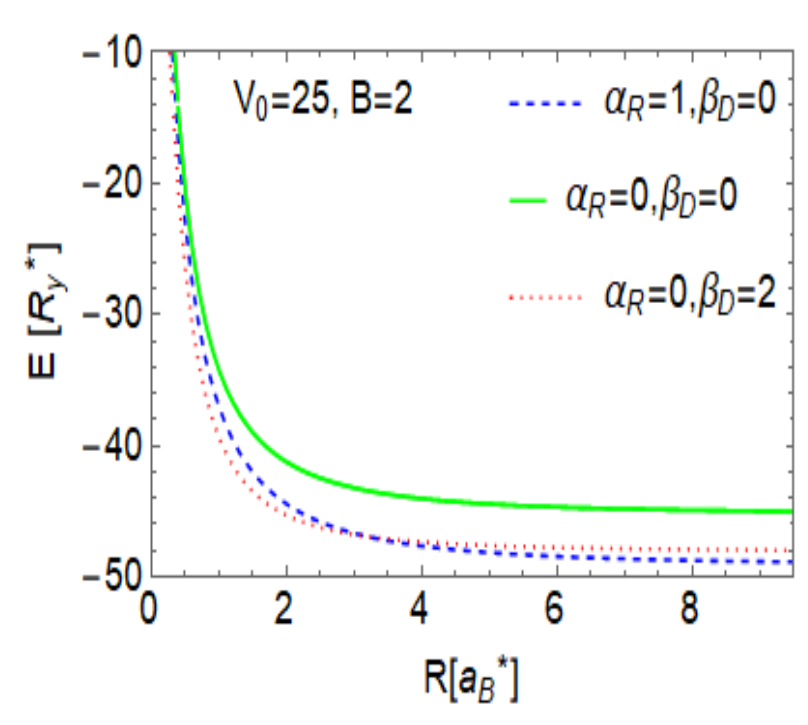


Fig.1 GS energy (*E*) of a D^- complex vs. R for a GaAs GQD with $V_0 = 25 \text{ R}_y^*$, B = 2 T and for a few combination of α_R (R_y^* - α_B^*) and β_D (R_y^* - α_B^*).

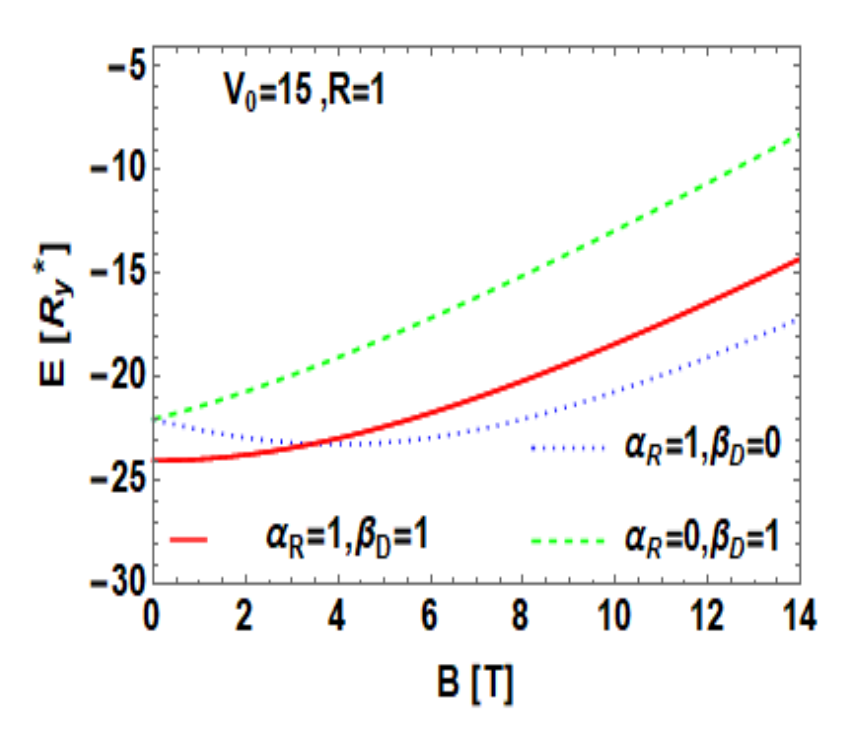


Fig. 2 E vs. B for a D^- system in a GaAs GQD with $V_0 = 15 R_y^*$, $R = 1 \alpha_B^*$ for different sets of α_R (R_y^* - α_B^*) and β_D (R_y^* - α_B^*).

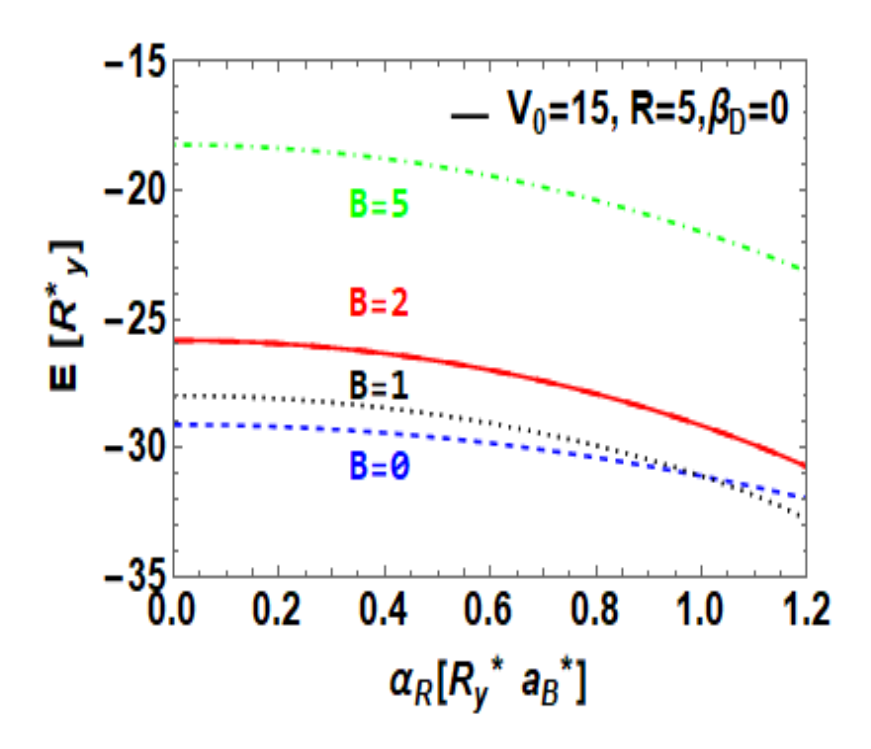


Fig. 3 *E* vs. α_R . for a D^- system in a GaAs GQD with $V_0 = 15 R_y^*$, $R = 1 \alpha_B^*$, $\beta_D = 0 R_y^* - \alpha_B^*$ for different sets of B (T).

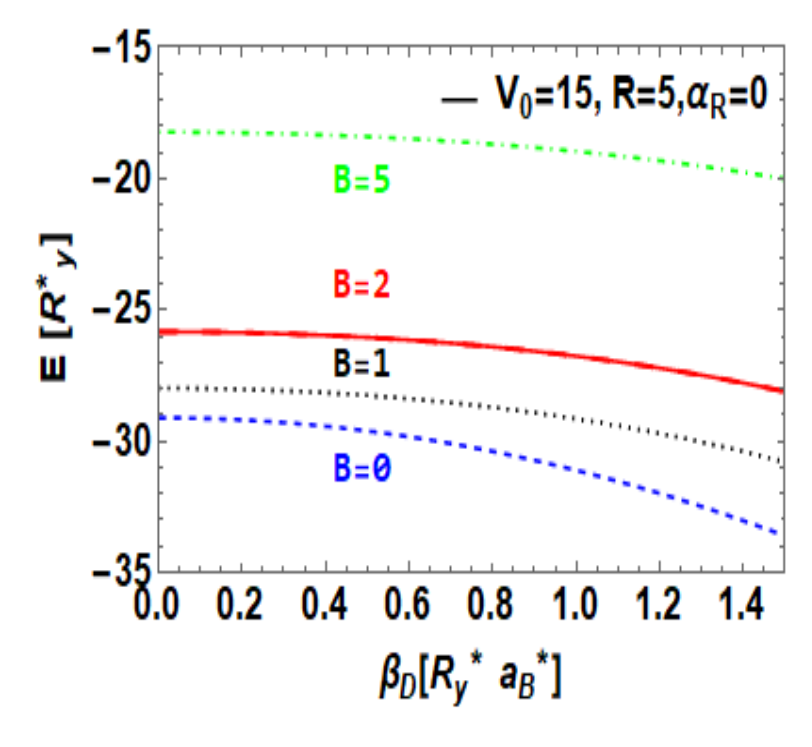


Fig. 4 E vs. β_D for a D⁻ complex in a GaAs GQD with $V_0 = 15 R_y^*$, $R = 1 a_B^*$, $\alpha_R = 0 R_y^* - a_B^*$ for different sets of B (T).

Fig. 3 exhibits the behaviour of E with α_R for a few values of B with $V_0 = 15R_y^*$, $R = 1\alpha_B^*$ in the case of $\beta_D = 0$, while Fig. 4 shows the behaviour with β_D for $\alpha_R = 0$. Though, both the Rashba and Dresselhaus interactions reduce the energy, it is evident that the Rashba effect is more dominant than the Dresselhaus one.

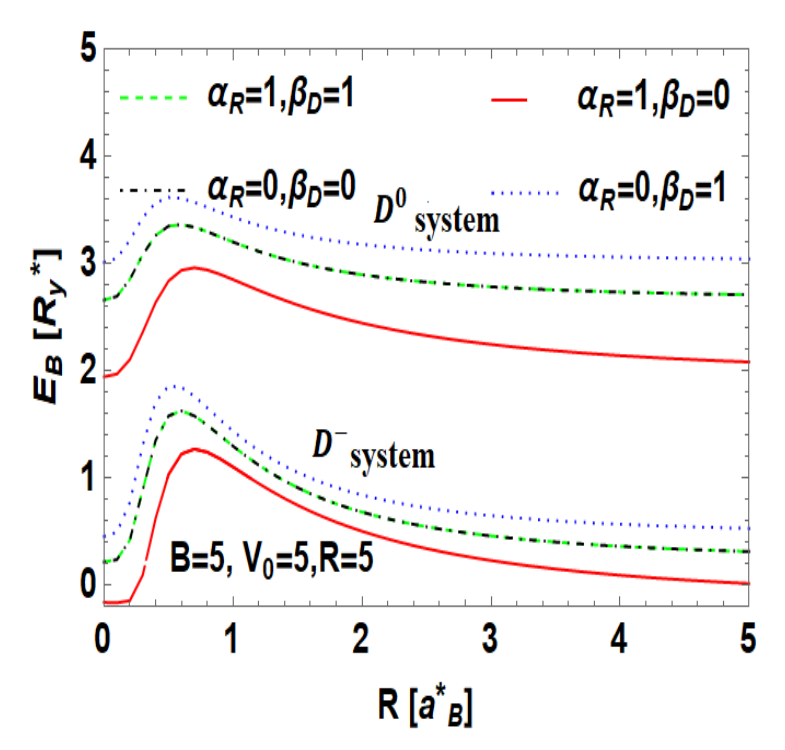


Fig. 5 GS binding energy E_B vs. R for a D⁰ and D⁻ complex in a GaAs GQD with B = 5 T, $V_0 = 15$ R_y^* , R = 1 a_B^* for different sets of α_R (R_y^* - a_B^*) and β_D (R_y^* - a_B^*).

Fig. 5 displays the behaviour of the BE (E_B) of the D^- centres with respect to R for a few sets of values of α_R and β_D . The figure shows that BE of a D^- impurity in a GaAs QD is positive which suggests that one can have a stable D^- in this material. The figure also shows the BE curves for a D^0 system and it is clear that in a GaAs GQD, D^- has a much weaker binding than D^0 , which is of course an expected result. In both the systems, however, DSOI increases the binding, while RSOI decreases it. One can see that the stability is maximum at a critical size (R_c) of the QD and below this size BE falls off rather sharply. The diminution in the strength of binding at small R is solely a quantum phenomenon. The critical length R_c depends on both the Rashba and Dreseelhaus interactions. The peak of the BE is increased by DSOI. From BE we can have an estimate of the binding temperature (T_B) i. e., the temperature above which the D^- will become unbound. Fig. 6 shows the T_B versus R plot for certain combinations of α_R and β_D values and thus the bound and the unbound regions.

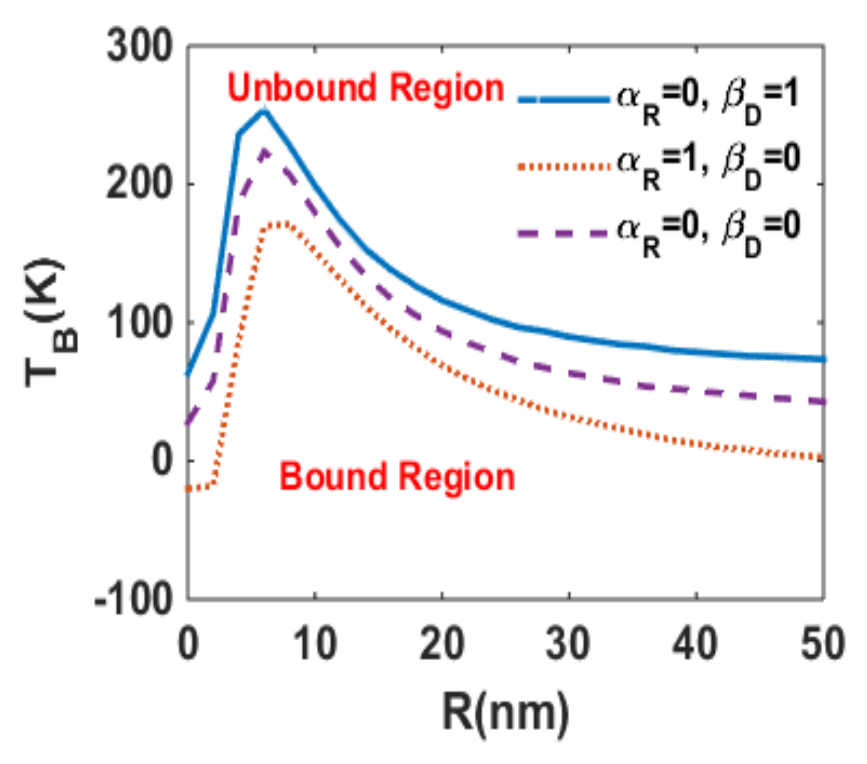


Fig. 6 GS binding temperature vs R for different sets of α_R (R_y^* - a_B^*) and β_D (R_y^* - a_B^*).

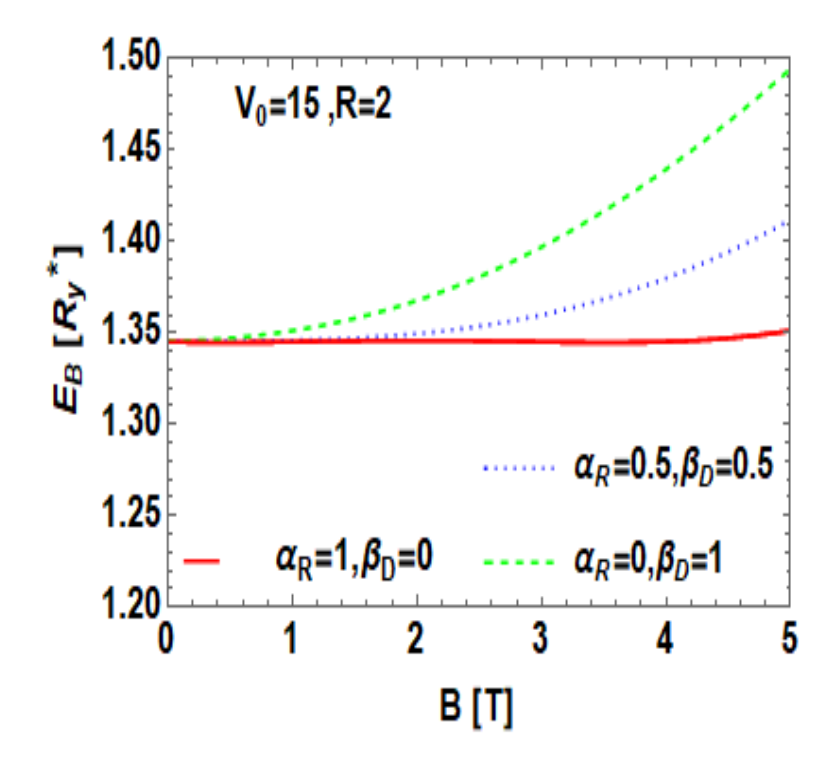


Fig. 7 E_B vs. B of a D^- complex in a GaAs GQD with $V_0 = 15 R_y^*$, $R = 2 a_B^*$ for different sets of $\alpha_R (R_y^* - a_B^*)$ and $\beta_D (R_y^* - a_B^*)$.

Fig. 7 presents the behaviour of E_B with B for a few combinations of α_R and β_D . One may note that in the presence of DSOI, BE increases with B. As we switch on a small RSOI together with DSOI, BE still increases with B but the rate of increase decreases. In the presence of RSOI alone, BE is essentially independent of B. We do not have the experimental values of BE of a D^- complex in a QD and so we cannot test the veracity of our results, but our results are of the same order of magnitude as the ones experimentally found for GaAs/AlGaAs heterostructure [3].

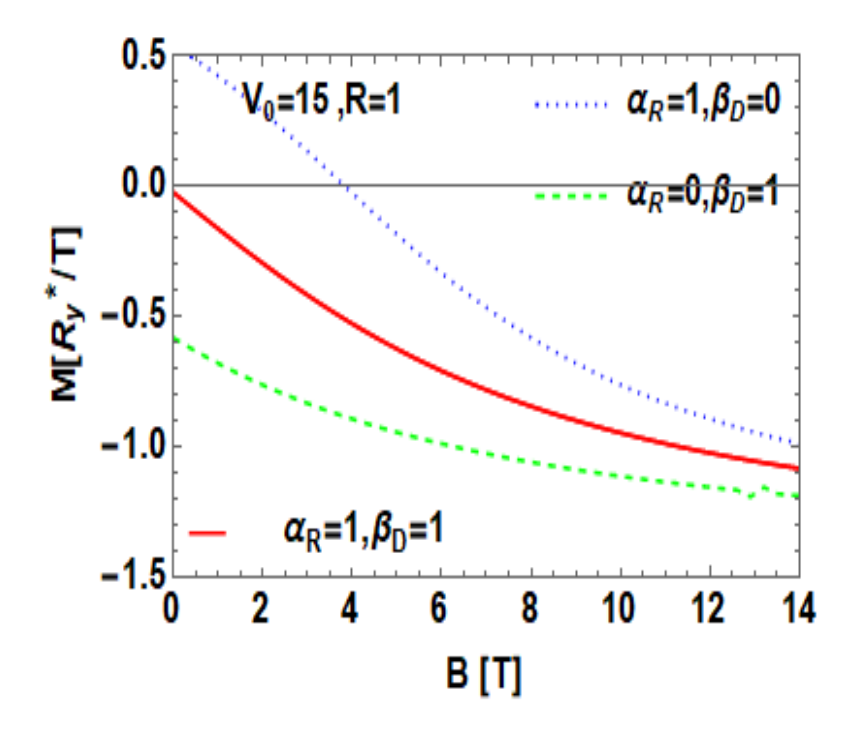


Fig. 8 Magnetic moment vs B of a D^- system in a GaAs GQD with $V_0 = 15 R_y^*$, $R = 1 \alpha_B^*$ for different sets of $\alpha_R (R_y^* - \alpha_B^*)$ and $\beta_D (R_y^* - \alpha_B^*)$.

In Fig. 8, we plot the magnetic moment M as a function of B for the D^- system with $V_0 = 15 R_y^*$, $R = 1 a_B^*$ and for different sets of values of α_R and β_D . |M| increases with increasing B. In the case of $\alpha_R = \beta_D$, M exhibits a purely diamagnetic behaviour. In the presence of DSO interaction alone, M is strongly diamagnetic. In the presence of RSO interaction alone, the behaviour of M is more interesting. It shows a paramagnetic behaviour at small B and a diamagnetic behaviour above a certain value of B.

Fig. 9 depicts how in the presence of RSOI and DSOI, the magnetic susceptibility S of the D^- system varies with B. One can see that S is negative for all values of B. Thus we reiterate that D^- is diamagnetic like D^0 . With DSOI alone, |S| increases with increasing B. With RSOI alone, the

behavior of S is more interesting. As B increases from zero, |S| initially decreases, then reaches a minimum at a critical B and finally increases with a further increase in B. When both the SOIs are present, |S| shows only an increasing behaviour with B.

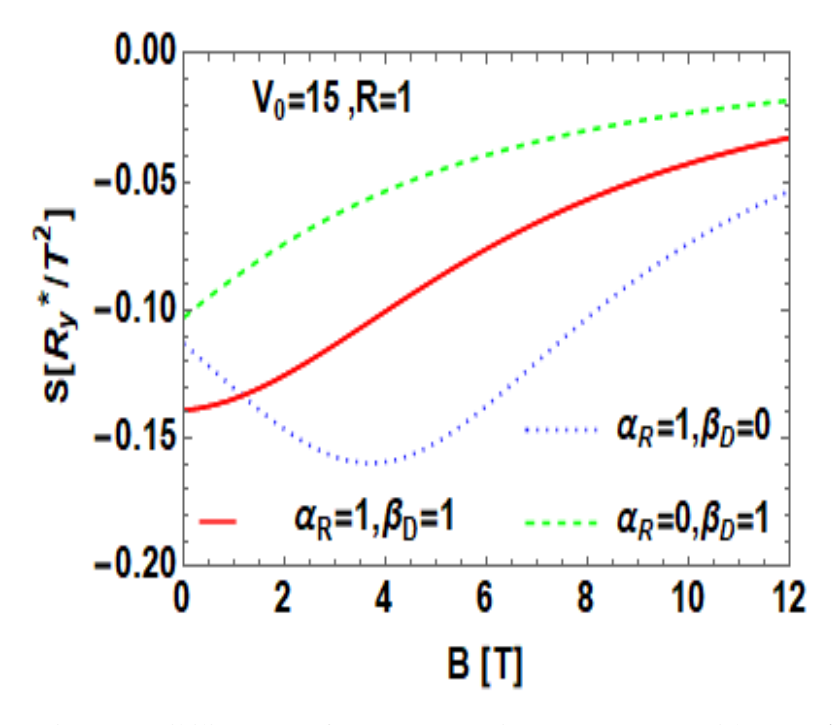


Fig. 9 Magnetic susceptibility vs B of a D^- system in a GaAs GQD with $V_0 = 15 R_y^*$, $R = 1 a_B^*$ for different sets of $\alpha_R (R_y^* - a_B^*)$ and $\beta_D (R_y^* - a_B^*)$.

Because of Coulomb correlation and quantum fluctuations, a D^- centre can develop a dipole moment (P). In Fig. 10, we show the variation of P with the Rashba parameter α_R for a few values of B in the absence of DSOI. For B=0, P turns out to be independent of α_R , while for $B\neq 0$, P is found to be an growing function of α_R , the rate of increase being much larger at higher α_R . For nonzero B, as B increases, P decreases at small values of α_R , while it increases at large α_R , giving rise to a crossing behaviour. The reason is understandable. As B increases, the motion of the electrons is restricted in the close proximity of the nucleus because of the confining effect of the field and consequently P reduces. Thus there is a competition between the effects of the magnetic field and RSOI on P. At small α_R , the magnetic field wins and dipole moment decreases with B whereas at large α_R , RSOI wins and the dipole moment increases with B. Fig.11 describes the behaviour of P with respect to β_D for a few B values in the absence of RSOI. For B=0, P is independent of β_D and for $B\neq 0$, P is a decreasing function of β_D . In the present case, the magnetic field reduces P for all β_D .

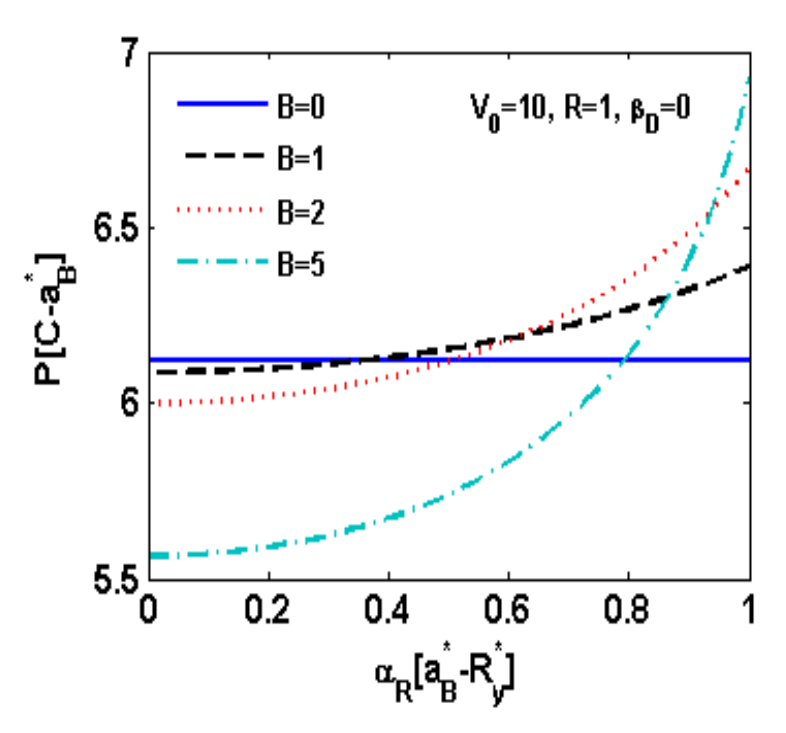


Fig. 10 dipole moment (*P*) vs α_R of a D⁻ system in a GaAs GQD with $V_0 = 10 R_y^*$, $R = 1 a_B^*$, $\beta_D = 0 R_y^* - \alpha_B^*$ for different sets of B (T).

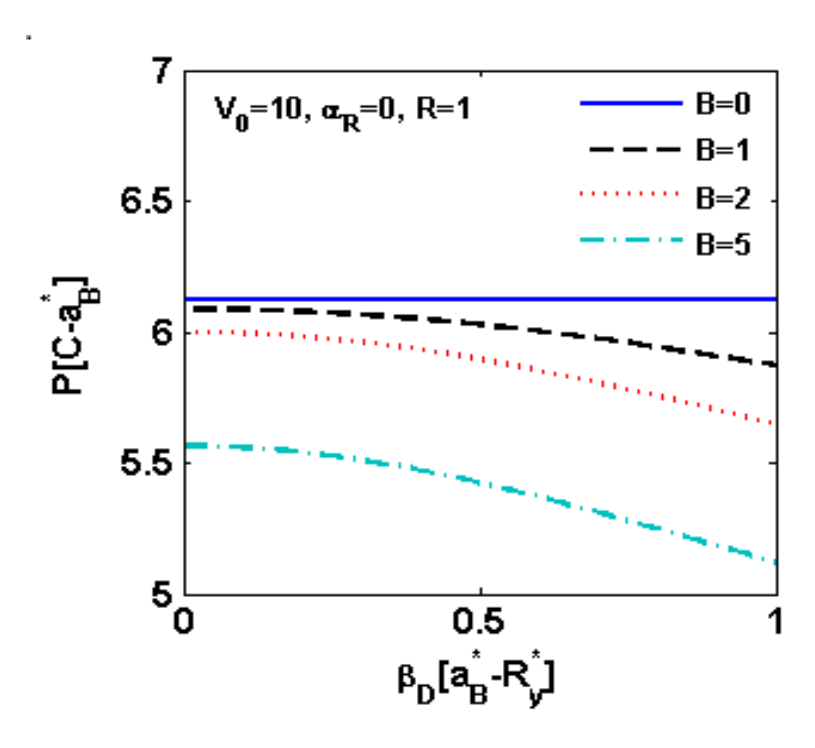


Fig. 11 P vs β_D of a D^- system in a GaAs GQD with $V_0 = 10 \text{ R}_y^*$, $R = 1 \text{ a}_B^*$, $\alpha_R = 0 \text{ R}_y^* - \alpha_B^*$ for different values of B (T).

In Fig.12, we show the variation of the the dipole moment P with respect to B for different sets of α_R and β_D . P decreases almost linearly with respect to B and the reason is again easy to understand in view of the confining effect of the field.

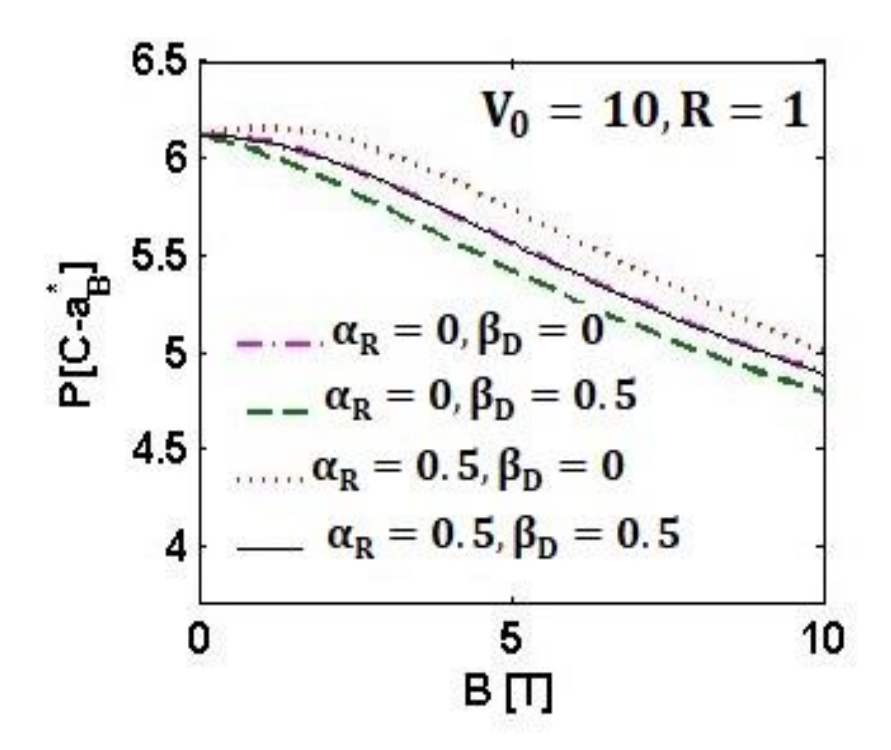


Fig. 12 P vs. B of a D^- complex in a GaAs GQD with $V_0 = 10 R_y^*$, $R = 1 \alpha_B^*$ for different sets of $\alpha_R (R_y^* - \alpha_B^*)$ and $\beta_D (R_y^* - \alpha_B^*)$.

Fig. 13 provides the plot of P versus R for a few sts of α_R and β_D . It is clear from the figure that P decreases with decreasing dot size even in the presence of SOIs. This is again not difficult to understand. The upturn in P at an extremely small R seems to be an artefact of the numerics. At large R, P attains the bulk value. One can also see from the figure that RSOI enhances P while DSOI reduces it. These observations are consistent with the results shown in Figs.10 and 11.

In Fig.14 we show the behaviour of P with respect to the depth of the QD potential (V_0) for a few combinations of α_R and β_D . P turns out to be a decreasing function of V_0 . The explanation for this behaviour is rather simple. For a given R, E decreases with increasing V_0 and consequently, BE increases. In this case, electrons also get closer to the nucleus leading to a reduction in P.

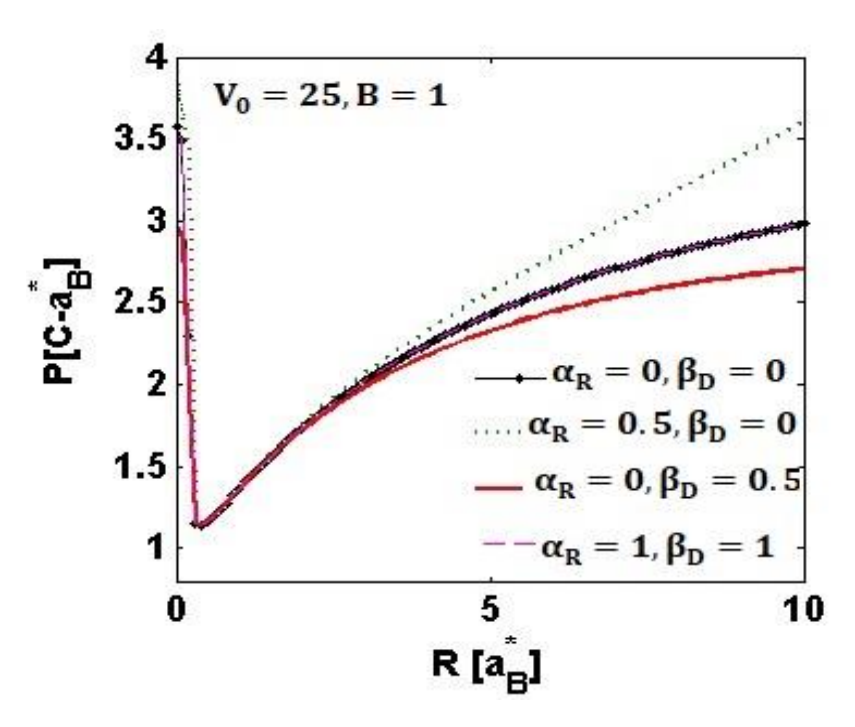


Fig. 13 P vs. R of a D^- complex in a GaAs GQD with $V_0 = 25 R_y^*$, B = 1 T for different sets of $\alpha_R (R_y^* - a_B^*)$ and $\beta_D (R_y^* - a_B^*)$.

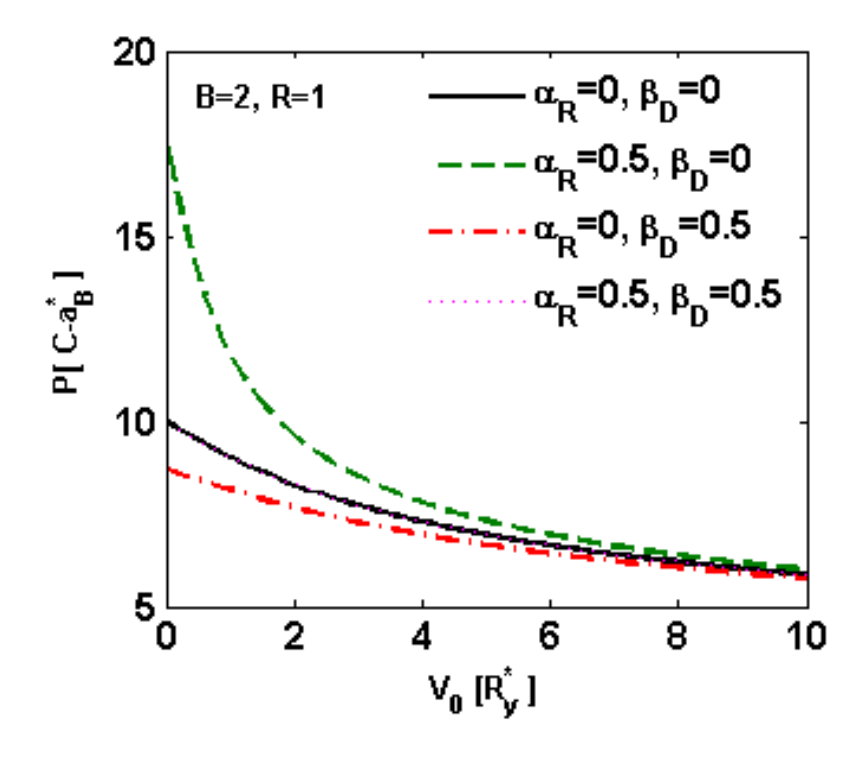


Fig. 14 P vs. V_0 of a D^- complex in a GaAs GQD with B=2 T, R=1 a_B^* for different sets of α_R $(R_y^*-a_B^*)$ and β_D $(R_y^*-a_B^*)$.

6.4 Conclusion

We have analysed variationally the role of spin-orbit interactions on the GS energy, binding energy, susceptibility and the dipole moment of a negative donor centre in a Gaussian QD of GaAs placed in a magnetic field. The Coulomb correlation has been taken into account by using the Jastrow method. Our results show unequivocally that a stable bound system of D^- complex can exist in a GaAs QD which should be experimentally observable. We have also shown that spinorbit interactions play an effective role in this problem. The Dresselhaus interaction enhances the binding energy while the Rashba coupling seems to reduce it. The binding becomes stronger with increasing magnetic field in the presence of the Dresselhaus interaction while it remains almost unaffected by the Rashba coupling. We have also calculated the susceptibility which has turned out to be diamagnetic in character. Interestingly, in the presence Rashba interaction, the susceptibility curve exhibits a minimum. Finally we have shown the behaviour of the dipole moment of the D^- system as a function of several QD parameters. We have shown that in the magnetic fied's absence, the dipole moment D^- in a GQD is not affected by the spin-orbit interactions. However, if the magnetic field is present, the Rashba coupling enhances the dipole moment of the negative donor impurity, while the Dresselhaus coupling reduces it. The strength of the dipole moment also rises with the QD size and reduces with the increasing potential depth and the magnetic field.

6.5 References

- [1] M.A. Lampert, Phys. Rev. Lett. 1, 450 (1958).
- [2] R.N. Hill, Phys. Rev. Lett. 38 643 (1977).
- [3] S. Huant, S.P. Najda, B. Etienne, Phys. Rev. Lett. 65, 1486 (1990).
- [4] D.E. Phelps, K.K. Bajaj, Phys. Rev. B 26 (1982) 912; D.E. Phelps, K.K. Bajaj, Phys. Rev. B 27 4883 (1983).
- [5] C.J. Armistead, S.P. Najda, P.A. Makado, R.A. Stradling, P.C. Coulter, G.E. Stillman, Solid State Commun. 48, 51 (1983).
- [6] Jie-Hua Zhao, Wen-Hui Duan, Gu Bing-Lin, Phys. Rev. B 46, 12 (1992);
 J.L. Zhu, Xi Chen, Phys. Rev. B 50, 4497 (1994);
 Wen-Fang Xie, Chinese Phys Lett. 22, 1768 (2005);

Gu Juan, Jiu-Qing Liang, Phys. Lett. A 335, 451 (2005);

Wen-Fang Xie, Commun. Theor. Phys. (Beijing, China) 47, 167 (2007);

Yuan-Peng Bao, Wen-Fang Xie, Commun. Theor. Phys. (Beijing, China) 50, 1449 (2008);

L. Chang, Wen-Fang Xie, Commun. Theor. Phys. (Beijing, China) 45, 1117 (2008);

Dong-Ming Liu, Wen-Fang Xie, Commun. Theor. Phys. (Beijing, China) 51, 919 (2009);

S.S. Gomez, R.H. Romero, Physica E 42, 1563 (2010);

Aalu Boda, A. Chatterjee, Physica E 45, 36 (2012);

A. Boda, B. Boyacioglu, A. Chatterjee, J. Appl. Phys. **114**, 044311 (2013).

- [7] A. Boda, M. Gorre, A. Chatterjee, Superlattices and Microstructures **71**, 261 (2014).
- [8] P. Saini, A. Boda, Ashok Chatterjee, J. Mag. Mag. Mat. 485, 407 (2019);
 P. Saini, S. Mukhopadhyay, Ashok Chatterjee, Physica B Condensed matter, 617, 413099 (2021).

Chapter ~7

Thermoelectric properties of single molecular transistor

7.1 Introduction

With recent advances in molecular scale electronics, areas like Spintronics and Spin caloritronics [1-3] have received considerable attention. Controlling electron-spin and consequently the spin current is the hallmark of spintronics. In contrast, in spin caloritronics [4], the spin current is primarily controlled and manipulated by thermal bias generated through a temperature gradient applied to the system's various ends. This is an area that can be considered as a fusion of thermoelectricity and spintronics. Spin transport in semiconductors is expected to give rise to dissipation-less information transfer with pure spin currents. For instance, spin-based transistors do not rely on the raising or lowering of electrostatic barriers and therefore can bypass scaling limitations that occur in charge-based transistors. The spin Seebeck effect (SSE), one of the most fascinating phenomena in spin caloritronics, is the formation of a spin current as a result of a temperature gradient. In a quantum dot (QD) junction, SSE has lately been the subject of extensive investigations. Several materials or heterojunctions including magnetic metals [5], semiconductors [6] and insulators [7,8] have shown evidence of SSE and some unique spin-based thermodynamic properties. Theoretical investigation shows that SSE can be considerably enhanced by inserting a QD between a metal lead and a magnetic insulator. This enhancement happens because of spin flipping and quantum resonance.

SSE was first discovered by Uchida et al. [9] in a ferromagnetic metal. It has also been observed in ferromagnetic insulators [10] and semiconducting materials [11], nonmagnetic materials with a magnetic field [12], paramagnetic materials [13], antiferromagnetic materials [14], metal-

ferromagnet insulators [15] and also topological insulators [16]. More recently, antiferromagnetic SSE has been predicted and measured in MnF_2 . When two charge carriers of spin components, S_{\uparrow} and S_{\downarrow} exhibit equal magnitude of charge but of opposite sign, the charge Seebeck coefficient $(S_c \propto (S_{\uparrow} + S_{\downarrow}))$ vanishes while the spin Seebeck coefficient becomes finite $(S_s \propto S_{\uparrow} - S_{\downarrow})$ resulting in the net spin voltage with the charge voltage being zero. SSE can be described by the spin-resolved Seebeck coefficient (or thermo-power).

Recently, there has been an upsurge in the interest in single molecular transistors, which can play a crucial role in nano-electronics. A single molecular transistor (SMT) is a nano-device with a molecule or QD [17] in its centre that has discrete energy levels and is connected to a source and a drain by metallic leads. The conduction electrons in S and D are considered to be free so that they can be described by continuous energy levels. The entire arrangement is placed on an insulating substrate which is mounted on a gate. The current flowing through the SMT device can be effectively manipulated by tuning the gate voltage. The first SMT device was fabricated in 2000 by linking the source and the drain with a single C60 molecule. A large number of investigations have revealed that SMT transport shows low-temperature correlated phenomena such as the Coulomb blockade and the Kondo effect [18-20]. However, in polar QDs, the interaction of electrons with phonons produces polarons which are electrons dressed with the cloud of virtual phonons and are the quasi-particles that participate in the transport process in these systems. Both electron-electron (el-el) and electron-phonon (el-ph) interactions affect the transport parameters of a correlated polar SMT device in general.

In the present study, we consider an SMT system placed in an external magnetic field and is mounted on an insulating substrate that contains a collection of uncoupled harmonic oscillators and acts as a heat bath giving rise to a dissipative effect to the current in SMT. We assume that QD has a single phonon mode that interacts with the substrate phonons and also with the QD electrons. We use the non-equilibrium Keldysh Green function formalism to study the effect of elel and el-ph interactions, magnetic field and dissipation on the thermal transport characteristics of the SMT device. In particular, we calculate the charge and spin-Seebeck effect.

7.2 The Modal

We assume that the QD electrons of the SMT system interact with each other through the Hubbard onsite Coulomb interaction and with the single QD phonon via Holstein-type el-ph coupling. We

model the tunneling of electrons from S to QD and QD to D and vice versa by the Anderson Hamiltonian and assume that the QD phonon and the substrate phonons interact with each other via a linear Caldeira-Leggett (CL) interaction. This interaction renormalizes the frequency of the QD phonon leading to a dissipative effect in the SMT current. An external magnetic field is applied to the SMT system as shown in Fig. 1. This magnetic field lifts the spin degeneracies of the electronic levels. Due to the lifting of the spin degeneracy, the QD setup acts

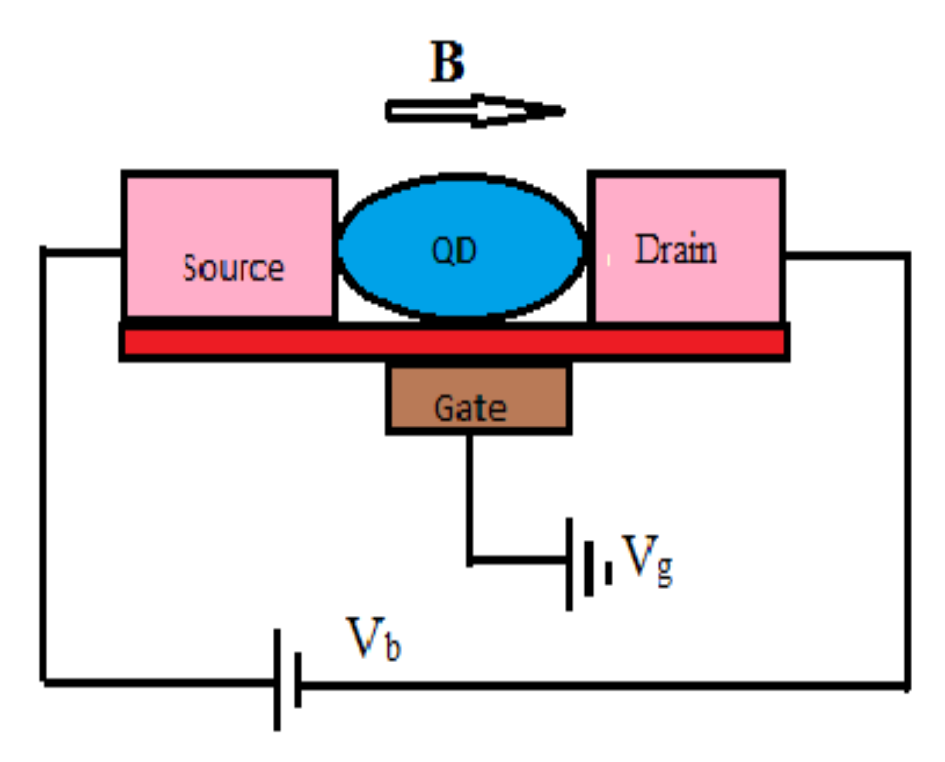


Fig.1 Schematic representation of an SMT device.

as a spin-filtering device and produces a current that is spin-polarized. The system can be modelled by the Anderson-Holstein-Caldeira-Leggett Hamiltonian given by

$$H = H_l + H_{QD} + H_t + H_B. (7.1)$$

The first term H_l in Eq. (1) denotes the Hamiltonian of the leads, i.e., the source (l = S) and the drain (l = D) and is given by

$$H_l = \sum_{k\sigma \in S, D} \varepsilon_k \, n_{k\sigma} \,, \tag{7.2}$$

where $n_{k\sigma}(=c_{k\sigma}^{\dagger}c_{k\sigma})$ represents the number operator for the conduction electrons with momentum k and spin σ in the metallic leads, $c_{k\sigma}^{\dagger}(c_{k\sigma})$ being the creation (annihilation) operator for the corresponding electrons. The second term, H_{QD} refers to the Hamiltonian of the QD and can be written as

$$H_{\rm QD} = \sum_{\sigma} (\varepsilon_d - eV_g) n_{d\sigma} + U n_{d,\sigma} n_{d,-\sigma} + \frac{1}{2} g \mu_B B S_d^z + \left(\frac{p_0^2}{2m_0} + \frac{1}{2} m_0 \omega_0^2 x_0^2 \right) + \gamma \sum_{\sigma} n_{d\sigma} x_0 , \qquad (7.3)$$

where $n_{d\sigma}$ (= $c_{d\sigma}^{\dagger}c_{d\sigma}$) represents the number operator for the QD electrons with energy ε_d and spin σ , $c_{d\sigma}^{\dagger}$ ($c_{d\sigma}$) being the creation (annihilation) operator of the electrons, V_g denotes the gate voltage, U gives the measure of the onsite e-e interaction, B (0,0,B) refers to the magnetic field, S_d^z describes the z-component of the QD spin, μ_B is the Bohr magneton, g is the gyromagnetic ratio, (x_0 , p_0) are the coordinate and the corresponding canonical momentum of the QD lattice mode, ω_0 being the mode frequency and γ is the e-p coupling coefficient. The third term in (1) describes the tunneling of electrons from the leads to QD and vice versa and is given by

$$H_t = \sum_{k\sigma \in S.D} (V_k c_{k\sigma}^{\dagger} c_{d\sigma} + h.c), \tag{7.4}$$

where V_k is known as the hybridization coefficient, which essentially determines the strength of electron tunneling between the QD and the source or drain. H_B represents the phonon bath and its interaction with the local QD phonon mode and is given by

$$H_B = \sum_{j=1}^{N} \left[\frac{p_j^2}{2m_j} + \frac{1}{2} m_j \omega_j^2 x_j^2 \right] + \sum_{j=1}^{N} \beta_j x_j x_0 , \qquad (7.5)$$

where (x_j, p_j) are the generalized variables of the *j*-th substrate oscillator, ω_j its frequency and β_j denotes the strength of the CL coupling between the *j*-th oscillator of the substrate and the QD oscillator. The spectral density of the substrate phonons $(J(\omega))$ is described by the function:

$$J(\omega) = \sum_{i=1}^{N} \left[\frac{\beta_j^2}{2m_j \omega_j} \right] \delta(\omega - \omega_j). \tag{7.6}$$

7.3 Formulation

7.3.1 Decoupling of coupling between QD and bath phonons interaction

In order to decouple the local QD phonon from the bath phonons partially, we perform the unitary transformations,

$$\widetilde{x}_j = x_j + \frac{\beta_j x_0}{m_j \omega_j^2} \quad , \tag{7.7}$$

$$\tilde{p}_j = -\iota \hbar \frac{\partial}{\partial \tilde{x}_j} \,, \tag{7.8}$$

which renormalize the local phonon frequency to

$$\widetilde{\omega}_0 = \sqrt{(\omega_0^2 - \Delta \omega^2)},\tag{7.9}$$

where

$$\Delta\omega = \left(\sum_{j=1}^{N} \frac{{\beta_j}^2}{m_0 m_j \omega_j^2}\right)^{1/2}.$$
 (7.10)

From now onwards, we will concentrate on SMT only. Using Eq. (7.6) for the spectral density, $(\Delta\omega)^2$ can be written as

$$(\Delta\omega)^2 = \frac{2}{m_0} \int_0^\infty \frac{J(\omega)}{\omega} d\omega, \tag{7.11}$$

In the Ohmic situation, the spectral density $I(\omega)$ follows the relationship:

$$J(\omega) = 2m_0 \gamma \omega \tag{7.12}$$

for all frequencies, where the Ohmic damping coefficient can be expressed as

$$\gamma = \frac{1}{2m_0} \sum_{j=1}^{N} \left(\frac{\beta_j^2}{2m_j \omega_j^2} \right) \delta(\omega - \omega_j) . \tag{7.13}$$

One can see from Eq. (7.13) that γ diverges in the limit: $\omega \to \infty$ and therefore the form of γ given by (7.13) is not a realistic expression for a pure Ohmic spectral density. To salvage the situation, one introduces a cut-off frequency. In this regard, various forms have been proposed. We employ the Lorentz-Drude form [6], which gives $J(\omega)$ as follows:

$$J(\omega) = \frac{2m_0\gamma\omega}{\left[1 + \left(\frac{\omega}{\omega_c}\right)^2\right]},\tag{7.14}$$

where ω_c denotes the cut-off frequency. It is evident that in the limit: $\omega \to \infty$, $J(\omega) \to 0$, and in the limit: $\omega \to 0$, one obtains the pure Ohmic spectral density. Finally, we can express the change in the frequency of QD phonon as:

$$\Delta\omega^2 = 2\pi\gamma\omega_c \,. \tag{7.15}$$

The reduction in the frequency of the QD phonon gives rise to a resistive effect which is precisely the role of the substrate towards dissipation. We neglect the higher-order dissipative effects. The total transformed Hamiltonian is given by

$$\overline{H} = \sum_{k\sigma\in S,D} \varepsilon_k n_{k\sigma} + \sum_{\sigma} (\varepsilon_d - eV_g) n_{d\sigma} + \sum_{k\sigma\in S,D} (V_k c_{k\sigma}^{\dagger} c_{d\sigma} + h.c) + U n_{d,\sigma} n_{d,-\sigma} + g\mu_B B S_d^z + \hbar \widetilde{\omega}_0 b^{\dagger} b + \lambda \hbar \widetilde{\omega}_0 \sum_{\sigma} n_{d\sigma} (b^{\dagger} + b).$$
(7.16)

where λ is the renormalized el-ph coupling constant (renormalized by the QD-bath interaction).

7.3.2 Elimination of phonons

To decouple this interaction, we apply the celebrated Lang-Firsov transformation (LFT) [43] with a unitary operator: $U = e^s$, where

$$S = \lambda(b^{\dagger} - b) \sum_{\sigma} n_{d\sigma} \,. \tag{7.17}$$

It is well-known that this transformation works better for in the anti-adiabatic regime. The transformed Hamiltonian can be written as

$$\widetilde{H} = e^S H e^{-S} \quad , \tag{7.18}$$

The electron operators of the system are transformed as follows:

$$\tilde{c}_{d\sigma} = c_{d\sigma}\hat{\chi}, \qquad \tilde{c}_{d\sigma}^{\dagger} = c_{d\sigma}^{\dagger}\hat{\chi}^{\dagger} \quad , \tag{7.19}$$

where

$$\hat{\chi} = e^{-\lambda(b^{\dagger} - b)}, \quad \hat{\chi}^{\dagger} = e^{+\lambda(b^{\dagger} - b)}, \qquad (7.20)$$

and the phonon operators are transformed as:

$$\tilde{b} = b - \sum_{\sigma} \lambda n_{d\sigma} , \qquad \tilde{b}^{\dagger} = b^{\dagger} - \sum_{\sigma} \lambda n_{d\sigma} .$$
 (7.21)

Thus the transformed Hamiltonian reads

$$\widetilde{H} = \sum_{k\sigma\in S,D} \varepsilon_k \, n_{k\sigma} + \sum_{\sigma} \widetilde{\varepsilon}_d n_{d\sigma} + \, \widetilde{U} n_{d,\sigma} n_{d,-\sigma} + \hbar \widetilde{\omega}_0 b^{\dagger} b + \sum_{k\sigma\in S,D} (\widetilde{V}_k \, c_{k\sigma}^{\dagger} c_{d\sigma} + h. \, c), \quad (7.22)$$

with

$$\tilde{\varepsilon}_{d\sigma} = \varepsilon_d - eV_g - \mu_B \sigma B - \lambda^2 \hbar \widetilde{\omega}_0 , \qquad (7.23)$$

$$\widetilde{U} = U - 2\hbar \widetilde{\omega}_0 \lambda^2, \tag{7.24}$$

$$\widetilde{V}_k = V_k \hat{\chi} = V_k e^{\lambda(b-b^{\dagger})} . \tag{7.25}$$

where $\tilde{\varepsilon}_{d\sigma}$ is the QD energy renormalized by the el-ph interaction, \tilde{U} denotes the modified Coulomb correlation strength and \tilde{V}_k represents the phonon-mediated hybridization strength.

7.3.3 Tunnelling current: Non-equilibrium Keldysh Green function formalism

We calculate the expression for the current density employing Keldysh method. We present here the derivation of the tunnelling current expression in the presence of the el-el, el-ph interactions and quantum dissipation. The current from the source to the QD in SMT can be written as the average value of the rate of change of charge operator:

$$Q = -eN_s (7.26)$$

where N_s is the number operator for the source electrons which is given by

$$N_{s\sigma} = \sum_{k\sigma \in S} c_{k\sigma}^{\dagger} c_{k\sigma}. \tag{7.27}$$

Thus the tunnelling charge current flowing through the central interacting QD can be written as:

$$J_{S\sigma} = -e \left\langle 0 \left| \frac{dN_{S\sigma}}{dt} \right| 0 \right\rangle = -\frac{\iota e}{\hbar} \left\langle 0 \right| \left[\widetilde{H}, N_{S\sigma} \right] \left| 0 \right\rangle , \qquad (7.28)$$

where \widetilde{H} refers to the transformed Hamiltonian in equation (7.22) and the averaging state $|0\rangle$ is the ground state of the whole system i.e., $|0\rangle = |0\rangle_{el} |0\rangle_{ph}$. Since N_s commutes with all but the hybridization term of \widetilde{H} , we obtain

$$J_{s\sigma} = \frac{\iota e}{\hbar} \sum_{k\sigma \in s} \left[\overline{\tilde{V}}_k < c_{k\sigma}^{\dagger} c_{d\sigma} > -h.c \right] , \qquad (7.29)$$

where $\overline{\tilde{V}}_k$ is the average of \tilde{V}_k with respect to the phonon state of the system. Eq. (7.29) can be written as

$$J_{s\sigma} = \frac{2e}{\hbar} Re \left\{ \sum_{k\sigma \in s} \left[\overline{\tilde{V}}_k \ G_{k\sigma,d}^{<}(t,t) \right] \right\}, \tag{7.30}$$

where $G_{k\sigma,d}^{<}(t,t')$ and $G_{d,k\sigma}^{>}(t,t')$ are the Keldysh lesser and greater tunnelling Green functions defined as

$$G_{k\sigma,d}^{\leq}(t,t') = i\langle 0|c_d^{\dagger}(t')c_{k\sigma}(t)|0\rangle, \tag{7.31a}$$

$$G_{d,k\sigma}^{\leq}(t,t') = i\langle 0|c_{k\sigma}^{\dagger}(t')c_d(t)|0\rangle, \tag{7.31b}$$

with the property:

$$G_{k\sigma,d}^{\leq}(t,t) = -\left[G_{d,k\sigma}^{\leq}(t,t)\right]^{*}, \qquad (7.32)$$

$$c_{d\sigma}(t) = e^{-i\tilde{H}_{el}t}c_{d\sigma}e^{i\tilde{H}_{el}t} . (7.33)$$

Eq. (7.30) can be written as

$$J_{S} = \frac{2e}{\hbar} Re \left\{ \sum_{k\sigma \in S} \widetilde{V}_{k} G_{d,k\sigma}^{\leq}(t,t) \right\} . \tag{7.34}$$

 $G_{d,k\sigma}^{\leq}(t)$ can be obtained through the equation of motion (EOM) method. Due to the structural similarity between the non-equilibrium theory and the equilibrium theory, we consider the zero temperature time-ordered Green function and its equation of motion. So, let us define the retarded and the advanced tunnelling Green functions as

$$G_{d,k\sigma}^{r(a)}(t-t') = \mp i\theta(\pm t \mp t')\langle 0 | \{\tilde{c}_d(t), c_k^{\dagger}(t')\} | 0 \rangle, \qquad (7.35)$$

which satisfies the following inhomogeneous equation:

$$\left(-i\frac{\partial}{\partial t'} - \varepsilon_k\right) G_{d,k\sigma}^{r(a)}(t - t') = V_k^* G_{dd}^{r(a)}(t - t') , \qquad (7.36)$$

where the retarded (advanced) QD Green function $G_{dd}^{r(a)}(au=t-t')$ is defined as

$$G_{dd}^{r(a)}(\tau) = \mp i \; \theta(\pm t \mp t') \langle 0 | \{ \tilde{c}_d(t), \tilde{c}_d^{\dagger}(t') \} | 0 \rangle . \tag{7.37}$$

Therefore, Eq. (7.36) can be easily solved to give

$$G_{d,k\sigma}^{r(a)}(\tau) = \int d\tau \, V_k^* G_{dd}^{r(a)}(\tau) g_{k\sigma}^{r(a)}(\tau) , \qquad (7.38)$$

where $g_{k\sigma}^{r(a)}(au)$ is the non-interacting lead Green function given by

$$g_{k\sigma}^{r(a)}(t-t') = \mp i\theta \left((\pm t \mp t') \right) \langle \left\{ c_{k\sigma}^{\dagger}(t), c_{k\sigma}(t') \right\} \rangle$$

$$= \mp i\theta ((\pm t \mp t'))e^{-i\varepsilon_k(t-t')}. \tag{7.39}$$

where the averaging state is the ground state of the non-interacting electron system. $g_{k\sigma}^{r(a)}$ satisfies the equation

$$\left(-i\frac{\partial}{\partial t} - \varepsilon_k\right) g_{k\sigma}^{r(a)}(t) = \delta(t) . \tag{7.40}$$

According to the analytical continuum rule, $C(\tau) = A(\tau)B(\tau)$, which can be explicitly written as

$$C(t,t') = \int dt_1 A(t,t_1)B(t_1,t') , \qquad (7.41)$$

on the real axis, can be written as

$$C^{<}(t,t') = \int \left[A^{<}(t,t_1)B^{(a)}(t_1,t') + A^{r}(t,t_1)B^{<}(t_1,t') \right] dt_1.$$
 (7.42)

So we can write

$$G_{d,k\sigma}^{\leq}(t,t') = \int dt_1 V_k^* [G_{dd}^{\leq}(t,t_1)g_{k\sigma}^a(t_1,t') + G_{dd}^r(t,t_1)g_{k\sigma}^{\leq}(t_1,t')], \qquad (7.43)$$

where

$$G_{dd}^{<}(\tau) = i\langle 0|c_d^{\dagger}(t')c_d(t)|0\rangle, \tag{7.44}$$

$$G_{dd}^{>}(\tau) = i\langle 0|c_d(t) c_d^{\dagger}(t')|0\rangle, \tag{7.45}$$

$$g_{k\sigma}^{\leq}(t-t') = i\langle c_{k\sigma}^{\dagger}(t')c_{k\sigma}(t)\rangle = i f(\varepsilon_k)e^{-i\varepsilon_k(t-t')}, \tag{7.46}$$

 $f(\varepsilon_k)$ denoting the Fermi-Dirac (FD) distribution function. The Fourier transforms of the different Green functions are defined as

$$G_{d,k\sigma}^{<}(\tau) = \frac{1}{2\pi} \int d\varepsilon \ e^{-i\varepsilon\tau} G_{d,k\sigma}^{<}(\varepsilon), \tag{7.47}$$

$$G_{dd}^{r}(\tau) = \frac{1}{2\pi} \int d\varepsilon \, e^{-i\varepsilon\tau} G_{dd}^{r}(\varepsilon) \,, \tag{7.48}$$

$$G_{dd}^{<}(\tau) = \frac{1}{2\pi} \int d\varepsilon \ e^{-i\varepsilon\tau} \ G_{dd}^{<}(\varepsilon), \tag{7.49}$$

$$g_{k\sigma}^{a}(\tau) = \frac{1}{2\pi} \int d\varepsilon \ e^{-i\varepsilon\tau} \ g_{k\sigma}^{a}(\varepsilon) , \qquad (7.50)$$

where $G_{dd}^{r(a)}(\varepsilon)$ and $G_{dd}^{<}(\varepsilon)$ represent the retarded (advanced) and lesser Keldysh Green functions respectively for the QD electron in the energy space and $g_{k\sigma}^{a}(\varepsilon)$ refers to the advanced Green function for the non-interacting electrons in the ε -space. The first term of $G_{d,k\sigma}^{<}(t,t')$ can be calculated as follows.

$$G_{d,k\sigma}^{\leq}(t,t') = \int dt_1 V_k^* G_{dd}^{\leq}(t,t_1) g_{k\sigma}^a(t_1,t')$$

$$= \left(\frac{1}{2\pi}\right)^2 \int dt_1 V_k^* \int d\varepsilon \, e^{-i\varepsilon(t-t_1)} G_{d,k\sigma}^{\leq}(\varepsilon) \int d\varepsilon' \, e^{-i\varepsilon'(t_1-t')}$$

$$= \frac{1}{2\pi} \int d\varepsilon \, V_k^* \, G_{d,k\sigma}^{\leq}(\varepsilon) g_{k\sigma}^a(\varepsilon) \, e^{-i\varepsilon(t-t')} \quad . \tag{7.51}$$

Similarly, we can calculate the second term of $G_{d,k\sigma}^{\leq}(t,t')$ and thus $G_{d,k\sigma}^{\leq}(t,t')$ is given by

$$G_{d,k\sigma}^{\leq}(t,t') = \int \frac{d\varepsilon}{2\pi} V_k^* \left[G_{d,k\sigma}^{\leq}(\varepsilon) g_{k\sigma}^a(\varepsilon) + G_{dd}^r(\varepsilon) g_{k\sigma}^{\leq}(\varepsilon) \right] e^{-i\varepsilon(t-t')}. \tag{7.52}$$

We obtain the expression for the source current as

$$J_{s\sigma} = \frac{2e}{\hbar} \int \frac{d\varepsilon}{2\pi} Re \left\{ \sum_{k} \tilde{V}_{k} V_{k}^{*} [G_{dd}^{r}(\varepsilon) g_{k\sigma}^{<}(\varepsilon) + G_{dd}^{<}(\varepsilon) g_{k\sigma}^{a}(\varepsilon)] \right\}, \qquad (7.53)$$

where $g_{k\sigma}^{<}(\varepsilon)$ is given by:

$$g_{k\sigma}^{<}(\varepsilon) = \int d\tau \ e^{i\varepsilon\tau} \ g_{k\sigma}^{<}(\tau) = 2\pi i \ f(\varepsilon_k) \delta(\varepsilon - \varepsilon_k). \tag{7.54}$$

We first consider the first term in the current expression (7.54). We denote this term by $J_{s\sigma}(1)$.

$$J_{s\sigma}(1) = \frac{2e}{\hbar} \int \frac{d\varepsilon}{2\pi} Re \left\{ \sum_{k} \tilde{V}_{k} V_{k}^{*} [G_{dd}^{r}(\varepsilon) g_{k\sigma}^{<}(\varepsilon)] \right\}.$$
 (7.55)

We convert the momentum summation into energy integration and get

$$J_{s\sigma}(1) = \frac{2e}{\hbar} \int \frac{d\varepsilon}{2\pi} \int d\varepsilon_k \, \Gamma_S(\varepsilon_k) \, Re[G^r_{dd}(\varepsilon)i\delta(\varepsilon - \varepsilon_k)f_S(\varepsilon_k)] \,, \tag{7.56}$$

where

$$\Gamma_{S}(\varepsilon_{k}) = 2\pi \varrho_{S}(\varepsilon_{k}) \overline{\tilde{V}}_{k} V_{k}^{*}, \qquad (7.57)$$

 ρ_S and $f_S(\varepsilon)$ being respectively the density of states and the Fermi distribution function of the source. Integration over ε_k gives

$$J_{s}(1) = \frac{2e}{\hbar} \int \frac{d\varepsilon}{2\pi} f_{s}(\varepsilon) \Gamma_{s}(\varepsilon) Re\{iG_{dd}^{r}(\varepsilon)\} = -\frac{2e}{\hbar} \int \frac{d\varepsilon}{2\pi} f_{s}(\varepsilon) \Gamma_{s}(\varepsilon) Im\{G_{dd}^{r}(\varepsilon)\}$$

$$= \frac{ie}{\hbar} \int \frac{d\varepsilon}{2\pi} f_{s}(\varepsilon) \Gamma_{s}(\varepsilon) [G_{dd}^{r}(\varepsilon) - G_{dd}^{a}(\varepsilon)] , \qquad (7.58)$$

where we have used the relation

$$G_{dd}^{r}(\varepsilon) = [G_{dd}^{a}(\varepsilon)]^{*}. \tag{7.59}$$

The other part of the current expression can be manipulated similarly. Finally, we obtain

$$J_{S\sigma(D\sigma)} = \frac{ie}{\hbar} \int \frac{d\varepsilon}{2\pi} \Gamma^{S(D)}(\varepsilon) \{ G_{dd}^{<}(\varepsilon) + f_{S(D)} [G_{dd}^{r}(\varepsilon) - G_{dd}^{a}(\varepsilon)] \}, \tag{7.60}$$

where $\Gamma_{S(D)}(\varepsilon)$ measures the hybridization interaction of the QD with the source (drain) and is given by

$$\Gamma_{S,D}(\varepsilon) = 2\pi \varrho_{S,D}(\varepsilon) \overline{\widetilde{V}}_k V_k^* \,, \tag{7.61}$$

In the steady-state, the current will be uniform and we have:

$$J_{\sigma} = J_{S\sigma} = -J_{D\sigma} , \qquad (7.62)$$

and after symmetrizing, we can write:

$$J_{\sigma} = \frac{(J_{S\sigma} - J_{D\sigma})}{2} \tag{7.63}$$

which can be expressed as

$$J_{\sigma} = \frac{e}{2h} \int \left[\{ f_{S} \Gamma_{S} - f_{D} \Gamma_{D} \} A(\varepsilon) + (\Gamma_{S} - \Gamma_{D}) G_{dd}^{<}(\varepsilon) \right] d\varepsilon , \qquad (7.64)$$

where $f_{S(D)}(\varepsilon)$ denotes the Fermi function for the S (D) electrons:

$$f_{S(D)}(\epsilon) = \frac{1}{e^{(\epsilon - \mu_{S(D)})/k_B T_{S(D)}} + 1} , \qquad (7.65)$$

 $\mu_{S(D)}$ and $k_B T_{S(D)}$ being respectively the chemical potential and the thermal energy of the source (drain) and $A(\varepsilon)$ is the spectral function which describes the excitations and is related to the Green functions as

$$A(\varepsilon) = i[G_{dd}^{r}(\varepsilon) - G_{dd}^{a}(\varepsilon)] = i[G_{dd}^{<}(\varepsilon) - G_{dd}^{>}(\varepsilon)] . \tag{7.66}$$

We assume that the QD is symmetrically coupled to the left and the right leads and so we can write:

$$\Gamma = \frac{\Gamma_S(\varepsilon) + \Gamma_D(\varepsilon)}{2} = 2\pi\rho(0)|V_k|^2 e^{-\lambda^2/2},$$
(7.67)

and consequently, the expression for the tunnelling charge current reduces to

$$J_{\sigma} = \frac{e\Gamma}{2h} \int \left[\{ f_s - f_D \} A(\varepsilon) \right] d\varepsilon . \tag{7.68}$$

To obtain $A(\varepsilon)$ and hence J_{σ} , we need to calculate $G_{dd}^{r(a)}(\varepsilon)$ or $G_{dd}^{<(>)}(\varepsilon)$. $G_{dd}^{r(a)}(t,t')$ can be written as

$$G_{dd}^{r(a)}(t,t') = \left[\tilde{G}_{dd}^{r(a)}(t,t')\right]_{el} \langle \hat{\chi}(t)\hat{\chi}^{\dagger}(t')\rangle_{ph} = \left[\tilde{G}_{dd}^{r(a)}(t,t')\right]_{el} e^{-\varphi(\tau)}, \qquad (7.69)$$

where $\left[\tilde{G}_{dd}^{r(a)}(t,t')\right]_{el}$ is defined as

$$\left[\tilde{G}_{dd}^{r(a)}(t,t')\right]_{el} = \mp i \,\theta(\pm t \mp t')\langle 0 | \left\{c_{d\sigma}(t), c_{d\sigma}^{\dagger}(t')\right\} | 0 \rangle_{el}, \tag{7.70}$$

and $\langle \hat{\chi}(t) \hat{\chi}^{\dagger}(t') \rangle_{ph}$ is calculated as

$$\langle \widehat{\chi}(t)\widehat{\chi}^{\dagger}(t')\rangle_{ph} = \langle e^{-i\widetilde{H}_{ph}t}\widehat{\chi}e^{i\widetilde{H}_{ph}t}e^{-i\widetilde{H}_{ph}t'}\widehat{\chi}^{\dagger}e^{i\widetilde{H}_{ph}t'}\rangle_{ph} = e^{-\varphi(\tau)}, \tag{7.71}$$

with

$$\varphi(\tau) = \lambda^2 \left[2f_{ph} + 1 - 2\{f_{ph}(1 + f_{ph})\}^{1/2} \cos(\hbar \widetilde{\omega}_0(\tau + i\beta/2)) \right],$$

where f_{ph} is the phonon distribution function given by $f_{ph} = [exp(\hbar \widetilde{\omega}_0/k_BT) - 1]^{-1}$. After some algebraic manipulation, we obtain

$$\varphi(\tau) = \ln \left[\sum_{n=-\infty}^{\infty} L_n(z) e^{-in\hbar \widetilde{\omega}_0 \tau} \right], \tag{7.72}$$

where L_n is the spectral weight of the n^{th} phonon side band [24] and is given by

$$L_n(z) = exp\left[-\lambda^2 \left(2f_{ph} + 1\right) + \left(\frac{n\hbar\widetilde{\omega}_0}{2k_B T}\right)\right] I_n(z),\tag{7.73}$$

where $z = 2\lambda^2 [f_{ph}(1+f_{ph})]^{1/2}$, n is the number of phonons and I_n is the Modified Bessel function of the second kind. Thus, $G_{dd}^{r(a)}(\varepsilon)$ can be written in the ε -space as

$$G_{\mathrm{dd}}^{\mathrm{r(a)}}(\varepsilon) = \sum_{\mathrm{n}=-\infty}^{\infty} L_{\mathrm{n}}(z) \left[\widetilde{G}_{\mathrm{dd}}^{\mathrm{r(a)}}(\varepsilon \mp \mathrm{n}\hbar \widetilde{\omega}_{0}) \right]_{el}, \tag{7.74}$$

where the Green functions $\widetilde{G}^{r,a}_{dd}(\epsilon)$ are defined as

$$\tilde{G}_{\rm dd}^{r(a)}(\varepsilon) = \int \tilde{G}_{dd}^{r(a)}(\tau) e^{i\varepsilon\tau} d\tau , \qquad (7.75)$$

Using the equation of motion technique [19], $\tilde{G}_{dd}^{r,a}(\epsilon)$ is calculated as

$$\left[\widetilde{G}_{dd}^{r(a)}(\varepsilon \mp n\hbar\widetilde{\omega}_{0})\right]_{el} = \frac{1}{\varepsilon \mp n\hbar\widetilde{\omega}_{0} - \widetilde{\varepsilon}_{d\sigma} - \widetilde{U}\langle n_{d-\sigma}\rangle - \widetilde{\Sigma}^{r(a)}(\varepsilon)},$$
(7.76)

where n is the phonon number, $\langle n_{d\sigma} \rangle$ is the mean electron occupancy in QD and $\tilde{\Sigma}^{r(a)}(\varepsilon)$ is the retarded (advanced) self-energy which can be expressed as

$$\widetilde{\Sigma}^{r(a)}(\varepsilon) = \lim_{\eta \to 0} \sum_{k \in S, D} \left| < \widetilde{V}_k > \right|^2 (\varepsilon \mp n\hbar \widetilde{\omega}_0 - \varepsilon_k \pm i\eta)^{-1} = \widetilde{\Lambda}(\varepsilon) \mp i\widetilde{\Gamma}(\varepsilon), \tag{7.77}$$

where the real part of $\tilde{\Sigma}^{r(a)}(\varepsilon)$ can be clubbed with the QD energy and the imaginary part simplifies to

$$\tilde{\Gamma} = \Gamma e^{-\lambda^2 (N_{\text{ph}} + 1/2)}. \tag{7.78}$$

Substituting Eqs. (7.75) and (7.77) in Eq. (7.67), $A(\varepsilon)$ can be obtained as

$$A(\varepsilon) = \sum_{n=-\infty}^{\infty} \frac{2\widetilde{\Gamma} L_n(z)}{\left(\varepsilon \mp n\hbar\widetilde{\omega}_0 - \widetilde{\varepsilon}_{d\sigma} - \widetilde{U}\langle n_{d,-\sigma}\rangle\right)^2 + \widetilde{\Gamma}^2},$$
(7.79)

Following the same procedure as above, the mean electron occupancy $\langle n_{d\sigma} \rangle$ in the QD of a symmetric SMT is obtained as

$$\langle n_{d\sigma} \rangle = \int d\omega \, \frac{(f_s + f_D)}{2\pi} \, A(\varepsilon).$$
 (7.80)

 $A(\omega)$ can be determined by solving Eqs. (42) and (43) self-consistently and consequently J_{σ} can be calculated. We consider the temperature difference $\Delta T = T_S - T_D = T_S - T$ and the chemical potential difference $\Delta \mu = \mu_S - \mu_D = \mu_S - \mu$ as small and positive. In this limit, $(f_S - f_D)$ reduces to

$$f_S(\epsilon) - f_D(\epsilon) \approx \frac{1}{4k_B T \cosh^2\left(\frac{\epsilon - \mu}{2k_B T}\right)} \left(\Delta \mu + \frac{\epsilon - \mu}{T} \Delta T\right),$$
 (7.81)

so that Eqs. (7.69) becomes

$$J_{\sigma} = \frac{e}{h} \int \left[\left\{ \frac{1}{4k_{B}T \cosh^{2}\left(\frac{\epsilon - \mu}{2k_{B}T}\right)} \left(\Delta \mu + \frac{\epsilon - \mu}{T} \Delta T\right) \right\} \tau_{\sigma}(\epsilon) \right] d\epsilon . \tag{7.82}$$

In the linear response regime for small values of ΔV and ΔT [20,21], we can write

$$J_{\sigma} = \sum_{\sigma} (eK_{0\sigma}\Delta\mu + \frac{e}{T}K_{1\sigma}\Delta T) , \qquad (7.83)$$

where $K_{0\sigma}$ and $K_{1\sigma}$ are known as the kinetic Onsagar coefficients and are given by

$$K_{0\sigma} = \frac{e}{h} \int \left[\left\{ \frac{1}{4k_B T \cosh^2\left(\frac{\epsilon - \mu}{2k_B T}\right)} \right\} \tau_{\sigma}(\epsilon) \right] d\epsilon . \tag{7.84}$$

$$K_{1\sigma} = \frac{e}{h} \int \left[\left\{ \frac{(\epsilon - \mu)}{4k_B T \cosh^2\left(\frac{\epsilon - \mu}{2k_B T}\right)} \right\} \tau_{\sigma}(\epsilon) \right] d\epsilon . \tag{7.85}$$

The charge and spin currents are defined as [19]:

$$J_c = (J_\uparrow + J_\downarrow) , \qquad (7.86)$$

$$J_s = (J_\uparrow - J_\downarrow) \quad , \tag{7.87}$$

and the energy current is defined as

$$J_{\epsilon} = \frac{e}{h} \int \epsilon \{ f_{s}(\epsilon) - f_{D}(\epsilon) \} [\tau_{\sigma}(\epsilon)] d\epsilon.$$
 (7.88)

7.2.4 Conductance, charge and spin-Seebeck coefficients

The heat current can be defined as [20]:

$$J_h^{\sigma} = J_{\epsilon} - \mu J_{\sigma} = \sum_{\sigma} (K_{1\sigma} \Delta \mu - \frac{1}{T} K_{2\sigma} \Delta T), \tag{7.89}$$

where $K_{1\sigma}$ is defined in (7.86) and $K_{2\sigma}$ is given by

$$K_{2\sigma} = \frac{e}{h} \int \left[\left\{ \frac{(\epsilon - \mu)^2}{4k_B T \cosh^2 \left(\frac{\epsilon - \mu}{2k_B T} \right)} \right\} \tau_{\sigma}(\epsilon) \right] d\epsilon . \tag{7.90}$$

The kinetic (Onsager) coefficient $K_{n,\sigma}(\mu)$ [20,21] can be written in general as:

$$K_{n,\sigma}(\mu) = \frac{1}{\hbar} \int \left[-\frac{\partial f(\epsilon, \mu)}{\partial \epsilon} \right] (\epsilon - \mu)^n \, \tau_{\sigma}(\epsilon) d\epsilon \quad , \tag{7.91}$$

where the transmission coefficient $\tau_{\sigma}(\varepsilon)$ can be written as [23]:

$$\tau_{\sigma}(\epsilon) = \frac{\Gamma_R \Gamma_L}{\Gamma_R + \Gamma_L} \left[-2 \, Im G_{\rm dd}^{\rm r}(\epsilon) \right]. \tag{7.92}$$

For symmetric leads, $\Gamma_R = \Gamma_L = \Gamma$ and we obtain

$$\tau_{\sigma}(\varepsilon) = \frac{\Gamma^{2}}{\left((\epsilon \pm n\hbar\omega_{0}) - \tilde{\varepsilon}_{d} - \tilde{u} < n_{d,-\sigma} > \right)^{2} + \tilde{\Gamma}^{2}} \quad . \tag{7.93}$$

We can relate the Onsager coefficients to the transport parameters like charge conductance and spin conductance [22]. For example, the charge conductance G^c can be written as:

$$G^{c} = G_{\uparrow} + G_{\downarrow} = e^{2} (K_{0\uparrow} + K_{0\downarrow}),$$
 (7.94)

and the Spin conductance is given by

$$G^{s} = G_{\uparrow} - G_{\downarrow} = e^{2} (K_{0\uparrow} - K_{0\downarrow}), \qquad (7.95)$$

while the thermal conductance can be written as [24]:

$$\kappa = \frac{1}{T} \left(\sum_{\sigma} K_{2\sigma} - \frac{|\sum_{\sigma} K_{1\sigma}|^2}{\sum_{\sigma} K_{0\sigma}} \right) \quad . \tag{7.96}$$

The thermo-power S is defined as the ratio of the generated voltage ΔV to the temperature difference ΔT in the absence of charge current:

$$S_{\sigma}(\mu) = -\frac{\Delta V}{\Delta T} = -\frac{1}{eT} \frac{K_{1,\sigma}}{K_{0,\sigma}}$$
 (7.97)

The charge Seebeck coefficient $S_c(\mu)$ and the spin Seebeck coefficient $S_s(\mu)$ are defined as [22]:

$$S_c(\mu) = S_{\uparrow}(\mu) + S_{\downarrow}(\mu) \quad . \tag{7.98}$$

$$S_{s}(\mu) = S_{\uparrow}(\mu) - S_{\downarrow}(\mu) \quad . \tag{7.99}$$

7.3 Results and discussions

For simplicity, we assume that the QD contains a single level with energy ε_d and is connected symmetrically to the source and the drain. From now on, we choose the phonon energy $\hbar\omega_0$ as the unit of energy and set $\Gamma=1$, $eV_g=0$, $\hbar\omega_0=1$. We also choose the temperature of the left lead slightly higher than that of the right lead. To study the effect of temperature, we plot in Fig. 2, the spin-resolved electronic conductances $(G_\sigma, \sigma=\uparrow,\downarrow)$, charge (spin) conductance G_c (G_s), as a function of QD energy level ε_d with el-ph coupling constant $\lambda=1$, chemical potential $\mu=0$, oscillator frequency $\omega_0=1$, magnetic field $\mu_B B=1$, cyclotron frequency $\omega_c=3$, damping factor g=0.03 and el-el interaction strength U=1 and for different values of

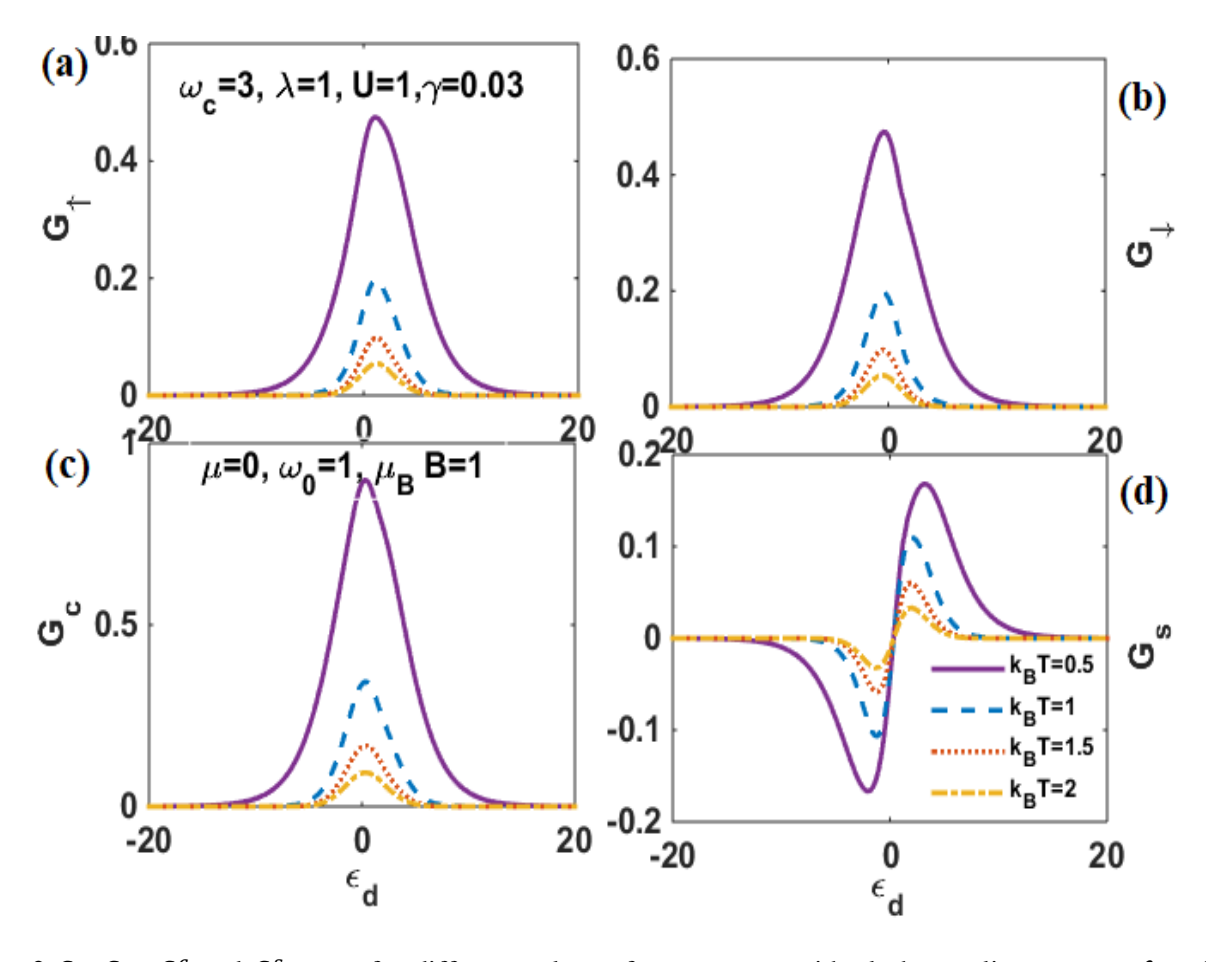


Fig. 2 G_{\uparrow} , G_{\downarrow} , G^c and G^s vs ϵ_d for different values of temperature with el-ph coupling constant $\lambda=1$, chemical potential $\mu=0$, oscillator frequency $\omega_0=1$, magnetic field $\mu_B B=1$, cyclotron frequency $\omega_c=3$, damping factor $\gamma=0.03$ and el-el interaction strength U=1.

temperature. In general, the qualitative behaviour of G_{\uparrow} and G_{\downarrow} with ε_d are similar. Both exhibit a peak structure at a certain value of ε_d (close to zero) and drop to zero on both sides of ε_d as $|\varepsilon_d|$ reaches a certain value. As temperature increases, both the spin-up and spin-down conductance peaks decrease in height. However, the spin-up conductance peak shifts towards the right, while the spin-down conductance peak shifts towards the left. The charge conductance curve also shows a peak which decreases in height with increasing temperature, but now the peak position does not change with temperature. Fig. 2 (d) shows that the behaviour of the spin conductance is different from the other conductances. The spin conductance increases with positive QD energy ε_d and exhibits a maximum and decreases with negative QD energy and exhibits a minimum. Here also the conductance vanishes as $|\varepsilon_d|$ reaches a certain value.

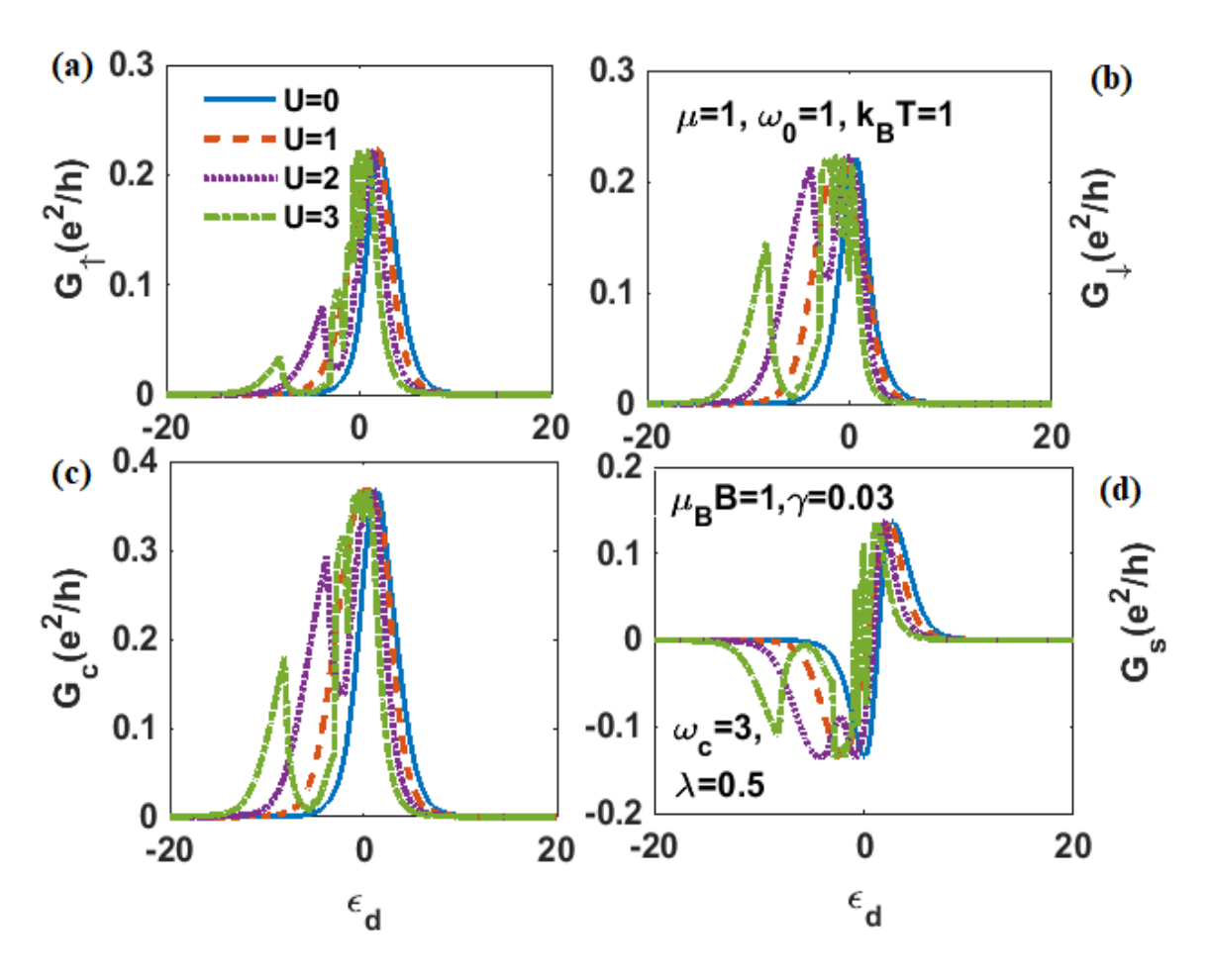


Fig. 3 G_{\uparrow} , G_{\downarrow} , G^c and G^s vs ϵ_d for different values of el-el interaction strength with el-ph coupling constant $\lambda = 0.5$, chemical potential $\mu = 1$, oscillator frequency $\omega_0 = 1$, magnetic field $\mu_B B = 1$, cyclotron frequency $\omega_c = 3$, damping factor $\gamma = 0.03$ and temperature $k_B T = 1$.

In Fig. 3, we plot the spin-up (-down) conductance G_{\uparrow} (G_{\downarrow}) and charge (spin) conductance G^c (G^s) (which is proportional to the Onsager coefficient K_0) as a function of ϵ_d for different values of the e-e interaction U. The figures show that at U=0, the conductance curves exhibit one maximum and as U increases, the number of peaks and also the fluctuation in the conductance increase. Also the peaks shift towards left with increasing U. Interestingly again, G_{\uparrow} , G_{\downarrow} and G^c behave qualitatively more or less in a similar way, while G^s displays a maximum-minimum structure around $\epsilon_d=0$ at U=0, which splits in many peaks at the presence of el-el interaction.

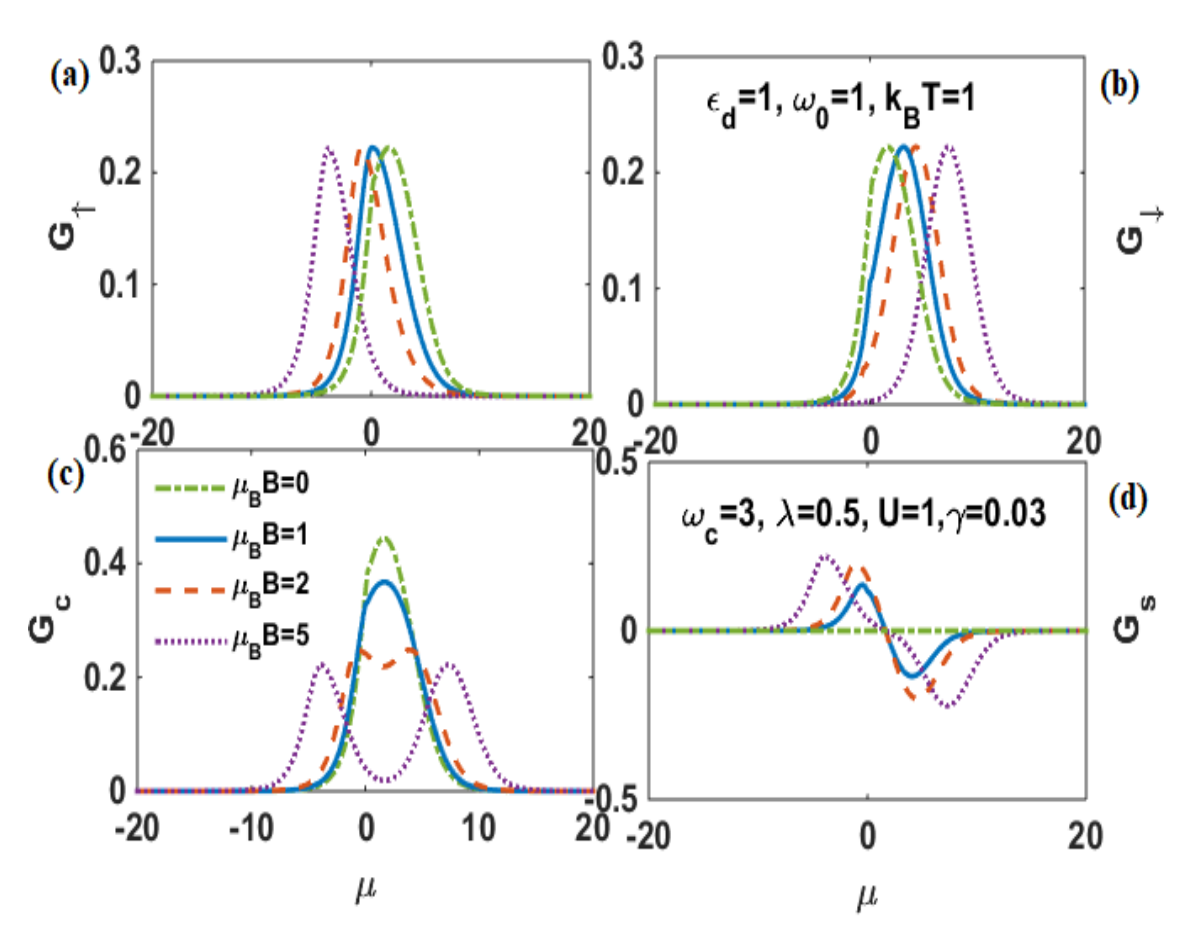


Fig. 4 G_{\uparrow} , G_{\downarrow} , G^c and G^s vs μ for different values of the magnetic field with el-ph coupling constant $\lambda = 0.5$, QD energy $\epsilon_d = 1$, oscillator frequency $\omega_0 = 1$, temperature $k_B T = 1$, cyclotron frequency $\omega_c = 3$, damping factor $\gamma = 0.03$ and el-el interaction strength U = 1.

In Figs. 4(a) and 4(b), we show the variation of G_{\uparrow} and G_{\downarrow} as a function of the chemical potential μ for a few different values of B. In the absence of the magnetic field, G_{\uparrow} and G_{\downarrow} show the same variation with μ . For $B \neq 0$, as B increases, the peak of G_{\uparrow} shifts towards left (i. e., towards negative μ), while G_{\downarrow} peak shifts towards right. However, the maximum height of the peak

remains same in both cases. Figs. 4 (c) and 4(d) display the behaviour of G^c and G^s . In the absence of a magnetic field, the charge conductance G^c as a function of μ , also shows a maximum, while the spin conductance G^s remains zero. As the magnetic field increases, the maximum of G^c decreases and splits into two symmetric maxima while G^s develops a maximum and a minimum structure around $\mu = 0$ which increase in height and width with increasing magnetic field

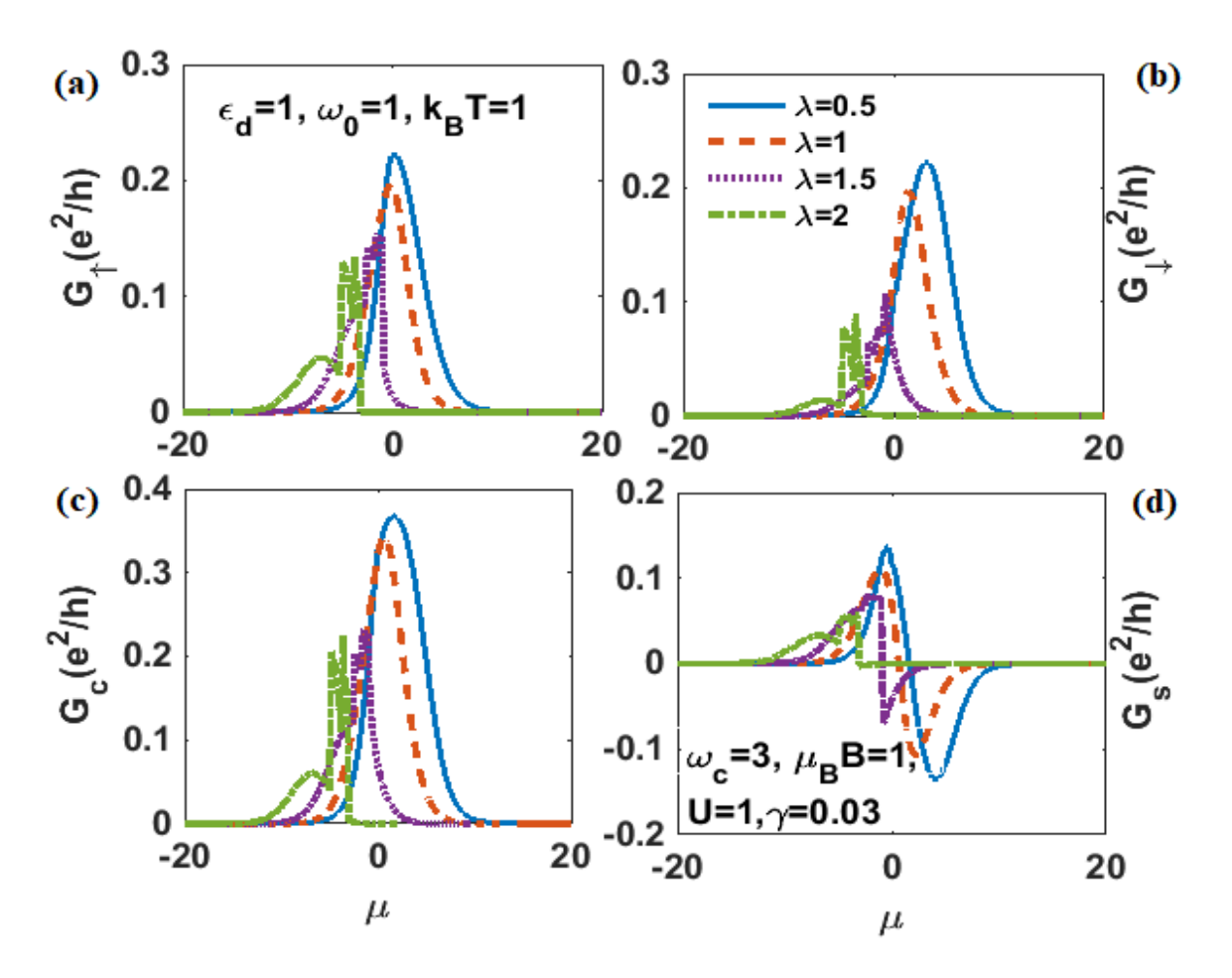


Fig. 5 G_{\uparrow} , G_{\downarrow} , G^c and G^s vs μ for different values of el-ph coupling constant with the magnetic field $\mu_B B = 1$, QD energy $\epsilon_d = 1$, oscillator frequency $\omega_0 = 1$, temperature $k_B T = 1$, cyclotron frequency $\omega_c = 3$, damping factor $\gamma = 0.03$ and el-el interaction strength U = 1.

In Fig. 5, we show the variation of G_{\uparrow} , G_{\downarrow} , G_{c} and G_{s} as a function of μ for a few values of the el-ph interaction strength λ . The conductance peaks in all cases decrease as λ increases and shift towards left. At higher values of el-ph interactions, the peak of the conductance splits in multiple peaks. Figs. 5(a) and 5(b) suggest that qualitatively, the spin-up and spin-down conductance curves behave more or less in the same way, but quantitatively, the magnitude of the spin-up conductance

is slightly larger. Figs. 5(c) and 5(d) show that the charge conductance and spin conductance also decrease as λ increases.

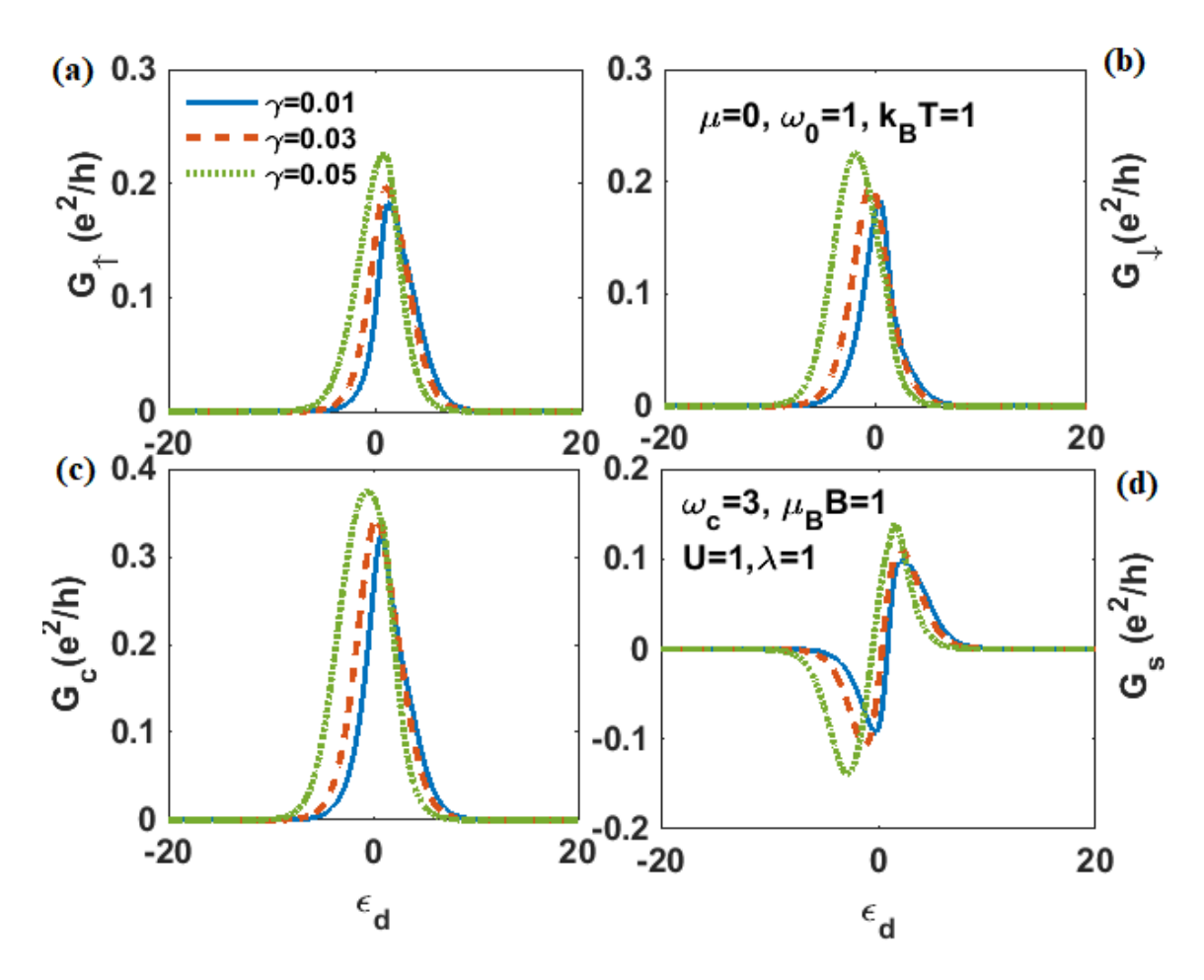


Fig. 6 G_{\uparrow} , G_{\downarrow} , G^c and G^s vs ϵ_d for different values of damping factor with el-ph coupling constant $\lambda=1$, chemical potential $\mu=0$, oscillator frequency $\omega_0=1$, temperature $k_BT=1$, cyclotron frequency $\omega_c=3$, magnetic field $\mu_BB=1$ and el-el interaction strength U=1.

In Fig. 6, we show the behaviour of G_{\uparrow} , G_{\downarrow} , G_{c} and G_{s} with respect to ϵ_{d} for a few different values of the damping factor. The figures show that the magnitude of the conductance increases with increasing damping parameter in all cases.

In Fig. 7, we plot the thermopowers ($(S_{\uparrow}, S_{\downarrow}, S_c, S_s)$) as a function of the magnetic field B for a few different values of el-ph coupling constant. The spin-up and spin-down Seebeck coefficients exhibit an maximum-minimum structure. Fig. 7(a) shows the behaviour of the spin-up Seebeck

coefficient (S_{\uparrow}) and the behaviour of the spin-down (S_{\downarrow}) Seebeck coefficient is shown in Fig.7(b). S_{\uparrow} and S_{\downarrow} are equal in the absence of the magnetic field and exhibit opposite behaviour as a function of the magnetic field. The el-ph interaction enhances the magnitude of the both spin-up and spin-down Seebeck coefficients. In Figs. 7 (c) and 7(d), we show the behaviour of the charge (spin) Seebeck coefficient S_c (S_s) with respect to the magnetic field for different values of el-ph interaction. The magnitude of the spin Seebeck coefficient is higher than the charge Seebeck coefficient because the spin-up and spin-down Seebeck coefficients have the

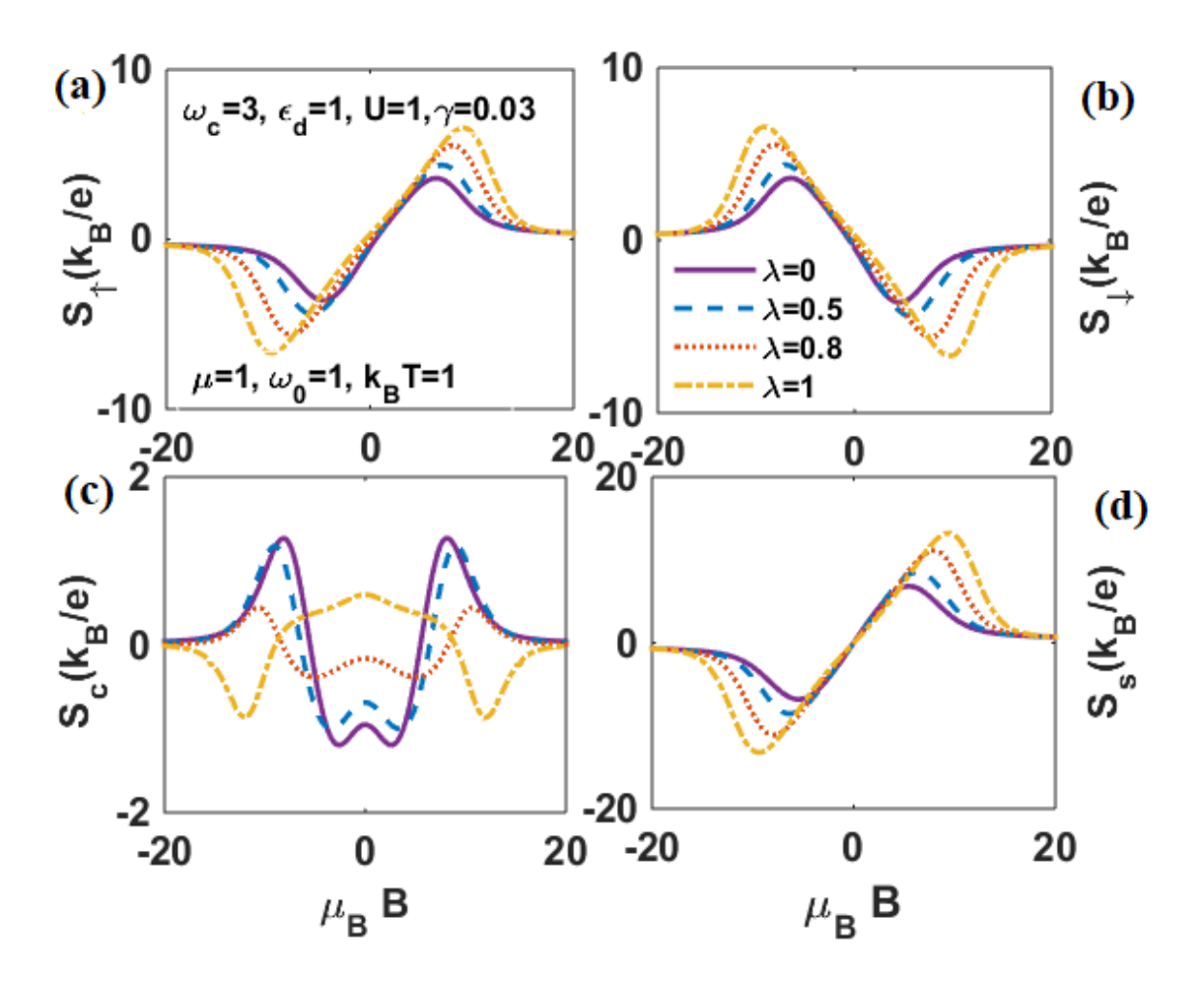


Fig. 7 Thermopowers as a function of magnetic field with QD energy $\epsilon_d = 1$, oscillator frequency $\omega_0 = 1$, temperature $k_B T = 1$, cyclotron frequency $\omega_c = 3$, damping factor $\gamma = 0.03$ and el-el interaction strength U = 1 and for a few different values of the el-ph coupling constant λ .

opposite behaviour. According the theory of metals, the thermopower vanishes in a half-filled band where the number of filled and empty states is equal which is a particle-hole symmetric condition. We have considered the left lead to be at a higher temperature than the right one and because of

this temperature gradient, the thermoelectric effect is created. The left lead also has more electrons above the chemical potential than the right one and consequently, more holes should exist below the chemical potential. The major carriers are holes (electrons) when the energy levels of QDs are below (above), and the thermo-power is therefore positive (negative). So the spin Seebeck coefficient graph is antisymmetric.

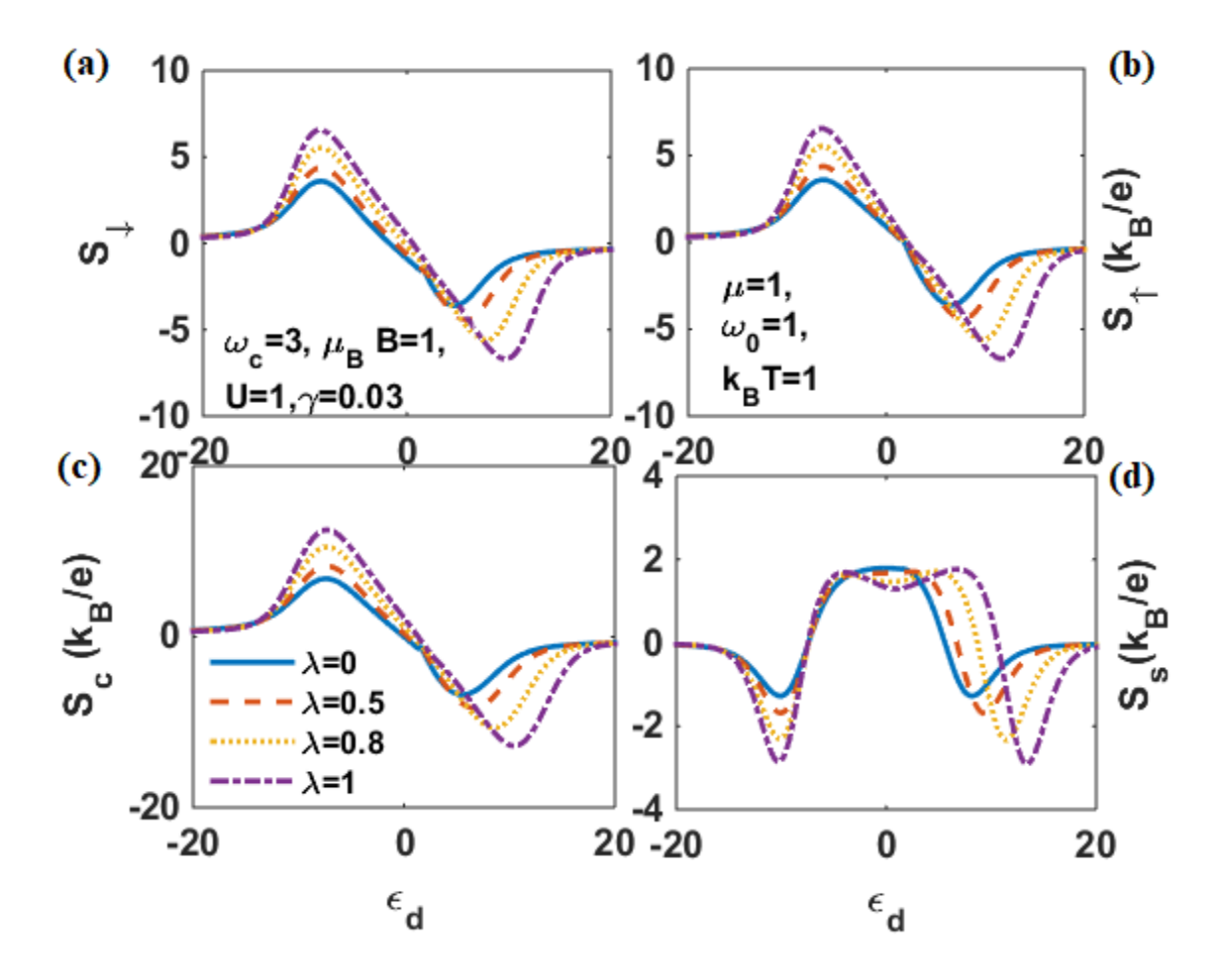


Fig. 8 Thermo-power as a function of QD energy ϵ_d for few values of el-ph coupling constant λ , oscillator frequency $\omega_0 = 1$, temperature $k_B T = 1$, cyclotron frequency $\omega_c = 3$, damping factor $\gamma = 0.03$ and el-el interaction strength U = 1.

In Fig. 8, we plot the thermopowers $(S_{\uparrow}, S_{\downarrow}, S_c, S_s)$ as a function of QD energy for a few different values of the el-ph coupling constant. In this case, the behaviour of the spin-up and spin-down Seeback coefficients are the same, but their amplitudes are slightly different. The thermopowers $(S_{\uparrow}, S_{\downarrow}, S_c)$ change their sign at $\epsilon_d = 0$ due to the compensation of electrons and holes in the case

of $\lambda=0$. the magnitude of the maxima and minima of the thermopowers $(S_{\uparrow},S_{\downarrow},S_{c})$ increase with increasing λ . Also, as λ increases, the maxima of the thermopowers continue to occur at the same value of ϵ_{d} but the minima of the thermopowers shift towards higher values of ϵ_{d} . The behaviour of spin Seebeck coefficient S_{s} is completely different from S_{c} . S_{s} exhibits a plateau around $\epsilon_{d}=0$ and as λ increases, the plateau splits into two peaks. The magnitude of S_{s} is very small compared to S_{c} , which implies that the spin current is much smaller than the charge current.

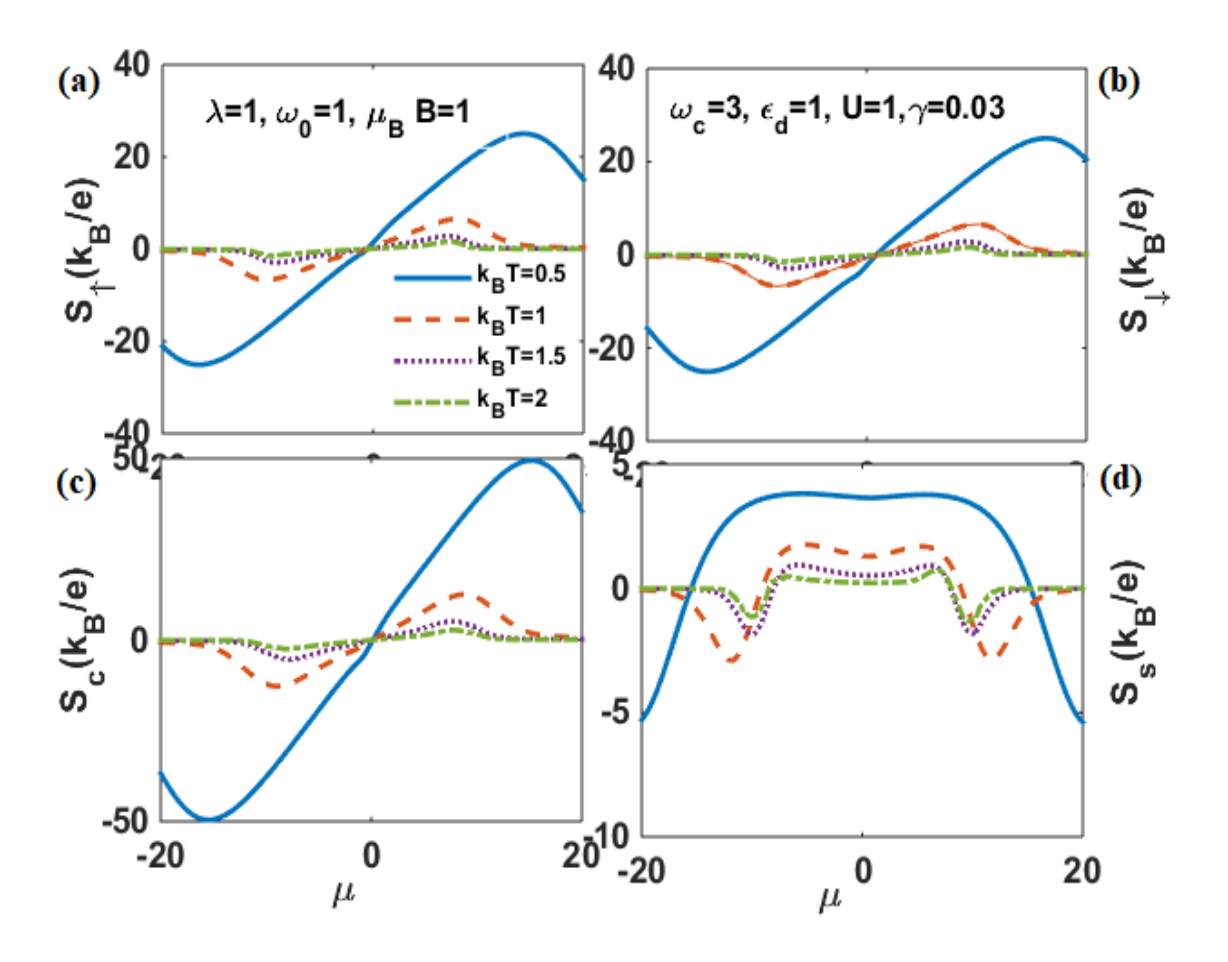


Fig. 9 Thermo-power as a function of chemical potential μ for a few different values of temperature k_BT and certain values of other parameters $\lambda=1$, $\omega_0=1$, $\mu_BB=1$, $\omega_c=3$, $\gamma=0.03$, $\epsilon_d=1$, and U=1.

In Fig. 9, we plot the thermopowers $(S_{\uparrow}, S_{\downarrow}, S_c, S_s)$ as a function of chemical potential μ for a few values of T. We observe that in all cases, the themopowers decrease as temperature increases. We also observe that the curves for S_{\uparrow} , S_{\downarrow} , and S_c are antisymmetric due to particle-hole symmetry and the positive (negative) thermopowers show holes (electrons) as the majority charge carriers. Fig. 9(d) shows that S_s , as a function of μ has a flat plateau that is symmetric around μ =

0. Temperature has an interesting effect on the spin Seebeck coefficient S_s . As temperature increases, the plateau height of S_s decreases and it splits into two maxima. We again notice that the magnitude of S_s is much smaller than that of S_c .

In Fig. 10, we show the results of thermopowers $(S_{\uparrow}, S_{\downarrow}, S_c, S_s)$ as a function of μ for different values of el-el interaction U. The peaks of the thermopowers have the same height for different values of U and they shift towards left on the μ -axis as U increases.

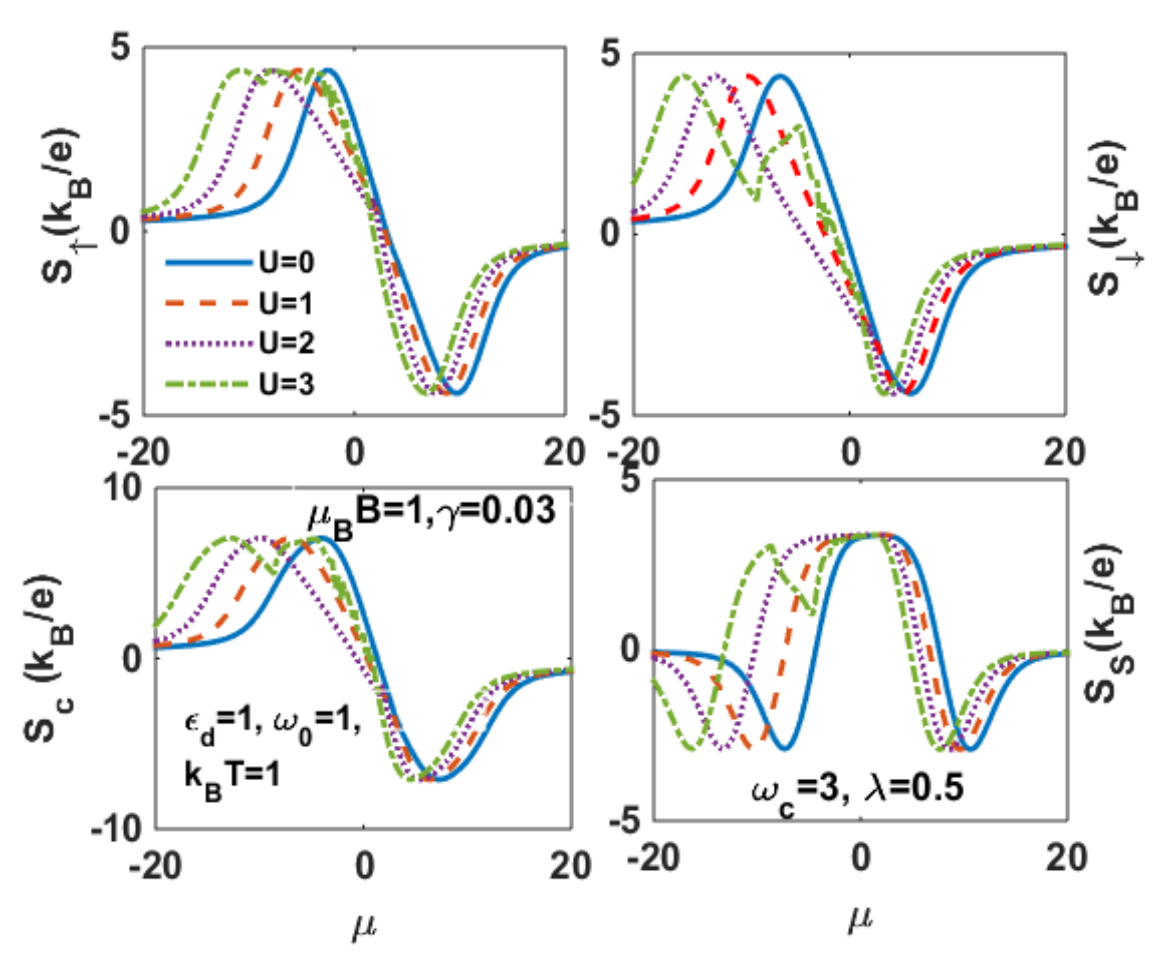


Fig. 10 Thermopowers as a function of chemical potential μ for different values of el-el interaction U and certain values of other parameters $\lambda=0.5$, $\omega_0=1$, $\mu_BB=1$, $\omega_c=3$, $\gamma=0.03$, $\epsilon_d=1$, and $k_BT=1$.

Fig. 11 presents the behaviour of the thermopowers $(S_{\uparrow}, S_{\downarrow}, S_c, S_s)$ with respect to chemical potential μ for different values of λ . One can see that as we increase λ , the magnitudes of the thermopowers and their peak values increase in all cases. Also the magnitude of the charge

Seebeck coefficient turns out to be larger than the spin Seebeck coefficient. The spin Seebeck coefficient peaks are split into two peaks at higher values of λ .

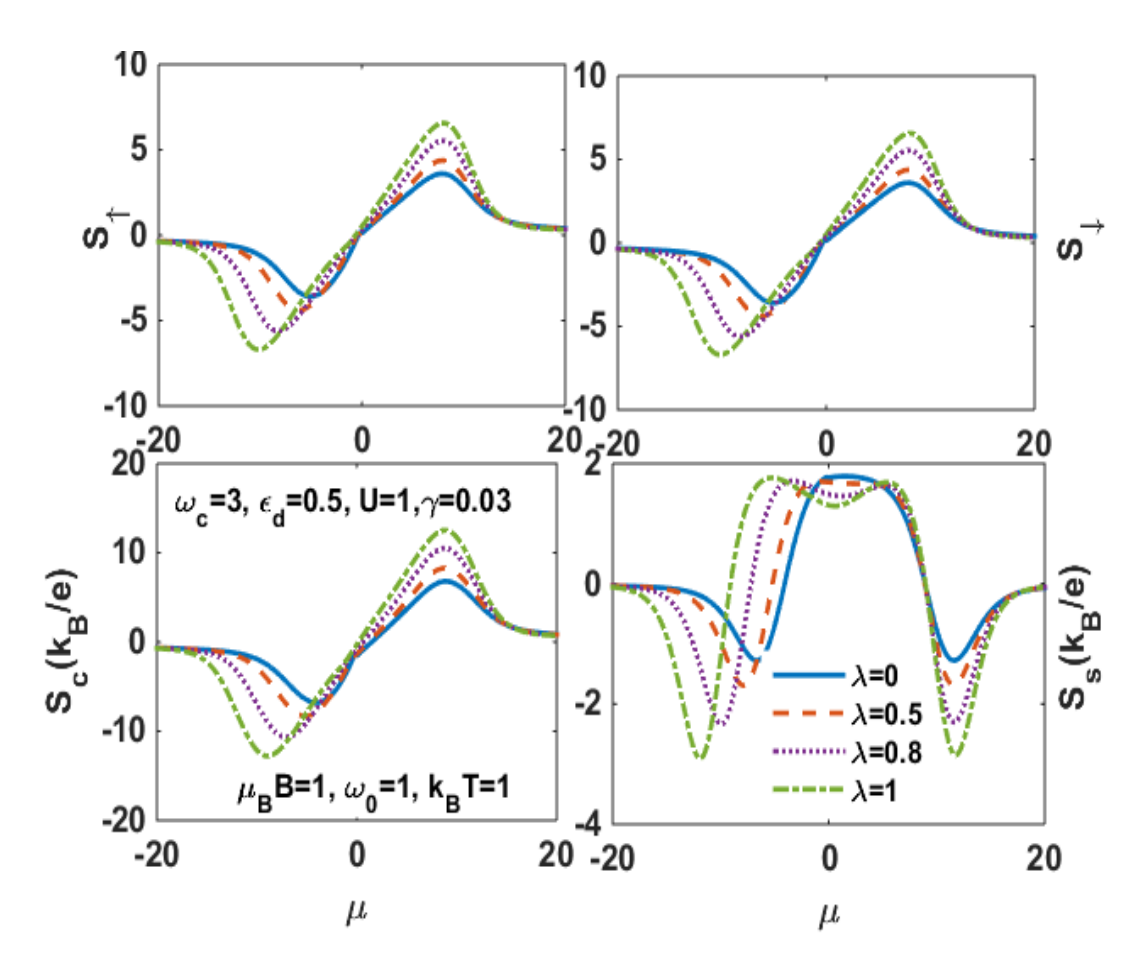


Fig. 11 Thermopowers as a function of chemical potential μ for different values of el-ph interaction λ and certain values of other parameters U=1, $\omega_0=1$, $\mu_BB=1$, $\omega_c=3$, $\gamma=0.03$, $\epsilon_d=1$, and $k_BT=1$.

In Fig. 12, we plot the thermopowers $(S_{\uparrow}, S_{\downarrow}, S_c, S_s)$ as a function of chemical potential μ for different values of the magnetic field B. The spin-up and spin-down thermopowers are the same at zero magnetic field. So the charge Seebeck coefficient is maximum and the spin Seebeck coefficient is zero in this case. Therefore, we will get maximum charge current and zero spin current in the absence of the magnetic field. The thermopowers S_{\uparrow} (S_{\downarrow}) shift towards left (right) at higher values of the magnetic field B. The maxima of S_{\uparrow} and S_{\downarrow} are equal for different values of B. However, S_c decreases and S_s increases at higher values of the magnetic field. Thus, the magnetic field increases the spin current and the spin Seebeck coefficient.

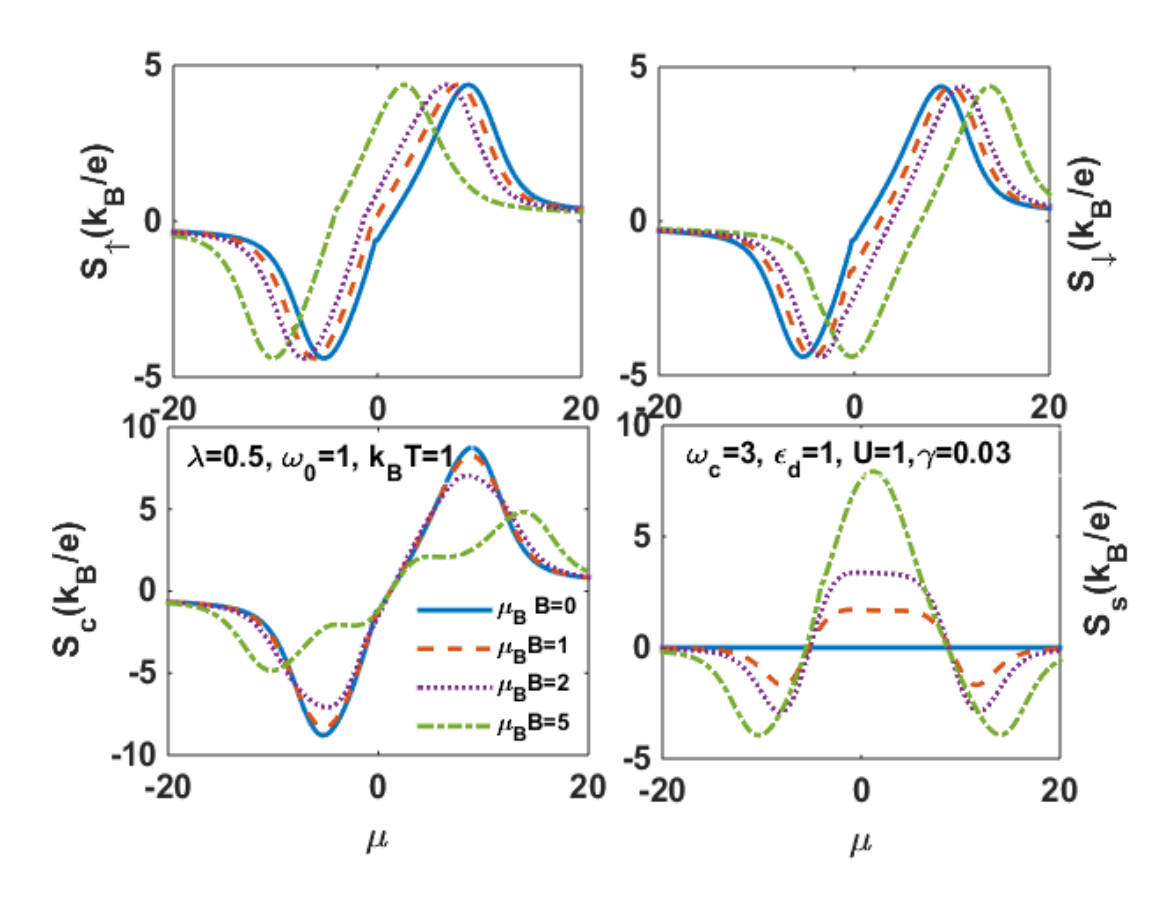


Fig. 12 Thermopowers as a function of chemical potential μ for different values of magnetic field $\mu_B B$ and certain values of other parameters U=1, $\omega_0=1$, $\lambda=0.5$, $\omega_c=3$, $\gamma=0.03$, $\epsilon_d=1$, and $k_B T=1$.

In Fig. 13, we present the results of the charge Seebeck coefficient S_c (dotted lines) and spin Seebeck coefficient S_s (solid lines) as a function of the QD energy for different values of the magnetic field B. Interestingly, S_c is positive for negative QD energy and negative for positive QD energy. At zero QD energy, S_c is zero and S_s is maximum and it decreases as the QD energy increases. In Fig. 14, we plot the charge Seebeck coefficient and the spin Seebeck coefficient with respect to the chemical potential μ for different values of the damping factor γ . The effect of dissipation on the charge and spin Seebeck coefficients appears to be marginal.

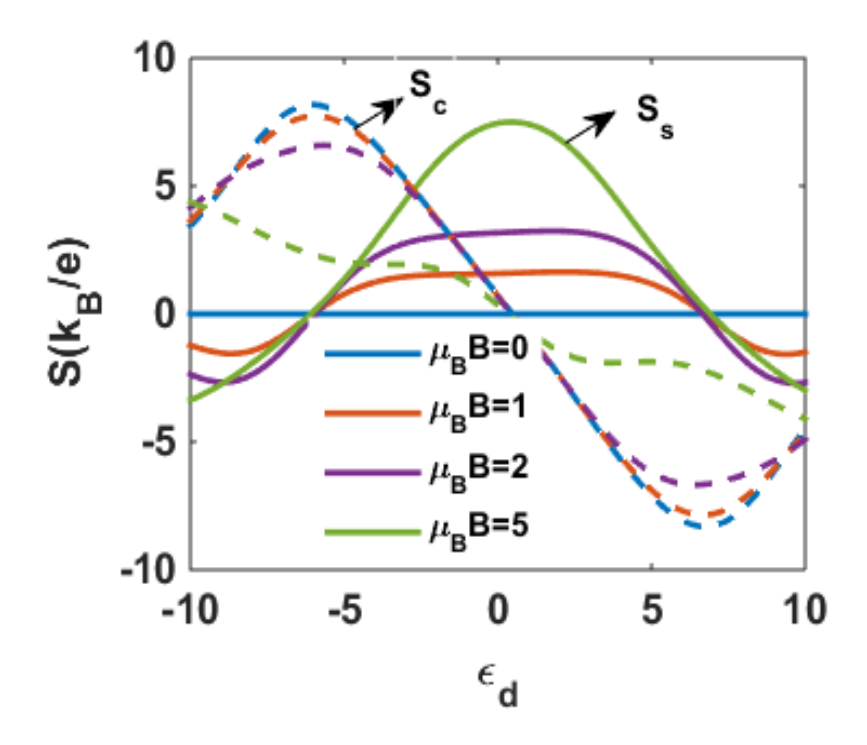


Fig. 13 Charge Seebeck coefficient (dotted lines) and spin Seebeck coefficient (solid lines) vs QD energy ϵ_d for different values of magnetic field $\mu_B B$.

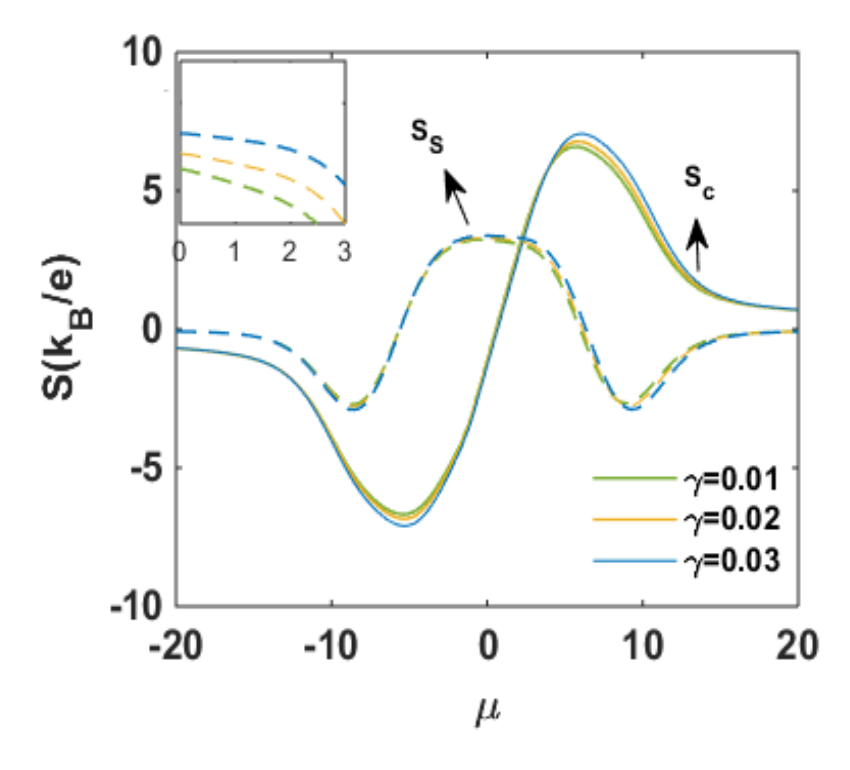


Fig.14 Thermopowers as a function of μ for different values of dissipation parameters γ .

7.4 Conclusion

In this chapter, we have studied the thermal transport properties of a dissipative SMT device with e-e and e-p interactions and magnetic field. The e-e interaction has been described by the Hubbard term and the e-p interaction has been taken care of by the Holstein model. The dissipative effect which arises because of the interaction of the substrate phonons with the QD phonon has been incorporated by the linear Caldeira-Leggett model. The dissipation has been approximately treated by a canonical transformation which reduces the QD frequency which is precisely the damping effect. Using the Lang-Firsov transformation followed by a zero-phonon averaging, the e-p interaction is eliminated. Finally using the Keldysh method, the effect of magnetic field, dissipation, e-e and e-p interactions on thermal parameters has been studied. In particular, we studied the behaviour of the conductance conductance $(G_{\uparrow}, G_{\downarrow}, G^c)$ and G^s) with respect to different parameters such as the temperature, e-e interaction, e-p interaction, damping parameter, magnetic field, quantum dot energy and chemical potential. It is found that the charge conductance G^c is maximum while the spin conductance G^s is zero in the absence of the magnetic field. However, as the magnetic field increases, the peak height of G^c decreases and the peaks split into two peaks while the peak height of G^s increases and shifts towards right on the chemical potential axis. We have also shown that temperature, magnetic field and the above-mentioned interactions have interesting effects on the thermopowers $(S_{\uparrow}, S_{\downarrow}, S_c \text{ and } S_s)$. As a function ϵ_d , the behaviour of the spin-up and spin-down Seeback coefficients are the same, but their amplitudes are slightly different. The spin-up and spin-down thermopowers are the same at zero magnetic field. So the charge Seebeck coefficient is maximum and the spin Seebeck coefficient is zero in this case. However, S_c decreases and S_s increases at higher values of the magnetic field. Thus, the magnetic field increases the spin current and the spin Seebeck coefficient.

The thermopowers $(S_{\uparrow}, S_{\downarrow}, S_c)$ change their sign at $\epsilon_d = 0$ due to the compensation of electrons and holes in the case of $\lambda = 0$. the magnitude of the maxima and minima of the thermopowers $(S_{\uparrow}, S_{\downarrow}, S_c)$ increase with increasing λ . Also, as λ increases, the maxima of the thermopowers continue to occur at the same value of ϵ_d but the minima of the thermopowers shift towards higher values of ϵ_d . The behaviour of spin Seebeck coefficient S_s is completely different from S_c . S_s exhibits a plateau around $\epsilon_d = 0$ and as λ increases, the plateau splits into two peaks. The magnitude of S_s is very small compared to S_c , which implies that the spin current is much smaller than the charge current. The effect of dissipation on the charge and spin Seebeck coefficients appears to be marginal.

7.5 References

- 1. Prinz GA (1998) Magnetoelectronics. Science 282:1660
- Wolf SA, Awschalom DD, Buhrman RA, Daughton JM, von Molnár S, Roukes ML, Chtchelkanova AY, Treger DM (2001) Spintronics: A Spin-Based Electronics. Science 294:1488
- **3.** Zuti ´c I, Fabian J, Sarma SD (2004) Spintronics: Fundamentals and ´applications. Rev Mod Phys (London) 76:323
- **4.** Bauer GE, Saitoh E, van Wees BJ (2010) Spin caloritronics. Nat Mater 150:391–399
- 5. H. Adachi, K. Uchida, E. Saitoh, and S. Maekawa, Rep. Prog. Phys. 76, 036501 (2013).
- 6. Jaworski CM, Yang J, Mack S, Awschalom D, Heremans J, Myers R (2010) Observation of the spin-Seebeck effect in a ferromagnetic semiconductor. Nat Mater 9:898–903.
- 7. Uchida K, Adachi H, Ota T, Nakayama H, Maekawa S, Saitoh E (2010) Observation of longitudinal spin-Seebeck effect in magnetic insulators. Appl Phys Lett 97:172505.
- 8. Uchida K, Xiao J, Adachi H, Ohe J, Takahashi S, Ieda J, Ota T, Kajiwara Y, Umezawa H, Kawai H, Bauer GEW, Maekawa S, Saitoh E (2010) Spin Seebeck insulator. Nat Mater 9:894–897
- 9. K. Uchida, S. Takahashi, K. Harii, J. Ieda, W. Koshibae, K. Ando, S. Maekawa, and E. Saitoh, Nature 455, 778 (2008).
- Uchida K, Adachi H, Ota T, Nakayama H, Maekawa S, Saitoh E (2010) Observation of longitudinal spin-Seebeck effect in magnetic insulators. Appl Phys Lett 97:172505
- 11. Uchida K, Xiao J, Adachi H, Ohe J, Takahashi S, Ieda J, Ota T, Kajiwara Y, Umezawa H, Kawai H, Bauer GEW, Maekawa S, Saitoh E (2010) Spin Seebeck insulator. Nat Mater 9:894–897
- 12. Jaworski C, Myers R, Halperin JE, Heremans J (2012) Giant spin Seebeck effect in a non-magnetic material. Nature (London) 487:210–212
- 13. Wu SM, Pearson JE, Bhattacharya A (2015) Paramagnetic spin seebeck effect. Phys Rev Lett 114:186602
- 14. Wu SM, Zhang W, Kc A, Borisov P, Pearson JE, Jiang JS, Lederman D, Hoffmann A, Bhattacharya A (2016) Antiferromagnetic Spin Seebeck Effect. Phys Rev Lett 116:097204

- 15. Tang GM, Chen XB, Ren J, Wang J (2018) Rectifying full-counting statistics in a spin Seebeck engine. Phys Rev B 97:081407(R)
- 16. Chang PH, Mahfouzi F, Nagaosa N, Nikolic BK (2014) Spin-Seebeck effect on the surface of a topological insulator due to nonequilibrium spin-polarization parallel to the direction of thermally driven electronic transport. Phys Rev B 89:195418
- 17. Jiwoong Park B.S. Electron Transport in Single Molecule Transistors (Seoul National University) 1996.
- 18. Nordlander, P., Pustilnik, M., Meir, Y., Wingreen, N. S. & Langreth, D. C. How long does it take for the kondo efect to develop. Phys. Rev. Lett. 83, 808 (1999)
- 19. G. Tang, J. Thingna and J. Wang, Thermodynamics of the energy, charge and spin currents in a thermoelectric quantum dot spin valve, Phys. Rev. B **97**, 155430 (2018).
- 20. Liu YS, Chi F, Yang XF, Feng JF (2011) Pure spin thermoelectric generator based on a rashba quantum dot molecule. J Appl Phys 109:053712
- 21. Andrade JRP, Peña FJ, González A, Ávalos-Ovando O, Orellana PA (2017) Spin-Seebeck effect and spin polarization in a multiple quantum dot molecule. Phys. Rev. B **96**:165413
- 22. L.M. Liu, F. chi, Z. G. Fu, S. C. Yu and H. W. Chen (2018) Spin polarized transport and spin Seebeck effect in triple quantum dots with spin dependent interdot coupling, Nanoscale research letters 13: 358.
- 23. F. chi, Z-G Fu, J. Liu, K M Li, Z. Wang and P. Zhang Nanoscale Research Lett. 15:79, 2020.
- P. Trocha and J. Barnas, Large enhancement of thermoelectric effects in a double quantum dot system due to interference and Coulomb correlation phenomena, Phys. Rev. B 85 085408, (2012)

Chapter-8

Conclusions

In this thesis, we have studied the effect of spin-orbit interactions on electronic states in quantum dots and also on the thermo-electric properties of a single molecular transistor. In particular, we have studied the effect of spin-orbit interactions on the hydrogenic donor impurity systems in a QD and applied our results to a GaAs QD for the sake of concreteness. We have finally studied the effect of electron-electron and electron-phonon interactions on the thermopower and spin-Seebeck effect in a single molecular transistor in the presence of quantum dissipation and an external magnetic field.

We began the thesis with a general overview of QDs in Chapter 1 where we covered some of the fundamental characteristics of QDs such as the nature of their energy spectrum, the density of states, the confinement potential and briefly mentioned some of their applications. We have next presented a brief introduction to the Rashba and Dresselhaus spin-orbit interactions. Finally, we have introduced the subject of single molecular transistor and presented the derivation of conductance and thermopower using the non-equilibrium Keldysh Green function technique.

In Chapter 2, we have considered the combined effect of Rashba and Dresselhaus spin-orbit interactions on a D^0 hydrogenic impurity in a Gaussian QD of GaAs in the presence of a magnetic field. To decouple the spin-orbit interactions, we have used a unitary transformation and calculated the GS energy and the binding energy (E_B) of the D^0 impurity using the Ritz variational method. We have shown that the Rashba term reduces the GS energy more than the Dresselhaus term in the presence of the magnetic field but in the absence of the magnetic field, both the terms reduce the GS energy by the same amount. We have also demonstrated that the binding energy reaches its maximum at a particular dot size and rapidly decreases below this critical size. Furthermore, in the presence of the magnetic field, the GS binding energy increases with decreasing Rashba coupling constant (α_R) but it increases with the Dresselhaus interaction coefficient (β_D) , whereas,

in the case of zero magnetic field, the GS binding energy remains unaffected by both the Rashba and Dresselhaus interactions. Next we have shown that the susceptibility S increases with B. Also |S| increases with increasing QD size at small magnetic fields, but above a critical magnetic field, it decreases with increasing QD radius. This leads to a crossing behaviour in the diamagnetic susceptibility. Finally, we have shown that in general, as the QD size decreases, the electron localization becomes stronger. However, the behaviour starts reversing below a certain QD size because of the uncertainty principle.

In Chapter 3, we have studied the impact of spin-orbit interactions on the binding energy of an off-centre D^0 impurity in a 2D Gaussian QD of GaAs in a magnetic field by the Ritz variational method. We have shown that the binding of a D^0 complex is strongest for the on-centre complex (D = 0) and binding energy decreases with increasing D and eventually saturates. Our results reveal that the effect of spin-orbit interactions on the D-dependence of the binding energy is rather weak, though the magnetic field can influence the D-dependence at small D values. However, if D is large, then none of QD parameters would have any effect on the E_B vs D curve. Finally, we determined the susceptibility (S) of the off-centre D^0 complex using statistical mechanics. It turns out that S is diamagnetic. With increasing D, |S| initially increases and eventually saturates to a constant. It is observed that when Rashba coupling is absent and only Dresselhaus coupling is present, |S| decreases both with β_D and B. However, in the case when the Dresselhaus coupling is absent and only Rashba coupling present, at small values of B, |S| initially increases with increasing α_R , reaches a maximum and then decreases with α_R , but at large B, |S| increases monotonically with α_R .

In chapter 4, we have studied the role of spin-orbit interactions on the energetics of an on-centre D^0 complex in a power-exponential quantum dot (PEQD) in an external magnetic field. We have shown that below a certain QD size, the GS energy increases with the steepness parameter p, while above that critical size, it decreases. However, in both cases, the GS saturates as p becomes large. This is because when p becomes large, the confinement potential hardly changes with p. For a small dot, the binding energy exhibits a peak at a small p and saturates to a constant as p increases. As the QD size (R) increases, the peak becomes flatter though its height increases. Furthermore, the peak shifts towards higher values of p. As R becomes still larger, the peak disappears and the binding energy just monotonically increases with p at small p and eventually saturates. As a function of R too, BE shows peaks and the peak height increases as p increases. After reaching the

peak, the binding energy decreases with R faster for higher p giving rise to a crossing behavior. Finally, we show that the susceptibility of a D^0 impurity in PEQD is diamagnetic and this diamagnetic susceptibility (S) increases with p at small B and at large B, it decreases with increasing p. At intermediate B, S first decreases with increasing p, develops a minimum at some value of p and then increases with further increase in p. Eventually, however, S saturates to a constant as p becomes large.

In Chapter 5, we have considered the D^0 impurity in a 3D asymmetric Gaussian QD. We have shown that GS energy increases with the asymmetry parameter b. We have also shown that with respect to the QD size R, the binding energy exhibits a peak that shifts towards larger R as b increases. Furthermore, the binding energy decreases with increasing b. Finally, the magnitude of S (which is diamagnetic) has been shown to decrease with increasing B. However, it increases as the asymmetry increases at small B and decreases with increasing asymmetry at large B. This gives rise to an interesting crossing behavior. The Rashba coupling decreases the binding energy, while the Dresselhauss coupling increases it and the asymmetry in the confinement potential enhances these effects.

In Chapter 6, we have studied the spin-orbit interaction effects on the binding energy of a D^- complex in a 3D GQD of GaAs in the presence of a magnetic field using a variational method with a modified Jastrow-type correlation factor. We have observed that, in general, the Dresselhaus coupling enhances the binding energy of D^- whereas the Rashba interaction reduces it. Also, as a function of the magnetic field, the binding energy increases in the presence of Dresselhaus interaction whereas, it remains almost constant in the presence of Rashba interaction. Next we have shown that the susceptibility of a D^- impurity in a GaAs QD is diamagnetic. Interestingly, in the presence Rashba interaction, the susceptibility curve exhibits a minimum. We have shown that in the absence of a magnetic field, the dipole moment of D^- remains unaffected by the spin-orbit interactions. However, if the magnetic field is present, the Rashba coupling enhances its dipole moment, while the Dresselhaus coupling reduces it. The strength of the dipole moment also rises with the QD size and reduces with the increasing potential depth and the magnetic field.

In chapter 7, we have studied some thermo-electric properties of a correlated polar SMT device with dissipation in the presence of a magnetic field using the Holstein-Hubbard-Caldeira-Leggett model. The dissipation and electron-phonon interaction have been treated by canonical transformations and the charge and spin currents have been calculated using the Keldysh method.

In the absence of a magnetic field, the charge conductance G^c as a function of the chemical potential μ , shows a maximum, while the spin conductance G^s remains zero. As the magnetic field increases, the maximum of G^c decreases and splits into two symmetric maxima while G^s develops a maximum and a minimum structure around $\mu=0$ which increase in height and width with increasing magnetic field. We have observed that at zero magnetic field, the spin-up and spin-down Seebeck coefficients are equal and therefore at zero field, the charge Seebeck coefficient (S_c) is maximum and the spin Seebeck coefficient (S_s) vanishes. However, as a function of the magnetic field, the spin-up and spin-down Seebeck coefficients exhibit an opposite behaviour. We have also shown that the el-ph interaction suppresses the charge and spin conductance but enhances the thermopower. Finally, we have shown that the charge and spin Seebeck coefficients decrease as the temperature difference between the leads increases.

ORIGINALITY REPORT

SIMILARITY INDEX

INTERNET SOURCES

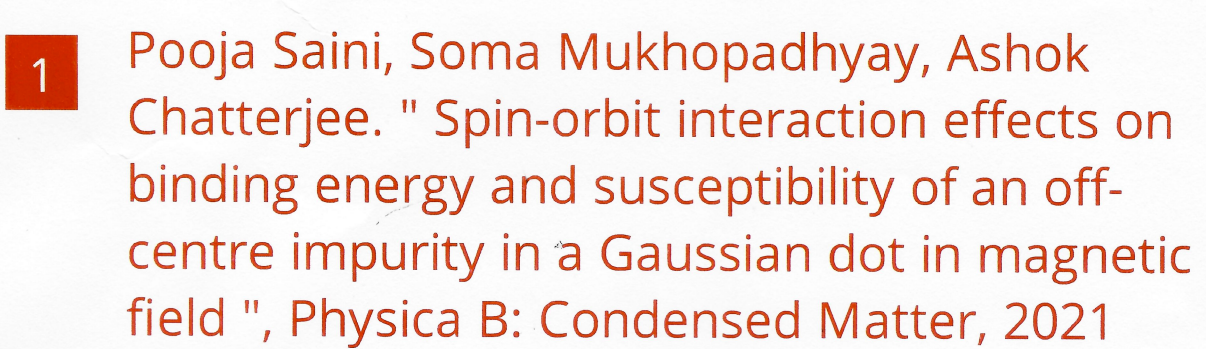
43%

PUBLICATIONS

1 %

STUDENT PAPERS

PRIMARY SOURCES



Publication

Pooja Saini, Aalu Boda, Ashok Chatterjee. " Effect of Rashba and Dresselhaus spin-orbit interactions on a impurity in a twodimensional Gaussian GaAs quantum dot in the presence of an external magnetic field ", Journal of Magnetism and Magnetic Materials, 2019



Publication

Pooja Saini, Ashok Chatterjee. "Confnement shape effect on impurity in a GaAs quantum dot with spin-orbit coupling in a magnetic field ", Superlattices and Microstructures, 2020

Publication

The total Similarity index he lown publications. Therefore it don't indep is 9 to which is I

HYDERABAD - 500 046, INDIA

4	Pooja Saini, Aalu Boda, Ashok Chatterjee. " Spin-orbit interaction effects on a complex in a GaAs quantum dot in a magnetic field ", Micro and Nanostructures, 2022 Publication	8%
5	Submitted to University of Hyderabad, Hyderabad Student Paper	1 %
6	www.ncbi.nlm.nih.gov Internet Source	1 %
7	Kuntal Bhattacharyya, Manasa Kalla, Ashok Chatterjee. "Temperature dependent nonequilibrium magneto-transport in a correlated polar single molecular transistor with quantum dissipation", Journal of Applied Physics, 2022	1%
8	Aalu Boda, Madhusudhan Gorre, Ashok Chatterjee. "Effect of external magnetic field on the ground state properties of D– centres in a Gaussian quantum dot", Superlattices and Microstructures, 2014 Publication	1 %
9	worldwidescience.org Internet Source	<1%
10	Manasa Kalla, Ch. Narasimha Raju, Ashok Chatterjee. "Magneto-transport properties of	<1%

a single molecular transistor: Anderson-Holstein-Caldeira-Leggett model", AIP Publishing, 2019

Publication

Publication

Manasa Kalla, Narasimha Raju Chebrolu, Ashok Chatterjee. "Quantum transport in a single molecular transistor at finite temperature", Scientific Reports, 2021

<1%

Feng Liang, Dong Zhang, Ben-Ling Gao, Yan-Zong Wang, Yu Gu. "Spin thermoelectric transport in a four-quantum-dot ring:
Influence of quantum dots magnetization",
Modern Physics Letters B, 2018

<1%

Manasa Kalla, Narasimha Raju Chebrolu, Ashok Chatterjee. "Magneto-transport properties of a single molecular transistor in the presence of electron-electron and electron-phonon interactions and quantum dissipation", Scientific Reports, 2019

<1%

Ch. Narasimha Raju, Ashok Chatterjee.
"Specific heat of a localized magnetic impurity in a non-magnetic host: A spectral density method for the Anderson–Holstein model", Physica B: Condensed Matter, 2015

Publication

<1%

Zhi-Cheng Yang, Qing-Feng Sun, X C Xie. "Spincurrent Seebeck effect in quantum dot systems", Journal of Physics: Condensed Matter, 2014

<1%

Publication

Pooja Saini, Aalu Boda, Ashok Chatterjee.
"Effect of Rashba and Dresselhaus spin-orbit interactions on the ground state properties of a D0 impurity in a Gaussian GaAs quantum dot placed in a magnetic field", AIP Publishing, 2019

<1%

Publication

A. Cehovin, C. M. Canali, A. H. MacDonald. "Magnetization orientation dependence of the quasiparticle spectrum and hysteresis in ferromagnetic metal nanoparticles", Physical Review B, 2002

<1%

Publication

Peng-Bin Niu, Lixiang Liu, Xiaoqiang Su, Lijuan Dong, Yunlong Shi, Hong-Gang Luo. "Spinresolved transport through a quantum dot driven by bias and temperature gradient", Physica E: Low-dimensional Systems and Nanostructures, 2020

<1%

Publication

Yu-Shen Liu, Feng Chi, Xi-Feng Yang, Jin-Fu Feng. "Pure spin thermoelectric generator

<1%

based on a rashba quantum dot molecule", Journal of Applied Physics, 2011

Publication

20	repository.najah.edu Internet Source	<1%
21	Lan Hong, Feng Chi, Zhen-Guo Fu, Yue-Fei Hou, Zhigang Wang, Ke-Man Li, Jia Liu, Haiyan Yao, Ping Zhang. "Large enhancement of thermoelectric effect by Majorana bound states coupled to a quantum dot", Journal of Applied Physics, 2020 Publication	<1%
22	N F Johnson. "Quantum dots: few-body, low-dimensional systems", Journal of Physics: Condensed Matter, 1995 Publication	<1%
23	Xiao, Jing-Lin. "Influences of temperature and impurity on excited state of bound polaron in the parabolic quantum dots", Superlattices and Microstructures, 2014. Publication	<1%
24	Kuntal Bhattacharyya, Manasa Kalla, Ashok Chatterjee. "Effect of finite temperature and external magnetic field on non-equilibrium transport in a single molecular transistor with quantum dissipation: Anderson-Holstein- Caldeira-Leggett model", Materials Today: Proceedings, 2021	<1%

Michael Yu.. "Chapter 17 Analysis of <1% 25 Axisymmetric and Non-Axisymmetric Wave Propagation in a Homogeneous Piezoelectric Solid Circular Cylinder of Transversely Isotropic Material", IntechOpen, 2010 Publication www.arxiv-vanity.com <1% Internet Source <1% Lei-Lei Nian, Long Bai, Wenting Yu, Jun Tang, Huichao Li, Rong Zhang, Rui-Qiang Wang, Xue-Feng Wang, M. Wierzbicki. "Exploration of Spin-Dependent Thermoelectricity in the Chiral Double-Stranded DNA Molecule Coupled to Ferromagnetic Leads", Physical Review Applied, 2019 Publication Goyal, Swati, and P K Sen. "Dynamic Stark <1% 28 effects in a semiconductor quantum dot exhibiting a two-hole species valence band", Journal of Physics Conference Series, 2012. Publication K. Luhluh Jahan, Bahadir Boyacioglu, Ashok <1% 29 Chatterjee. "Effect of confinement potential shape on the electronic, thermodynamic, magnetic and transport properties of a GaAs

quantum dot at finite temperature", Scientific

Reports, 2019

- Rong Lü. "Time-dependent electron transport through molecular quantum dots in the presence of external irradiation", Journal of Physics Condensed Matter, 09/21/2005
- <1%

<1%

- Aalu Boda, Ashok Chatterjee. "Effect of an external magnetic field on the binding energy, magnetic moment and susceptibility of an offcentre donor complex in a Gaussian quantum dot", Physica B: Condensed Matter, 2014
- Jianhua Liu, Kun Luo, Hudong Chang, Bing Sun, Zhenhua Wu. "Ultrahigh Spin Filter Efficiency, Giant Magnetoresistance and Large Spin Seebeck Coefficient in Monolayer and Bilayer Co-/Fe-/Cu-Phthalocyanine Molecular Devices", Nanomaterials, 2021

<1%

- John Schliemann, J. Carlos Egues, Daniel Loss.
 "Variational study of the quantum Hall
 ferromagnet in the presence of spin-orbit
 interaction ", Physical Review B, 2003
- <1%

34 www.mrs.org
Internet Source

Publication

Publication

<1%

35	P. Hashemi, M. Servatkhah, R. Pourmand. "The effect of rashba spin–orbit interaction on optical far-infrared transition of tuned quantum dot/ring systems", Optical and Quantum Electronics, 2021 Publication	<1%
36	Aalu Boda. "Effect of spin-orbit interactions on the energy, magnetic moment and susceptibility of an off-center donor impurity in a Gaussian quantum dot", AIP Publishing, 2020 Publication	<1%
37	Brataas, A "Non-collinear magnetoelectronics", Physics Reports, 200604	<1%
38	Kumar, D. Sanjeev, Aalu Boda, Soma Mukhopadhyay, and Ashok Chatterjee. "Effect of Rashba spin-orbit interaction on the ground state energy of a D0 centre in a GaAs quantum dot with Gaussian confinement", Superlattices and Microstructures, 2015. Publication	<1%
39	Golnaz Khanlar, Sahar Izadi Vishkayi, Hamid Rahimpour Soleimani. "The spin-dependent properties of silicon carbide/graphene nanoribbons junctions with vacancy defects", Scientific Reports, 2021	<1%



X.F. Yang, H.L. Wang, X.K. Hong, Y.S. Liu, J.F. Feng, X.F. Wang, C.W. Zhang, F. Chi, M.S. Si. "Tunable half-metallic properties and spin Seebeck effects in zigzag-edged graphene nanoribbons adsorbed with V atom or V-benzene compound", Organic Electronics, 2015

<1%

Publication

Exclude quotes On

Exclude bibliography (

Exclude matches

< 14 words